ANALYSIS OF NOVEL 3D FIBRE REINFORCED NATURAL FIBRE HYBRID COMPOSITES FOR HIGH PERFORMANCE BONDED JOINTS

HENRIQUE FERNANDES MEDEIROS DE QUEIROZ

Tese apresentada ao Programa/Curso de Pós-Graduação em Engenharia Mecânica e Tecnologia dos Materiais - PPEMM, do Centro Federal de Educação Tecnológica Celso Suckow da Fonseca, CEFET/RJ, como parte dos requisitos necessários à obtenção do título de Doutor em Engenharia Mecânica e Tecnologia dos Materiais

Orientadora: Doina Mariana Banea

Rio de Janeiro

Fevereiro/2025

ANALYSIS OF NOVEL 3D FIBRE REINFORCED NATURAL FIBER HYBRID COMPOSITES FOR HIGH PERFORMANCE BONDED JOINTS

Dissertação apresentada ao Programa de Pós-Graduação em Engenharia Mecânica e Tecnologia dos Materiais - PPEMM, do Centro Federal de Educação Tecnológica Celso Suckow da Fonseca, CEFET/RJ, como parte dos requisitos necessários à obtenção do título de Doutor em Engenharia Mecânica e Tecnologia dos Materiais.

HENRIQUE FERNANDES MEDEIROS DE QUEIROZ

Banca Examinadora:

_____

Presidente, Professora Dra. DOINA MARIANA BANEA (CEFET/RJ) (orientadora)

_____

Professor Dr. RICARDO ALEXANDRE AMAR DE AGUIAR (CEFET/RJ)

_____

Professor Dr. JOÃO MARCIANO LAREDO DOS REIS (UFF/RJ)

_____

Professor Dr. MARCELO LEITE RIBEIRO (USP/SP)

_____

Professora Dra. ROSEMERE DE ARAÚJO ALVES LIMA (TU Delft/NL)

Rio de Janeiro

Fevereiro/2025

Ficha catalográfica elaborada pela Biblioteca Central do CEFET/RJ

Q3 Queiroz, Henrique Fernandes Medeiros de
Analysis of novel 3D fibre reinforced natural fibre hybrid composites for high performance bonded joints / Henrique Fernandes Medeiros de Queiroz – 2025.
40f : il. color. + anexos , enc.

Tese (Doutorado). Centro Federal de Educação Tecnológica Celso Suckow da Fonseca, 2025.
Bibliografia : f. 36-40.
Orientadora: Doina Mariana Banea.

1. Polímeros. 2. Nanocompósitos (Materiais). 3. Compósitos naturais. 4. Fibras vegetais. 5. Tecnologia de materiais. I. Banea, Doina Mariana (Orient.). II Título.

CDD 620.192

Elaborada pelo bibliotecário Leandro Mota de Menezes – CRB/7 nº 5281

DEDICATION

To my father's final smile.

ACKNOWLEDGEMENTS

Primeiramente,
A minha família que me apoiaram durante todo meu percurso acadêmico.

Aos Professores,
A minha orientadora e mentora, Dra; Doina Mariana Banea pela visão, orientação, amizade e encorajamento durante o processo (da graduação ao doutorado!).

Aos pesquisadores Jorge Neto, Daniel Cavalcanti, Rogério Junior (CEFET/RJ) e Natália Victória (PUC), que não somente foram cruciais para o processo de pesquisa, mas se tornaram grandes amigos.

Ao antigo técnico (e salvador da pátria) Brenno Duarte (LASEI/CEFET) e Hiron Akira (LAMAT) e Técnico Leonardo da Silva pelo suporte e utilização de maquinário. Ao Técnico de assuntos acadêmicos Fernando Berçot.

Ao pesquisador Raffaele Ciardiello, técnica Ana Pagnoncelli, doutorando Francesco Bandinelli e pesquisador Alberto Ciampaglia (Politecnico di Torino) pela amizade e suporte durante a pesquisa na Itália. Agradeço também a Alessia, Valentin, Adriano e Francesca pela amizade e risos.

Alla mia amata Aurora Pressutti, il mio grande regalo dall'Italia.

Ao Centro Federal de Educação Tecnológica Celso Suckow da Fonseca (CEFET/RJ), pela oportunidade de obtenção do grau de Engenheiro, Mestre e Doutor. E finalmente a CAPES pela oportunidade de pesquisa internacional.

RESUMO

ANÁLISE DE COMPÓSITOS NATURAIS HÍBRIDOS 3D PARA JUNTAS COLADAS DE ALTA PERFORMANCE

A indústria humana moderna se encontra em um ponto crucial. Cada setor deve enfrentar os efeitos inevitáveis das mudanças climáticas devido ao aquecimento global. Isso está ligado às emissões causadas pela queima de combustíveis fósseis não renováveis. Nesse contexto, as aplicações de materiais renováveis de fontes naturais e com impacto ambiental muito reduzido são imperativas. Na ciência dos materiais compósitos, isso se apresenta na forma de compósitos reforçados com fibras naturais. (NFRCs). Entre os muitos desafios enfrentados por qualquer novo material a ser utilizado por diversos setores industriais, a junção desses materiais a estruturas maiores deve ser abordada. Assim, esta pesquisa focou no desenvolvimento e caracterização de uma abordagem inovadora para melhorar o desempenho das juntas coladas de NFRCs. A questão surge das propriedades mecânicas inferiores das fibras naturais (i.e., juta, sisal e curauá) quando comparadas às fibras sintéticas clássicas. (i.e., vidro e carbono). Essas propriedades inferiores das fibras se traduzem em propriedades inferiores do compósito, que, por sua vez, sob as cargas de uma junta de sobreposição simples (SLJ), falha prematuramente. A técnica inovadora aplicada nesta pesquisa utiliza a arquitetura das fibras de reforço para melhorar as propriedades transversais (fora do plano) dos compósitos, de modo que falhas prematuras de delaminação devido à rotação da borda de sobreposição (tensões de arrancamento) sejam diminuídas ou evitadas. O objetivo desta técnica era melhorar o desempenho da junta colada (ou seja, a carga de falha) dos NFRCs, de modo que

correspondesse ao das juntas sintéticas de vidro e carbono. (i.e., GFRP e CFRP). A técnica de reforço ortogonal tridimensional através da espessura (3D OTT) conseguiu ter sucesso nesse esforço com duas fibras de reforço secundárias distintas, SISAL e CURAUÁ. Tendo alcançado o principal objetivo desta pesquisa, permanece um amplo espectro de caracterização de materiais para facilitar uma aplicação industrial mais ampla desses novos NFRCs 3D. Portanto, foram realizadas análises mecânicas quasi-estáticas e dinâmicas, bem como análises pós-falha por meio de microscopia e microtomografia por raios X para caracterizar esses materiais. Foi encontrado, de maneira geral, que para as propriedades clássicas de materiais quasi-estáticos no plano, o reforço 3D não apresentou variações altamente significativas, o que está alinhado com a literatura predominante para compósitos 3D sintéticos. Além disso, para as propriedades de impacto de queda, foi encontrado que a arquitetura 3D apresenta uma melhoria altamente significativa na vida útil de fadiga de impacto de baixa velocidade (LVI) ou seja, foram encontradas melhorias de até 2x e 3,6x para os espécimes 3D de CURAUÁ e SISAL, respectivamente. Além disso, a análise de microCT demonstra que a técnica simples de moldagem por compressão utilizada nesta pesquisa conseguiu fabricar NFRCs com frações de vazios inferiores a 5%, que é o limite aceitável para aplicações automotivas. Portanto, esta pesquisa aplicou materiais inovadores com a clara intenção de melhorar o desempenho SLJ dos NFRCs. Ao alcançar seu objetivo, foi aplicado uma grande gama experimental de modo a melhorar a compreensão desses novos materiais para aplicações industriais mais amplas.

Palavras-chave: Compósitos naturais, juntas coladas, reforços tridimensionais.

ABSTRACT

ANALYSIS OF NOVEL 3D FIBRE REINFORCED NATURAL FIBER HYBRID COMPOSITES FOR HIGH PERFORMANCE BONDED JOINTS

The modern human industry finds itself at a pivotal point. Every sector must address the unavoidable effects of climate change due to global warming. This is linked to the emissions caused by non-renewable fossil fuels. In this context, the applications of renewable materials with natural sources with much decreased environmental impact is imperative. In composite material science, this comes in the form of natural fibre-reinforced composites (NFRCs). Among the many challenges faced by any new material to be used by various industrial sectors, the joining of these materials to larger structures must be addressed. As such, this research focused on the development and characterization of a novel approach in order to enhance the bonded joint performance of NFRCs. The issue arises from the lower mechanical properties of natural fibres (i.e., jute, sisal and curauá) when compared to classical synthetic fibres (i.e., glass and carbon). These lower fibre properties translate to lower composite properties, which in turn, under the loads of a single lap joint (SLJ), fails prematurely. The novel technique applied in this research leverages the reinforcement fibre architecture to enhance the transverse (out-of-plane) composite properties such that premature delamination failures due to overlap edge rotation (peel stresses) are decreased or avoided. The aim of this technique was to enhance the bonded joint performance (i.e., failure load) of NFRCs, such that it matched that of the synthetic joints of glass and carbon (i.e., GFRP and CFRP). The 3-dimensional orthogonal-through-the-thickness reinforcement technique (3D OTT) managed to

succeed in this effort with two distinct secondary reinforcement fibres, SISAL and CURAUÁ. Having reached the main objective of this research, a large envelope of material characterization remains in order to facilitate a wider industrial application of these novel 3D NFRCs. Therefore, quasi-static and dynamic mechanical analysis were conducted as well as post-mortem analysis via microscopy and X-ray microtomography was used to characterize these materials. It was found generally, that for the classical in-plane quasi-static material properties, the 3D reinforcement did not present highly significant variations, which is aligned with the prevailing literature for synthetic 3D composites. Furthermore, for the drop-dart impact properties, it was found that the 3D architecture presents a highly significant improvement in the low velocity impact (LVI) fatigue life (i.e., enhancements of up to 2x and 3.6x were found for the CURAUÁ and SISAL 3D specimens, respectively. Moreover, the microCT analysis demonstrates that the simple compression molding technique used in this research managed to fabricate NFRCs with void fractions lower than 5%, which is the acceptable threshold for automotive applications. Therefore, this research effort applied novel materials with a clear intent of enhancing the SLJ performance of NFRCs. Upon reaching its goal, a large experimental envelope towards a better understanding of these novel materials for wider industrial applications was demonstrated.

Keywords: Natural composites, bonded joints, three-dimensional reinforcement.

LIST OF FIGURES

Figure 1. Representative tensile properties of composite constituents [2]. 1

Figure 2. Roadmap of NFRC applications in the automotive industry [3]..... 2

Figure 3. Typical 3D woven composite architectures (a) and a representative visualization (b) [18, 19]. 11

Figure 4. Effect of z-binder yarn content on the (a) mode I load–displacement curves and the (b) initiation and steady-state fracture toughness values. The error bars in (b) represent two standard deviations [16]..... 13

Figure 5. 3D woven carbon fibre plane motor blade (a) and landing gear brace (b) [25]. 14

Figure 6. Example of 3D woven natural fibre architecture analyzed in the literature: a) Layer-to-layer 3D woven angle interlock structure, b) Semi-automatic Dobby loom (modified with 4 beam arrangement) and c) Image showing stuffer yarns and binding yarns (photographed after manual peeling of fabric) [27]..... 16

Figure 7. Preparation of 3DOWSBCs. (a) Schematic diagram of 3D orthogonal woven preform preparation and structure. (b) Schematic diagram of VARTM curing process and (c) physical diagram of 3DOWSBC and (c) Detailed morphologies of the 3DOWSBCs [40]..... 17

Figure 8. Representative 3D OTT architecture [41] (a) and curauá fibre-reinforced jute fabrics with 2D (b), 3D (c), while the cross-section of the fabricated composite can be seen in the bottom (d), e) representative 2D curauá weaving process and f) 2D curauá intralaminar reinforcement geometry. 20

Figure 9. Representative schematic of composite fabrication process, a) laminated fibres on steel mould, b) compression molding process, c) fabrication stages of the 3D woven

composites and c) representative fabricated SISAL 3D composite plate. 22

Figure 10. Testing machine used for quasi-static tests (a) and tensile test set-up with extensometer (b). 25

Figure 11. Flexural test set-up. 26

Figure 12. Short beam test set-up. 27

Figure 13. Example of stress distribution across the overlap zone of an aluminum/epoxy bonded joint [48]. 28

Figure 14. Representative schematic of (a) mould and spaers used and (b) fabricated bonded joint. 29

Figure 15. Charpy impact machine used. 30

Figure 16. Drop dart impact fatigue machine used (a) and a 100x100 mm representative specimen used (b). 31

Figure 17. Fatigue machine used (a) and a close u of the fatigue test set-up (b). 32

LIST OF TABLES

Table 1. Recommendation table for the selection of reinforcement architectures [22]. 14

CONTENTS

SUMMARY OF THESIS 1

1. Introduction 1

1.1 Background 1

1.2 Objectives 4

1.3 Research methodology 5

1.4 Outline of the thesis 6

2. 3D woven composite state of the art 10

2.1 General trends in 3D woven synthetic composites 10

2.2 General trends in 3D woven natural composites 15

3. Materials and Methods 19

3.1 Quasi-static tests 24

3.1.1 Tensile tests 24

3.1.2 Flexural tests 25

3.1.3 Short beam tests 26

3.1.4 Single lap joints 27

3.2 Dynamic tests 29

3.2.1 Charpy impact tests 30

3.2.2 Drop weight tests 31

3.2.3 Fatigue tests 32

4. Conclusions 33

5. Future work 35

References 36

Paper 1 41

Paper 2 26

Paper 3 61

Paper 4 84

Paper 5 163

LIST OF PUBLICATIONS

1. de Queiroz HFM, Banea MD. Methods to increase the mechanical performance of composite adhesive joints: An overview with focus on joints with natural fibre composite adherends. Journal of Composite Materials. 2022;56(26):3993-4010. doi:10.1177/00219983221125906

2. H.F.M. de Queiroz, J.S.S. Neto, D.K.K. Cavalcanti & M.D. Banea (2023): A novel 3D fibre-reinforcement architecture for high performance natural fibre reinforced composite adhesively bonded joints, The Journal of Adhesion, DOI: 10.1080/00218464.2023.2200173

3. H.F.M. de Queiroz, N. V. dos Santos J.S.S. Neto, D.K.K. Cavalcanti & M.D. Banea (2024): Mechanical characterization of novel natural fibre-reinforced composites via a three-dimensional fibre architecture, Composites Science and Technology, DOI: 10.1016/j.compscitech.2024.110996

4. H.F.M. de Queiroz, R. Ciardiello & M.D. Banea (2024): Perforation and impact fatigue response of 3D hybrid natural fibre-reinforced composites, submitted to Composites Part A: Applied Science and Manufacturing.

5. H.F.M. de Queiroz, R. Ciardiello & M.D. Banea (2024): Fatigue analysis of novel 3D natural fibre-reinforced composites, to be submitted.

SUMMARY OF THESIS

1. Introduction

1.1 Background

Composite materials are very common nowadays due to their excellent performance in weight-critical applications such as automotive, naval, sport and aerospace industries [1]. These materials are simply defined as a merger of two or more distinct phases that come together to form a new material whose properties are superior to each individual constituent part. Fibre-reinforced composite materials usually refer to the use of a polymer matrix and a fibre reinforcement of different kinds. The resulting material will inevitably present superior properties such as tensile strength, when compared to the individual materials (see Fig 1.) [2].

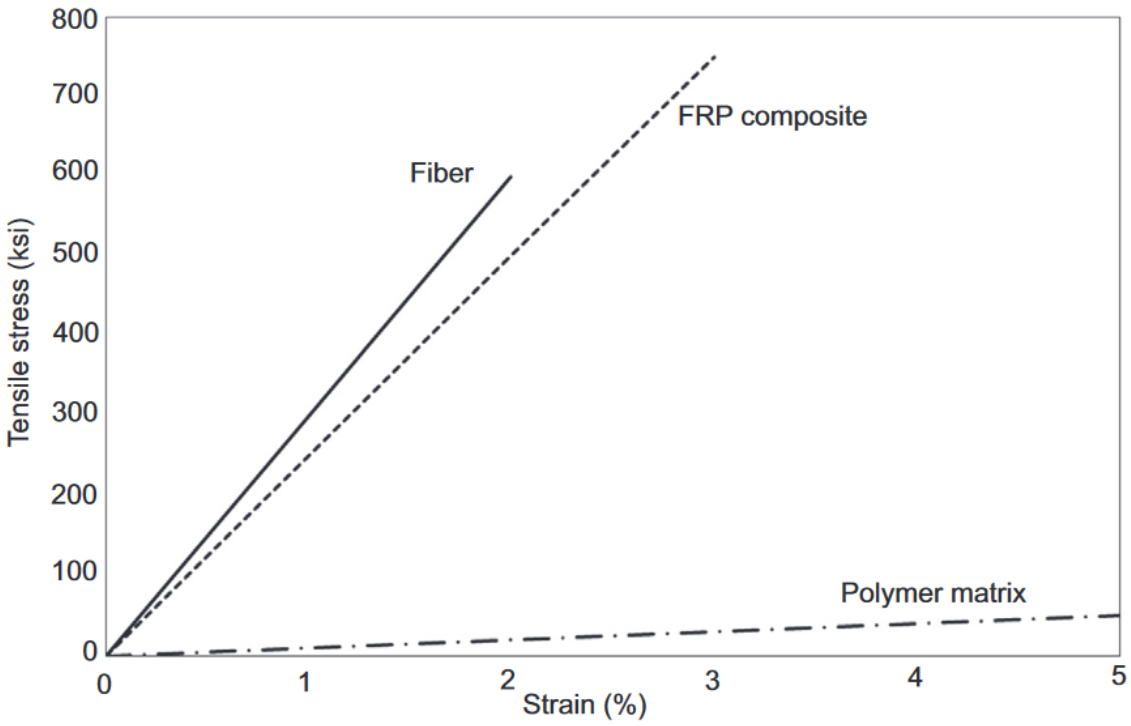


Figure 1. Representative tensile properties of composite constituents [2].

The application of natural fiber-reinforced composites (NFRCs) in the automotive industry, among others, is only expected to increase due to the pressure from society and every government on every industrial sector do decrease or eliminate the carbon footprint of goods and services [1]. Specifically, to the automotive sector, natural fibre-reinforced composites have been used since the very beginning with Henry Ford, albeit in very non-structural applications. In fact, semi-structural applications have become a reality only very recently (c.a. 2018) with the advent of high-performance flax fiber composites by BComp® (see Fig. 2) [3].

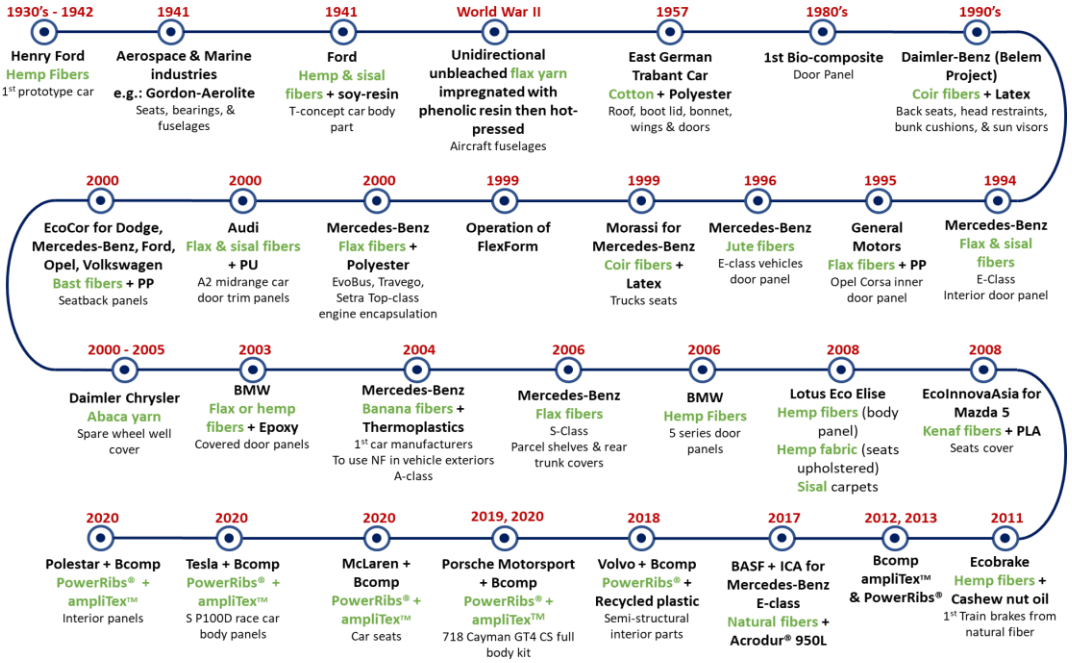


Figure 2. Roadmap of NFRC applications in the automotive industry [3].

NFRCs present a variety of compelling reasons for their application in the automotive sector, such as low weight and cost, high vibration absorption (damping), low environmental impact due to low energy required for processing, no toxic fumes when exposed to flames and may present high enough mechanical properties depending on the application [4-6]. However, there are some significant drawbacks that have retarded the widespread application of these materials, such as high hydrophilic tendency, lower mechanical properties in general when compared to classical synthetic fibre composites and low interfacial strength with common matrices such as epoxy. Despite these

drawbacks, the advantages of NFRCs usually outweigh their drawbacks, especially concerning cost and weight [7].

Finally, and directly linked to this research, there is the issue of the joining of these materials to the structure of the vehicle. It is well established in the literature that the optimum joining method for composites in general is adhesive bonding [8]. This is due to the specific advantages afforded by an adhesive when compared to classical mechanical joining methods such as bolts and rivets [9]. These will be discussed at length in **Paper 1**. Suffice it to say that as far as composites are concerned, it is far better to use an adhesive bonding technique in order to join it to any other structure.

However, for NFRCs in particular, due to their mechanical properties, their bonded joint performance has been hitherto hindered by their failure mechanisms, mainly delamination, which significantly decreases the bonded joint failure load [10-13]. Previous works by the author aimed to solve the same issue by different techniques. Hybrid intralaminar reinforcements were attempted and a jute + glass 2D intralaminar hybrid reached 77% of the GFRP failure load [10]. Following this, a simples interlaminar jute + glass hybrid was attempted (i.e., glass fabrics around a jute core) and it reached 100% of the neat GFRP joint failure load, however this was still not a fully NFRC joint [11]. With this particular problem in mind, this research work came to be, such that it aimed to enhance the transverse properties of NFRCs [14-16] in order to combat the particularly high peel stresses suffered by the adherend in a classical single lap joint (SLJ). This has been published in **Paper 2** and the goal was finally achieved.

This work presents a methodology which applied three-dimensional (3D) orthogonal - through-the-thickness (OTT) reinforcements in NFRC composites, such that the transverse (out of plane) strength and fracture toughness were significantly enhanced. These novel materials were then tested under SLJ with a modern tough automotive-grade adhesive and it was found that the bonded joint performance matched that of the synthetic glass and carbon composites (i.e., GFRP and CFRP). The materials that managed to reach this milestone were the CURAUÁ and SISAL variants, and further architectural and fabrication details will be discussed in the appended papers. Furthermore, upon discovering which materials can reach the synthetic benchmark, further mechanical studies were conducted to better understand these novel materials in other applications that are relevant to the automotive industry, such as low velocity impact (LVI), impact

fatigue and tension-tension fatigue, as well as the more classical mechanical characterizations. This research represents the first reported literature result in which NFRC bonded joints reached their synthetic counterparts in SLJ performance. Furthermore, the 3D OTT architecture also presented significant improvements in impact, impact fatigue and classical tension-tension fatigue. However, this still represents a very new research field, and much work still needs to be done for wider industrial applications.

1.2 Objectives

The main objective of this research was to investigate the effect of transverse (3D) fibre reinforcement in NFRCs in order to enhance their bonded joint performance. Several different natural fibres were used with a fixed 3D architecture. The bonded joint failure load to be reached was that of fully synthetic composites (i.e. GFRP and CFRP).

The specific objectives are listed below:

- First a comprehensive analysis of the available techniques in the literature was condensed in a first of its kind review, which determined that 3D architectures presented a very promising path for SLJ load enhancement.
- Second, an experimental effort was carried out to determine the viability of 3D OTT architectures in the improvement of NFRC bonded joint performance up to the failure load of synthetic composite joints with an epoxy automotive-grade adhesive.
- Further analysis was carried out to ascertain the in-plane quasi-static mechanical properties of the materials that succeeded in satisfying the previous objective.
- Finally, these satisfactory materials were tested in dynamic loads (i.e., low velocity impact and tension-tension fatigue) which are more in line with real world applications.

1.3 Research methodology

In order to reach all of the aims of this research, the following methodology was adopted.

- First, a comprehensive review of all of the available and possible techniques that may be applied in order to enhance the bonded joint performance of composites was carried out to single out the best possible path forward. This was published in **Paper 1**. It was found that the most promising way forward for this research was the application of 3D OTT reinforcements, which were completely novel, presented a relatively simple fabrication technique, was low cost and within the fabrication capabilities of the laboratory facility.
- Following the decision of the technique, preliminary tests were carried out to choose an architecture. Once chosen, an experimental SLJ testing program was devised to fabricate and test novel 3D hybrid NFRCs under SLJ bonding as well as their 2D counterparts. The results were published in **Paper 2**. It was found that the goal was reached and the technique successful.
- Once the novel materials were proven to reach the synthetic benchmark for SLJ performance, it was necessary to further characterize them in monotonic quasi-static tests. Tensile and flexural tests as well as Charpy impact tests were carried out on both 2D and 3D specimens of the successful materials. Furthermore, the failure modes were analyzed via SEM images and undamaged specimens were also analyzed via microCT scanning. The results were summarized in **Paper 3** (submitted, not yet published).
- Finally, further dynamic tests were chosen to analyze more realistic scenarios such as low velocity impact and impact fatigue as well as tension-tension fatigue life of both 2D and 3D specimens. MicroCT scanning was also used to analyze the specimens. The results will be published as **Paper 4** and **5** (**Paper 5** is still being written**)**.

1.4 Outline of the thesis

This thesis consists of five appended papers and a summary. Chapter one presents the general background and reasoning for the research effort, while Chapter 2 summarizes the general trends in the state of the art of 3D woven synthetic and natural composites. Chapter 3 presents the materials and methods used throughout the research. Chapter 4 presents the general conclusions while Chapter 5 formulates the general steps envisioned for the future of the research. Finally, five papers, both published, submitted and still to be submitted are appended individually. The following summary of the papers is provided:

Paper 1 de Queiroz HFM, Banea MD. Methods to increase the mechanical performance of composite adhesive joints: An overview with focus on joints with natural fibre composite adherends. Journal of Composite Materials. 2022;56(26):3993-4010. doi:10.1177/00219983221125906

Abstract of Paper 1: *Methods to increase the mechanical performance of composite adhesive joints: An overview with focus on joints with natural fibre composite adherends*. This paper presents an overview of the recent developments in the main methods used to increase the mechanical performance of composite adhesive joints with focus on joints with natural fibre reinforced composite (NFRC) adherends. First, the main factors that affect the performance of composite adhesive joints were briefly discussed. Further, the main methods used to increase the mechanical performance of natural fibre-reinforced composite adhesive joints are presented. Since, the literature regarding these methods applied to NFRC adherends is relatively scarce, in addition, promising techniques applied to synthetic fibre-reinforced composite joints, which behave in a similar manner and whose results can be extrapolated with a great deal of confidence to NFRCs are also briefly discussed. Finally, some conclusions and an outlook on critical challenges and future perspectives are summarized. The application of sustainable green composites may further increase in many structural and non-structural applications if their joining behaviour is well-known and established.

Paper 2 H.F.M. de Queiroz, J.S.S. Neto, D.K.K. Cavalcanti & M.D. Banea (2023): A novel 3D fibre-reinforcement architecture for high performance natural fibre reinforced composite adhesively bonded joints, The Journal of Adhesion, DOI: 10.1080/00218464.2023.2200173

Abstract of Paper 2: *A novel 3D fibre-reinforcement architecture for high performance natural fibre reinforced composite adhesively bonded joints*. In this paper, the effect of a novel fibre reinforcement architecture in the adhesively bonded joint efficiency of natural fibre reinforced composites (NFRC) was investigated. Two different reinforcement techniques were used: intralaminar reinforcement (2D) and orthogonal-through-the-thickness reinforcement (3D). The aim of the novel architecture is to enhance the transverse properties of the adherend (transverse strength and fracture toughness) in order to delay or avoid delamination failures. A jute bidirectional fabric was used as a base primary reinforcement phase and curauá, sisal, ramie, hemp and glass fibres were used as secondary reinforcement phases for the 2D and 3D fibre reinforcement architectures. Single lap joints (SLJs) bonded with an epoxy adhesive used in the automotive industry were fabricated with these adherends and the efficiency of the joints was investigated by comparing them to glass (GFRP) and carbon (CFRP) pure synthetic fibre reinforced composite joints. It was found that the novel architecture was successful in reaching the failure load of the synthetic composite joints for SISAL 3D, CURAUÁ 2D and CURAUÁ 3D SLJs. Therefore, NFRC bonded joints can be a viable replacement for synthetic fibre composite joints at no load-bearing loss.

Paper 3 H.F.M. de Queiroz, N. V. dos Santos J.S.S. Neto, D.K.K. Cavalcanti & M.D. Banea (2024): Mechanical characterization of novel natural fibre-reinforced composites via a three-dimensional fibre architecture, Composites Science and Technology, DOI: 10.1016/j.compscitech.2024.110996.

Abstract of Paper 3: *Mechanical characterization of novel natural fibre-reinforced composites via a three-dimensional fibre architecture.* This research focuses on the fabrication and analysis of novel natural fiber hybrid composites using two different reinforcement techniques: intralaminar reinforcement (2D) and orthogonal-through-the-thickness reinforcement (3D-OTT). Jute bidirectional fabric served as the main fiber phase, while secondary reinforcement phases (sisal, curauá, and glass fibers) were woven unidirectionally through the jute fabric for the 2D architecture (intralaminar reinforcement). For the 3D architecture, a transverse fiber phase was additionally woven orthogonally through the thickness of the fiber preforms. Pure jute and glass fiber-reinforced composites were also fabricated and tested for comparison. Tensile, flexural, and impact tests were performed to assess how the innovative 3D-OTT architecture influences in-plane composite properties. SEM analysis and X-ray microtomography were used to examine failure modes, interfacial quality and void volume fractions. The results support the viability of the novel composite materials for partial or complete substitution of glass fiber-reinforced materials (GFRP) in specific applications. For instance, curauá-reinforced specimens demonstrated comparable tensile and flexural stiffness to synthetic composites, while 3D-reinforced sisal specimens exhibited exceptional energy absorption during impact testing. Additionally, the simple fabrication process resulted in very low void fractions, making these composites suitable for the automotive industry.

Paper 4 H.F.M. de Queiroz, R. Ciardiello & M.D. Banea (2024): Perforation and impact fatigue response of 3D hybrid natural fibre-reinforced composites, submitted to Composites Part A: Applied Science and Manufacturing, 2024.

Abstract of Paper 4: *Perforation and impact fatigue response of 3D hybrid natural fibre-reinforced composites*. This research focuses on the dynamic response analysis of novel 3D natural fibre-reinforced hybrid composites. Novel sisal and curauá reinforced composites were fabricated and tested under low velocity impact (LVI). Both full perforation and repeated LVI impact fatigue tests were carried out to analyze both the maximum energy and load of the hybrid composites as well as the fatigue life expectancy

under diminished energy repeated impacts (similar to real life situations such as hailstorms or falling debris). It was found that for perforation the SISAL 2D specimens presented the highest absorbed energy and peak load due to the delamination of sisal fibres from the resin generating large debonding areas that absorb energy. Furthermore, for the 3D reinforcement, it was observed that the impact fatigue life was significantly enhanced (i.e., 3.6x and 2x for the SISAL and CURAUÁ specimens, respectively).

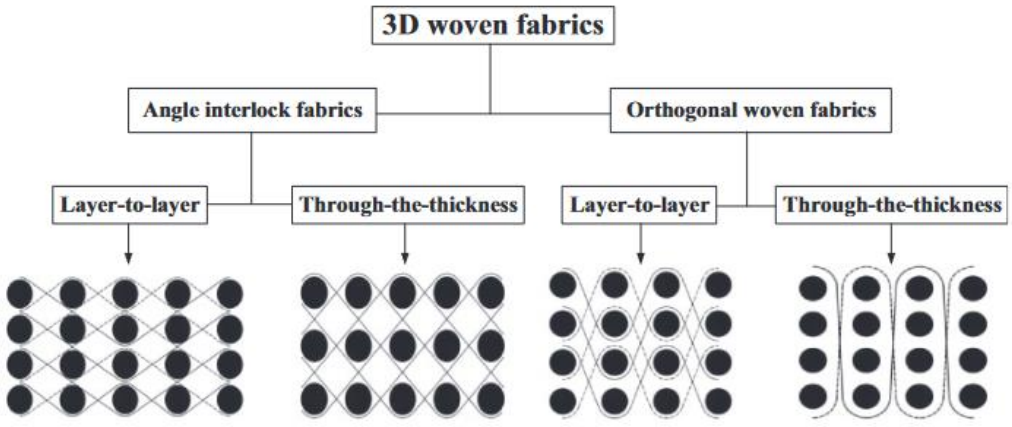
Paper 5 H.F.M. de Queiroz, R. Ciardiello & M.D. Banea (2024): Fatigue analysis of novel 3D natural fibre-reinforced composites, to be submitted.

Abstract of Paper 5: The increasing demand for sustainable materials in engineering applications has led to significant interest in natural fibre-reinforced composites (NFRCs). In this study, the fatigue behavior of a novel 3D woven orthogonal through-the-thickness natural fibre-reinforced composite was investigated. The unique structure of the composite, featuring a three-dimensional woven architecture, is examined for its impact on fatigue performance under cyclic loading conditions. Experimental testing is conducted to determine the fatigue life and failure modes, with a focus on the influence of fibre orientation, weave patterns, and matrix properties. The results show that the 3D woven structure significantly improves the fatigue resistance compared to conventional 2D fibre-reinforced composites, with enhanced through-the-thickness strength and durability. A detailed analysis of crack propagation, delamination, and damage evolution is presented, providing insights into the material's potential for automotive, aerospace, and other high-performance applications. This research contributes to the development of more sustainable, high-performance composites for advanced engineering applications, offering a promising alternative to traditional synthetic fibre-based materials.

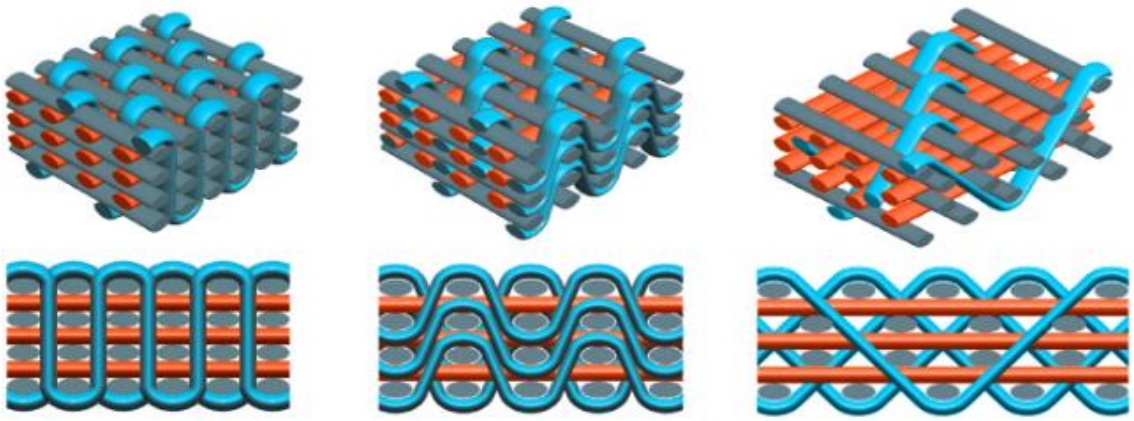
2. 3D woven composite state of the art

2.1 General trends in 3D woven synthetic composites

Three-dimensional fibre–polymer composites are an important class of advanced engineering materials containing a 3D network structure of planar and through-thickness reinforcing fibres. A variety of 3D fibre composites have been developed to overcome some of the problems that are inherent with conventional polymer laminates, such as their low delamination resistance and poor impact damage tolerance. Many types of 3D fibre composite materials have been created, and they are classified according to the method by which the three-dimensional fibre reinforcement is produced. The most common types are 3D woven composites [17]. The fibre architecture for the various types of 3D woven composites can be seen in Fig. 3. The fibre architecture is designed with a large percentage of in-plane continuous fibres (like a conventional laminate) to provide high in-plane mechanical properties. The novel architectural feature of 3D composites is the inclusion of high-stiffness, high-strength fibres in the through-thickness (or z-) direction. The through-thickness fibres, which are given the general term z-binders, are used to provide 3D fibre composites with higher delamination fracture toughness and impact damage tolerance than conventional laminates (see Fig. 4). The volume fraction of z-binder reinforcement is usually low (typically under 5–10%), although this is sufficient to greatly increase the delamination resistance and damage tolerance [18].



a)



b)

Figure 3. Typical 3D woven composite architectures (a) and a representative visualization (b) [18, 19].

Through-thickness reinforcement of polymer laminates with woven tows is an effective method of increasing delamination toughness and damage tolerance. A large body of research published for synthetic composites has shown that through-thickness reinforcement also changes the in-plane static and fatigue properties [20]. The in-plane static properties of composites can be increased by through-thickness reinforcement with woven z-binders. The increase to the mechanical properties of 3D woven composites above their equivalent 2D material is typically under 20% and is not or only weakly dependent on the volume content or diameter of the z-binders. The property increase is presumably caused by an increase in the in-plane fiber volume fraction due to compaction of the woven laminate preform by the z-binders. The stiffness and strength of 3D woven composites can be reduced by their z-binders. The reduction to the properties, which is usually under 20%, does not correlate with the volume fraction or diameter of the z-binders. The reduction to stiffness is attributed to geometric defects (fiber crimp and waviness) which induce local softening in the volume of material surrounding each z-binder. Reductions to the strength properties are also controlled by microstructural defects, such as clusters of broken and damaged fibres reducing tensile strength and crimped fibres lowering compressive strength. The observation that the stiffness and strength of 3D woven and stitched composites do not correlate strongly with their z-binder content implies that increasing the volume fraction of through-thickness reinforcement to promote high delamination toughness and damage tolerance will not necessarily result in

a prohibitive reduction to the in-plane properties acceptable loss to the in-plane properties [17]. The fatigue properties of 3D woven synthetic composites are always reduced by the z-binders (with the exception of one stitched material) [21]. The fatigue properties are reduced in two ways. In the first, the fatigue life curve for the 3D composite is reduced by the z-binders, although it remains parallel with the S–N curve for the equivalent 2D laminate. In this case the loss in fatigue performance is due solely to the knockdown in monotonic strength caused by microstructural defects, and the fatigue mechanism is presumably not changed by the z-binders. However, comparative studies of the initiation and growth of fatigue-induced damage in 2D and 3D composites with parallel S–N curves have not been performed to confirm whether the fatigue process is always the same. In the second way, the fatigue life curves for the 2D and 3D materials are not parallel. This implies the z-binders are influencing the fatigue process and, in most cases, accelerating the loss in fatigue strength with increasing number of load cycles. Studies on 3D woven, stitched and pinned composites that show this trend reveal increased incidence of fatigue-induced damage at the z-binders, which accelerates the rate of degradation of fatigue strength [14]. Both 2D and 3D architectures have significant effects in several key parameters concerning composites [22]. The general effect for the fracture toughness is exemplified in Fig. 4. Table 1 presents recommendations for material architecture choices for both 2D and 3D reinforcement architectures. The grade (0 to 10) varies significantly as a function of architecture choice. Therefore, care must be taken when it comes to the choice of reinforcement material architecture. For the work developed in this research a mixed architecture of plain 2D woven and 3D woven was chosen since the goal was to improve or maintain the in-plane properties while enhancing the transverse properties and delamination resistance.

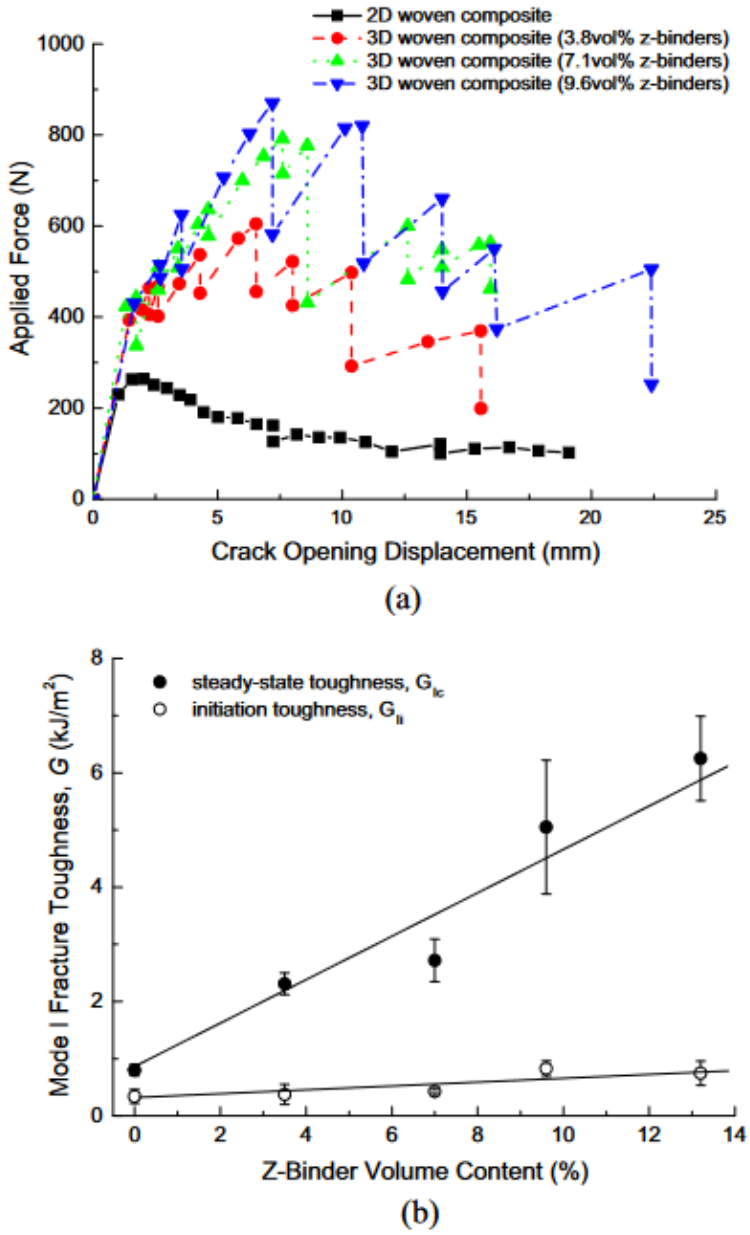


Figure 4. Effect of z-binder yarn content on the (a) mode I load–displacement curves and the (b) initiation and steady-state fracture toughness values. The error bars in (b) represent two standard deviations [16].

Various structural components, particularly in the aerospace industry, are equipped with fiber-reinforced composites manufactured by a 3D weaving process, for example, fan blades of airplane engines (manufactured by CFM International, France) and landing gear braces for the Boeing 787 (manufactured by Safran Landing Systems, France, see Fig. 5) [19]. 3D synthetic composites may also be used for radar absorbing capabilities in

advanced weapons systems [23]. Finally, regarding 3D woven architectures, the transverse reinforcement may be orthogonal or angled, and the former enhances mode I resistance while the latter (preferably at +-45 degrees) enhances shear cracks (i.e., mode II) [24].



a) b)

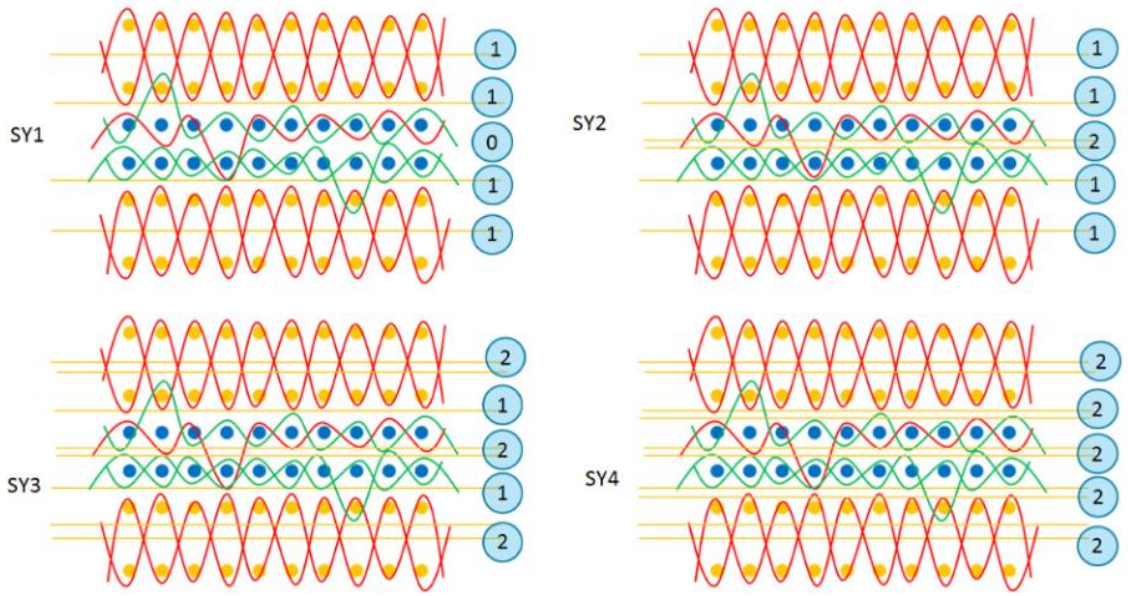
Figure 5. 3D woven carbon fibre plane motor blade (a) and landing gear brace (b) [25].

Table 1. Recommendation table for the selection of reinforcement architectures [22].

Reinforcement	In-plane strength	Out-of-plane strength	Flexural strength	Drapability	Surface finish	Ease of manufacturing	Delamination resistance	Crack propagation resistance
Noncontinuous	1	4	1	1	1	9	6	4
Plain woven 2D	**8**	**3**	**8**	**3**	**8**	**8**	**3**	**3**
Twill woven 2D	10	1	10	4	9	7	2	2
Satin woven 2D	9	2	9	6	10	6	1	1
Woven 3D	**5**	**10**	**7**	**2**	**6**	**3**	**10**	**6**
Knitted 2D	6	5	3	8	4	4	5	7
Knitted 3D	3	8	5	10	2	1	8	9
Braided 2D	7	6	4	7	5	5	4	8
Braided 3D	4	9	6	9	3	2	9	10
Needle punched	2	7	2	5	7	10	7	5

2.2 General trends in 3D woven natural composites

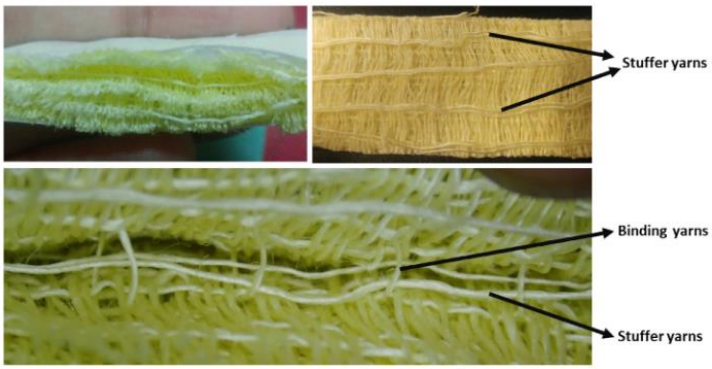
The field of 3D woven natural composites is still in its infancy; however, a good number of research efforts have been published in recent years [26-40]. The majority of these works have focused on layer-to-layer angle interlocks and natural/synthetic hybridization. Furthermore, the architectures tend to be denser and the spacing between the transverse fibres quite short. A similar trend was also observed for the synthetic 3D woven composite literature. Furthermore, no study has been currently found to analyze the direct fracture toughness and delamination resistance improvement. The majority of the works focused on the in-plane properties (i.e., tensile, flexural, Charpy impact, drop weight impact) and thermal stability. No study was found on the effect of 3D woven architecture on the tensile-tensile and impact fatigue life of the composites. The materials found in the literature were all fabricated by ways of modified dobby or Jacquard looms and generally preferred layer-to-layer angle interlock architectures (see Fig. 6).



a)



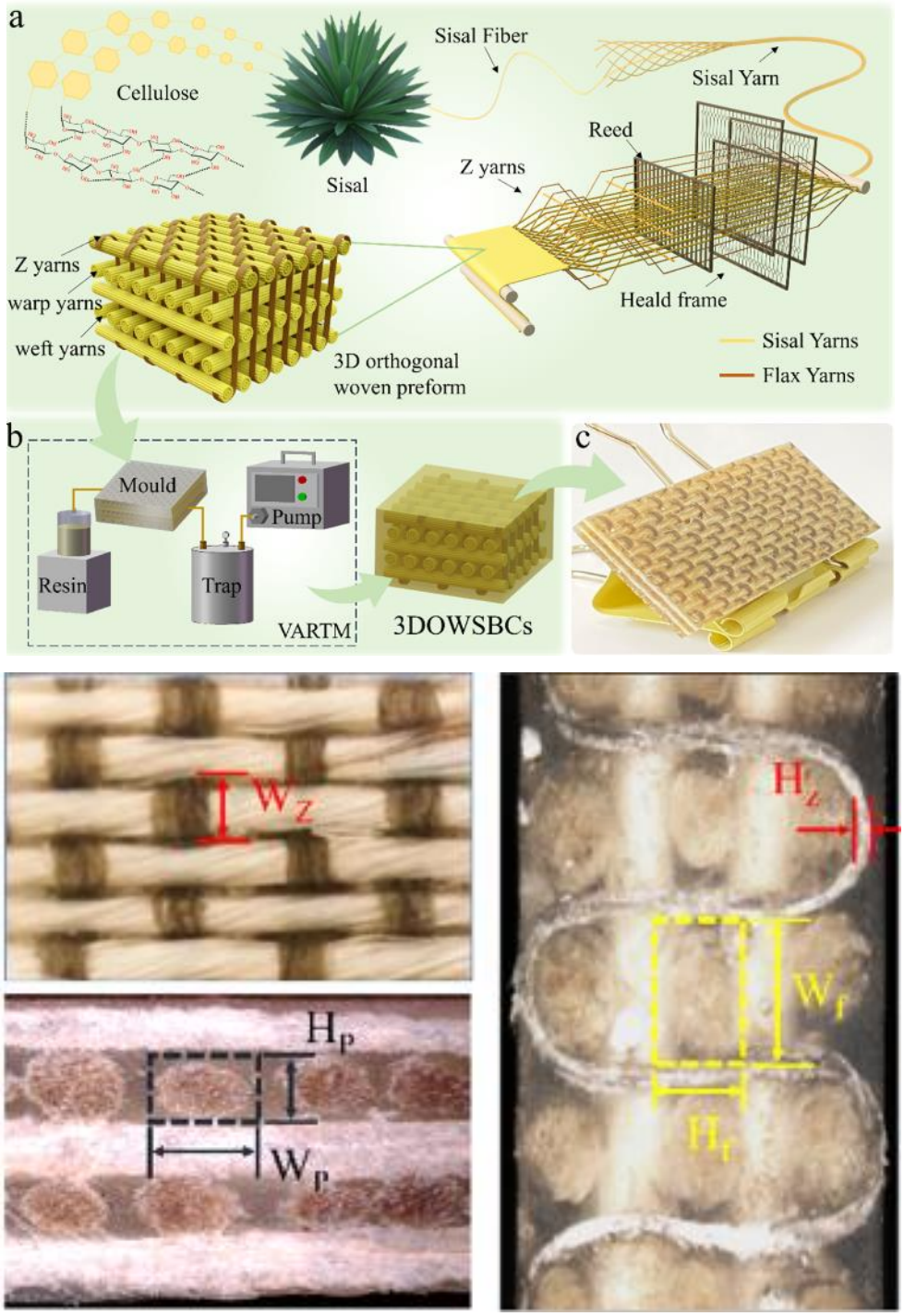
b)



c)

Figure 6. Example of 3D woven natural fibre architecture analyzed in the literature: a) Layer-to-layer 3D woven angle interlock structure, b) Semi-automatic Dobby loom (modified with 4 beam arrangement) and c) Image showing stuffer yarns and binding yarns (photographed after manual peeling of fabric) [27].

Recently, Su et al. [40] analyzed a three-dimensional technique for fabrication of sisal/flax hybrid fiber green composites in order to enhance the mechanical, thermal and sound isolation properties. Sisal yarns were used as warp and weft, while flax yarns were used as z-binders. A 3D loom was used to fabricate the preforms and the composite was fabricated via the vacuum-assisted resin transfer molding process (VARTM) with an epoxy resin. The z-binder density was 2.5 yarns/cm. A schematic can be seen in Fig. 7. The novel composites were tested in tensile and compression as well as shear aligned with the warp direction. The thermal and acoustic performance was also analyzed.



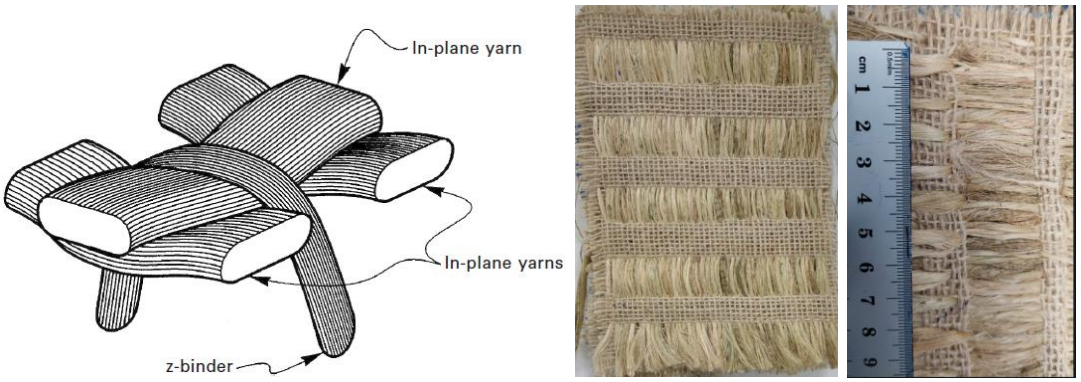
c)

Figure 7. Preparation of 3DOWSBCs. (a) Schematic diagram of 3D orthogonal woven preform preparation and structure. (b) Schematic diagram of VARTM curing process and (c) physical diagram of 3DOWSBC and (c) Detailed morphologies of the 3DOWSBCs [40].

It was found that the novel 3D hybrid NFRCs enhanced mechanical properties in comparison to traditional lamination composites. Notably, the bending and shear strengths were increased by 37.9% and 86.9%, respectively. The impact of Z-yarns on the mechanical properties in out-of-plane direction was found to be more significant than that in in-plane direction. Furthermore, the predominant failure modes observed in the 3D composites included fiber breakage under tensile and compressive loads, as well as matrix cracking under bending and shear loads. They exhibit low thermal conductivity (0.29 W/m·K) and favorable sound transmission loss characteristics (63 dB). During the radiative heat resistance test, the temperature differential between the two surfaces along the thickness reached 13 ^{o}C. These findings suggest potential applications for thermal and sound insulation in engineering.

3. Materials and Methods

In this thesis, several novel hybrid natural fiber composites were fabricated with the aim of enhancing the bonded joint performance of NFRCs. Specifically, the 3D OTT architecture technique was used (see Fig. 8). Intralaminarly reinforced jute bidirectional fabrics were used as well as intralaminar + transverse reinforcement (z-binder), see Fig. 8b. The novel weaves were fabricated manually via commercially available jute fabrics as a base and long fibres of glass, sisal, ramie, hemp and curauá for the bonded joint experimental program.



a) b) c)



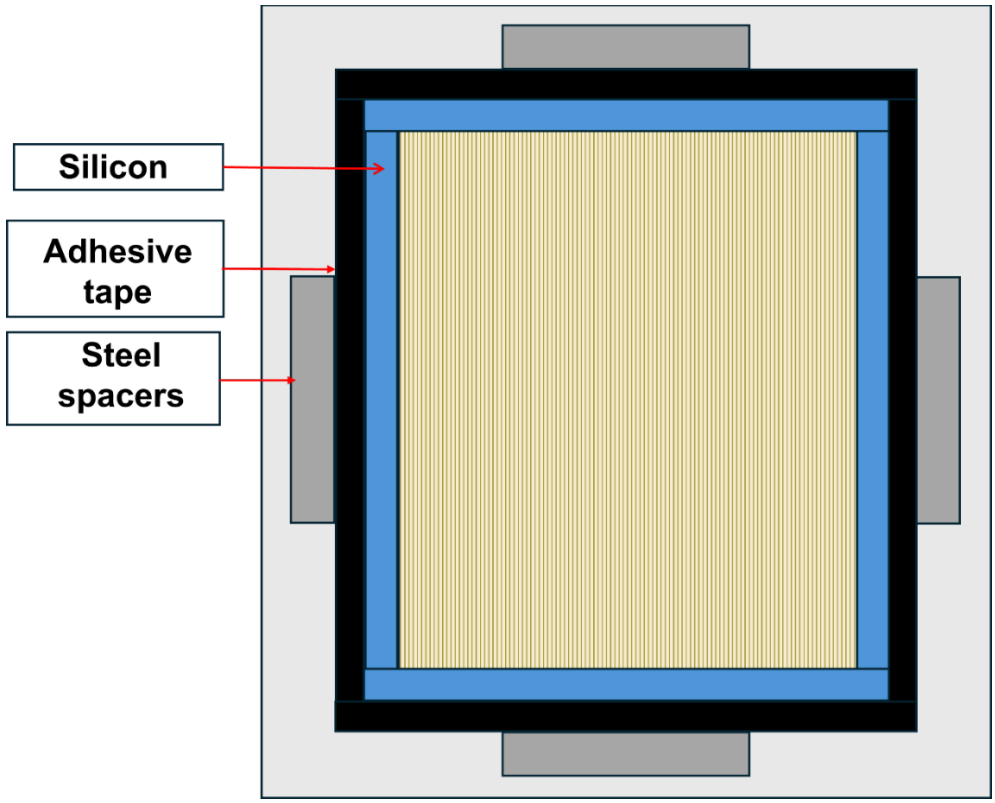
d)



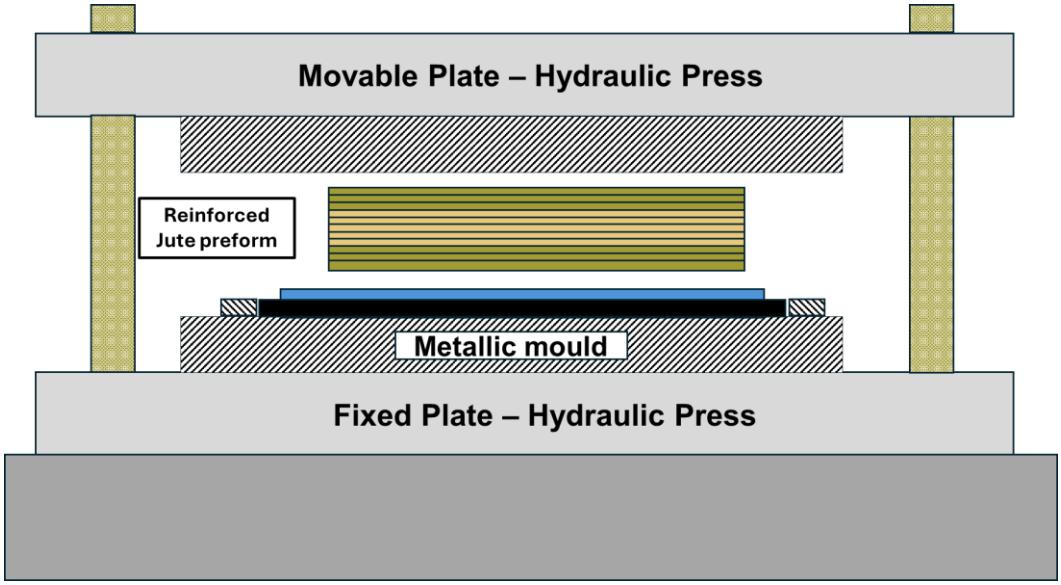
e) f)

Figure 8. Representative 3D OTT architecture [41] (a) and curauá fibre-reinforced jute fabrics with 2D (b), 3D (c), while the cross-section of the fabricated composite can be seen in the bottom (d), e) representative 2D curauá weaving process and f) 2D curauá intralaminar reinforcement geometry.

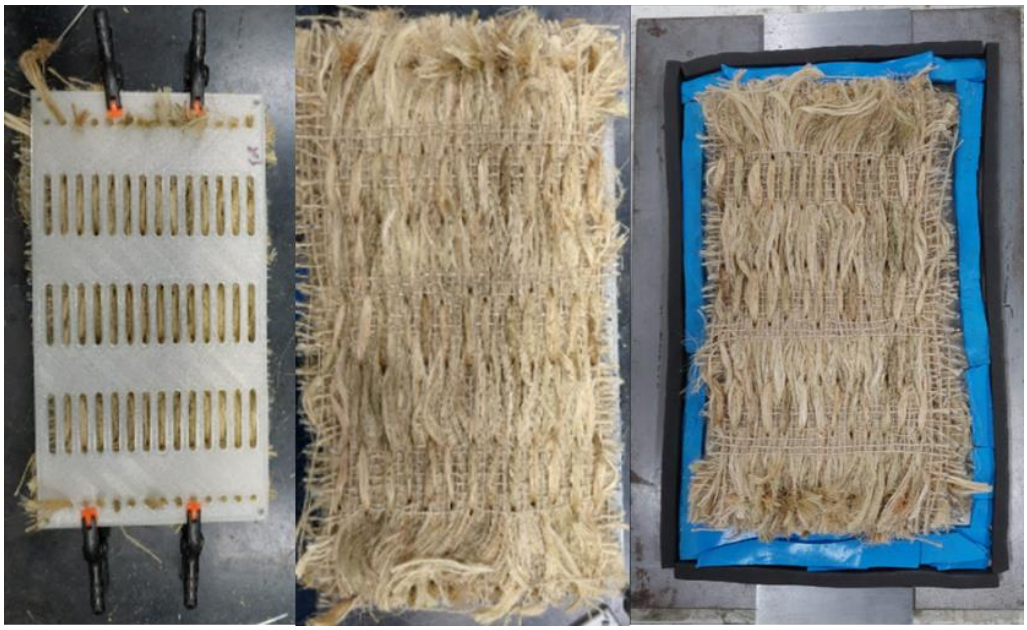
These natural fibres were chosen due to their ease of acquisition and ubiquitous implementations in various sectors (i.e., jute, sisal, hemp and ramie). The curauá fibres, however, do not yet have a scale economy and are very difficult to acquire, being endemic to Amazonas. On the other hand, as demonstrated by this research, it represents a fibre with very high capabilities when applied to high performance NFRCs. Moreover, glass and carbon (Barracuda Advanced Composites, SP/Brazil) neat synthetic composites were also fabricated and used as benchmarks for the bonded joint performance of the composites. A bi-component brittle structural epoxy was used (i.e., HEX SLOW 135, Barracuda Advanced Composites, SP/Brazil) along with the compression molding fabrication technique (see Fig. 9). This moulding technique allows for very hydrostatic pressures afforded by the silicone while decreasing resin runaways. This results in high quality composite plates with minimum internal voids (see **Paper 3**). Further details on materials and manufacturing can be found on **Paper 2**. Following the completion of this task, the most promising results (i.e., SISAL and CURAUÁ) were further analyzed in quasi-static and dynamic tests.


Silicon
Adhesive tape
Steel spacers

a)


Movable Plate – Hydraulic Press
Reinforced Jute preform
Metallic mould
Fixed Plate – Hydraulic Press

b)



c)



d)

Figure 9. Representative schematic of composite fabrication process, a) laminated fibres on steel mould, b) compression molding process, c) fabrication stages of the 3D woven composites and c) representative fabricated SISAL 3D composite plate.

The fibre weight fractions (in relation to the total weight of the fibre phases, resin and hardener) were approx. 30%, 24%, 20%, 22% and 18% for the curauá, sisal, ramie, hemp and glass intralaminar (2D) specimens, respectively. For the 3D fibre reinforcements, the weight fractions were approx. 3%, 2%, 4%, 1% and 2%, respectively. The composite panel thickness varied slightly as a function of fibre type and architecture (the JFRP was approx. 2 mm, while the SISAL 2D was 5.33 ± 0.11 mm, the SISAL 3D was 5.37 ± 0.06 mm, the CURAUÁ 2D was 5.09 ± 0.09 mm, and the CURAUÁ 3D was 4.96 ± 0.36 mm). The 3D reinforcement was chosen specifically to combat the peel stresses that develop at the edges of a SLJ under load. These stresses are key in the delamination and early onset of failure in composite materials. It is expected from the prevailing synthetic 3D reinforced composite literature that the in-plane properties will vary for woven composites approx. ±20% [14]. This was observed for the materials analyzed in this research in **Papers 2-5**. This field is still very new for 3D NFRCs and few works exist to date [26-30, 32, 33, 36, 38, 42]. However, regarding the 3D OTT of NFRCs, with hybrid reinforcement such as analyzed in this research, no research efforts exist in the literature to date. Regarding the 3D OTT reinforcement architecture and manufacture, more details can be found in **Paper 2**.

For the adhesive, a ductile bi-component automotive-grade epoxy was chosen for the SLJ tests (i.e., BETAMATE® 2096, DuPont) [43]. This research fabricated novel composite materials with the aim of solving the issue of low bonded joint performance of NFRCs when compared to synthetic composites in order to widen their industrial application envelopes. Specifically, the automotive industry, where low cost and structural weight are key factors. However, before any large-scale applications can be considered, these materials have to be characterized mechanically in static and dynamic loads.

The tests chosen were all based on ASTM standards and represent a good basis for understanding the behavior of these novel materials. Common testing methods such as tensile, flexural, impact, short beam, drop weight impact and fatigue have been applied as well as SLJ tests. Furthermore, SEM microscopy coupled with microCT scanning was used to further analyze the failure modes and the presence of voids and cracks.

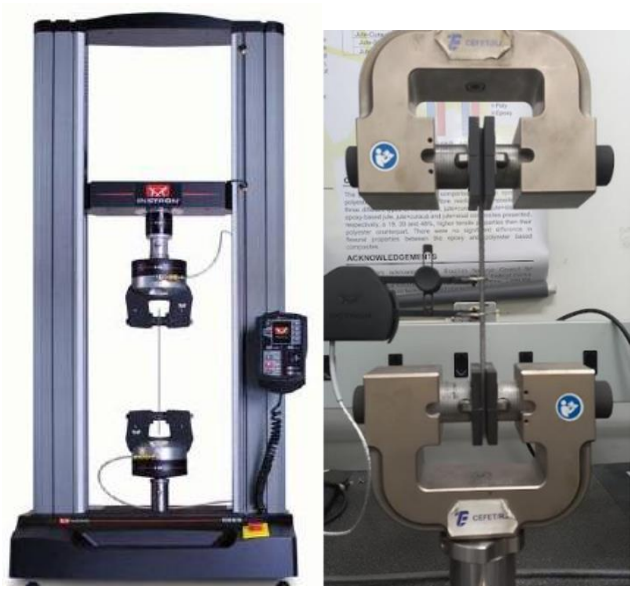
3.1 Quasi-static tests

In this thesis the following quasi-static tests were performed for the determination of the basic composite material mechanical properties:

- Tensile tests were performed to obtain the tensile properties of the composites.
- Three-point bending tests were performed to ascertain the flexural properties of the composites.
- Short-beam tests were performed to analyze the interlaminar shear strength (ILSS) of the composites.
- Single lap bonded joint tests were carried out to analyze the bonded joint efficiency of the novel composites.

3.1.1 Tensile tests

Determining the tensile properties is crucial as they provide information regarding the modulus of elasticity, elastic limit, elongation, reduction in area, tensile strength, ultimate strength, fracture strength, among other properties. Tensile properties vary depending on the material and are generally presented in the form of a stress x strain curve. For composite materials (reinforced polymers), the standards used are ASTM D638 [44] and ASTM D3039 [45] depending on the type of composite [2]. The machine used was the INSTRON® 5966 universal traction machine, see Fig. 10, located in the composites and adhesives laboratory (LADES – CEFET/RJ). A clip gauge extensometer was used to measure true strain as well as load cells of 10 kN and 1 kN. A rate of 1 mm/min and room temperature were used. At least 4 specimens were tested for each configuration and specimen geometry was kept at 220 x 13 x t mm, t being specimen thickness which varied as a function of fibre type.



a) b)

Figure 10. Testing machine used for quasi-static tests (a) and tensile test set-up with extensometer (b).

3.1.2 Flexural tests

Stiffness and flexural strength was determined by applying the ASTM D7264 standard [46] for reinforced polymeric materials. The test consists of a two-point support where a third point of contact moves the specimen in the middle (see Fig. 11). The same UTS machine was used as for the tensile tests with a load cell of 1 kN and a rate of 1 mm/min. The span/depth ratio was approx. 20. The stress and strain values were calculated via the equations given by the standard. The applied force results in a deflection of the midpoint that is measured and recorded until failure occurs on one of the faces. Due to the nature of the test, the upper face that is in contact with the load point is undergoing compression while the lower face is under tension. Failure will then occur depending not only on the mechanical characteristics of the resin and laminated fibre (i.e., fibre properties and reinforcement architecture), but also on small imperfections in the symmetry of the specimen.



Figure 11. Flexural test set-up.

3.1.3 Short beam tests

Short beam tests are designed to elicit a sliding between the composite layers and therefore a measurement of the interlaminar shear strength (ILSS) can be made. The ILSS is important in quantifying the interfacial quality and out of plane shear stress at a lamina/matrix level [5]. The test is essentially a three-point bending test where the span to depth ratio is 4, therefore the small specimen dimensions facilitate the interlaminar sliding mechanism. The international standard ASTM D2344 [47] was used along with the same UTS machine and a 1 mm/min test speed. The ILSS was calculated by was of a simple equation as described in the standard.

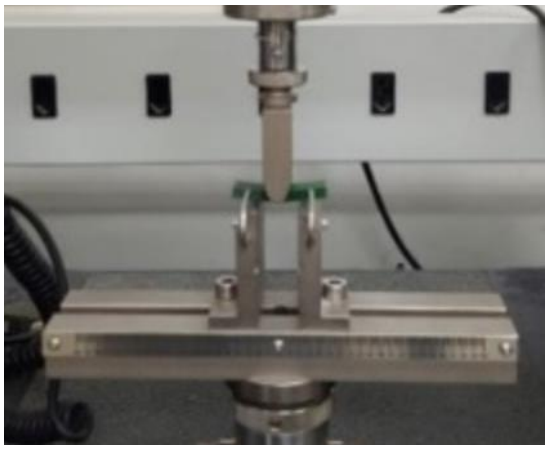


Figure 12. Short beam test set-up.

3.1.4 Single lap joints

The bottom line of this entire research effort revolved around the enhancement of the bonded joint performance of NFRCs. This is a crucial factor as bonding is the preferred and superior joining technology for any composite material. Therefore, this represents a significant bottleneck in the wider application of NFRCs in many industries, especially the automotive [8]. Up until now, the bonded joint performance of NFRCs was held back by the lower mechanical properties of the adherends 9such as stiffness) which significantly increased the rotation of the overlap zone during SLJ loading, leading to high peel stresses (see Fig. 13).

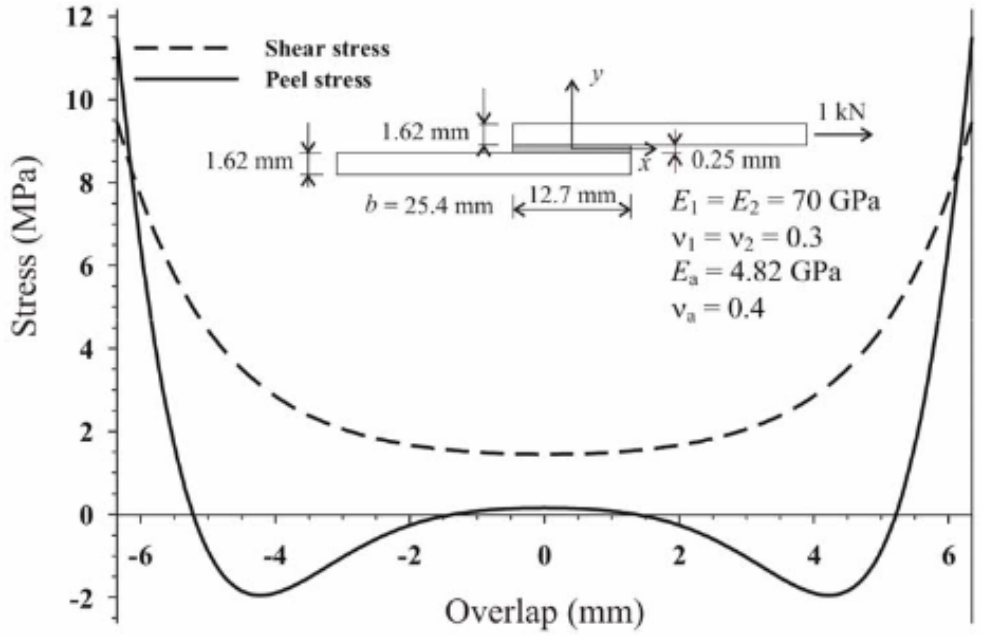


Figure 13. Example of stress distribution across the overlap zone of an aluminum/epoxy bonded joint [48].

As will be explained in greater depth in **Paper 1**, the stress state of the overlap zone, in conjunction with the adherend and adhesive material properties will control the failure onset. And in this equation, the *transverse* properties of a composite adherend are key. In a well fabricated bonded joint where the matrix/adhesive interface is of good quality with good mechanical interlocking, said interface is usually of higher resistance than the matrix/fibre interface. Furthermore, for classical synthetic composites, the adherends tend to have very high stiffness such as CFRP, with moduli around 65 GPa, therefore presenting little rotation at the edges [13].This manifests as a mixed mode of TLC/LFT near the edges (high peel stresses) and a predominantly cohesive failure near the middle of the overlap failure zone. There are other failure mechanisms that are architecture-dependent (i.e., where a bidirectional fabric or a UD is used). For NFRCs, whose Young's moduli tend to range from 6-20 GPa (this research), the dominant failure mode tends to be delamination. Delamination is the removal, partial or complete, of usually the first or second layer of a composite SLJ. This failure mode is responsible for drastically reducing the bonded joint performance of NFRC SLJs. This is where the 3D OTT architecture comes into play, by directly restraining the layers of the composite in the out-of-plane direction, it significantly increases the energy necessary to initiate and propagate a crack.

This means a higher fracture toughness, delamination resistance, transverse strength and impact resistance. Regarding SLJs, the 3D reinforcement acts against the peak peel stresses at the overlap edges that occur during loading, which can be thought of as a predominantly mode I state, therefore, significantly retarding or altogether avoiding the delamination failure and increasing the bonded joint failure load.

The bonded joints in this research were fabricated via a steel mould which controlled the overlap length (12.5 mm) and thickness (~0.2 mm) via steel spacers, see Fig. 14. They were fabricated under pressure and temperature as per adhesive manufacturer guidelines.

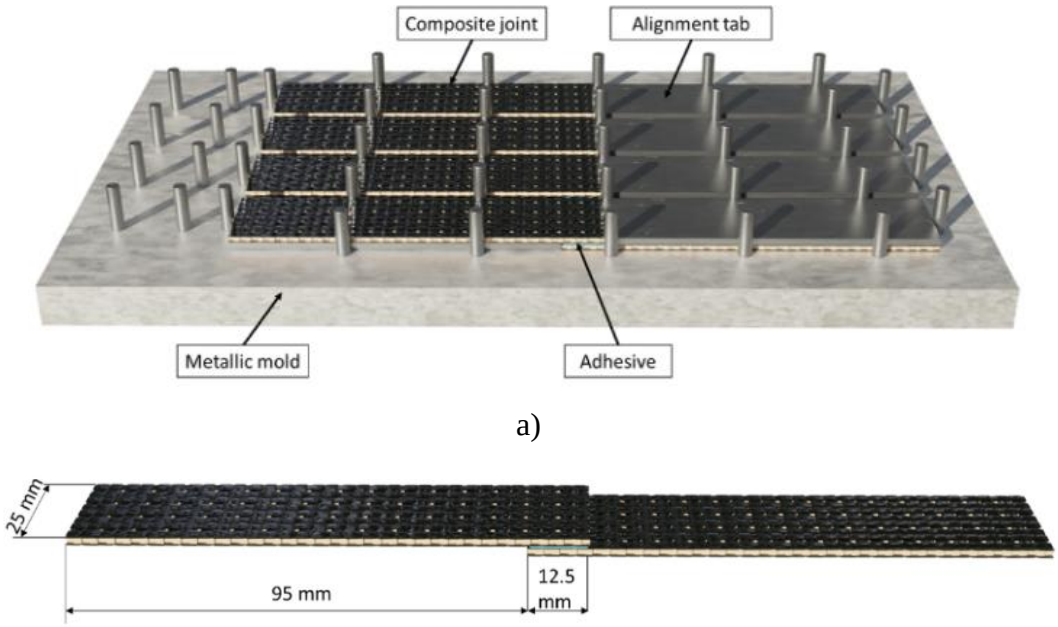


Figure 14. Representative schematic of (a) mould and spaers used and (b) fabricated bonded joint.

The joints were fabricated and tested based on the ASTM D3163 [49] international standard, with the same UTS testing machine, a load cell of 10 kN and a test speed of 1 mm/min. The failure modes were visually inspected and assessed based on the ASTM D5573 [50] international standard.

3.2 Dynamic tests

It is crucial to characterize these novel materials in dynamic loads for these types of

loading conditions are more aligned with real world applications such as low velocity impacts and fatigue loading scenarios. In this research the novel composite materials that reached the desired synthetic SLJ benchmark moved forward to dynamic analysis. These materials were tested via classical Charpy impact tests, drop dart impact, both perforation and repeated impacts (impact fatigue) as well as tension-tension fatigue.

3.2.1 Charpy impact tests

Impact testing is designed to determine how a specimen of a known material responds to suddenly applied stress. The test is used to evaluate the energy absorption efficiency of the material. The ability to quantify the impact property is a huge advantage when it comes to safety. Test specimens may have notches of varying geometries or no notch. In this work, the ASTM D4812 [51] standard was used as a basis for the Charpy style impact test (although it is Izod) because the geometry and machine available are Charpy (WPS Leipzig 30, error of 0.0075 kgf, see Fig. 15), and a small difference is observed in the case of reinforced composites between the notch or no [52]. The specimen geometry was 80 x 13 x t mm, t being the specimen thickness.



a) b)

Figure 15. Charpy impact machine used.

3.2.2 Drop weight tests

Drop dart impact tests were performed at Politecnico di Torino on laminate specimens with dimensions of 100 mm × 100 mm, using a drop tower machine (Instron/CEAST Fractovis Plus, see Fig. 16) equipped with a hemispherical impactor instrumented with a piezoelectric load cell of 12.7 mm diameter at room temperature. The samples were clamped between two steel plates with a circular opening of 40 mm diameter. Three different energy levels were tested: 3 J, 7 J, and 12 J, respectively for the repeated impact of the different materials. The lowest energy level was used for the JFRP and GFRP specimens, while 7 J was used for the CFRP, CURAUÁ 2D and 3D specimens. The highest energy level was used for the SISAL hybrid composites, both 2D and 3D. This was done in order to obtain reasonable impact repeats (i.e., at lower energy levels the hybrid SISAL composites did not fail at over 200 impacts). This is likely due to the difference in composite thickness [53]. For the perforation tests a higher energy of 45 J was used to ensure full penetration of the impactor.



a) b)

Figure 16. Drop dart impact fatigue machine used (a) and a 100x100 mm representative specimen used (b).

3.2.3 Fatigue tests

For the fatigue testing of the composite materials, a WinTest TA ElectroForce testing machine present at the DYNLAB facility at Politecnico di Torino with a 15 kN load cell was used, see Fig. 17. The size and geometry of the specimens were based on the ASTM D3479 [54] international standard. The testing was conducted with a targeted R ratio of 0.1, sine wave and a test frequency of 5 Hz in all cases. The load levels analyzed were chosen to be 0.7, 0.6 and 0.5 of the UTS of the individual materials. Specimen geometry was the same as the tensile tests.



a) b)

Figure 17. Fatigue machine used (a) and a close u of the fatigue test set-up (b).

4. Conclusions

In this thesis, novel NFRC materials were fabricated and tested in quasi-static and dynamic experiments. A novel 3D OTT architecture was applied to the NFRCs with the express purpose of enhancing the delamination resistance of the adherends in a SLJ load state. Furthermore, a more classical 2D intralaminar reinforcement was used in tandem with the 3D OTT. The architecture was successful in this goal with two main fibres (i.e., SISAL and CURAUÁ).

The main conclusions of this research are summarized below:

The SLJ performance of both 2D and 3D NFRCs were analyzed in **Paper 2** for a range of hybrid composites. It was found that for resistance and ductile natural fibres such as CURAUÁ and SISAL, the 3D reinforcement was successful in enabling the SLJ failure load to reach the level of the synthetic composites (i.e., CFRP and GFRP). Furthermore, for the case of the CURAUÁ, it was found that the 2D case was also able to reach this level due to the stiffness of the adherend. This marks the first time in the available literature that this has been observed. Moreover, the adhesive used was an automotive grade ductile epoxy bicomponent, further demonstrating the possible application of this technique in the industry.

In **Paper 3**, the materials that were successful in the SLJ objective plus synthetic neat and hybrid points of comparison were analyzed in quasi-static testing as well as SEM and microCT imaging. It was found that the variations in mechanical properties when the 2D are compared to the 3D specimens never exceeded 15%. This trend is in accordance with the expected trends for synthetic 3D composites as per the current available literature. This result means that the current fabrications methods and numerical analysis available for 3D synthetic composites may be modified and adapted to encapsulate NFRCs without significant difficulties. Furthermore, it was observed that the void fractions of the NFRCs were not significantly affected by the 3D architecture and never exceeded 3.9%. The acceptable range for automotive applications is 5%, therefore this simple fabrication methodology is acceptable. Moreover, complex anisotropy and significant deviations from the idealized architecture were observed during microCT imaging, such as misalignment of the fibres and crushing of the zbinder due to compression when consolidating the composite plates. However, this did not translate to significant

decreases in the mechanical properties.

In **Paper 4**, the dynamic mechanical properties of the successful NFRCs were analyzed under drop dart impact testing. The impact tests were twofold: perforation and repeated impacts. Furthermore, the perforated specimens were analyzed via microCT imaging to ascertain the crack propagation. It was found that for perforation, the SISAL 2D presented the highest absorbed energy and peak load. However, for repeated impacts it was found that for both SISAL and CURAUÁ the 3D architecture significantly increased the impact fatigue life (i.e., 3.6x and 2x, respectively). Furthermore, the microCT images revealed that for both SISAL and CURAUÁ, the 3D reinforcement significantly decreased the internal crack propagation of the specimens, demonstrating the crack blunting mechanism that is expected of this architecture.

Finally, in **Paper 5**, the tensile-tensile fatigue of these novel 3D OTT NFRC hybrid composites was analyzed at 5 Hz and an R=0.1 ratio at three distinct load levels (i.e., 0.7, 0.6 and 0.5 UTS). It was found that for the load levels of 0.8 and 0.7, the 3D OTT architecture increased the fatigue life of both CURAUÁ and SISAL composites, while for the 0.5 UTS load level a tendency of stabilization was found. Furthermore, at the 0.5 UTS level, all cases presented run outs (i.e., specimens that survived 10^6 cycles) and these specimens were tested in uniaxial quasi-static tension and compared to the virgin composites. It was found that significant tensile strength deterioration occurred for all specimens, however, the 3D composites presented significant stiffness retention when compared to the 2D.

5. Future work

The experimental envelope needed for a wider industrial implementation of these novel materials must account for out-of-plane material properties as well as how the behaviour changes as a function of environmental factors. In this context, the following next steps are suggested.

Fracture testing

In this thesis the effect of 3D OTT reinforcement in NFRCs was analyzed in a variety of mechanical tests. However, for a quantitative analysis of the enhancement of the fracture toughness, mode I and II experiments must be conducted.

Shear modulus

Another crucial property that must be analyzed experimentally is the shear modulus. Without this value comprehensive numerical modelling is not feasible.

Environmental ageing

These materials are primarily aimed to be used in industries such as sport, automotive and marine. Therefore, it is necessary to analyze how their behavior changes as a function of environmental ageing such as water immersion, salt-fog spray and UV ageing.

References

1. Neto, J., et al., *A Review of Recent Advances in Hybrid Natural Fiber Reinforced Polymer Composites.* Journal of Renewable Materials, 2022. **10**(3): p. 561--589.
2. Rahman, R. and S. Zhafer Firdaus Syed Putra, *5 - Tensile properties of natural and synthetic fiber-reinforced polymer composites*, in *Mechanical and Physical Testing of Biocomposites, Fibre-Reinforced Composites and Hybrid Composites*, M. Jawaid, M. Thariq, and N. Saba, Editors. 2019, Woodhead Publishing. p. 81-102.
3. Elseify, L., et al., *Manufacturing Automotive Components from Sustainable Natural Fiber Composites*. 2021.
4. Neto, J.S.S., et al., *A Review on the Thermal Characterisation of Natural and Hybrid Fiber Composites.* Polymers, 2021. **13**(24): p. 4425.
5. de Araujo Alves Lima, R., et al., *Effect of surface treatments on interfacial properties of natural intralaminar hybrid composites.* Polymer Composites, 2020. **41**(1): p. 314-325.
6. Rahman, M.Z., *Mechanical and damping performances of flax fibre composites – A review.* Composites Part C: Open Access, 2021. **4**: p. 100081.
7. Shahinur, S., et al., *Current Development and Future Perspective on Natural Jute Fibers and Their Biocomposites.* Polymers, 2022. **14**(7): p. 1445.
8. Banea, M.D., et al., *Multi-material adhesive joints for automotive industry.* Composites Part B: Engineering, 2018. **151**: p. 71-77.
9. Kupski, J. and S. Teixeira de Freitas, *Design of adhesively bonded lap joints with laminated CFRP adherends: Review, challenges and new opportunities for aerospace structures.* Composite Structures, 2021. **268**: p. 113923.
10. de Queiroz, H., M. Banea, and D. Cavalcanti, *Experimental analysis of adhesively bonded joints in synthetic- and natural fibre-reinforced polymer composites.* Journal of Composite Materials, 2020. **54**(9): p. 1245-1255.
11. de Queiroz, H.F.M., M.D. Banea, and D.K.K. Cavalcanti, *Adhesively bonded joints of jute, glass and hybrid jute/glass fibre-reinforced polymer composites for automotive industry.* Applied Adhesion Science, 2021. **9**(1): p. 2.
12. de Queiroz, H.F.M., et al., *Mechanical characterization of short Curauá/glass fiber-reinforced interlaminar hybrid composite adhesive joints.* Journal of

Adhesion Science and Technology, 2024. **38**(9): p. 1473-1490.

13. de Queiroz, H.F.M., et al., *Effect of hybridization and composite architecture symmetry in the bonded joint performance of jute/carbon fibre-reinforced composites.* International Journal of Adhesion and Adhesives, 2024. **133**: p. 103745.
14. Mouritz, A.P. and B.N. Cox, *A mechanistic interpretation of the comparative in-plane mechanical properties of 3D woven, stitched and pinned composites.* Composites Part A: Applied Science and Manufacturing, 2010. **41**(6): p. 709-728.
15. Behera, B.K. and B.P. Dash, *Mechanical behavior of 3D woven composites.* Materials & Design, 2015. **67**: p. 261-271.
16. Stegschuster, G., et al., *Experimental determination of the mode I delamination fracture and fatigue properties of thin 3D woven composites.* Composites Part A: Applied Science and Manufacturing, 2016. **84**: p. 308-315.
17. Mouritz, A.P., *Three-dimensional (3D) fiber reinforcements for composites*, in *Composite reinforcements for optimum performance*. 2011, Elsevier. p. 159-197.
18. Ma, Z., P. Zhang, and J. Zhu, *Review on the fatigue properties of 3D woven fiber/epoxy composites: testing and modelling strategies.* Journal of Industrial Textiles, 2022. **51**(5_suppl): p. 7755S-7795S.
19. Gereke, T. and C. Cherif, *A review of numerical models for 3D woven composite reinforcements.* Composite Structures, 2019. **209**: p. 60-66.
20. Fan, W., et al., *Fatigue behavior of the 3D orthogonal carbon/glass fibers hybrid composite under three-point bending load.* Materials & Design, 2019. **183**: p. 108112.
21. Aymerich, F., P. Priolo, and C.T. Sun, *Static and fatigue behaviour of stitched graphite/epoxy composite laminates.* Composites Science and Technology, 2003. **63**(6): p. 907-917.
22. Ahmad, F., N. Yuvaraj, and P.K. Bajpai, *Effect of reinforcement architecture on the macroscopic mechanical properties of fiberous polymer composites: A review.* Polymer Composites, 2020. **41**(6): p. 2518-2534.
23. Fan, W., et al., *Enhanced mechanical and radar absorbing properties of carbon/glass fiber hybrid composites with unique 3D orthogonal structure.* Polymer Testing, 2018. **69**: p. 71-79.

24. Sitnikova, E., et al., *Controllable parameters as the essential components in the analysis, manufacturing and design of 3D woven composites.* Composites Science and Technology, 2022. **230**: p. 109730.
25. De Luycker, E., et al., *Simulation of 3D interlock composite preforming.* Composite Structures, 2009. **88**(4): p. 615-623.
26. Jabbar, M., et al., *Mechanical Response of Novel 3D Woven Flax Composites with Variation in Z Yarn Binding.* Journal of Natural Fibers, 2020. **17**(6): p. 890-905.
27. Jabbar, M., et al., *Effect of the stuffer yarns on the mechanical performance of novel 3D woven green composites.* Composite Structures, 2021. **269**: p. 114023.
28. Kashif, M., et al., *Effect of interlocking pattern on short beam strength of 3D woven composites.* Journal of Composite Materials, 2019. **53**(20): p. 2789-2799.
29. Kashif, M., et al., *Optimization of 3D woven preform for improved mechanical performance.* Journal of Industrial Textiles, 2019. **48**(7): p. 1206-1227.
30. Khan, M.I., et al., *Development of composites, reinforced by novel 3D woven orthogonal fabrics with enhanced auxeticity.* Journal of Industrial Textiles, 2019. **49**(5): p. 676-690.
31. Yang, J., et al., *Effects of Kevlar volume fraction and fabric structures on the mechanical properties of 3D orthogonal woven ramie/Kevlar reinforced poly (lactic acid) composites.* Journal of Industrial Textiles, 2018. **47**(8): p. 2074-2091.
32. Paul, P., M. Ahirwar, and B.K. Behera, *Acoustic behavior of three-dimensional woven fabrics and their composites: role of fiber type and weave architecture.* The Journal of The Textile Institute: p. 1-14.
33. Olhan, S., et al., *Mechanical, thermal, and viscoelastic behavior of sisal fibre-based structural composites for automotive applications: Experimental and FEM analysis.* Composite Structures, 2023. **322**: p. 117427.
34. Olhan, S., B. Antil, and B.K. Behera, *Low-velocity impact and quasi-static post-impact compression analysis of woven structural composites for automotive: Influence of fibre types and architectural structures.* Composite Structures, 2025. **352**: p. 118676.
35. Olhan, S., et al., *Investigating the impact of different machinability processes and fibre architecture on the bearing performance of pin-loaded textile structural composites for automotive applications: Experimental and finite element analysis.*

Journal of Manufacturing Processes, 2023. **86**: p. 30-55.

36. Nawab, Y., et al., *Development & Characterization of Green Composites Using Novel 3D Woven Preforms.* Applied Composite Materials, 2018. **25**(4): p. 747-759.
37. Safdar, M.M., et al., *Effect of fillers and weave architecture hybridization on the impact performance of 3D woven hybrid green composites.* Polymer Composites, 2024. **45**(2): p. 1776-1792.
38. Islam, M.A., et al., *Development of three dimensional (3D) woven flax/PLA composites with high mechanical and thermal properties using braided yarns.* Industrial Crops and Products, 2024. **222**: p. 119580.
39. Wodag, A.F., et al., *Three-dimensional (3D) woven flax fiber/polylactic acid (PLA) composites for high flexural strength.* Polymer Composites, 2024. **45**(14): p. 13242-13255.
40. Su, J., et al., *Advanced three-dimensional textile technique for fabrication of sisal/flax hybrid fiber green biocomposite with enhanced mechanical, thermal, and sound isolation properties.* Industrial Crops and Products, 2025. **223**: p. 120174.
41. Cox, B.N., et al., *Failure mechanisms of 3D woven composites in tension, compression, and bending.* Acta Metallurgica et Materialia, 1994. **42**(12): p. 3967-3984.
42. Awais, H., et al., *Effect of comingling techniques on mechanical properties of natural fibre reinforced cross-ply thermoplastic composites.* Composites Part B: Engineering, 2019. **177**: p. 107279.
43. dos Reis, M.Q., et al., *Mechanical characterization of a modern epoxy adhesive for automotive industry.* Journal of the Brazilian Society of Mechanical Sciences and Engineering, 2019. **41**(8): p. 340.
44. Standard, A., *D638: Standard test method for tensile properties of plastics.* West Conshohocken (PA): ASTM International, 2010.
45. ASTM, A.M., *ASTM D3039-standard test method for tensile properties of polymer matrix composite materials.* Book ASTM D3039-standard test method for tensile properties of polymer matrix composite materials (ASTM International, 2017), 2017. **360**.

46. Standard, A., *D 7264/D 7264M–07 Standard Test Method for Flexural Properties of Polymer Matrix Composite Materials.* Annual Book of ASTM Standards, 2007: p. 1-11.
47. ASTM, D., *2344.* D 2344M Standard test method for short-beam strength of polymer matrix composite materials and their laminates, 2000.
48. Banea, M.D. and L.F.M. da Silva, *Adhesively bonded joints in composite materials: An overview.* Proceedings of the Institution of Mechanical Engineers, Part L: Journal of Materials: Design and Applications, 2009. **223**(1): p. 1-18.
49. ASTM, A., *D3163-01, Standard Test Method for Determining Strength of Adhesively Bonded Rigid Plastic Lap-Shear Joints in Shear by Tension Loading.* ASTM International, 2014.
50. Standard, A., *D5573-99.* Standard practice for classifying failure modes in fibre-reinforced-plastic (FRP) joints" Annual Book of ASTM standards, 1999. **15**: p. 03.
51. ASTM, D., *D4812-11, Standard Test Method for Unnotched Cantilever Beam Impact Resistance of Plastics.* ASTM book of standards, 2011. **8**.
52. Erkliğ, A., N.F. Doğan, and M. Bulut, *Charpy impact response of glass fiber reinforced composite with nano graphene enhanced epoxy.* Periodicals of Engineering and Natural Sciences, 2017. **5**(3).
53. Sadighi, M. and R. Alderliesten, *Impact fatigue, multiple and repeated low-velocity impacts on FRP composites: A review.* Composite Structures, 2022. **297**: p. 115962.
54. ASTM, D., *3479.* Standard Test Method for Tension-Tension Fatigue of Polymer Matrix Composite Materials. ASTM International, West Conshohocken, PA, 2007: p. 19428-2959.

Paper 1

Literature review

Methods to increase the mechanical performance of composite adhesive joints: an overview with focus on joints with natural fibre composite adherends

H.F.M. de Queiroz[1], M.D. Banea[1]

[1]Federal Centre of Technological Education in Rio de Janeiro (CEFET/RJ), Brazil.

ABSTRACT

This paper presents an overview of the recent developments in the main methods used to increase the mechanical performance of composite adhesive joints with focus on joints with natural fibre reinforced composite (NFRC) adherends. First, the main factors that affect the performance of composite adhesive joints were briefly discussed. Further, the main methods used to increase the mechanical performance of natural fibre-reinforced composite adhesive joints are presented. Since, the literature regarding these methods applied to NFRC adherends is relatively scarce, in addition, promising techniques applied to synthetic fibre-reinforced composite joints, which behave in a similar manner and whose results can be extrapolated with a great deal of confidence to NFRCs are also briefly discussed. Finally, some conclusions and an outlook on critical challenges and future perspectives are summarized. The application of sustainable green composites may further increase in many structural and non-structural applications if their joining behaviour is well-known and established.

Keywords: Natural fibre reinforced polymer composites (NFRCs), hybrid composites, adhesive joints, mechanical properties, delamination.

1. Introduction

Natural fibre reinforced composites (NFRCs) are gaining increasing attention in many industries, owing to their specific properties and environmental benefits [1]. Consequently, there has been an increasing growth in research and innovation in the NFRC materials, mainly due to the advantages of these materials compared to synthetic fibre-reinforced composites, such as low environmental impact and low cost which support their potential across a wide range of applications. NFRCs are nowadays used in non-structural car body parts, such as: door panels, package trays, hat racks, instrument panels, internal engine covers, sun visors, boot liners, oil air filters and even progressing to more structurally demanding parts such as seat backs and exterior underfloor panelling [2]. Nowadays, most of the automotive makers such as Audi, Volkswagen, Toyota, Daimler-Benz, Volvo, Ford, etc. use NFRCs to produce components [3]. The continually growing demands for lightweight and fuel-efficient vehicles will further push the growth of NFRCs in the automotive market. There are other exciting market trends going forward in many different industries. For example, tri-dimensional hybrid natural fibre reinforcement preforms have been used recently by sports cars manufacturers such as Porsche and even McLaren in Formula 1 [4]. Other applications of NFRCs include sport equipment, musical instruments, aerospace, construction industry [4-6] and ballistic armour [7, 8]. Several types of natural fibres currently used in industry such as: jute, sisal, oil palm, kenaf, and flax, are well established on the global market with a well-defined production line. However, new promising natural fibres are being discovered and used on a smaller scale or are still being used only for research. It is the case of the buriti and curauá fibres, for example, that still need some improvements in their production line to be more commercially affordable and reach widespread use [9-11]. Natural fibres are used as reinforcing fibres in thermoset or thermoplastic polymeric matrix in a variety of applications. The growing importance of natural fibre reinforced composites is reflected by the increasing number of publications (e.g., reviews, patents, book chapters and books) during the recent years [12-19]. Therefore, it is important to study their joining behaviour in order to utilize the full potential of natural fibre- reinforced composites.

Adhesive bonding is the preferred method for joining of fibre-reinforced composite materials [20, 21]. The use of adhesive bonding rather than mechanical fasteners offers

the potential for reduced weight and cost [20, 22]. However, NFRCs have inferior mechanical properties and higher water absorption capabilities compared to synthetic fibre-reinforced composites. Intense research efforts are continuously made and some of these shortcomings were addressed by recent advancements in fibres treatments and modifications, exploration of new natural fibres and hybridization [1]. The fibre modification techniques provide improved fibre-matrix interfacial adhesion, improved fibre roughness and wettability and depends on the particular fibre/matrix used and the composite application, while the hybridization methods provide flexibility in fibre selection for the material properties according to the end-use application requirements.

The behaviour of adhesively bonded joints with NFRC adherends was investigated by several researchers [23-35]. However, as per author's knowledge, there is no literature review available on this subject. This paper provides an overview of the recent developments in adhesive joining of natural fibre reinforced polymer composites. First, the main factors that affect the mechanical performance of adhesive joints of natural fibre-reinforced composites are briefly discussed. Further, the main methods used to increase the robustness of fibre-reinforced composite adhesive joints are presented. Since, the literature regarding these methods applied to NFRC adherends is relatively scarce, in addition, promising techniques applied to synthetic fibre-reinforced composite joints, which behave in a similar manner (e.g. behaviour up to failure, failure modes) and whose results can be extrapolated to natural fibre-reinforced composites are also briefly discussed.

2. Factors affecting the mechanical performance of composites adhesive joints

It is well known that different materials and joint geometries give rise to distinct stress states in the adhesive layer, and the mechanical performance of adhesive joints depends on several factors (e.g., the joint geometry and the mechanical properties of the adhesive and adherends) [36, 37]. In this section, the main factors that affect the mechanical performance of fibre-reinforced polymer composite (FRP) adhesive joints, are briefly discussed.

2.1 Effect of joint configuration and failure mode

There are a wide variety of adhesive joints available in the literature. Common joint configurations used in composite structures include single-lap joints (SLJs), double-lap

joints, scarf joints, and stepped-lap joints. Many other configurations exist, with their specific benefits, such as peel joints, the joggle-lap joints and L-section joints among others. However, the SLJ is the most common joint used and studied in the literature mainly due to its simplicity and efficiency [38]. On the other hand, one of the problems associated to this joint is the fact that the stress distribution (shear and peel) is concentrated at the ends of the overlap. For FRP adhesive joints, several other factors influence the failure behaviour and strength of the joint (see Fig. 1). An out-of-plane bending moment is generated on the overlap zone of a SLJ due to the load path eccentricity (mixed mode stress state) and the transverse composite material properties (the inter- and intra-laminar strength of composites) play a significant role on the overall joint mechanical performance and failure mode.

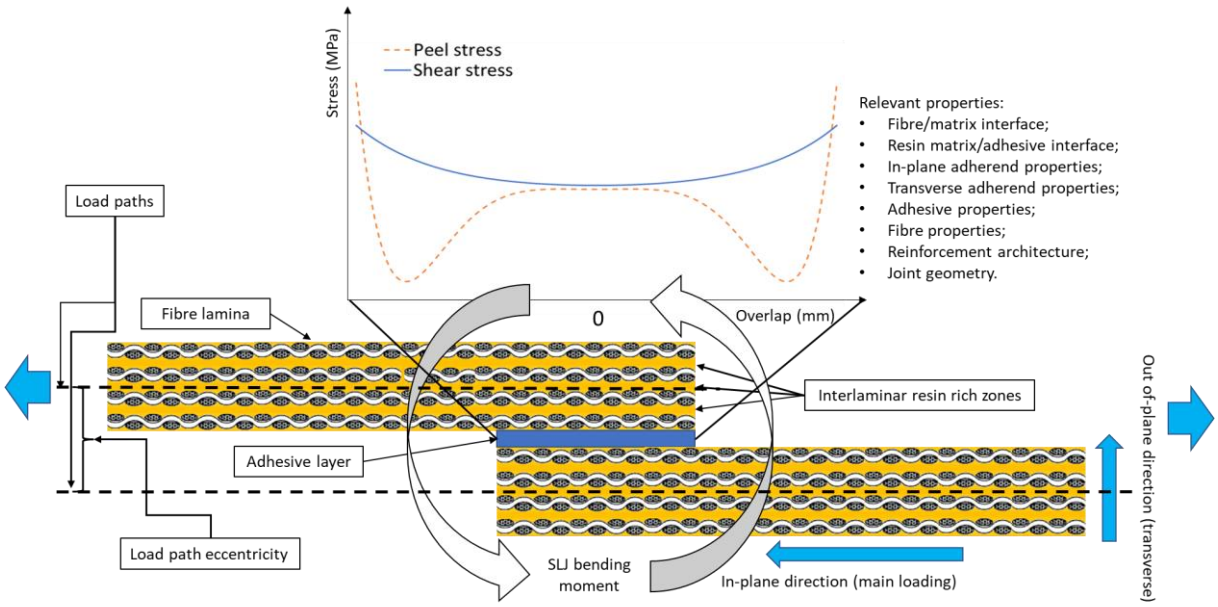


Figure 1. Schematic illustration of an FRP adhesive joint with the main relevant parameters that affect the strength and failure mode.

Gonzalez-Murillo and Ansell [25] studied the effect of joint geometry on the strength of natural fibre composite joints using three different joint geometries: SLJs, co-cured joints (the curing and joining process occurred at the same time) and termed intermingled fibre joins (IFJs) and laminated fibre joints (LFJs) of henequen and sisal fibre composite. They found that the IFJs and LFJs presented higher lap shear strengths than the single lap shear

joints. Melese et al. [26] investigated the effect of joint configuration and hybridization in pure jute, sisal and jute/sisal hybrid joints using SLJs, double strap butt joint and scarf-45^{o} joint. The highest joint strength reported was for the hybrid butt composite joints, followed closely by the sisal butt joint.

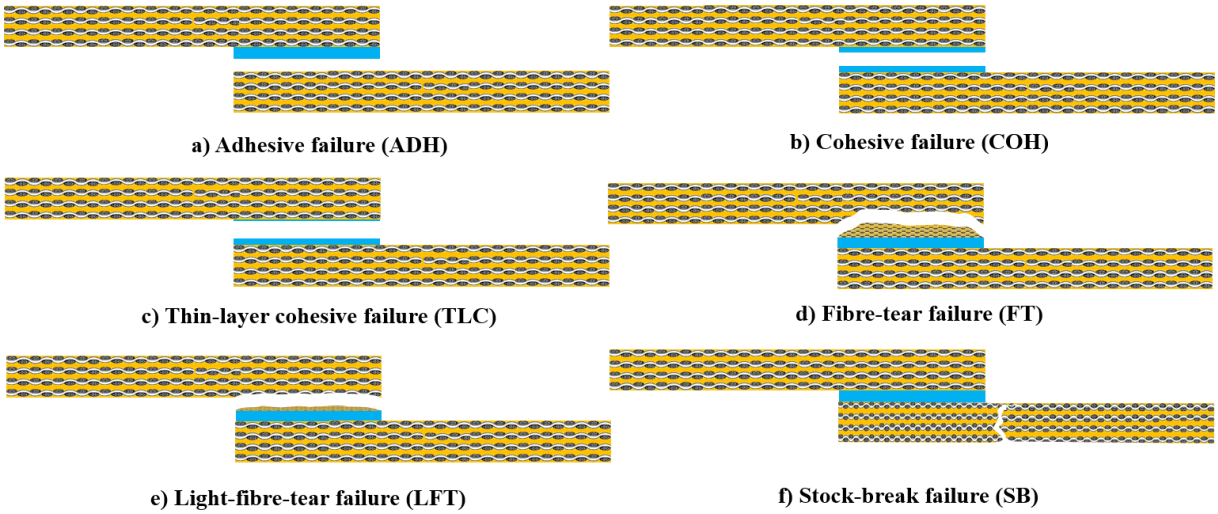
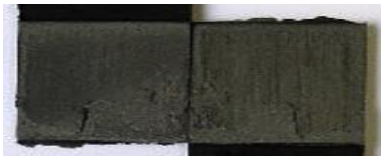


Figure 2. Possible failure modes in bonded joints between FRP composite adherends.

It is well established in the literature that the joint failure mode is extremely important for the ultimate load carrying capacity of a bonded joint. When the failure mode is well reported, it can give an accurate and deep understanding on the crack propagation, stress concentrations and significant material properties that are affecting the joint performance [7]. Typical failure modes for fibre reinforced polymer (FRP) composite joints can be seen in Fig. 2 as per international standard ASTM D 5573 [39]. The type of failure is ruled by the adherend and adhesive properties, joint geometry as well as the adherend/adhesive interfacial quality. Generally, cohesive within the adhesive failures (COH) lead to the highest failure loads. It is well known that, one of the issues in bonding composite adherends is the delamination (fibre tear failure). This is particularly true if the composite adherends are made of layers with different fibre orientations. It is well known, that in the fibre direction, unidirectional composites can be very strong and stiff, whereas the transverse and shear properties are much lower. Thus, in order to avoid premature failure of the composite adherends (both natural and synthetic), it is recommended to have the outer layers of the adherend with a direction parallel to the loading direction to avoid intralaminar failure of these layers [36]. Table 1 presents the standard definition for all

the failure modes, as well as representative bonded FRP joint failure surfaces for each case.

Table 1. ASTM D 5573 standard failure mode definition and examples.

Failure mode	**Standard definition** [39]	**Example/Reference**
Adhesive failure/interfacial failure (ADH)	Rupture of the adhesively bonded joint, such that the separation appears to be at the adhesive-adherend interface. After failure, the FRP and adhesive surfaces may have a shiny appearance and there is no evidence that any adhesive or FRP, or both, have transferred to the other surface	 T300 CFRP adhesive joint [40]
Cohesive failure (COH)	Rupture of an adhesively bonded joint, such that the separation is within the adhesive.	 CFRP adhesive joint [41]
Stock break (SB)	A break of the FRP substrate outside the adhesively bonded-joint region, often occurring near it.	 Sisal fibre reinforced composite adhesive joint [24]
Thin-layer cohesive failure/Interphase failure (TLC)	Failure similar to cohesive failure, except that the failure is very close to the adhesive-substrate interface, characterized by a "light dusting" of adhesive on one substrate surface and a thick layer of adhesive left on the other. (Sometimes referred to as interphase failure.)	 Sisal/glass intralaminar hybrid composite joint (glass reinforced sisal fabric) [24]
Light-fibre tear failure (LFT)	Failure occurring within the FRP substrate, near the surface, characterized by a thin layer of the FRP resin matrix visible on the adhesive, with few or no glass fibres transferred from the substrate to the adhesive.	 Jute/glass interlaminar hybrid composite joint (glass fabric around jute core) [42]

Delamination/Fibre tear failure (FT)	Failure occurring exclusively within the FRP matrix, characterized by the appearance of reinforcing fibres on both ruptured surfaces.	 Jute/glass intralaminar hybrid composite joint (glass reinforced jute fabric) [24]

Delamination and adherend failure (stock break failure) are the prominent failure modes found in the current literature on the topic of NFRC bonded joints [24-27, 30, 31, 33, 43, 44]. In fact, delamination is a significant issue for NFRC bonded joints, hampering the improvement of the load bearing capacity of these joints [42]. This failure is characterized by the removal, either partial or complete, of composite layers as the crack progresses in the interlaminar space of the composite adherend instead of within the adhesive or close to the adhesive/adherend interface. Close to the interface failures such as thin layer cohesive (TLC) and light fibre tear (LFT) failures are also common [42]. The TLC failure is characterized by crack propagation very close to the adherend/adhesive interface, where one side of the joint will present a thick adhesive layer while the other will show a light adhesive dusting with few delaminated fibres. On the other hand, the LFT failure type is characterized by the entirety of the adhesive layer on one side of the joint while the other presents some interface surface resin removal and the tearing of a few fibres. Currently, the international standard ASTM D 5573 is generally used for the failure mode determination of composite bonded joints [39] (see Table 1).

It was shown that NFRCs using sisal and jute fibre tend to fail by stock break very close or exactly at the overlap edge of the bonded SLJ due to the maximum shear and peel stresses and the brittle nature of the fibres [24, 26, 44]. This type of failure has also been observed in DLJ (double lap joint) NFRCs as well as being a function of the overlap length [27]. Premature stock break crack propagation at the SLJ overlap edge has also been reported in composites reinforced with coconut fibres [45]. In previous research efforts it was observed that the failure modes of NFRC bonded joints presented significant differences as a function of adherend material [24, 42]. For the intralaminar hybridization technique (i.e., natural and synthetic fibres in the same lamina), the failure modes were delamination for the jute/glass specimens and delamination/TLC mixed modes for the sisal/glass specimens (see Table 1) [24]. These trends in failure modes are linked to the

fibre type, fibre/matrix interface quality, lay-up architecture and stress state of the overlap, among other factors. For example, in the above-mentioned study, the LFT failure type was observed for both the Glass Fibre Reinforced Plastic (GFRP) and hybrid joints. The failure mode of adhesive joints with NFRC adherends is also influenced by the fibre type and location (i.e., stacking sequence). It was shown in the literature that certain stacking sequences can retard delamination [21]. For instance, Yoon et al. [30], investigated the effect of bamboo fibre layer positioning on the failure strength of SLJ with natural fibre composites adherends (i.e., bamboo fibre and polyester matrix, purely polyester and mild steel mesh reinforcement) and found that the fibre positioning had a significant effect in stress concentration of the adhesive joint. The position of the reinforcement layer studied was: fibre layer close to the adherend/adhesive interface (narrow) or away from the interface (wide) types. For instance, narrow type mild mesh steel specimens presented higher strength than wide type ones. This was linked to the stress reducing effect in the overlap edge afforded by the reinforcement. For the bamboo narrow specimens, the bonded joint strength was decreased due to poor fibre/matrix interface leading to premature adherend failure.

Another important joint geometry parameter that affects the adhesively bonded joints performance is the adhesive thickness [46]. For SLJs, it was shown that the joint's strength decreases as the adhesive thickness increases, with the exception of SLJs bonded with elastomeric adhesives [47, 48]. The highest strength is obtained for adhesive thicknesses of the order of 0.1 to 0.5 mm [49, 50]. Moreover, this observation is not generally applicable as there are other factors involved, such as the type of loading, the adherend behaviour (elastic or plastic), and the type of adhesive (ductile or brittle), which can modify the behaviour of joints as their thickness is varied [46].

The overlap length is another parameter that can affect the joint strength [51]. While increasing the joint width increases the strength proportionally, the effect of the overlap length on the adhesive joint strength depends on the type of adhesive (i.e., ductile or brittle) and also on the type of adherend [52]. For instance, for bonded joints with elastic adherends and ductile adhesives, the strength is proportional to the overlap length. This occurs because ductile adhesives deform plastically as the load increases and make use of the whole overlap. In this case the global yielding failure criterion is suitable. For joints with elastic adherends and brittle adhesives, the joint strength is not proportional to the

overlap and a limit strength is attained. In this case the adhesive does not accommodate peak stresses at the ends of the overlap and failure is ruled by these peaks. On the other hand, for composite adherends the overlap effect on the strength of the joints is mainly dictated by the composite transverse strength (the transverse (out-of-plane) composite properties are very different (lower) than the in-plane mechanical properties) [53].

Several researchers have conducted investigations to study the effect of overlap length on the behaviour of the adhesively bonded joint of natural fibre-reinforced composites. For example, Mittal et al. [27] studied the behaviour of jute-based composites while varying the overlap length and curing temperature in single and double lap joints. Delamination was found to be the dominant failure mode. The mean shear stress (calculated as failure load over bonded area) was reported to be similar for both single and double lap joints (DLJ) irrespective of overlap length, even though the double lap joint presented higher failure loads. Moreover, for jute/epoxy DLJs, an increase in overlap length quickly leads to the failure of the substrate at the overlap edge, nevertheless, the failure load is still significantly higher than the SLJ counterpart.

Choudhury and Debnath [33] studied experimentally the effect of different overlap lengths (20, 40, and 60 mm) and widths (20, 26, and 32 mm) on the performance of SLJs of green composites (bamboo fibre/Polylactic acid (PLA)). Three adhesives were used (epoxy, polyurethane, and parent polymer (PLA)) for joining of the bamboo/PLA composites. The epoxy joints had a superior strength compared to polyurethane and PLA joints (e.g., the strength of SLJs was reduced by 49% and 81% when PLA and polyurethane are used). Higher strength of the adhesively bonded joint was achieved by increasing the bonding area.

2.2. Effect of mechanical properties of adhesive and adherend material on the mechanical performance of adhesive joints

The adhesive and adherend material influence the bonded joints performance and its effect should be taken into consideration in the design of composite adhesive joints [54]. There are many different types of adhesives available, each with their own advantages and disadvantages: epoxies (having high strength and temperature resistance), cyanoacrylates (fast bonding capability to plastic and rubber but poor resistance to moisture and temperature), anaerobics (suitable for bonding cylindrical shapes), acrylics

(versatile adhesives with capabilities of fast curing and tolerate dirtier and less prepared surfaces), polyurethanes (good flexibility at low temperatures and resistant to fatigue) and high-temperature adhesives (phenolics, polyimides and bismaleimides). The selection of a suitable adhesive is not an easy task, as there is no universal adhesive that will fulfil every application and the selection of the proper adhesive is often complicated by the wide variety of available options [20, 52, 54]. Adhesive selection includes several factors such as: type and nature of adherends to be bonded, cure and adhesive application method and the expected environments and stresses that the joint will face in service. Also, the cost of the adhesive may sometimes be an important factor of adhesive selection in a particular production situation [54].

The first criteria for choosing an adhesive is that it can create a proper bond between the materials chosen for the structure. Datasheets from adhesive manufacturers provide basic information about what type of materials can be bonded. Some adhesive suppliers provide software tools to help the engineer or designer to select the adhesive, although for critical components expert assistance is still needed. For joining natural fibre composite materials, the selection of a proper adhesive is critical because of the natural fibre reinforced composites temperature processing.

The adherend material influences the adhesively bonded joints performance and its effect should be also taken into consideration in the design of adhesive joints. It is well known that composite adherends have relatively low out-of-plane strength and shear stiffness compared to their in-plane material properties. Therefore, it is important to understand the mechanisms of failure involved for each specific material and how they are affected by these properties [36]. It was shown in the literature that, in general, increasing the adherend stiffness improved the joint's strength [38]. There are several methods available to enhance the natural fibre adherends properties, for example, the hybridization technique. Synthetic fibres such as glass and carbon have been widely used along with natural fibres such as jute and flax and significant property improvements have been observed [55-59]. The hybridization technique using different natural fibres has also been widely studied, [13, 14, 60-62] and it was shown that the natural/natural hybridization also presents significant positive effects in the mechanical properties of the composites owing to the differences in the mechanical properties of the fibres [63]. Mechanical and physical properties of typical natural fibres used as reinforcements in NFRCs are shown

in Table 2.

Table 2. Mechanical and physical properties of typical natural fibres used as reinforcements in NFRCs [60, 62].

Properties	Jute fibre	Sisal fibre	Ramie fibre	Curauá fibre
Density (g/cm^3)	1.3	1.33-1.45	1.5	1.4
Bundle diameter (mm)	0.55-0.65	1.2-1.3	0.55-0.65	0.6-0.7
Tensile strength (MPa)	393-773	468-700	400-968	500-1150
Young's modulus (GPa)	26.5	9.4-38	44-128	11.8
Elongation at break (%)	1.5-1.8	2-7	1.2-3.8	3.7-4.3
Cellulose (%)	58-63	60.5	76	58.8
Hemicellulose (%)	12	25.7	17	23.8
Lignin content (%)	12-14	12.1	1	14.7
Lumen area (μm^2)	1014	5796	-	162
Cellular wall thickness (μm)	2.5	2.6	2.8	3.5
Lumen diameter (μm)	6.7	12.8	8.2	4
Microfibril angle	8^o	10-22^o	7.5^o	-

Further, the stacking sequence is also a highly relevant factor to take into consideration, especially concerning the flexural and moisture barrier properties of the natural fibre composite. This is due to the nature of the stress distribution during three-point-bending (flexural testing) of a specimen, where the top layer (punch contact) will be under maximum compression and the bottom layer will experience maximum tensile stresses, decreasing linearly towards the neutral line (middle of the composite). Therefore, in a natural/synthetic hybrid composite for example, external synthetic fibres will provide an increased resistance under bending loads and improve joint performance. The synthetic phase improves the general mechanical properties as well as providing a barrier to humidity given its hydrophobic nature, while the natural phase contributes to decreasing the weight and carbon footprint of the composite structure [57]. Therefore, a two-fold improvement can be achieved as a function of stacking sequence for bonded joints with composite adherends. A reduction in overlap edge peak peel stresses due to an increase in adherend flexural rigidity (increase in delamination failure onset load) and an overall lower moisture uptake. In this way, the service lifetime of the bonded structure is enhanced and extended.

To summarise, the transverse properties of the composite adherend, the elastic properties

of adhesive and adherend, adherend thickness and loading mode ultimately rule the failure mode and bonded joint efficiency. If the stresses in a composite adherend exceeds its transverse strength (i.e., the peel stress is higher than the out-of-plane tensile strength), delamination failure within the composite will initiate, and propagate interlaminarly as a function of its toughness. These stresses will increase with loading mode mixicity, high adherend axial modulus, low adherend thickness and high adhesive toughness [64]. Therefore, tailoring the properties of the adherend and adhesive (elastic properties in the in-plane and transverse directions as well as careful geometry selection) is crucial for maximizing composite bonded joint efficiency and decreasing or eliminating delamination failures.

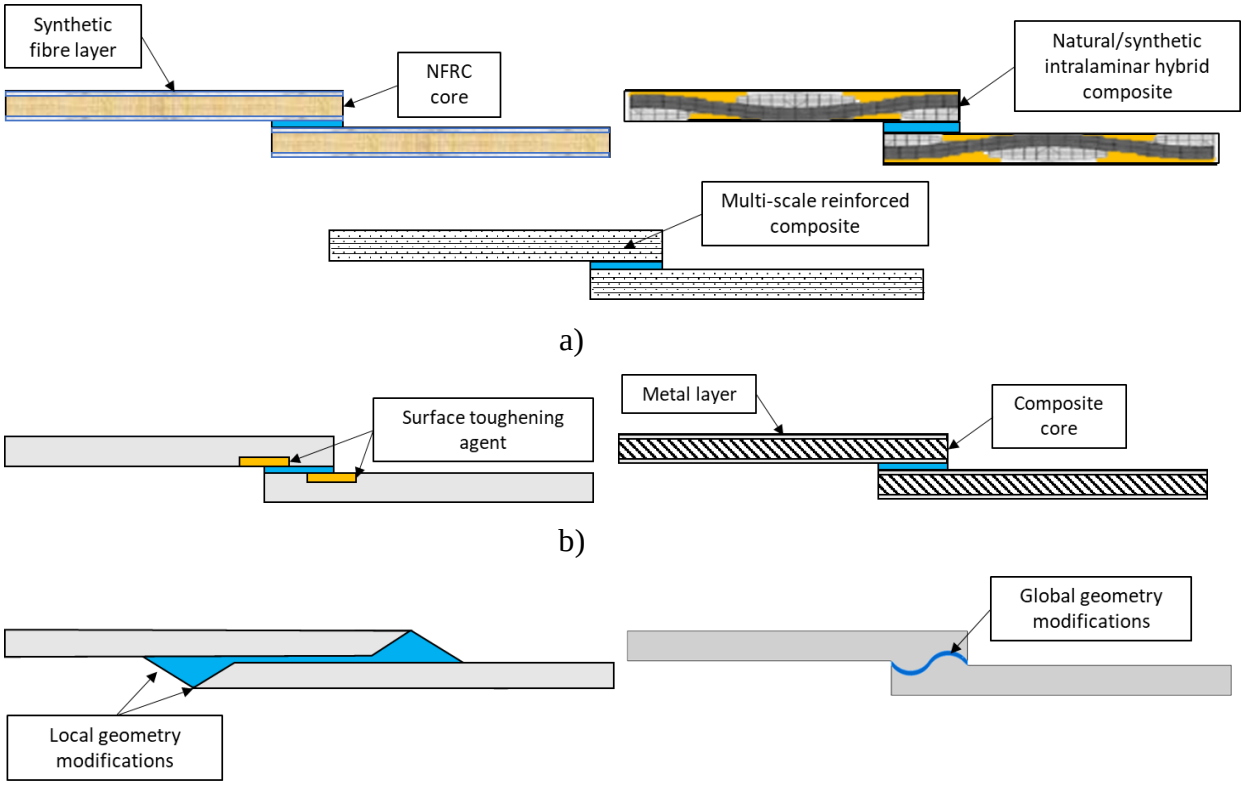
3. Methods to increase the robustness of natural fibre-reinforced composite adhesive joints

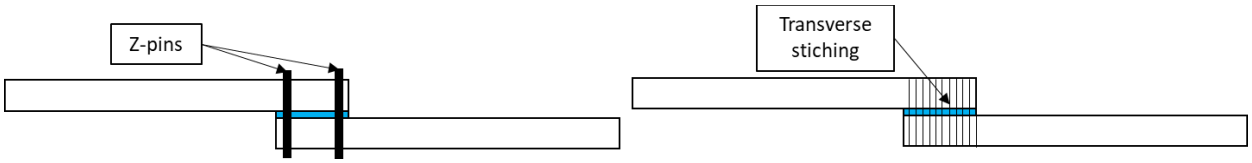
In this section, the main methods explored so far to increase the robustness of natural fibre-reinforced composite adhesive joints are presented. These methods can be categorised into two main groups: material and geometrical modifications of the adherend and adhesive. The available literature from the perspective of the mechanical performance optimisation of the NFRC adhesive joints is discussed. However, since, the literature regarding these methods applied to NFRC adherends is relatively scarce, in addition, several promising techniques applied to synthetic fibre-reinforced composite joints, which behave in a similar manner and whose results can be extrapolated to natural fibre-reinforced composites are also briefly presented.

3.1 Modification of the adherend

The material characteristics of the adherend play a crucial role in the overall properties of a bonded joint[36]. However, it is well known that natural fibres and their composites generally present lower properties when compared to their synthetic counterparts [42]. There are different methods to improve the performance of natural-fibre reinforced composites, such as: hybridization, multi-scale reinforcements, coatings, geometrical modifications and transverse toughening. The hybridization technique uses different fibres (natural/natural or natural/synthetic) in the same composite to fabricate a novel material with superior properties to the single fibre case. On the other hand, the multi-

scale reinforcement technique involves the addition of micro and nano scale fillers in the matrix phase of a fibre-reinforced composite aiming to improve the interlaminar fracture toughness of the composite [65]. Other solution is adding additives with different scales (e.g., multiwall carbon nanotube coating, nano clay and short fibres) into the interface to improve its bonding strength and toughness by forming an interweaving and bridging effect [66]. Similarly, the coating technique induces an increase of the delamination toughness of the composite through the application of tough resins or modified resins to the surface of the adherends [67]. The modification of the adherend geometry is a technique that involves tailoring a more suitable stress distribution at the bonded joint overlap edges. Finally, the transverse toughening of the adherend is a technique that involves the use of metal layers in the case of fibre metal laminates (FMLs) or through-the-thickness 3D reinforcements [68]. A schematic of the main adherend modification techniques investigated in the current literature can be seen in Fig. 3. The following sub-sections present the most relevant methods used to improve the adherend properties and consequently the performance of their adhesive joints.





d)

Figure 3. Schematic examples of the main adherend modification techniques: a) adherend material hybridization, b) adherend surface modification, c) adherend/adhesive geometry modification and d) transverse toughening.

3.1.1 Adherend material hybridization

Hybridization is the most well-established technique used for improving adherend properties and has been investigated by several researchers [24, 26, 30, 31, 42, 44, 65]. Ferreira et al. [31] studied the influence of stacking sequence and natural fibre content of hybrid composite in the fatigue strength of bonded joints. Hybrid fibre reinforced composites with a polypropylene/hemp natural fibre layer adjacent to the bond interface which was expected to produce more uniform stresses in transient regions joints were compared to single fibre reinforced composites. They found that the fatigue strength of hybrid stacked joints was lower than the single fibre reinforced composite joints due to lower adhesion between hemp and adhesive layer. The finite element model (FEM) showed that peak stresses in critically referenced sections are significantly higher in hybrid stacked fibre composites than single fibre ones. It is concluded that hybrid stacked composites could be an alternative if economic costs are considered along with ecological concerns. De Queiroz et al. [24], have shown that intralaminar synthetic hybridization of jute and sisal composites via glass fibre had a significant effect on both adherend material properties and bonded joint strength. The synthetic fibre hybridization significantly improved the adherend material properties which also led to bonded joint performance enhancements. The highest bonded joint performance improvement was found for the jute/glass intralaminar hybrid specimens, for both similar and dissimilar joints. Melese et al. [26] investigated the effect of joint configuration and hybridization in the mechanical behaviour of pure jute, sisal and jute/sisal hybrid composite adherend bonded joints using SLJs, double strap butt joint and scarf-45^{o} joint. The highest joint strength reported was for the hybrid composite adherend joints, while the most efficient joint configuration was found to be the double strap butt joint.

More recently, de Queiroz et al [42] studied experimentally the behaviour of SLJs made of natural, synthetic and interlaminar hybrid fibre-reinforced polymer composites. The effect of the number of the interlaminar synthetic layers required to match the bonded joint efficiency of a fully synthetic GFRP bonded joint was studied by testing SLJs bonded with a modern tough structural adhesive used in the automotive industry. A significant variation of joint behaviour as a function of adherend material was found (see Fig. 4). The failure load of the hybrid adherend joints increased by increasing the number of external synthetic layers (i.e., the failure load of hybrid 3-layer joint increased by 28.6% compared to hybrid 2-layer joint) and reached the pure synthetic adherends joint efficiency. The authors state that this is due to the optimum compromise between the adherend material property (i.e., stiffness and strength) and a diminished bondline peel stress state as a result of lower rotation of the adherend during loading, which leads to lower stresses and delayed delamination failure onset.

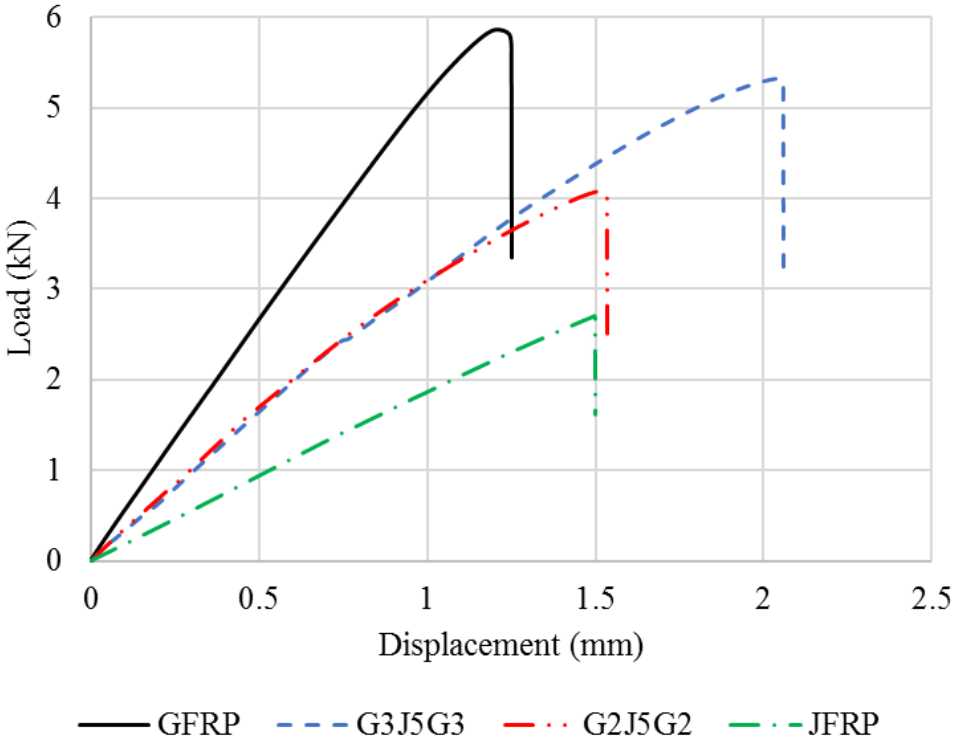


Figure 4. Representative load-displacement curves of SLJs as a function of adherend material (where GFRP is Glass Fibre Reinforced Polymer Composites, JFRP is Jute fibre Reinforced Polymer Composites, G2J5G2 and G3J5G3 represent Jute/glass hybrid composites with 2 and 3 exterior glass layers around a 5 layer jute core, respectively) [42].

3.1.2 Surface modification

The surface modification technique allows for a decrease in unwanted stress peaks at the overlap edges (common in SLJs), without significantly increasing fabrication complexity and costs [69]. Schollerer et al [67] investigated the effect of a novel local adherend surface toughening concept via a thermoplastic polyvinylidene fluoride (PVDF) layer and compared it to classical local geometrical modifications. The expected benefit was twofold: a reduction of peak stresses at the overlap edges and maintaining a simple fabrication methodology so that additional expenses are avoided. A prepreg adherend made from Hexcel Hexply® 8552 was used along with Hysol® EA 9695 adhesive system. The PVDF thermoplastic was added to the uncured prepreg and then the laminate was cured in an autoclave. The PVDF layer length effect was studied, and an optimum dimension was found. The adherend surface treatment was atmospheric pressure plasma. The results from 4 PVDF length joint specimen groups (i.e., 5, 10, 17.5 and 30 mm) were compared to the unmodified (neat) case along with local adhesive geometry modifications (i.e., half triangle, arc and chamfering). Significant improvements were observed for the 5, 10 and 17 mm PVDF layer cases, where an approx. 28, 84 and 30% joint efficiency increase was reported compared to the unmodified joint, respectively. Moreover, this PVDF case also presented significant improvements when compared to the classical geometrical modifications. It was remarked that only the overlap edges benefit from a more ductile material in the stress transfer zone, which acts to transfer peel stresses from one adherend to the other without a crack up to joint failure. Similarly, Kanani et al. [70] studied the effect of embedding patches of higher stiffness material in lower stiffness adherends in order to diminish the peak stresses at the overlap edge. The technique was applied in order to increase the efficiency of dissimilar multi-material bonded joints. Numerical and experimental investigations were carried out on bonded joints with aluminum alloy 6082 T6 and Polyphtalamide (PPA) adherends. PPA adherend's surface was modified by the addition of aluminum patches at the overlap edge, see Fig. 5. A two-component room temperature cure adhesive was used, Loctite EA 9497. The length of the aluminum patches was studied (i.e., 5, 7.5, 10 and 25 mm) and the optimum configuration was found. It was reported that, in a dissimilar joint, the stress distribution is asymmetric with the higher peak value toward the lower stiffness adherend. The novel

technique presented higher global adherend stiffness which led to decreased bending rotation and lower peak peel stresses at the overlap edge. The most efficient model was reported for the Model-II case with an aluminium patch of 0.4 mm thickness and 5 mm length.

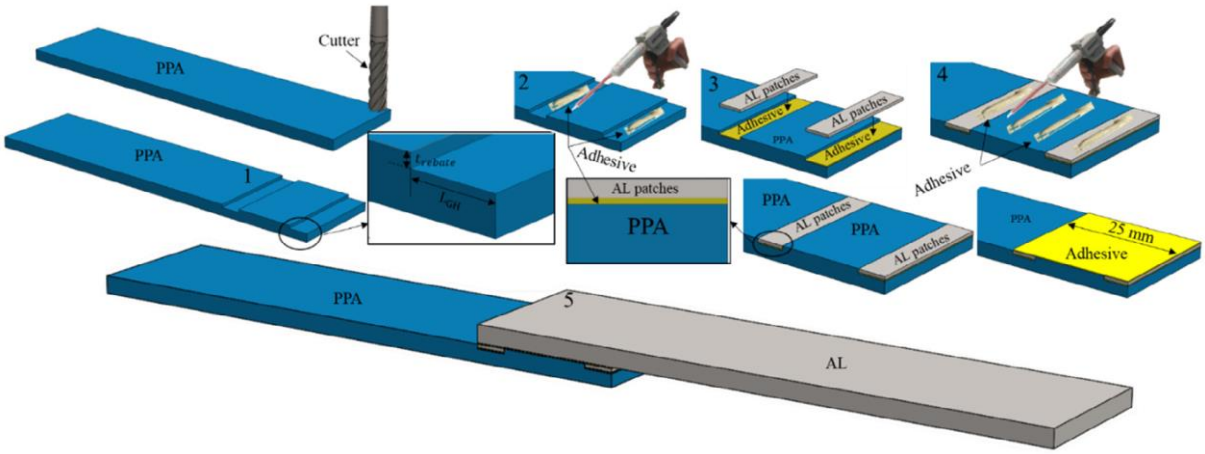


Figure 5. The manufacturing process of the modified PPA SLJs with aluminium patches. [70].

The adherend may also be modified in other ways, such as: the addition of fibres to the interface on a macro scale or fibre/resin matrix interface improvement by modifying the surface of the fibre via chemical treatments, among others. These techniques have been investigated by several researchers [43, 44, 71]. Estevez et al. [43], studied experimentally the effect of different surface treatments of SLJs with sisal fibre reinforced composite adherends bonded with an epoxy resin. Fibre reinforcement was 25% in volume and random oriented. They found that the tensile strength of the joints was a function of surface treatment. The failure modes were all cohesive in the adherend with the damage initiation at the overlap edge. This indicated a poor fibre matrix interfacial adhesion despite the treatment. Melese et al [44] investigated the effect of drilled holes in the overlap area of sisal/jute hybrid composite bonded joints. Pure jute, sisal and jute/sisal composites were bonded with the same polymer resin used as a matrix for composite fabrication (Araldite LY-559). Four different holes arrangement were tested (i.e., 2, 4, 6 and 8). It was found that the adhesive-filled hole provided a hinge effect during joint loading and the best results were generally observed for the four and eight-hole configurations.

3.1.3 Geometry modification

The tailoring of the geometry of bonded joints has a significant effect in its load-bearing capabilities. Improper joint geometry design leads to undesired stress distributions and concentrations. There are many types of joint geometries as described in section 2.1 and the most common joint studied is the SLJ. However, due to its eccentric load path, peak shear and peel stresses occur at the overlap edges. The geometry modification can be global or local. The global geometry includes different joint configuration, such as SLJ, DLJ or scarf joints, and other general geometric features such as: non-linear overlap, overlap length and bond line thickness. On the other hand, the local geometry design focuses mostly on the overlap edges, to address the stress concentrations that arise due to the material discontinuities of both the adhesive and adherend. Techniques such as adhesive fillets and adherend tapering/rounding are commonly used in this context. Shang et al. [72] described in detail in a recent review, the research efforts on this subject. It was noted by the authors that improvements to bonded joint efficiency as a function of the applied techniques invariably led to significant increases in manufacturing complexity and cost. Combinations of global and local geometries showed improvements of up to 200% of joint efficiency. It is important to note that a qualitative scale of fabrication difficulty was used and the highest improvements at low manufacturing difficulty were: adherend inside taper coupled with adhesive spew fillet [73] and wavy joints [74]. Particularly for composite adherends, the wavy joint global configuration modification technique presents a significant improvement due to the conversion of dominant peel stress concentrations at the overlap edges to almost entirely compressive stresses [74]. The relevance of this modification is found in the fact that peel stresses play a crucial role in delamination failure onset. This technique has been used in synthetic fibre-reinforced composite bonded joints and significant improvements have been reported [74-77]. An example of the effect of this type of global geometry modification can be seen in Fig. 6. The negative bond shape changes the stress state of the overlap edge significantly, improving the joint failure load. Similarly, this technique is well suited for application in NFRC bonded joints considering the known brittle nature of commonly used natural composites and its propensity for SB and delamination failures. Delamination will tend to diminish due to the shift from a predominantly peel stress state to a compressive state

at the overlap edge.

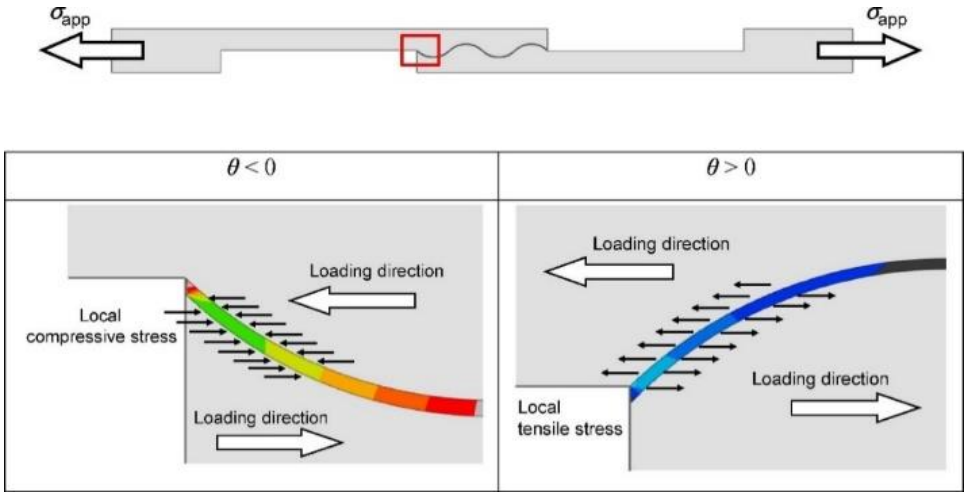


Figure 6. Schematic of horizontal compressive stress distribution for non-flat SLJs with negative bond shape [78].

3.1.4 Fibre Metal Laminates (FMLs)

As already mentioned, the transverse properties of a composite material are crucial for the performance of a bonded joint as it is one of the ruling factors for the maximum load-bearing capacity as well as the type of failure. One of the available techniques for improving these properties is the use of metal layers around the composite material, a Fibre Metal Laminate (FML). The most widely used families of FMLs are Glass reinforced aluminium laminates (GLARE), carbon reinforced Aluminium Laminate (CARAL) and Aramid-Reinforced Aluminium Laminate (ARALL) [79]. FMLs based on natural fibres are called Natural Fibre Metal Laminates (NFMLs). Although, the material properties of natural fibre NFMLs have been reported by several researchers and significant improvements were observed [68, 80-85], there are no natural fibres FML bonded joint research efforts to date.

3.1.5 Transverse reinforcements

Another method to improve the joint performance explored in the literature is by enhancing the transverse properties of the composite adherend and the overlap area via transverse reinforcements: Z-pin [86-91], stitching [92-94], micro [95] and nano-fillers [96]. One of the main improvements reported by these techniques is an increase in delamination resistance of the adherends provided by the through-the-thickness direction

reinforcement. The transverse reinforcements in general, increase the fracture toughness of the composite adherend (modes I and II) [97-99]. For instance, Bogdanovich et al. [92] studied both co-cured and adhesively bonded joints of composite adherends reinforced with non-crimp 3D orthogonal woven glass fibre fabrics (see Fig. 7). Single-lap and double butt-strap joints were fabricated via co-curing and adhesive bonding and tested in uniaxial tension. Stitching the co-cured single-lap joints resulted in significant increase in joint strength. Moreover, the delamination failure was not observed within any of the unitary 3D woven composite adherends owing to the effect of the z-binders, even in relatively low weight fraction (~2%).

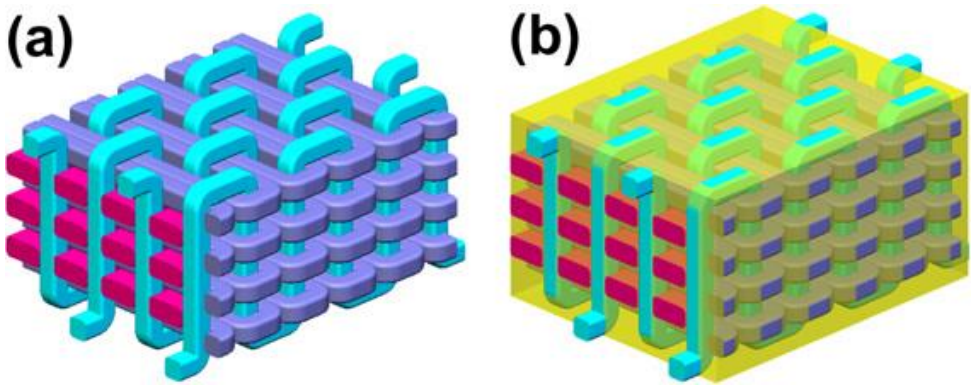


Figure 7. Representative non-crimp orthogonal 3D woven fabric composite element (a) and fabricated (transparent resin) (b) [92].

Islam and Tong [86] studied experimentally the effect of trough-the-thickness pin reinforcement in the static joint strength of hybrid steel/glass fibre joints, see Fig. 8. Stainless steel pins were used as mechanical fasteners near the overlap edge of the adhesively bonded joints. It was reported that the pins increase the strength of the joints via a bridging mechanism as a function of number and location of pins by up to 58%. Regarding the application of this method in NFRC joints, it is likely that a significant increase in the load necessary to cause failure in a transversely reinforced overlap zone would change the failure mode to a stock break. As it has already been discussed in this paper, most of the NFRCs tend to display this failure type, and therefore, this method may be best suited for natural/synthetic hybrid adherends or in conjunction with other adherend material property enhancements, where SB failures will be less likely.

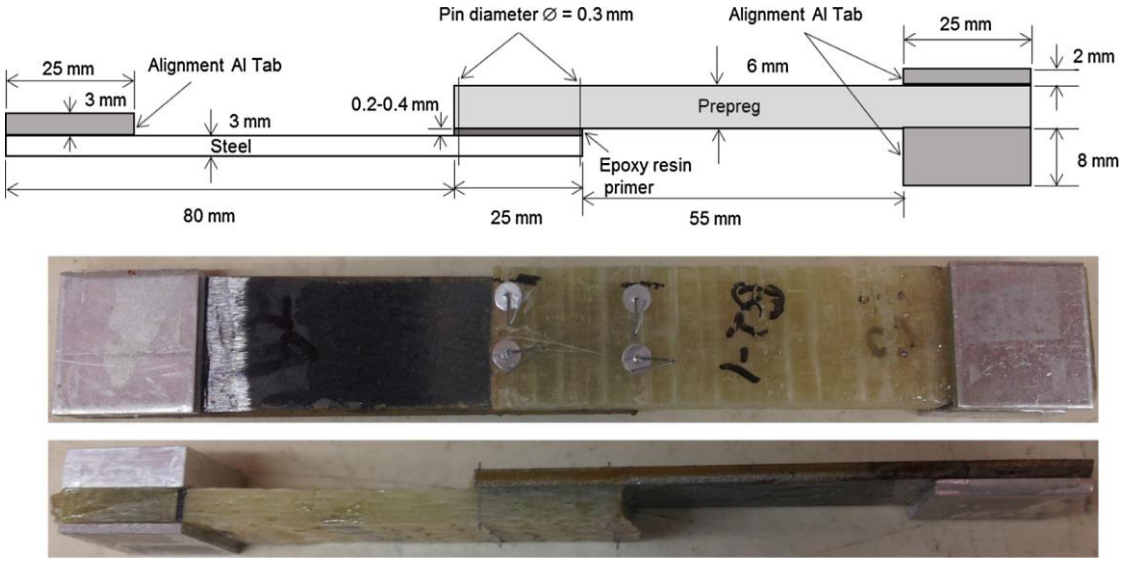


Figure 8. Test configuration for pinned SLJ specimen [86].

3.2 Modification of the adhesive

The general trends in adhesive modification with the focus on improving the load-bearing capacity of bonded joints are either local adhesive geometry tailoring (spew fillets) or reinforcements by fibres or fillers (natural or synthetic) [72, 100]. The benefits from spew fillets to the efficiency of composite bonded joints is well documented in the literature [101-105] and was briefly discussed in the previous subsection (3.1.3 Geometry modification). These benefits stem from a more uniform stress distribution at the overlap edges as well as a larger adherend-adherend load transfer region.

The use of filler reinforcements (natural or synthetic) in both micro and nano scale to modify the adhesive material properties has also been extensively investigated [66, 106-110]. The improvements observed come from the toughening effect of the adhesive by the fillers, especially for epoxy adhesives [100, 111]. Moreover, increased durability in humid environments is also an improvement afforded by using synthetic nano-fillers as an adhesive material modification [109].

There are several studies on using natural reinforcement materials such as natural fibres or particles (e-g. cork) on adhesive or adhesive joints properties [111-114]. For instance, Delzendehrooy et al. [71] studied the effect of date palm fibres (short and long), extracted from different parts of the plant (i.e. mesh, rachis, petiole and bunch), on the static strength of aluminum bonded joints. The influence of different parameters (fibre length, weight ratio and alkali treatment) on the joint strength was studied. Fibre lengths of 0.5-

2 mm were studied as well as long fibre (30 mm) while the weight ratios were 2, 5 and 10%. The long fibres (length similar to the overlap length) were placed parallel along the bondline, on the adhesive layer (see Fig 6). It was found that the addition of date palm fibres to the bonded joints significantly increased the failure load. The best case reported was for the 2 wt% short rachis fibre treated by 6% NaOH solution where an increase of 141% in joint strength was found. The reason for the increase in joint strength of joints modified with date palm fibres was reported to be the change in the path and arresting the crack propagation.

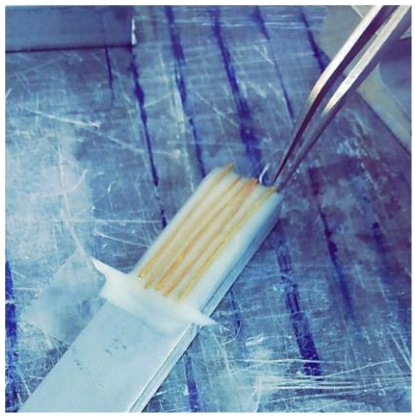


Figure 9. Long parallel date palm fibre arrangement along the bondline [71].

Researchers also investigated the effects of cork particles on the micro failure mechanisms and static strength of an epoxy adhesive, they found that cork acts as a crack stopper, stabilizes the crack propagation and prevents unstable crack growth inside the adhesive layer [115].

Several researchers were inspired by bones and trees to improve the interfacial bonding of adhesive joints [116-119]. For example, recently Wagih et al. [119] proposed a bio-inspired adhesive joint with improved interlaminar fracture toughness by generating sacrificial cracks inside the adhesive layer with specific topology that activates nonlocal dissipation damage mechanisms through the development of bridging ligaments. However, more research has to be done to simplify the manufacturing process in order to apply this method to real-life composite bonded structures,

There are other available methods for adhesive property tailoring in order to improve the overall bonded joint performance, such as: mixed-adhesive technique or functionally graded adhesive [72]. However, these methods are difficult to implement in practice due

to difficulties to manufacture these adhesive joints. Nevertheless, the application of adhesive modification method to adhesive joints with NFRC adherends is very limited; thus these techniques are not discussed in detail in this review.

It should be noted that when NFRC bonded joints are concerned, the properties of the adhesive have a drastic effect owing to the usually high mechanical properties of the commercially available structural adhesives. As has been previously discussed in this review, high adhesive toughness will directly influences the transverse stresses in the bonded adherends and this is directly linked to the initiation of intralaminar delamination failures. Thus, careful adhesive selection for NFRC adherend bonding is fundamental.

4. Challenges and future developments

Figure 10 summarizes the main effects on the performance of composite bonded joints as a function of the optimization technique used. It can be seen that each method has positive effects on the performance of the bonded joint, but also presents certain downsides. The selection of the most suitable technique for performance improvement of NFRC bonded joints is therefore a complex task. So far, the hybridization technique has clearly demonstrated its ability to improve the NFRC adherend properties and the bonded joint efficiency at relatively low fabrication complexity. In addition, synthetic interlaminar hybridization also provides benefits by acting as a barrier to moisture, increasing the service life of natural/synthetic fibre reinforced composite structures.

The joint strength can also be improved by local geometry modification, including the local modification of adherends or adhesive. Geometry local optimization through taper and spew fillet shaping represent an effective way to reduce the high peak peel stresses at the bondline edges. However, the overall joint topology must be designed carefully so that both local and global modifications complement each other.

Local, or global adherend surface toughening and adhesive tailoring are also promising techniques to improve the efficiency of NFRCs bonded joints. These methods can be used together with the methods that focus on reducing the local peel stress concentration in NFRC adherends.

Despite the higher fabrication complexity, the field of multi-dimensional fibre architectures (i.e., stitching, knitting, braiding, through-the-thickness reinforcements) also presents many possible applications for toughening both the adherend and the entire

overlap zone. Especially when coupled with hybrid natural/natural and natural/synthetic architectures to leverage the specific advantages of each fibre. This would significantly decrease the delamination tendency of NFRC bonded joints by increasing the transverse properties of the adherend/joint.

The comparison of different techniques to improve the joint strength show that most of the techniques available come with an increase in the complexity of the manufacturing process, which will increase the cost of the final products. Thus, a balance of the strength gain and cost increase should be taken into account when more complex design and optimization processes are considered. In addition, increasing the complexity of design stands in contradiction to the need for simple, cheap and robust solutions for products based on NFRC.

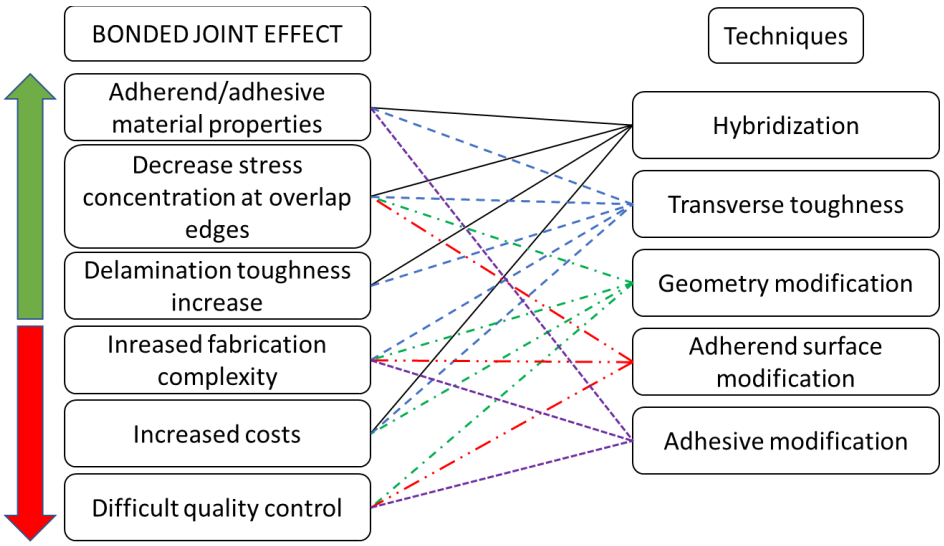


Figure 10. General trends of main effects on the performance of composite bonded joints as a function of the optimization technique.

Some of the main challenges and opportunities for adhesive bonded structures with NFRC adherends, that will need significant research efforts going forward, are listed below:

- Given their complexity and relatively recent development, there is a need for the development of robust design and process simulation tools for NFRC joining processes. The development of predictive numerical models would allow for a better understanding of all the phenomena involved. This would greatly advance the understanding of these processes and promote further process development and optimization to expand their area of applications in industry.

- There is a need to investigate the effect of environmental factors (e.g., the influence of radiation, humidity and temperature) on the NFRC adhesive joints. These issues will need to be addressed before any potential implementation of joining technologies involving NFRCs in industry.
- In several industries (e.g., automotive, rail and naval transport industries), the use of NFRCs could be considered as a potential solution, in order to reduce the mass as well as the manufacturing cost and mainly due to the increasing aspirations for more environmental-friendly technologies and light-weight materials. The joining of polymers, composites, and multi-material structures for industrial applications is still a growing research and development area. Thus, there is a need for new developments on joining technologies for these materials.
- Finally, another area currently developing fast is the application of natural reinforcements in additive manufacturing (AM, 3D printing). This technology allows for the fabrication of complex geometries without the need for expensive tooling and moulds. The use of natural fibres as filament reinforcement presents many advantages such as being environmentally friendly, fabrication of renewable and recyclable parts with a high degree of property tailoring. However, significant challenges remain to be solved such as: fabricating composite filaments, difficult quality control due to voids and porosities, fibre orientation and natural fibre moisture content and tendency to absorb humidity.

5. Conclusions

The application of natural fibre composites, particularly in automotive, civil industry and sports is quite promising and will continually increase in the future due to the significant pressure on reducing costs and increasing demand for material recyclability. This paper presents an overview of recent advancements in the main methods used to increase the performance of composite adhesive joints with focus on joints with natural fibre reinforced composite adherends. There are several techniques available that aim at improving adherend/adhesive properties as well as local/global stress distributions. In general, the goal of these techniques is to ultimately eliminate delamination failures and maximize efficiency through joint design. The hybridization of the NFRC adherends is the most studied and successful technique used so far. However, there is still a wide scope

for further improvement using other techniques discussed in this paper, which have not yet been applied in NFRC bonded joints. In this context, the most promising methods focus on improving the adherend properties (i.e., in-plane and transverse) and overlap edge stress state tailoring (i.e., hybridization, wavy overlap geometries, fillets/tapers, 3D reinforcements). Although, nowadays, several innovative and powerful techniques are available they still need detailed experimental validation for natural fibre composite joints. Emerging trends in manufacturing such as light weighting, increased use of multi-material structures and the need for more environmentally friendly materials motivate growing research efforts in the joining technologies of natural fibre composites.

REFERENCES

1. Neto, J., et al., *A Review of Recent Advances in Hybrid Natural Fiber Reinforced Polymer Composites.* Journal of Renewable Materials, 2022. **10**(3): p. 561--589.
2. Pickering, K.L., M.G.A. Efendy, and T.M. Le, *A review of recent developments in natural fibre composites and their mechanical performance.* Composites Part A: Applied Science and Manufacturing, 2016. **83**: p. 98-112.
3. Li, M., et al., *Recent advancements of plant-based natural fiber–reinforced composites and their applications.* Composites Part B: Engineering, 2020. **200**: p. 108254.
4. Akampumuza, O., et al., *Review of the applications of biocomposites in the automotive industry.* Polymer Composites, 2017. **38**(11): p. 2553-2569.
5. Fitzgerald, A., et al., *A Life Cycle Engineering Perspective on Biocomposites as a Solution for a Sustainable Recovery.* Sustainability, 2021. **13**(3): p. 1160.
6. Islam, M.S. and S.J.U. Ahmed, *Influence of jute fiber on concrete properties.* Construction and Building Materials, 2018. **189**: p. 768-776.
7. Benzait, Z. and L. Trabzon, *A review of recent research on materials used in polymer–matrix composites for body armor application.* Journal of Composite Materials, 2018. **52**(23): p. 3241-3263.
8. Braga, F.d.O., et al., *High energy ballistic and fracture comparison between multilayered armor systems using non-woven curaua fabric composites and aramid laminates.* Journal of Materials Research and Technology, 2017. **6**(4): p. 417-422.
9. Sanjay, M., et al., *A comprehensive review of techniques for natural fibers as reinforcement in composites: Preparation, processing and characterization.* Carbohydrate polymers, 2019. **207**: p. 108-121.
10. Silva, R.V. and E.M.F. Aquino, *Curaua Fiber: A New Alternative to Polymeric Composites.* Journal of Reinforced Plastics and Composites, 2008. **27**(1): p. 103-112.
11. Demosthenes, L.C.d.C., et al., *Thermal and structural characterization of buriti fibers and their relevance in fabric reinforced composites.* Journal of Materials Research and Technology, 2020. **9**(1): p. 115-123.
12. Chaudhary, V., P.K. Bajpai, and S. Maheshwari, *Effect of moisture absorption on*

the mechanical performance of natural fiber reinforced woven hybrid bio-composites. Journal of Natural Fibers, 2020. **17**(1): p. 84-100.

13. Maslinda, A.B., et al., *Effect of water absorption on the mechanical properties of hybrid interwoven cellulosic-cellulosic fibre reinforced epoxy composites.* Composite Structures, 2017. **167**: p. 227-237.
14. Yorseng, K., et al., *Influence of Accelerated Weathering on the Mechanical, Fracture Morphology, Thermal Stability, Contact Angle, and Water Absorption Properties of Natural Fiber Fabric-Based Epoxy Hybrid Composites.* Polymers, 2020. **12**(10): p. 2254.
15. Banea, M.D., J.S.S. Neto, and D.K.K. Cavalcanti, *Recent Trends in Surface Modification of Natural Fibres for Their Use in Green Composites*, in *Green Composites*, S. Thomas and P. Balakrishnan, Editors. 2021, Springer Singapore: Singapore. p. 329-350.
16. Choudhury, M.R. and K. Debnath, *Green Composites: Introductory Overview*, in *Green Composites*, S. Thomas and P. Balakrishnan, Editors. 2021, Springer Singapore: Singapore. p. 1-20.
17. El Messiry, M., *Green Composite as an Adequate Material for Automotive Applications*, in *Green Composites*, S. Thomas and P. Balakrishnan, Editors. 2021, Springer Singapore: Singapore. p. 151-208.
18. Mahmud, S., et al., *Comprehensive review on plant fiber-reinforced polymeric biocomposites.* Journal of Materials Science, 2021. **56**(12): p. 7231-7264.
19. Budhe, S., S. de Barros, and M.D. Banea, *Theoretical assessment of the elastic modulus of natural fiber-based intra-ply hybrid composites.* Journal of the Brazilian Society of Mechanical Sciences and Engineering, 2019. **41**(6).
20. Banea, M.D. and L.F.M. da Silva, *Adhesively bonded joints in composite materials: an overview.* Proceedings of the Institution of Mechanical Engineers Part L-Journal of Materials-Design and Applications, 2009. **223**(L1): p. 1-18.
21. Kupski, J. and S. Teixeira de Freitas, *Design of adhesively bonded lap joints with laminated CFRP adherends: Review, challenges and new opportunities for aerospace structures.* Composite Structures, 2021. **268**: p. 113923.
22. Banea, M.D., *Dissimilar Joining of PMCs to Metals – Adhesive Bonding*, in *Encyclopedia of Materials: Composites*, D. Brabazon, Editor. 2021, Elsevier:

Oxford. p. 324-333.

23. Campilho, R.D.S.G., et al., *Fracture toughness determination of adhesive and co-cured joints in natural fibre composites.* Composites Part B: Engineering, 2013. **50**: p. 120-126.
24. de Queiroz, H.F.M., M.D. Banea, and D.K.K. Cavalcanti, *Experimental analysis of adhesively bonded joints in synthetic- and natural fibre-reinforced polymer composites.* Journal of Composite Materials, 2020. **54**(9): p. 1245-1255.
25. Gonzalez-Murillo, C. and M.P. Ansell, *Co-cured in-line joints for natural fibre composites.* Composites Science and Technology, 2010. **70**(3): p. 442-449.
26. Melese, K.G. and I. Singh, *Joining Behavior of Jute/Sisal Fibers Based Epoxy Laminates Using Different Joint Configurations.* Journal of Natural Fibers, 2020: p. 1-12.
27. Mittal, A., A. Deb, and C. Chou, *A Study into the Mechanical Behavior of Adhesively-Bonded Jute Fiber-Reinforced Composite*. 2015, SAE International.
28. Mostafa, N.H., *Tensile and fatigue properties of Jute-Glass hybrid fibre reinforced epoxy composites.* Materials Research Express, 2019. **6**(8): p. 085102.
29. Ramesh, M., K. Palanikumar, and K.H. Reddy, *Mechanical property evaluation of sisal–jute–glass fiber reinforced polyester composites.* Composites Part B: Engineering, 2013. **48**: p. 1-9.
30. Yoon, H.C., et al., *Effects of Adhesive Joint on the Failure Strength Properties of Natural Fiber Reinforced Composite.* Key Engineering Materials, 2007. **353-358**: p. 1960-1964.
31. Ferreira, J.M., et al., *Stress analysis of lap joints involving natural fibre reinforced interface layers.* Composites Part B-Engineering, 2005. **36**(1): p. 1-7.
32. Hilton, A., S.Y. Lee, and K. Supar, *Static Strength of Adhesively-bonded Woven Fabric Kenaf Composite Plates.* IOP Conference Series: Materials Science and Engineering, 2017. **205**: p. 012019.
33. Roy Choudhury, M. and K. Debnath, *Experimental analysis of tensile and compressive failure load in single-lap adhesive joint of green composites.* International Journal of Adhesion and Adhesives, 2020. **99**: p. 102557.
34. Ramakrishnan, K.R., et al., *Experimental study of adhesively bonded natural fibre composite – steel hybrid laminates.* Composites Part C: Open Access, 2021: p.

100157.

35. Wang, S., et al., *Dynamic response and fracture analysis of basalt fiber reinforced plastics and aluminum alloys adhesive joints.* Composite Structures, 2021. **268**.
36. Banea, M.D., *Influence of adherend properties on the strength of adhesively bonded joints.* MRS Bulletin, 2019. **44**(8): p. 625-629.
37. Adams, R.D., *Strength Predictions for Lap Joints, Especially with Composite Adherends. A Review*. The Journal of Adhesion, 1989. **30**(1-4): p. 219-242.
38. Budhe, S., et al., *An updated review of adhesively bonded joints in composite materials.* International Journal of Adhesion and Adhesives, 2017. **72**: p. 30-42.
39. Astm, D., *5573-99. Standard practice for classifying failure modes in fiber-reinforced-plastic (FRP) joints.* Annual book of ASTM standards, 2002. **15**(03).
40. Li, S., et al., *A study of laser surface treatment in bonded repair of composite aircraft structures.* Royal Society Open Science, 2018. **5**(3): p. 171272.
41. Banea, M.D., et al., *Multi-material adhesive joints for automotive industry.* Composites Part B: Engineering, 2018. **151**: p. 71-77.
42. de Queiroz, H.F.M., M.D. Banea, and D.K.K. Cavalcanti, *Adhesively bonded joints of jute, glass and hybrid jute/glass fibre-reinforced polymer composites for automotive industry.* Applied Adhesion Science, 2021. **9**(1): p. 2.
43. Esteves, J.L. and C. Romão, *Adhesive joints for vegetal natural fibres reinforced composites.* IV International Materials Simposium, 2007.
44. Melese, K.G., T.P. Naik, and I. Singh, *Adhesive joining of sisal/jute/hybrid composites with drilled holes in lap area.* Proceedings of the Institution of Mechanical Engineers, Part L: Journal of Materials: Design and Applications, 2021. **235**(2): p. 255-264.
45. Pisanu, L., et al., *Strength shear test for adhesive joints between dissimilar materials obtained by multicomponent injection.* International Journal of Adhesion and Adhesives, 2018. **86**: p. 22-28.
46. Banea, M.D., L.F.M. Da Silva, and R. Campilho, *The Effect of Adhesive Thickness on the Mechanical Behavior of a Structural Polyurethane Adhesive.* Journal of Adhesion, 2015. **91**(5): p. 331-346.
47. Banea, M.D. and L.F.M. Da Silva, *Static and fatigue behaviour of room temperature vulcanising silicone adhesives for high temperature aerospace*

applications. Materialwissenschaft und Werkstofftechnik, 2010. **41**(5): p. 325-335.

48. Banea, M.D. and L.F.M. da Silva, *Mechanical characterization of flexible adhesives.* Journal of Adhesion, 2009. **85**(4-5): p. 261-285.
49. da Silva, L.F.M., et al., *Effect of adhesive type and thickness on the lap shear strength.* Journal of Adhesion, 2006. **82**(11): p. 1091-1115.
50. Gleich, D.M., M.L. Van Tooren, and A. Beukers, *Analysis and evaluation of bondline thickness effects on failure load in adhesively bonded structures.* Journal of Adhesion Science and Technology, 2001. **15**(9): p. 1091-1101.
51. Banea, M.D. and L.F.M. Da Silva, *The effect of temperature on the mechanical properties of adhesives for the automotive industry.* Proceedings of the Institution of Mechanical Engineers, Part L: Journal of Materials: Design and Applications, 2010. **224**(2): p. 51-62.
52. Banea, M.D., et al., *Effect of material on the mechanical behaviour of adhesive joints for the automotive industry.* Journal of Adhesion Science and Technology, 2017. **31**(6): p. 663-676.
53. Neto, J.A.B.P., R.D.S.G. Campilho, and L.F.M. Da Silva, *Parametric study of adhesive joints with composites.* International Journal of Adhesion and Adhesives, 2012. **37**: p. 96-101.
54. Banea, M.D., L.F.M. da Silva, and R.D.S.G. Campilho, *Principles of adhesive bonding*, in *Joining of Polymer-Metal Hybrid Structures: Principles and Applications*. 2018. p. 3-27.
55. Kureemun, U., et al., *Effects of hybridization and hybrid fibre dispersion on the mechanical properties of woven flax-carbon epoxy at low carbon fibre volume fractions.* Composites Part B: Engineering, 2018. **134**: p. 28-38.
56. Abd El-baky, M. and M. Attia, *Water absorption effect on the in-plane shear properties of jute–glass–carbon-reinforced composites using Iosipescu test.* Journal of Composite Materials, 2019. **53**(21): p. 3033-3045.
57. Cheng, M., et al., *Environmental durability of carbon/flax fiber hybrid composites.* Composite Structures, 2020. **234**: p. 111719.
58. Ahmed, K.S. and S. Vijayarangan, *Tensile, flexural and interlaminar shear properties of woven jute and jute-glass fabric reinforced polyester composites.*

Journal of Materials Processing Technology, 2008. **207**(1): p. 330-335.

59. Manteghi, S., et al., *Investigation of the mechanical properties and failure modes of hybrid natural fiber composites for potential bone fracture fixation plates.* Journal of the Mechanical Behavior of Biomedical Materials, 2017. **65**: p. 306-316.
60. Cavalcanti, D.K.K., et al., *Mechanical characterization of intralaminar natural fibre-reinforced hybrid composites.* Composites Part B: Engineering, 2019. **175**: p. 107149.
61. Neto, J.S.S., et al., *Effect of chemical treatment on the thermal properties of hybrid natural fiber-reinforced composites.* Journal of Applied Polymer Science, 2019. **136**(10): p. 47154.
62. de Araujo Alves Lima, R., et al., *Effect of surface treatments on interfacial properties of natural intralaminar hybrid composites.* Polymer Composites, 2020. **41**(1): p. 314-325.
63. Gholampour, A. and T. Ozbakkaloglu, *A review of natural fiber composites: properties, modification and processing techniques, characterization, applications.* Journal of Materials Science, 2020. **55**(3): p. 829-892.
64. Blackman, B.R.K., et al., *The fracture behaviour of adhesively-bonded composite joints: Effects of rate of test and mode of loading.* International Journal of Solids and Structures, 2012. **49**(13): p. 1434-1452.
65. Fernandes Medeiros de Queiroz, H., et al., *The effect of multiscale hybridization on the mechanical properties of natural fiber-reinforced composites.* Journal of Applied Polymer Science, 2021. **138**(41): p. 51213.
66. Razavi, S.M.J., et al., *Single lap joints bonded with structural adhesives reinforced with a mixture of silica nanoparticles and multi walled carbon nanotubes.* International Journal of Adhesion and Adhesives, 2018. **80**: p. 76-86.
67. Schollerer, M.J., et al., *Surface toughening – a concept to decrease stress peaks in bonded joints.* The Journal of Adhesion, 2019. **95**(5-7): p. 495-514.
68. Chandrasekar, M., et al., *Mechanical Properties of a Novel Fibre Metal Laminate Reinforced with the Carbon, Flax, and Sugar Palm Fibres.* Bioresources, 2018. **13**: p. 5725-5739.
69. Guo, Y., et al., *Novel interface strengthening and toughening method of*

steel/PEEK single lap joints with multi-scale combined features. Journal of Adhesion Science and Technology, 2021. **35**(15): p. 1637-1651.

70. Kanani, A.Y., X. Hou, and J. Ye, *A novel dissimilar single-lap joint with interfacial stiffness improvement.* Composite Structures, 2020. **252**: p. 112741.
71. Delzendehrooy, F., et al., *Strength improvement of adhesively bonded single lap joints with date palm fibers: Effect of type, size, treatment method and density of fibers.* Composites Part B: Engineering, 2020. **188**: p. 107874.
72. Shang, X., et al., *Review on techniques to improve the strength of adhesive joints with composite adherends.* Composites Part B: Engineering, 2019. **177**: p. 107363.
73. Adams, R.D. and J.A. Harris, *The influence of local geometry on the strength of adhesive joints.* International Journal of Adhesion and Adhesives, 1987. **7**(2): p. 69-80.
74. Zeng, Q.-G. and C.T. Sun, *Novel Design of a Bonded Lap Joint.* AIAA Journal, 2001. **39**(10): p. 1991-1996.
75. Nosouhi, F., M. Farahani, and M. Ansari, *Experimental and numerical study on the composite adhesive joint reinforcement using wavy edge.* Journal of Adhesion Science and Technology, 2018. **32**(9): p. 1007-1017.
76. Ávila, A.F. and P.n.d.O. Bueno, *Stress analysis on a wavy-lap bonded joint for composites.* International Journal of Adhesion and Adhesives, 2004. **24**(5): p. 407-414.
77. Ashrafi, M., et al., *Adhesively bonded single lap joints with non-flat interfaces.* International Journal of Adhesion and Adhesives, 2012. **32**: p. 46-52.
78. Razavi, S.M.J., et al., *Parametric study of adhesive joints with non-flat sinusoid interfaces.* Theoretical and Applied Fracture Mechanics, 2018. **93**: p. 44-55.
79. Salve, A., R. Kulkarni, and A. Mache. *A Review: Fiber Metal Laminates (FMl s) - Manufacturing, Test Methods and Numerical Modeling*. 2016.
80. Abd El-Baky, M.A., et al., *Fabrication of Cost Effective Fiber Metal Laminates Based on Jute and Glass Fabrics for Enhanced Mechanical Properties.* Journal of Natural Fibers, 2020: p. 1-16.
81. Qu, Z., et al., *Evaluation of Nano-Mechanical Behavior on Flax Fiber Metal Laminates Using an Atomic Force Microscope.* Materials, 2019. **12**(20): p. 3363.

82. Hussain, M., et al., *Properties and characterization of novel 3D jute reinforced natural fibre aluminium laminates.* Journal of Composite Materials, 2020. **55**: p. 1879 - 1891.
83. Mohammed, I., et al., *Mechanical Properties of Fibre-Metal Laminates Made of Natural/Synthetic Fibre Composites.* Bioresources, 2018. **13**: p. 2022-2034.
84. Vieira, L.M.G., et al., *Novel fibre metal laminate sandwich composite structure with sisal woven core.* Industrial Crops and Products, 2017. **99**: p. 189-195.
85. Bahari-Sambran, F., et al., *The effect of surface modified nanoclay on the interfacial and mechanical properties of basalt fiber metal laminates.* Thin-Walled Structures, 2019. **144**: p. 106343.
86. Islam, M.S. and L. Tong, *Influence of pinning on static strength of co-cured metal-GFRP hybrid single lap joints.* Composites Part A: Applied Science and Manufacturing, 2016. **84**: p. 196-208.
87. Chang, P., A.P. Mouritz, and B.N. Cox, *Properties and failure mechanisms of pinned composite lap joints in monotonic and cyclic tension.* Composites Science and Technology, 2006. **66**(13): p. 2163-2176.
88. Koh, T., et al., *Improving the structural properties and damage tolerance of bonded composite joints using z-pins.* Journal of Composite Materials, 2012. **46**(26): p. 3255-3265.
89. Beylergil, B., Y. Cunedioglu, and A. Aktas, *Experimental and numerical analysis of single lap composite joints with inter-adherend fibers.* Composites Part B: Engineering, 2011. **42**(7): p. 1885-1896.
90. Arnautov, A., et al., *Experimental Characterization of the Properties of Double-Lap Needled and Hybrid Joints of Carbon/Epoxy Composites.* Materials, 2015. **8**(11): p. 7578-7586.
91. Fei, S., et al., *Strengthening of composite T-joints using Ø 0.11 mm Z-pins via an ultrasound-guided insertion process.* Composites Part C: Open Access, 2022. **8**.
92. Bogdanovich, A.E., et al., *Experimental study of joining thick composites reinforced with non-crimp 3D orthogonal woven E-glass fabrics.* Composites Part A: Applied Science and Manufacturing, 2011. **42**(8): p. 896-905.
93. Aymerich, F., R. Onnis, and P. Priolo, *Analysis of the fracture behaviour of a stitched single-lap joint.* Composites Part A: Applied Science and Manufacturing,

2005. **36**(5): p. 603-614.

94. Reeder, J.R. and E.H. Glaessgen, *Debonding of Stitched Composite Joints under Static and Fatigue Loading.* Journal of Reinforced Plastics and Composites, 2004. **23**(3): p. 249-263.
95. Kumar, J., et al., *Joining behavior of polymeric composites fabricated using agricultural waste as fillers.* Journal of Adhesion Science and Technology, 2021. **35**(15): p. 1652-1663.
96. Bagheri, M.R., et al., *The effect of nanoparticles in single-lap composite joints studied by experimental and numerical analyses.* Iranian Polymer Journal, 2015. **24**(8): p. 629-640.
97. Prasad, V., et al., *Enhancing Mode I and Mode II interlaminar fracture toughness of flax fibre reinforced epoxy composites with nano TiO2.* Composites Part A: Applied Science and Manufacturing, 2019. **124**: p. 105505.
98. Quan, D., J.L. Urdániz, and A. Ivanković, *Enhancing mode-I and mode-II fracture toughness of epoxy and carbon fibre reinforced epoxy composites using multi-walled carbon nanotubes.* Materials & Design, 2018. **143**: p. 81-92.
99. Ladani, R.B., et al., *Delamination toughening and healing performance of woven composites with hybrid z-fibre reinforcement.* Composites Part A: Applied Science and Manufacturing, 2018. **110**: p. 258-267.
100. Nemati Giv, A., et al., *Effect of reinforcements at different scales on mechanical properties of epoxy adhesives and adhesive joints: a review.* The Journal of Adhesion, 2018. **94**(13): p. 1082-1121.
101. Doru, M.O., et al., *Effect of the Spew Fillet on Adhesively Bonded Single-Lap Joint Subjected to Tensile Loading: Experimental and 3-D Non-Linear Stress Analysis.* The Journal of Adhesion, 2014. **90**(3): p. 195-209.
102. Akpinar, S., et al., *The effect of the spew fillet on an adhesively bonded single-lap joint subjected to bending moment.* Composites Part B: Engineering, 2013. **55**: p. 55-64.
103. Zheng, G., et al., *Effect of spew fillet on adhesively bonded single lap joints with CFRP and aluminum-alloy immersed in distilled water.* International Journal of Adhesion and Adhesives, 2020. **99**: p. 102590.
104. Moya-Sanz, E.M., I. Ivañez, and S.K. Garcia-Castillo, *Effect of the geometry in*

the strength of single-lap adhesive joints of composite laminates under uniaxial tensile load. International Journal of Adhesion and Adhesives, 2017. **72**: p. 23-29.

105. Kim, K.-S., et al., *Failure mode and strength of uni-directional composite single lap bonded joints with different bonding methods.* Composite Structures, 2006. **72**(4): p. 477-485.
106. Marathe, U., M. Padhan, and J. Bijwe, *Carbon nanotubes- A powerful nano-filler for enhancing the performance properties of polyetherketoneketone composites and adhesives.* Composites Science and Technology, 2021. **210**: p. 108813.
107. Upadhyaya, P., et al., *Multiscale modeling of strength and failure behavior of carbon nanostructure reinforced epoxy composite adhesives in bonded systems.* European Journal of Mechanics - A/Solids, 2020. **80**: p. 103932.
108. Saraç, İ., H. Adin, and Ş. Temiz, *Investigation of the effect of use of Nano-Al2O3, Nano-TiO2 and Nano-SiO2 powders on strength of single lap joints bonded with epoxy adhesive.* Composites Part B: Engineering, 2019. **166**: p. 472-482.
109. Jojibabu, P., et al., *Effect of carbon nano-filler addition on the degradation of epoxy adhesive joints subjected to hygrothermal aging.* Polymer Degradation and Stability, 2017. **140**: p. 84-94.
110. Jouyandeh, M., et al., *High-performance epoxy-based adhesives reinforced with alumina and silica for carbon fiber composite/steel bonded joints.* Journal of Reinforced Plastics and Composites, 2016. **35**(23): p. 1685-1695.
111. Akhavan-Safar, A., et al., *Influence of Date Palm Tree Fibers on the Tensile Fracture Energy of an Epoxy-based Adhesive.* Journal of Natural Fibers, 2022.
112. Barbosa, A.Q., et al., *Methods to increase the toughness of structural adhesives with micro particles: An overview with focus on cork particles.* Materialwissenschaft und Werkstofftechnik, 2016. **47**(4): p. 307-325.
113. Mahdavi, S., H. Kermanian, and A. Varshoei, *Comparison of mechanical properties of date palm fiber- polyethylene composite.* BioResources, 2010. **5**(4): p. 2391-2403.
114. Kaddami, H., et al., *Short palm tree fibers - Thermoset matrices composites.* Composites Part A: Applied Science and Manufacturing, 2006. **37**(9): p. 1413-1422.
115. Akhavan-Safar, A., et al., *Micro failure analysis of adhesively bonded joints*

enhanced with natural cork particles: Impact of overlap length and particles volume fraction. Frattura ed Integrita Strutturale, 2018. **12**(46): p. 266-274.

116. Akrami, R., et al., *High-performance bio-inspired composite T-joints.* Composites Science and Technology, 2019. **184**.
117. Burns, L., et al., *Bio-inspired hierarchical design of composite T-joints with improved structural properties.* Composites Part B: Engineering, 2015. **69**: p. 222-231.
118. Munzinger, M., O. Kraft, and C. Mattheck, *Computer aided adhesive and assembly optimization method: Biomimetic optimization of adhesive joints.* Journal of Materials Research, 2006. **21**(8): p. 2011-2017.
119. Wagih, A., R. Tao, and G. Lubineau, *Bio-inspired adhesive joint with improved interlaminar fracture toughness.* Composites Part A: Applied Science and Manufacturing, 2021. **149**: p. 106530.

Paper 2

Bonded joint performance of novel 3D natural hybrid composites

A novel 3D fibre-reinforcement architecture for high performance natural fibre reinforced composite adhesively bonded joints

H.F.M. de Queiroz[1], J.S.S. Neto[1], D.K.K. Cavalcanti[1], M. D. Banea[1]
[1]Federal Center of Technological Education in Rio de Janeiro, Brazil.

Abstract

In this paper, the effect of a novel fibre reinforcement architecture in the adhesively bonded joint efficiency of natural fibre reinforced composites (NFRC) was investigated. Two different reinforcement techniques were used: intralaminar reinforcement (2D) and orthogonal-through-the-thickness reinforcement (3D). The aim of the novel architecture is to enhance the transverse properties of the adherend (transverse strength and fracture toughness) in order to delay or avoid delamination failures. A jute bidirectional fabric was used as a base primary reinforcement phase and curauá, sisal, ramie, hemp and glass fibres were used as secondary reinforcement phases for the 2D and 3D fibre reinforcement architectures. Single lap joints (SLJs) bonded with an epoxy adhesive used in the automotive industry were fabricated with these adherends and the efficiency of the joints was investigated by comparing them to glass (GFRP) and carbon (CFRP) pure synthetic fibre reinforced composite joints. It was found that the novel architecture was successful in reaching the failure load of the synthetic composite joints for SISAL 3D, CURAUÁ 2D and CURAUÁ 3D SLJs. Therefore, NFRC bonded joints can be a viable replacement for synthetic fibre composite joints at no load-bearing loss.

Keywords: natural fibres, mechanical properties, 3D architecture, bonded joints, hybrid composites.

1. INTRODUCTION

Environmentally conscious design has become front and centre in many industrial sectors owing to the mounting pressure to drastically decrease carbon emissions and overall environmental impact. Fibre-reinforced composite materials have been one of the go-to methods for decreasing the use of certain materials with very high energy required for fabrication (i.e., substituting metals for carbon fibre-reinforced composites (CFRPs)) as well as decreasing the overall structural weight while maintaining the required material properties [1]. However, while this was, and remains a highly valuable and used strategy, the need to further decrease the carbon footprint of composite structures continues to increase. In this context, natural fibre composites present a suitable solution for many of the issues presently facing composite materials owing to their much lower cost, energy to produce, weight and overall carbon footprint when compared to their synthetic counterparts. Though, there are still many challenges that need to be addressed such as the high variability in fibre quality and properties as well as their hydrophilic nature [2-5].

The joining of materials is also a vital area of intense study over the last few decades. Since many complex structures are fabricated with a large variety of different materials, an equally large variety of joining mechanisms are applied. Regarding composite materials specifically, it is well documented that the adhesive joining is the optimum technology given its advantages when compared to the classical mechanical joining techniques (i.e., bolts, screws, and rivets) [6]. However, this technology, while being the most suitable for joining composite materials to other composites as well as other materials, has its own challenges that need to be addressed, so that the highest efficiency may be achieved in the bonded joint. For instance, it is well known that delamination is the main problem in joining composites due to the high peel stress that occurs in the joints and the low transverse strength of the composites [6]. If the normal stress in a composite adherend exceeds its transverse strength, delamination failure within the composite will initiate, and propagate interlaminarly (usually between the first and second layers) as a function of its toughness. These stresses will increase with loading mode mixicity, high adherend axial modulus, low adherend thickness and high adhesive toughness [7]. Therefore, tailoring the properties of the adherend (elastic properties in the in-plane and transverse directions as well as careful geometry selection) is crucial for maximizing

composite bonded joint efficiency and decreasing or eliminating delamination failures [8, 9]. This is even more critical when joining NFRC composites. In a recent review article, the possible techniques that may be applied to NFRC bonded joints, to enhance the bonded joint efficiency were described in detail [10]. The adherend hybridization method (i.e., the use of different fibre types in the same composite) both natural/natural and natural/synthetic has presented the most promising results in both the intralaminar (both fibre phases in the same layer) and interlaminar (each fibre phase in a different layer) configurations [11-13]. For instance, de Queiroz et al. [14] have shown that intralaminar synthetic hybridization of jute and sisal composites via glass fibre had a significant effect on both adherend material properties and bonded joint strength. The synthetic fibre hybridization significantly improved the adherend material properties which also led to bonded joint performance enhancements. Melese et al. [13] investigated the effect of joint configuration and hybridization in the mechanical behaviour of pure jute, sisal and jute/sisal hybrid composite adherend bonded joints using SLJs, double strap butt joint and scarf-45^{o} joint. The highest joint strength reported was for the hybrid composite adherend joints, while the most efficient joint configuration was found to be the double strap butt joint. More recently, de Queiroz et al [11] studied experimentally the behaviour of SLJs made of natural, synthetic and interlaminar hybrid fibre-reinforced polymer composites. The effect of the number of the interlaminar synthetic layers required to match the bonded joint efficiency of a fully synthetic GFRP bonded joint was studied and a significant variation of joint behaviour as a function of adherend material was found (the failure load of the hybrid adherend joints increased by increasing the number of external synthetic layers (i.e., the failure load of hybrid 3-layer joint increased by 28.6% compared to hybrid 2-layer joint) and reached the pure synthetic adherends joint efficiency. Furthermore, other techniques such as local and global geometrical modifications, use of surface toughening agents, multi-scale reinforcement hybridization and transverse toughening, are also promising [10].

One of the possibilities explored in the literature to delay or avoid the onset of delamination failures within the composite adherends is to reinforce the adherends in the transverse direction by using different fibre reinforcement architectures [8]. There are a wide variety of reinforcement architectures available, and each present a different set of effects on the macroscopic mechanical properties of the composites (e.g., knitted, woven

or braided as well as orthogonal (OTT) or angular through-the-thickness or layer to layer interlocks) [15-20]. However, regarding specifically the enhancement of the out-of-plane (transverse) strength and delamination resistance of the composite, the woven 3D OTT fibre architecture was reported to be the most suitable [16]. The design of a 3D fibre reinforced composite allows for a relatively simple and effective solution to the known issue of low interlaminar properties in a classical composite laminate. A 3D woven composite is defined as consisting of in-plane layers that are interlocked in the transverse direction by z-binder fibres in the through-the-thickness direction with the aim of enhancing transverse strength and delamination toughness. Furthermore, the modes I and II fracture toughness are also expected to significantly increase [21]. On the other hand, there is an expected cost increase with more complex fibre architectures depending on many factors such as, type of loom, fibre, fibre treatments and preform architecture [22]. It is important to note that the in-plane properties of 3D woven composites are expected to be lower than their 2D counterparts, due to in-plane crimp [23].

Several researchers investigated the effect of 3D woven composite architectures in the mechanical behaviour of joints with synthetic fibre-reinforced composites [15, 24-26]. For instance, Bogdanovich et al. [24] studied both co-cured and adhesively bonded joints of composite adherends reinforced with non-crimp 3D orthogonal woven glass fibre fabrics and found that stitching resulted in significant increase in joint strength. Furthermore, the delamination failure was not observed within the 3D woven composite adherends due to the effect of the z-binders. Moreover, the application of novel techniques to delay the onset of delamination and to effectively improve the load carrying capability of adhesive joints with NFRC adherends is also necessary. To the best of the author's knowledge, a comprehensive experimental study on the effect of 3D architectures in NFRC bonded joint performance has not yet been published or assessed in the available literature. The main objective of this research was to investigate the use of a novel 3D orthogonal through-the-thickness fibre reinforcement along with an intralaminar reinforcement architecture (2D) to improve the mechanical properties of NFRC bonded joints. The main fibre phase was a jute bidirectional fabric, while the secondary reinforcement phases were curauá, sisal, hemp, ramie and glass fibres. Synthetic fibre reinforced composite bonded joints (i.e., CFRP and GFRP) were also fabricated and tested as points of comparison for bonded joint failure load. The failure modes of the

joints were analysed according to an ASTM standard.

2. EXPERIMENTAL DETAILS

2.1. Materials

Pure jute fibre bidirectional fabrics (P9, supplied by Sisalsul (São Paulo, Brazil)), were used as a base for the composite architecture. The intralaminar reinforcement technique was used in order to reinforce the jute fabrics. The reason for this is to essentially fabricate "unidirectional" (UD) fabrics with the secondary reinforcement fibre phases (i.e., curauá, sisal, ramie and hemp) since there are no commercially available UD fabrics of these fibres. The curauá fibres used were in-natura and supplied by the Federal University of Pará (Pará, Brazil). The curauá fibre bundles were manually selected and washed with distilled water in order to remove dirt and other impurities. They were then dried in an oven at 100 ºC until completely dry. Five layers of woven fabrics were used to fabricate the composite panels for all cases. The sisal (APAEB 700/1, Bahia, Brazil), ramie, hemp (Luli Têxtil, Blumenau, Brazil) and glass fibres (SE1200, Owens Corning, USA) were supplied as commercially available fibre rovings. The relevant physical and mechanical fibre properties can be seen in Table 1.

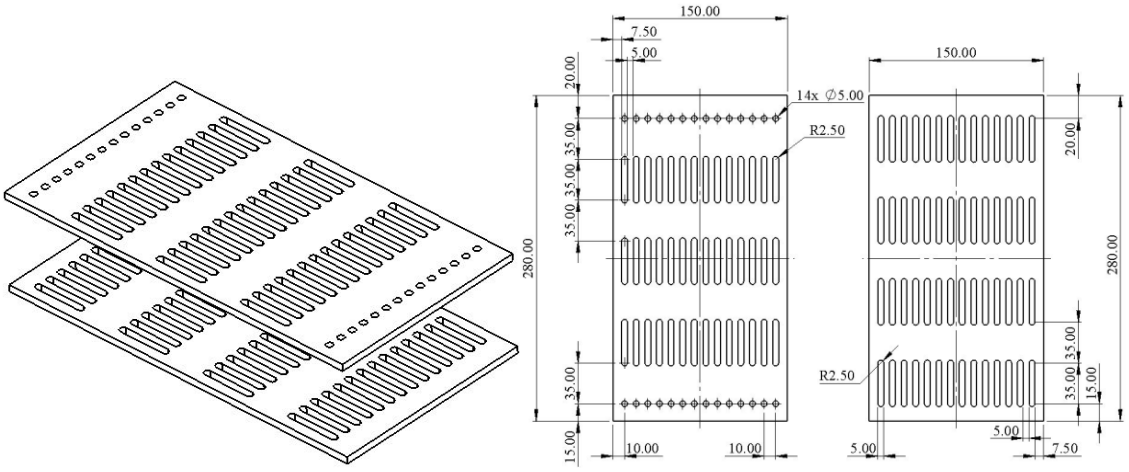
Table 1. Relevant physical and mechanical fibre properties [5, 27]

Fibres	Fibre diameter (μm)	Tensile strength (MPa)	Young's modulus (GPa)	Elongation at break (%)
Jute fibre	66 ± 13	254.46 ± 80.30	22.33 ± 10.10	2.52 ± 0.40
Sisal fibre	150 ± 1.0	398.48 ± 83.7	61.99 ± 25.3	2.74 ± 0.70
Ramie fibre	95 ± 50	212.32 ± 7.28	30.39 ± 10.8	2.62 ± 0.20
Curauá fibre	46 ± 13	1929.80 ± 249.50	87.23 ± 15.40	3.94 ± 0.60
Hemp fibre	305 ± 60	191 ± 38	20-70	1.0-4.0
Glass fibre*	-	2430	-	-

**Manufacturer data.*

The intralaminar reinforcement was fabricated via weaving the fibres through the plain weave jute base fabric in a pattern that skipped no columns and interweaved the weft rows by 8 spaces (see Fig. 1b and d). Next, for the 3D specimens, a 3D OTT reinforcement was woven through the 5 layers by way of a PLA 3D printed mask in order to control the architecture geometry of the dry preforms (see Fig. 1a and c). In other words, the

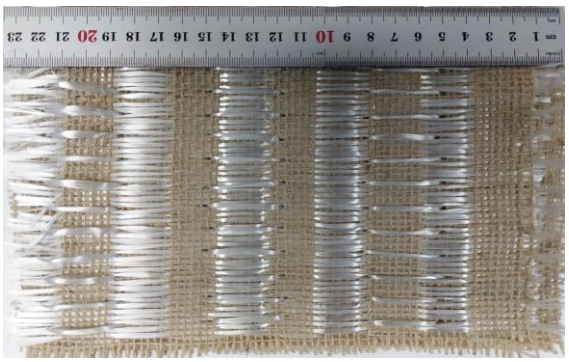
intralaminar only reinforced fabrics were placed between the 3D printed mask and the 3D reinforcement was woven through 5 layers to create the dry 3D fibre-reinforced preforms for all cases. The fibre weight fractions (in relation to the total weight of the fibre phases, resin and hardener) were approx. 30%, 24%, 20%, 22% and 18% for the curauá, sisal, ramie, hemp and glass intralaminar (2D) specimens, respectively. For the 3D fibre reinforcements, the weight fractions were approx. 3%, 2%, 4%, 1% and 2%, respectively. Pure synthetic fibre-reinforced specimens using bidirectional fabrics were also fabricated as points of comparison of bonded joint efficiency (GFRP and CFRP). Bidirectional fibre fabrics were used, and the same fabrication technique was applied (RE200P bidirectional glass fabrics as well as RC203P (800 tex and 193 g/m^2) for the carbon composite adherends (Barracuda Advanced Composites, SP, Brazil).



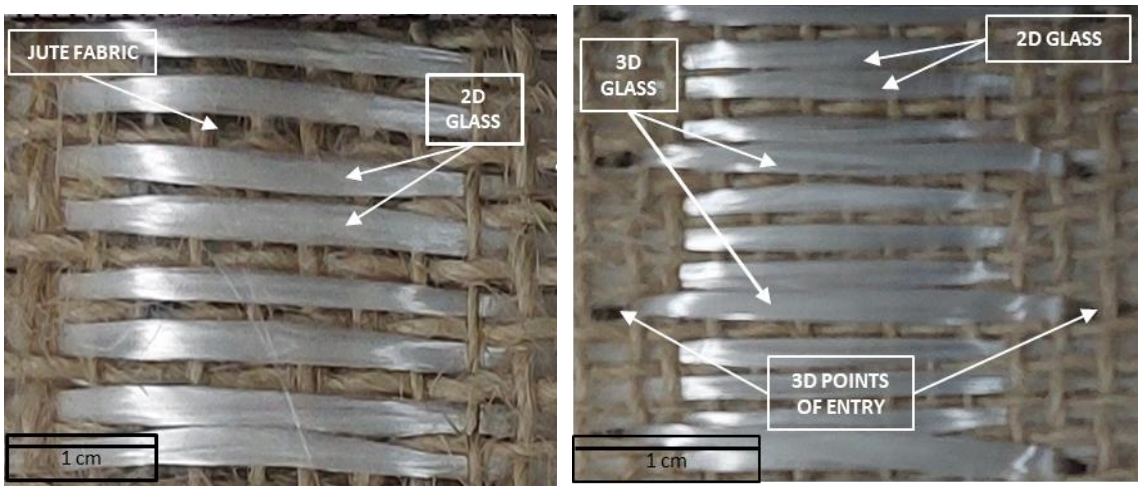
a)



b)



c)



d) e)

Figure 1. a) Scheme of the 3D reinforcement mask used to control the OTT reinforcement geometry, top and bottom (values in mm), b) representative photos of glass intralaminarly reinforced jute bidirectional fabric (2D), c) 3D glass reinforced dry preform (intralaminar reinforcement plus 3D), d) 2D reinforcement detail and e) 3D reinforcement detail.

A bicomponent epoxy resin matrix, HEX 135 SLOW (Barracuda Advanced Composites, SP, Brazil), was used in order to fabricate the composite panels. A bicomponent automotive-grade ductile epoxy structural modern adhesive, BETAMATE^{TM} 2096 (DuPont, Brazil), was used to fabricate the single lap joint specimens. The material properties can be seen in Table 2.

Table 2. Mechanical properties of the resin and adhesive used [11].

Polymer	Tensile strength (MPa)	Young's modulus (GPa)	Tensile strain (%)
BETAMATE^{TM} 2096	34.27 ± 1.52	1.6 ± 0.10	8.04 ± 0.39
HEX 135 SLOW	60.92 ± 1.42	3.25 ± 0.008	3.20 ± 0.20

2.2. Substrate specimen manufacture and characterization

The composites were fabricated using the compression moulding technique using a steel mould and a heated hydraulic press, Solab SL 20 (São Paulo, Brazil). The composite curing followed the manufacturer's guidelines at 70 degrees Celsius for 8 hours under pressure. The composite panel thickness was approx. 6 mm and it was controlled via steel

spacers. The tensile and SLJ specimens were cut from the panels via tungsten carbide blade. The tensile specimens followed the ASTM D3039 geometry guidelines.

The specimens received a simple nomenclature as a function of type of fibre reinforcement (nature and architecture). The 2D means only the intralaminar reinforcement is present, while the 3D means that both the intralaminar and 3D OTT reinforcement architectures are present simultaneously. For example, HEMP 2D: bidirectional jute fabric reinforced by hemp fibre roving intralaminarly (woven through the jute fabric in a 8-row configuration skipping no columns (see Fig. 1a).

All the composite materials used as adherends were characterised by tensile tests using a universal Instron®5966 testing machine (Norwood, Massachusetts, USA). A 10 kN load cell and a crosshead speed of 1 mm/min was used. The mechanical properties of the adherend materials are summarised in Table 3. It can be seen, somewhat surprisingly, that the 3D architecture reinforcement presented no significant variation when compared to the 2D specimens for all cases. According to the available literature (for synthetic fibre-reinforced composites), a decrease in the in-plane mechanical properties is to be expected as a trade-off for the higher fracture toughness and transverse composite properties afforded by the 3D architecture [23]. This is likely due to the chosen architecture, for two reasons; first, the ratio of the length of the 3D fibres in the main direction (the ones that are on the surfaces of the composite) compared to the ones in the transverse direction (going through-the-thickness), is approx. 6. That means that they are helping to resist the main direction of loading and manage to counter the deleterious effect of the orthogonal direction reinforcement. Second, the number of points in which the 3D fibre goes through the composite specimen in the useful area of the tensile coupon (the exposed specimen between the clamps of the machine) is approx. 5. This is relevant due to the fact that these points are likely high stress concentration points (high crimp of the fibre and a resin-rich zone, see Fig. 1e). The failure modes of the tensile specimens were generally brittle for the hybrid specimens, due to the brittle nature of the jute fibre. On the other hand, for the pure synthetic specimens a mixed mode of delamination was observed. Overall, it was found that the chosen 3D + 2D reinforcement architecture presented an optimum balance which affords the desired transverse property increase due to the presence of the OTT fibres as well as maintaining the mechanical properties of the composites.

Table 3. Mechanical properties of the adherends.

Composite type	Tensile strength (MPa)	Young's modulus (GPa)	Tensile strain (%)
JFRP	63.13 ± 0.78	6.06 ± 0.46	1.15 ± 0.0015
HEMP 2D	74.54 ± 3.12	8.04 ± 1.01	1.28 ± 0.001
HEMP 3D	87.78 ± 9.17	8.16 ± 0.99	1.46 ± 0.0032
RAMIE 2D	85.25 ± 4.27	10.69 ± 1.44	1.15 ± 0.0019
RAMIE 3D	84.77 ± 8.96	10.74 ± 1.66	1.26 ± 0.0032
SISAL 2D	96.98 ± 7.57	10.16 ± 0.12	1.04 ± 0.002
SISAL 3D	91.88 ± 7.04	9.90 ± 1.19	1.76 ± 0.006
CURAUÁ 2D	150.26 ± 12.72	17.79 ± 2.81	1.04 ± 0.002
CURAUÁ 3D	145.01 ± 10.81	15.78 ± 0.72	1.08 ± 0.001
GLASS 2D	161.26 ± 8.72	13.45 ± 1.66	1.59 ± 0.002
GLASS 3D	162.26 ± 9.72	13.83 ± 0.75	1.45 ± 0.0008
GFRP	197.85 ± 19.54	20.16 ± 4.86	2.00
CFRP	641.44 ± 26.20	65.88 ± 9.53	1.1 ± 0.20

2.3 SLJ specimen fabrication

The bonded joint was fabricated by first abrading the overlap area (12.5x25 mm) with a 100-grit sandpaper in a 45^{o} criss-cross pattern in order to remove impurities and demoulding agent remnants. Then, the surface was blown with compressed air to remove the debris and thoroughly cleaned with 99% acetone to completely degrease and clean the surface. The adhesive was then mixed and applied to the adherends. A metallic mould with steel spacers in order to control the joint geometry and avoid spew fillets was used [28]. The adhesive thickness was kept at 0.2 mm with the aid of steel spacers. Alignment tabs were used during testing to reduce the peel stresses. Figure 2 presents the representative scheme of the SLJ geometry.

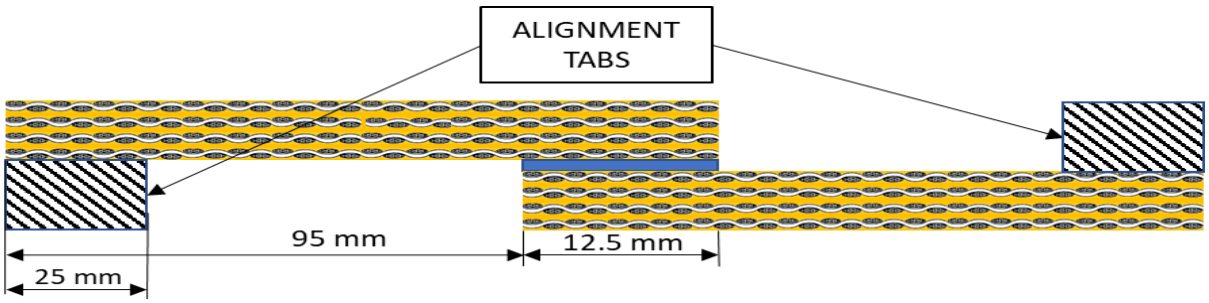


Figure 2. Representative SLJ geometry.

2.4. Test method

All specimens were tested in traction via a universal testing machine Instron®5966 equipped with a 10 kN load cell, at a crosshead speed of 1 mm/min (see Fig. 3). At least four specimens were tested for each case at room temperature. Load-displacement curves were recorded during the test.

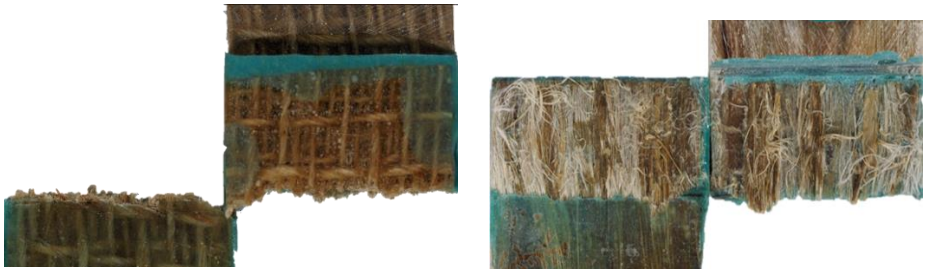


Figure 3. Representative SLJ test set-up.

3. RESULTS AND DISCUSSION

3.1. Failure analysis of the bonded joints

After the tests, the failure surface of the bonded joint specimens was visually analysed in accordance with the international standard ASTM D5573 [29]. Representative failure modes can be seen in Fig. 4 for the 2D and Fig. 5 for the 3D SLJ specimens.



a) b)

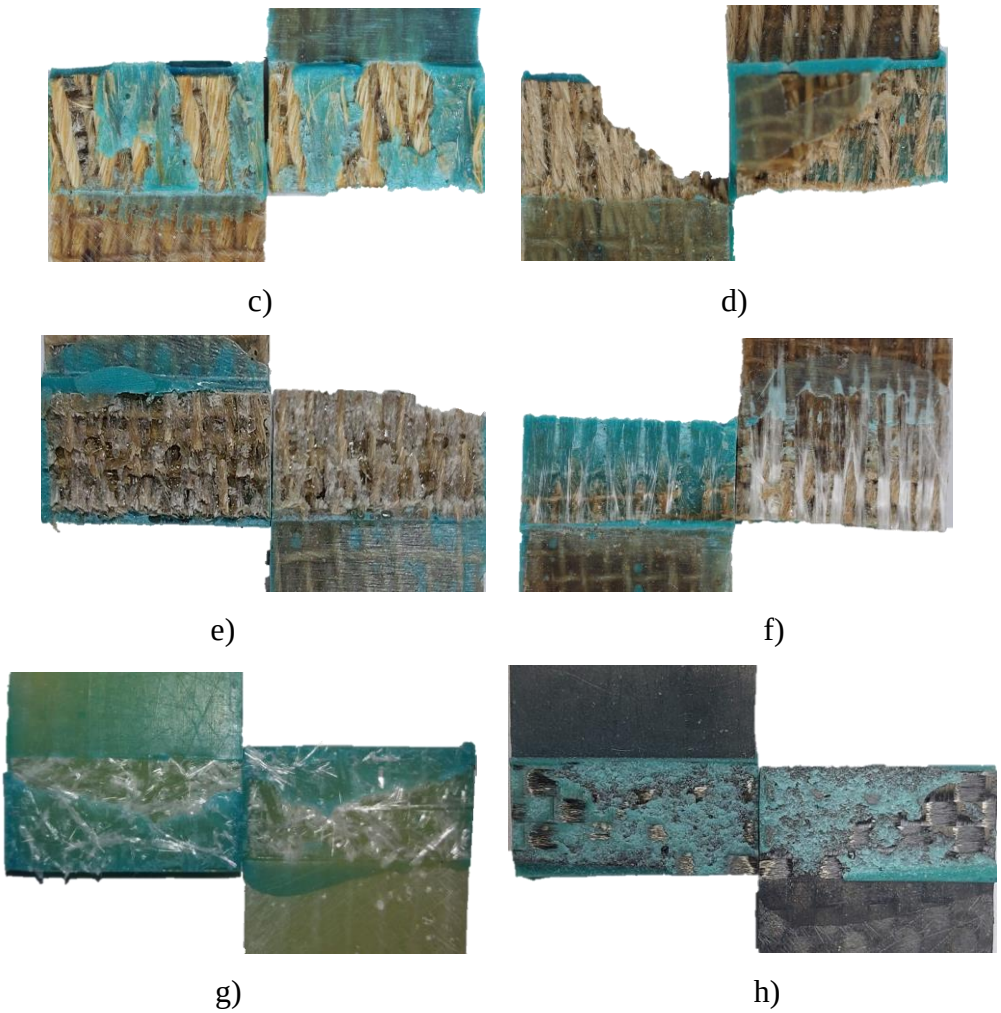


Figure 4. Representative failure surfaces of the tested 2D joint specimens, a) JFRP, b) CURAUÁ 2D, c) SISAL 2D, d) RAMIE 2D, e) HEMP 2D, f) GLASS 2D, g) GFRP and h) CFRP.

From Fig. 4 representative failure surfaces of the 2D bonded joint specimens can be seen. For the neat jute specimens (JFRP), a brittle failure at the overlap edge was observed and is consistent with previous works [14], (see Fig. 4a). For the CURAUÁ 2D SLJ specimens, a surface delamination failure mode was observed (see Fig. 4b). The adhesive layer is not visible, indicating that the entire first jute fabric layer was delaminated due to the high quality of the adhesive/resin interface. The crack propagation front was between the jute fabric and the curauá intralaminar reinforcement of the first layer, inducing a highly significant bridging failure (curauá bundles are visible). It should be noted that this bridging was the cause for the high failure load of the joints, which will be discussed in the next section (see Fig. 7) given the high material properties of the curauá fibre. From

Fig. 4c, a mixed failure mode of delamination and thin layer cohesive failure (TLC) can be seen for the SISAL 2D SLJ specimens. However, the TLC failure was predominant. A similar failure surface has been previously reported by the authors (i.e., intralaminar sisal reinforcement of a jute fabric) [14]. For the RAMIE 2D SLJ specimens a very brittle failure was found, where the crack initiated at the overlap edge and quickly progressed through one of the adherends crossing all the layers to the top (see Fig. 4d). A similar brittle failure was observed for the HEMP 2D SLJ specimens as can be seen in Fig. 4e. Since the primary reinforcement fibre is already brittle (jute), secondary reinforcement phases that are also brittle, such as ramie and hemp, will generate ultimately fragile failure modes. From Fig. 4f, for the GLASS 2D SLJ specimens, a mixed mode of delamination and TLC can be seen. Two crack fronts propagated from each adherend overlap edge. One of them propagated on the interlaminar space between the jute fabric of the first layer and its corresponding 2D glass reinforcement (bottom half of the image). This occurs due to the known tendency for the crack to nucleate near the overlap edge (highest stresses) and since the resin/adhesive interface is more resistant and tougher than the composite adherend, the crack propagates inwards and continues within the interlaminar space of the composite [7]. The opposing crack front presented a similar tendency, only it was much closer to the interface, with a mix of surface resin removal (TLC) and patches of cohesive failures (top half of the image). For the cases where delamination was observed (i.e., RAMIE, HEMP and GLASS) the initiation was always at the overlap edge due to the known stress state of the SLJ. Furthermore, the delamination progressed to a stock break failure through one of the adherends for the RAMIE and HEMP specimens. For the hybrid GLASS specimens, the first layer managed to contain the progression of the delamination and only the top jute bidirectional of the first layer was removed.

The CFRP bonded joint presented a mixed failure mode of cohesive within the adhesive and TLC failure (i.e., a thick adhesive layer is observed on one adherend and a thin layer of surface resin and light fibre delamination is visible on the other), however, the cohesive failure was predominant (see Fig. 4h). Finally, from Fig. 4g, the failure surface of the GFRP specimens can be seen and a light fibre tear (LFT) failure was observed. Two close to the interface cracks propagated from both overlap ends and generated a narrow transition zone in the middle. These failures are common for synthetic fibre reinforced composite joints [11, 30].

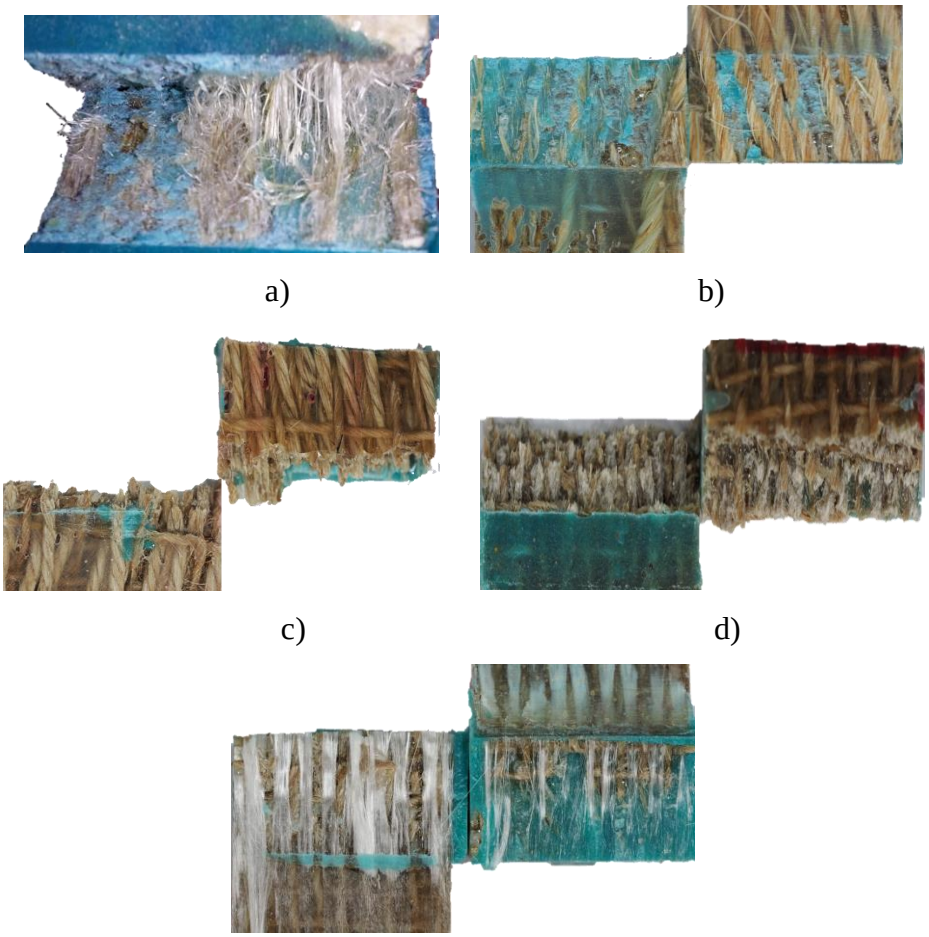


Figure 5. Representative failure surfaces of the tested 3D SLJ joint specimens, a) CURAUÁ 3D, b) SISAL 3D, c) RAMIE 3D, d) HEMP 3D and e) GLASS 3D.

The failure surface of the CURAUÁ 3D SLJ specimens can be seen in Fig. 5a. Differently from the 2D specimens, a mixed mode of cohesive failure and interlaminar curauá fibre bridging was observed. For or the SISAL 3D case, a mixed mode of TLC and cohesive failure patches was observed (see Fig 5b), however, the TLC failure is predominant. It is interesting to note that despite the similar predominant TLC failure mode (function of the similar interfacial properties between resin and adhesive), the failure had its onset at a higher load, indicating the enhancement granted by the 3D architecture (i.e., it takes longer for the peel stress to equal and surpass the transverse adherend strength). For the RAMIE 3D SLJ specimens, a similar brittle adherend failure was observed, however, the failure was closer to the overlap edge in its propagation through the adherend (see Fig. 5c). For the HEMP 3D specimens, a similar brittle adherend failure to the 2D case was

found (see Fig. 5d). However, such as the sisal specimens, there was a significant failure load enhancement as a function of the 3D architecture due to the same mechanism previously discussed. Similar to the 2D specimens, the GLASS 3D case presented a mixed delamination, TLC failure mode.

In summary, the failure mode of the bonded joints studied here is highly dependent on the type of fibre and reinforcement architecture.

3.2. Effect of fibre type and architecture in bonded joint efficiency

Figure 6 presents the representative load-displacement curves of the tested bonded joints, while Fig. 7 shows the quantitative bonded joint data. For the 2D architecture, in accordance with Table 2, a range of apparent joint stiffness can be seen going from the least stiff (JFRP) to the stiffest adherend (CFRP). Furthermore, a significant variation in behaviour up-to-failure of the joints can be seen. The least resistant and most brittle JFRP presents essentially no ductility in its behaviour, failing sharply at a low displacement. All other cases presented a more mixed behaviour (see Fig. 6).

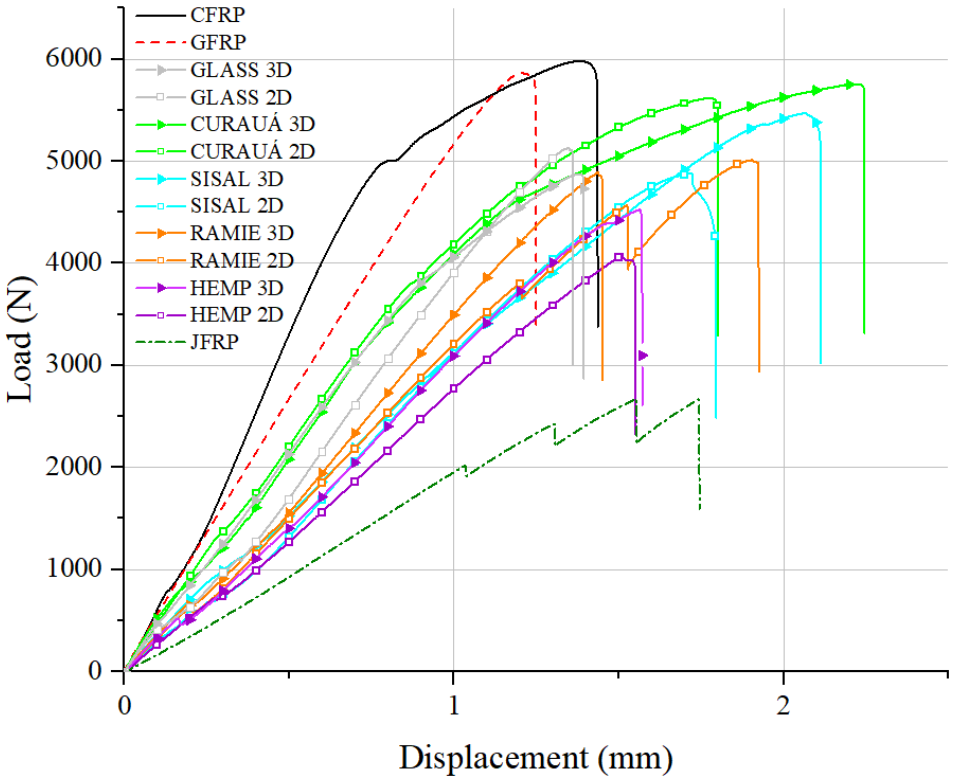


Figure 6. Representative load-displacement curves of the tested bonded joints.

From Fig. 7 the statistical quantitative bonded joint failure load data can be seen in bar

chart form. It can be seen that all intralaminar fibre reinforcement cases presented significant improvements in bonded joint failure load as a function of fibre type, in the classical 2D architecture, when compared to the JFRP SLJs. A failure load enhancement of approx. 34% was found for the HEMP 2D SLJ specimens, while for the RAMIE and SISAL 2D SLJ specimens an increase of approx. 46% was observed. The highest variation was found for the CURAUÁ 2D case at approx. 55% higher failure load when compared to the neat JFRP, while the GLASS 2D SLJ specimens presented an enhancement in failure load of approx. 49%. These significant enhancements are due to the improvements the secondary intralaminar fibre reinforcements had in the adherend properties, where higher resistance and stiffness was reported in all cases (see Table 3).

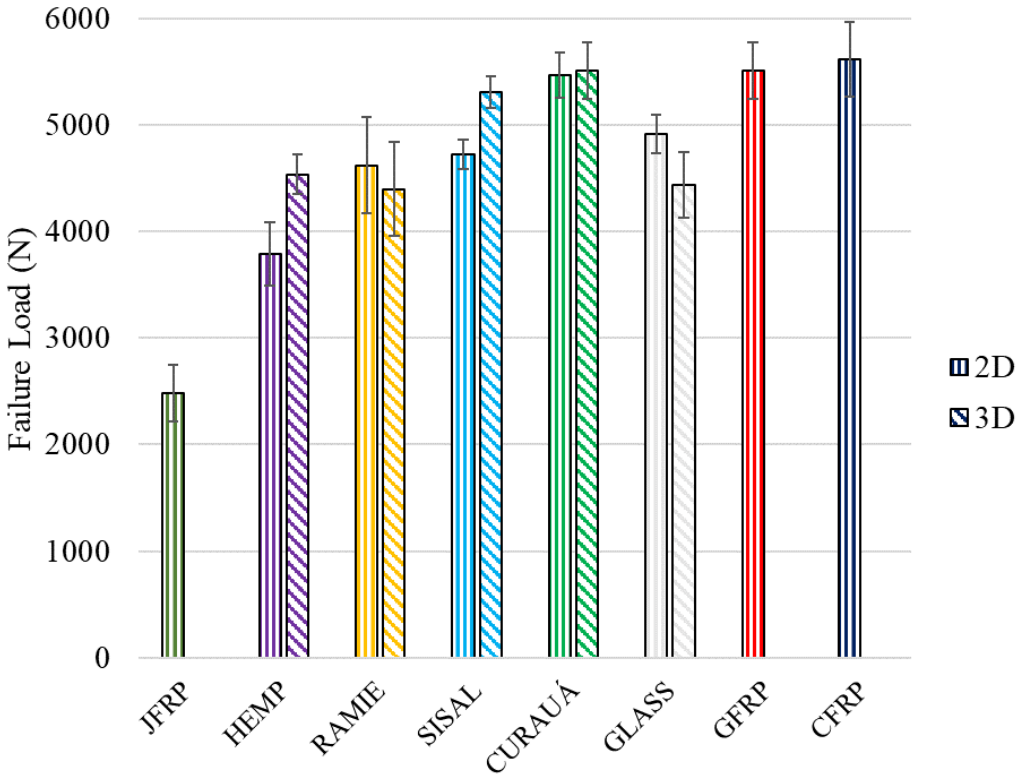


Figure 7. Average failure load of the tested SLJs as a function of reinforcement fibre and architecture.

When the effect of the fibre reinforcement architecture is analysed, different trends are observed as a function of fibre type. For example, for the HEMP 3D SLJ specimens, an enhancement in failure load of approx. 16% was found, while for the RAMIE 3D SLJ specimens a slight decrease of approx. 5% was found, when the 3D specimens are compared to the 2D (see Fig 7). For the SISAL specimens, an enhancement of approx.

11% in joint failure load was observed as a function of fibre reinforcement architecture. The enhancement in failure load observed for the SISAL 3D joints is related to the effect of the 3D reinforcement in improving the transverse properties of the adherend and delaying the onset of failure. In other words, the peel stress had to be higher in order to equal the transverse strength and initiate failure. This observation is reinforced by the higher area of cohesive failure zone visible on the joint failure surface of the 3D specimens (see Fig. 5b and 4c). The effect of the ductility and mechanical resistance of the secondary reinforcement fibre phase is thus significant, as evidenced by the fact that both SISAL and CURAUÁ 3D SLJ specimens presented the highest displacements. For the 2D and CURAUÁ 3D SLJ's, no significant failure load variation was observed as a function of fibre architecture. This is explained by the fact that the adherend have similar material properties and also similar joint´s failure modes (bridging) (see Fig. 4b, 5a and Table 3). Finally, for the GLASS SLJs a decrease of approx. 11% in joint failure load was found as a function of fibre architecture. This can be explained by the fact that although similar failure mode were observed (i.e. a mixed failure including the classical fiber-tear failure (or interlaminar failure) and TLC as can be seen in Fig. 4f and 5e), for the GLASS 2D SLJ specimens, the cohesive patches were more pronounced. Thus, the higher failure load for the GLASS 2D SLJs was directly related to the dimension of the cohesive failure area. GLASS 2D SLJs with the smallest TLC or delamination failure areas, however, showed higher joint strength than GLASS 3D SLJs.

When compared to the synthetic joints (GFRP and CFRP), the majority of the specimens presented lower joint failure loads with the exception of three groups: CURAUÁ 2D, 3D and SISAL 3D SLJ specimens. These groups managed to reach approx. 97%, 98% and 96% of the bonded joint failure load of the CFRP specimens, respectively. Thus, the fully natural fibre-reinforced composite joint matched the efficiency of fully synthetic composite joints. These results are mainly due to the adherend material properties and the effect of the 3D architecture.

From Table 2 little variation can be seen in terms of mechanical properties for CURAUÁ and SISAL adherends as a function of reinforcement architecture (i.e., when CURAUÁ 2D is compared to CURAUÁ 3D and SISAL 2D to SISAL 3D). However, the CURAUÁ 2D SLJ specimens present significantly higher joint failure load when compared to the SISAL 2D. This is due to the variation in adherend stiffness (see Table 3), where a more

stiff adherend will decrease the normal stresses (peeling) at the overlap edge, generating a lower mode mixicity and will decrease the propensity to delaminate [7]. This means that given the high mechanical properties of the curauá fibre, the 2D reinforcement architecture was already enough to reach an adherend stiffness capable of withstanding the peel stresses and to reach a failure load equal to the synthetic fibre-reinforced composites (yield stress limit of the resin/adhesive interface) [31, 32]. In other words, the crack initiated in the resin/adherend interface at the same stress state as the synthetic composite joints. However, increasing the adherend stiffness eventually reaches a limit and the load bearing capacity is a function of the maximum shear stresses that the adhesive/matrix interface are capable of withstanding (i.e., yield stress) [33]. This is evident from the stark differences in material properties (see Table 3), while the joint failure load is essentially the same between these natural and synthetic fibre-reinforced composite joints.

These results indicate that the effect of the 3D architecture in bonded joint failure load is highly dependent on the type of fibre, and significant improvements are achievable up to approx. 100% of even high-end synthetic fibre-reinforced composites. However, there are compromises involved in the application of this technique. The 3D architecture is a more complex reinforcement and therefore added costs to manufacture are expected [22]. Furthermore, the curauá fibre reinforced specimens, which presented a result equal to CFRP in its simpler reinforcement architecture (2D), while a very promising result, the fibre itself still lacks high scale production in the global market, especially compared to the alternatives such as the sisal fibre.

To summarize, in general, 3D fibre reinforcement architecture joints are more efficient than 2D architecture joints. This is related to the differences observed in the failure modes of the most promising specimens (i.e., SISAL and CURAUÁ). The failure mode changed from close to the interface failures (i.e., TLC and fibre bridging) to mixed modes with cohesive within the adhesive failures. The transverse reinforcement fibre acts against the tendency of the fibre layers to delaminate during the mode I loading (i.e., peel stresses caused by joint overlap edge tip rotation) as well as increase the transverse strength, delaying the initiation of the failure. However, this positive effect is dependant of a number of factors such as the type of through-thickness reinforcement fibre, the architecture geometry and the properties of the through-thickness reinforcement fibre

(i.e., more resistant and ductile fibres tend to present higher improvements). Thus, the 3D architecture proved to be a viable solution to enhancing the efficiency of NFRC bonded joints.

4. CONCLUSIONS

In this paper, the effect of a novel fibre reinforcement architecture in the adhesively bonded joint efficiency of natural fibre reinforced composites was investigated. Two different reinforcement techniques were used: intralaminar reinforcement (2D) and orthogonal-through-the-thickness reinforcement (3D). The aim of the novel architecture was to enhance the transverse properties of the adherend (transverse strength and fracture toughness) in order to delay or avoid delamination failures. A jute bidirectional fabric was used as a base primary reinforcement phase and curauá, sisal, ramie, hemp and glass fibres were used as secondary reinforcement phases for the 2D and 3D reinforcements. GFRP and CFRP composite bonded joints were fabricated and tested as points of comparison. The following conclusions can be drawn:

- All secondary fibre reinforced specimens presented an enhanced bonded joint failure load when compared to the JFRP SLJ specimens (e.g., enhancements from approx. 34% for the HEMP 3D to 55% for the CURAUÁ SLJ specimens. This is mainly due to the improvement of the adherend material properties as a function of the secondary fibre reinforcement.
- The bonded joints with 3D fibre reinforcement architecture adherends are more efficient than 2D fibre architecture joints. This is mainly due to the fact that the transverse (through-thickness) reinforcement fibre resist crack opening (peel stresses), as well as increase the adherend's transverse strength, therefore delay the initiation of the failure and increase the delamination resistance by creating a bridging zone behind crack tips during crack propagation.
- The most promising results reported are the SISAL 3D, CURAUÁ 2D and 3D SLJs, where nearly 100% of the bonded joint failure load of the fully synthetic counterparts (i.e., GFRP and CFRP) was reached. This clearly demonstrates that NFRC joints can be a viable replacement for synthetic composite joints at no load-bearing loss.
- The failure mode of the bonded joints studied here is highly dependent on the type

of fibre and reinforcement architecture and affected the bonded joint failure load. The JFRP, HEMP and RAMIE SLJs presented brittle stock break failures for both architectures. The SISAL and CURAUÁ SLJ specimens presented a variation of mixed failure modes as a function of architecture. The SISAL SLJ specimens presented delamination/TLC mixed modes, however, more pronounced cohesive failure patches were reported for the 3D specimens. For the CURAUÁ SLJ specimens, significant fibre bridging failure was reported for both 2D and 3D specimens, however, the 3D specimens also presented a significant cohesive failure zone.

REFERENCES

1. Budhe, S., et al., *An updated review of adhesively bonded joints in composite materials.* International Journal of Adhesion and Adhesives, 2017. **72**: p. 30-42.
2. Pickering, K.L., M.A. Efendy, and T.M. Le, *A review of recent developments in natural fibre composites and their mechanical performance.* Composites Part A: Applied Science and Manufacturing, 2016. **83**: p. 98-112.
3. Gholampour, A. and T. Ozbakkaloglu, *A review of natural fiber composites: properties, modification and processing techniques, characterization, applications.* Journal of Materials Science, 2020. **55**(3): p. 829-892.
4. Wankhede, B., et al., *A review on cotton fibre-reinforced polymer composites and their applications.* Proceedings of the Institution of Mechanical Engineers, Part L: Journal of Materials: Design and Applications, 2022: p. 14644207221143876.
5. de Araujo Alves Lima, R., et al., *Effect of surface treatments on interfacial properties of natural intralaminar hybrid composites.* Polymer Composites, 2020. **41**(1): p. 314-325.
6. Banea, M.D. and L.F.M. da Silva, *Adhesively bonded joints in composite materials: An overview.* Proceedings of the Institution of Mechanical Engineers, Part L: Journal of Materials: Design and Applications, 2009. **223**(1): p. 1-18.
7. Blackman, B.R.K., et al., *The fracture behaviour of adhesively-bonded composite joints: Effects of rate of test and mode of loading.* International Journal of Solids and Structures, 2012. **49**(13): p. 1434-1452.
8. Shang, X., et al., *Review on techniques to improve the strength of adhesive joints with composite adherends.* Composites Part B: Engineering, 2019. **177**: p. 107363.
9. Dhilipkumar, T. and M. Rajesh, *Influence of manufacturing process and GFRP pin loading on shear and dynamic behaviour of composite joints.* The Journal of Adhesion, 2022: p. 1-20.
10. de Queiroz, H.F.M. and M.D. Banea, *Methods to increase the mechanical performance of composite adhesive joints: An overview with focus on joints with natural fibre composite adherends.* Journal of Composite Materials, 2022. **56**(26): p. 3993-4010.
11. de Queiroz, H.F.M., M.D. Banea, and D.K.K. Cavalcanti, *Adhesively bonded*

joints of jute, glass and hybrid jute/glass fibre-reinforced polymer composites for automotive industry. Applied Adhesion Science, 2021. **9**(1): p. 2.

12. Melese, K., T. Naik, and I. Singh, *Adhesive joining of sisal/jute/hybrid composites with drilled holes in lap area.* Proceedings of the Institution of Mechanical Engineers Part L Journal of Materials Design and Applications, 2020. **235**.
13. Melese, K.G. and I. Singh, *Joining Behavior of Jute/Sisal Fibers Based Epoxy Laminates Using Different Joint Configurations.* Journal of Natural Fibers, 2022. **19**(6): p. 2053-2064.
14. de Queiroz, H.F.M., M.D. Banea, and D.K.K. Cavalcanti, *Experimental analysis of adhesively bonded joints in synthetic- and natural fibre-reinforced polymer composites.* Journal of Composite Materials, 2020. **54**(9): p. 1245-1255.
15. Yan, S., X. Zeng, and A. Long, *Experimental assessment of the mechanical behaviour of 3D woven composite T-joints.* Composites Part B: Engineering, 2018. **154**: p. 108-113.
16. Ahmad, F., N. Yuvaraj, and P.K. Bajpai, *Effect of reinforcement architecture on the macroscopic mechanical properties of fiberous polymer composites: A review.* Polymer Composites, 2020. **41**(6): p. 2518-2534.
17. Dai, S., et al., *Influence of fibre architecture on the tensile, compressive and flexural behaviour of 3D woven composites.* Composites Part A: Applied Science and Manufacturing, 2015. **69**: p. 195-207.
18. Stig, F. and S. Hallström, *Influence of crimp on 3D-woven fibre reinforced composites.* Composite Structures, 2013. **95**: p. 114-122.
19. Kier, Z.T., et al., *Estimating mechanical properties of 2D triaxially braided textile composites based on microstructure properties.* Composites Part B: Engineering, 2015. **68**: p. 288-299.
20. Jabbar, M., et al., *Effect of the stuffer yarns on the mechanical performance of novel 3D woven green composites.* Composite Structures, 2021. **269**: p. 114023.
21. Stegschuster, G., et al., *Experimental determination of the mode I delamination fracture and fatigue properties of thin 3D woven composites.* Composites Part A: Applied Science and Manufacturing, 2016. **84**: p. 308-315.
22. Clarke, J., et al., *A Cost Model for 3D Woven Preforms.* Journal of Composites Science, 2022. **6**(1): p. 18.

23. Stig, F. and S. Hallström, *Assessment of the mechanical properties of a new 3D woven fibre composite material.* Composites Science and Technology, 2009. **69**(11): p. 1686-1692.
24. Bogdanovich, A.E., et al., *Experimental study of joining thick composites reinforced with non-crimp 3D orthogonal woven E-glass fabrics.* Composites Part A: Applied Science and Manufacturing, 2011. **42**(8): p. 896-905.
25. Aymerich, F., R. Onnis, and P. Priolo, *Analysis of the effect of stitching on the fatigue strength of single-lap composite joints.* Composites Science and Technology, 2006. **66**(2): p. 166-175.
26. Aymerich, F., R. Onnis, and P. Priolo, *Analysis of the fracture behaviour of a stitched single-lap joint.* Composites Part A: Applied Science and Manufacturing, 2005. **36**(5): p. 603-614.
27. Guillebaud-Bonnafous, C., et al., *Experimental and numerical investigation of the interface between epoxy matrix and hemp yarn.* Composites Part A: Applied Science and Manufacturing, 2012. **43**(11): p. 2046-2058.
28. Banea, M.D., L.F.M. Da Silva, and R.D.S.G. Campilho, *Moulds design for adhesive bulk and joint specimens manufacturing.* Assembly Automation, 2012. **32**(3): p. 284-292.
29. ASTM D5573-99, *Standard practice for classifying failure modes in fiber-reinforced-plastic (FRP) joints.* Annual book of ASTM standards, 2002. **15**(03).
30. Hunter-Alarcón, R.A., et al., *Effect of the natural aging process on the shear strength of FRP composite single lap joints.* International Journal of Adhesion and Adhesives, 2018. **86**: p. 4-12.
31. Banea, M.D., et al., *Effect of material on the mechanical behaviour of adhesive joints for the automotive industry.* Journal of Adhesion Science and Technology, 2017. **31**(6): p. 663-676.
32. Banea, M.D., et al., *Multi-material adhesive joints for automotive industry.* Composites Part B: Engineering, 2018. **151**: p. 71-77.
33. Reis, P.N.B., J.A.M. Ferreira, and F. Antunes, *Effect of adherend's rigidity on the shear strength of single lap adhesive joints.* International Journal of Adhesion and Adhesives, 2011. **31**(4): p. 193-201.

Paper 3

Mechanical characterization of novel 3D hybrid composites

Mechanical characterization of novel natural fibre-reinforced composites via a three-dimensional fibre architecture

H.F.M. de Queiroz[1], N.V. dos Santos[2], J.S.S. Neto[1], M.D. Banea[1,3]

[1]Federal Centre of Technological Education in Rio de Janeiro (CEFET/RJ), Brazil
[2]Pontifical Catholic University of Rio de Janeiro - PUC-Rio
[3]CICECO - Aveiro Institute of Materials, Department of Materials and Ceramic Engineering, University of Aveiro, 3810-193, Aveiro, Portugal

Abstract

This research focuses on the fabrication and analysis of novel natural fiber hybrid composites using two different reinforcement techniques: intralaminar reinforcement (2D) and orthogonal-through-the-thickness reinforcement (3D-OTT). Jute bidirectional fabric served as the main fiber phase, while secondary reinforcement phases (sisal, curauá, and glass fibers) were woven unidirectionally through the jute fabric for the 2D architecture (intralaminar reinforcement). For the 3D architecture, a transverse fiber phase was additionally woven orthogonally through the thickness of the fiber preforms. Pure jute and glass fiber-reinforced composites were also fabricated and tested for comparison. Tensile, flexural, and impact tests were perfomed to assess how the innovative 3D-OTT architecture influences in-plane composite properties. SEM analysis and X-ray microtomography were used to examine failure modes, interfacial quality and void volume fractions. The results support the viability of the novel composite materials for partial or complete substitution of glass fiber-reinforced materials (GFRP) in specific applications. For instance, curauá-reinforced specimens demonstrated comparable tensile and flexural stiffness to synthetic composites, while 3D-reinforced sisal specimens exhibited exceptional energy absorption during impact testing. Additionally, the simple fabrication process resulted in very low void fractions, making these composites suitable for the automotive industry.

Keywords: Composite structures, hybrid composites, natural fibre composites, 3D architecture.

1. INTRODUCTION

Natural fibre-reinforced composites (NFRCs) have continued to grow across a multiple and ever-increasing array of applications in many industrial sectors such as automotive, civil, marine, sports among others [1, 2]. This trend stems directly from the environmental pressures originating from both governments and societies that are growing more environmentally conscious. The threat of climate change and its effects on global economies and markets are continually pushing every industrial sector to significantly decrease their carbon-footprints. In this context, the use of NFRCs is quite clear when it comes to replacing classical synthetic fibre composites, such as glass and carbon fibre-reinforced materials (GFRP and CFRP, respectively), partially or completely [3]. However, the fact remains that the mechanical properties of synthetic composites are significantly higher than their natural counterparts. There are a number of possible techniques that have been applied to address this, mostly via the hybridization of natural and synthetic fibres in the same composite [3-12]. It is also possible to increase the mechanical and thermal properties of NFRCs through chemical modifications at the microscopic scale [7, 13]. However, these micro and macroscale changes are not the only ways to improve the properties of fibre-reinforced composites. Altering the geometrical arrangement (architecture) of the fibre reinforcement structure itself is another method to enhance the properties of developed composites without the need to change the fibre and matrix materials. This would entail a mesoscale level change, a scale in between the micro and macro [14]. Due to the ever increasing demand of high performance reinforcements, the popularity of 3D reinforced composites is growing due to their enhanced out-of-plane mechanical properties [15-18]. For example, it is well known that the out-of-plane properties of classically laminated composites are significantly lower when compared to the in-plane direction, i.e., the direction of the main fibre reinforcement phase. This is because, in a classically laminated composite material, there is no reinforcement fibre in the transverse direction and the interlaminar space consist of resin matrix only. This significantly lowers the fracture toughness and delamination resistance of the composite [15]. Therefore, the technique of transverse reinforcement of composites comes into play

to address this weakness of the material properties, enhancing fracture toughness, fatigue life and impact resistance [14, 15, 17, 19, 20].

The 3D reinforcement architecture comprises a wide range of different architectures at different complexity levels [21]. They may be divided into categories such as: knitted, woven, or braided. Weaving is the most common technique for fibre reinforcement both for 2D and 3D architectures. Common 2D weaves include plain, twill, basket and satin and care must be taken when choosing the weave, as the style will significantly affect the drapability and crimp levels of the fabric [22]. The higher the interlacing points in a weave are, the lower the drapability and the higher the crimp levels will be. Therefore a compromise of mechanical and thermal properties, drapability, crimp levels and cost must be struck for the highest possible performance [14, 23]. The 3D weave architectures are divided into angle and orthogonal interlocks. Meaning that the z-binder (transverse) reinforcement is either at an angle or orthogonally directed as it enters the 2D fabrics. Furthermore, the architectures are further differentiated as layer-to-layer or through-the-thickness interlocks [22]. The choice of architecture significantly alters the properties of the composite such as, drapability, stiffness, strength and crimp levels [16]. Nawab et al. [24] has shown that the layer-to-layer tensile response was superior to that of the orthogonal-through-the-thickness (OTT) ones. However, for mode I fracture toughness, the OTT architecture has been shown to present superior performance [15]. On the other hand, Dai et al. [25] tested six types of 3D woven carbon fibre composites fabricated via a traditional weaving loom and resin transfer moulding. The tensile, compressive, flexural strength and modulus were experimentally analysed in the warp direction, revealing the influence of weave architectures. The tensile properties of the 3D composites were found to be affected by architecture waviness. Shorter binding spacing (increased density in z-binder) increases delamination resistance at the cost of increasing crimp and waviness. The angle interlock presented the highest performance overall; however, it also presented the highest delamination crack. Guenon et al. [26] investigated the effect of OTT 3D reinforcement in the mode I fracture toughness of carbon/epoxy composites. It was found that the presence of 1% z-binder fibres is equivalent to over a ten-fold increase in fracture toughness when the 3D composites are compared to the 2D ones. It is also noteworthy that regarding the numerical modelling capability of 3D composites, there are two main categories: predictive and descriptive. The descriptive model characterizes a real textile

fabric architecture by way of image processing techniques on X-ray tomographic images, which allow for a detailed view of the inside of the material [27]. X-ray microtomography also proves to be an invaluable tool for analysing imperfections within the material such as voids, waviness and crimp and damage analysis after mechanical destructive testing [28].

Several research works have addressed the application of 3D reinforcement on the mechanical properties of NFRCs [29-36]. Recently, Queiroz et al. [4], demonstrated that by using a transverse fibre reinforcement phase (OTT), a significant enhancement was observed in the single lap bonded joint performance of the composites. This was due to the likely significantly improved fracture toughness of the adherend. However, further mechanical characterization of these materials is needed, and the field of three-dimensional fibre reinforcement of NFRCs is currently in its infancy. The main focus of this research is the mechanical characterization of novel 3D fibre reinforced NFRCs in order to assess their viability in applications in the industry such as the automotive sector. The composites were analysed in tensile, flexural, impact and short-beam mechanical tests. Furthermore, SEM microscopy was used to examine the influence of the complex architecture in the failure modes and fibre/matrix interfaces, while X-ray microtomography was used to analyse the state of crimp, fibre and void volume fractions in selected specimens.

2. MATERIALS AND METHODS

2.1. Materials

Pure jute fibre bidirectional fabrics (type P9, supplied by Sisalsul (São Paulo, Brazil)), were the primary reinforcement phase while curauá, sisal and glass fibres were the secondary reinforcements for the 2D and 3D fibre preforms. In-natura curauá fibres supplied by the Federal University of Pará (Pará, Brazil) were used. The curauá fibre bundles were washed with distilled water for the removal of dirt and other impurities. Oven drying at 100 ºC was done subsequently. The intralaminar reinforcement architecture formed the base of the preforms. As such, “unidirectional” (UD) fabrics are fabricated by way of the secondary phases. The preforms were comprised of five layers each. The sisal (APAEB 700/1, Bahia, Brazil and glass fibres (SE1200, Owens Corning, USA) used were industrially made fibre rovings. The intralaminar reinforcement was

done through the weaving of the fibres across the plain weave jute base fabric in a way that no columns were skipped and stitched the weft rows by 8 spaces (see Fig. 1b). Moreover, regarding the 3D preforms, a 3D OTT architecture was stitched through 5 layers of 2D UD fabrics with the aid of a PLA 3D printed guide to maintain the architecture design of the dry preforms (see Fig. 1a). In other words, the 2D UD fabrics were put in between the guides and the transverse fibres were stitched through 5 layers to fabricate the dry 3D fabric architectures. Pure synthetic specimens (RE200P bidirectional glass fabrics, Barracuda Advanced Composites, SP, Brazil) were fabricated to act as a comparable point (GFRP). A two-component epoxy resin, HEX 135 SLOW (Barracuda Advanced Composites, SP, Brazil), was used as the matrix to fabricate the composites. The material properties of the resin matrix used can be seen in Table 1.

Table 1. Mechanical properties of the resin matrix used [4].

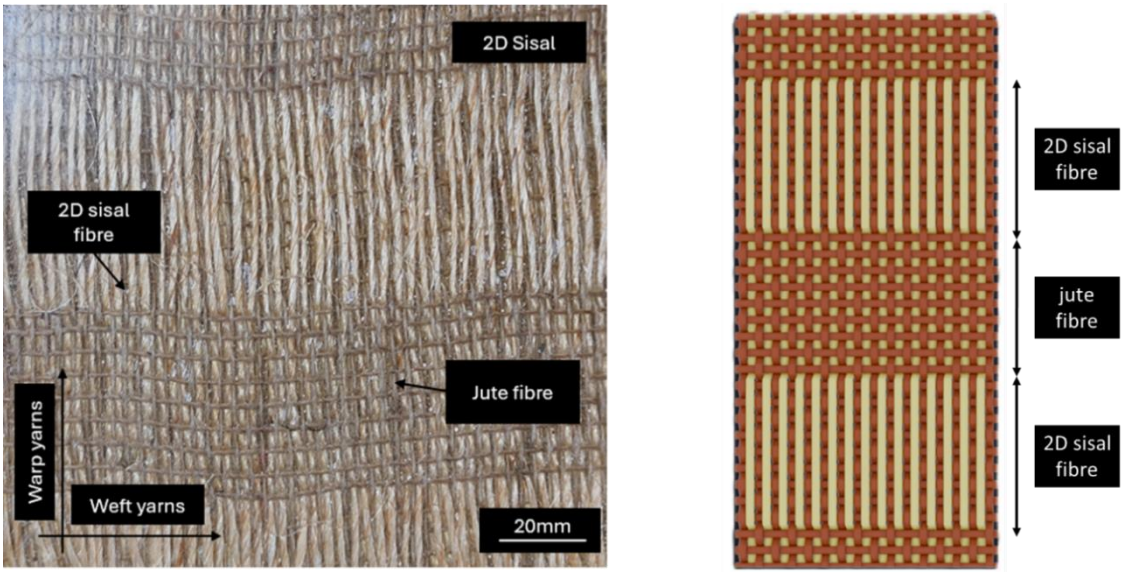
Polymer	Tensile strength (MPa)	Young's modulus (GPa)	Tensile strain (%)
HEX 135 SLOW	60.92 ± 1.42	3.25 ± 0.008	3.20 ± 0.20

2.2 Specimens manufacturing

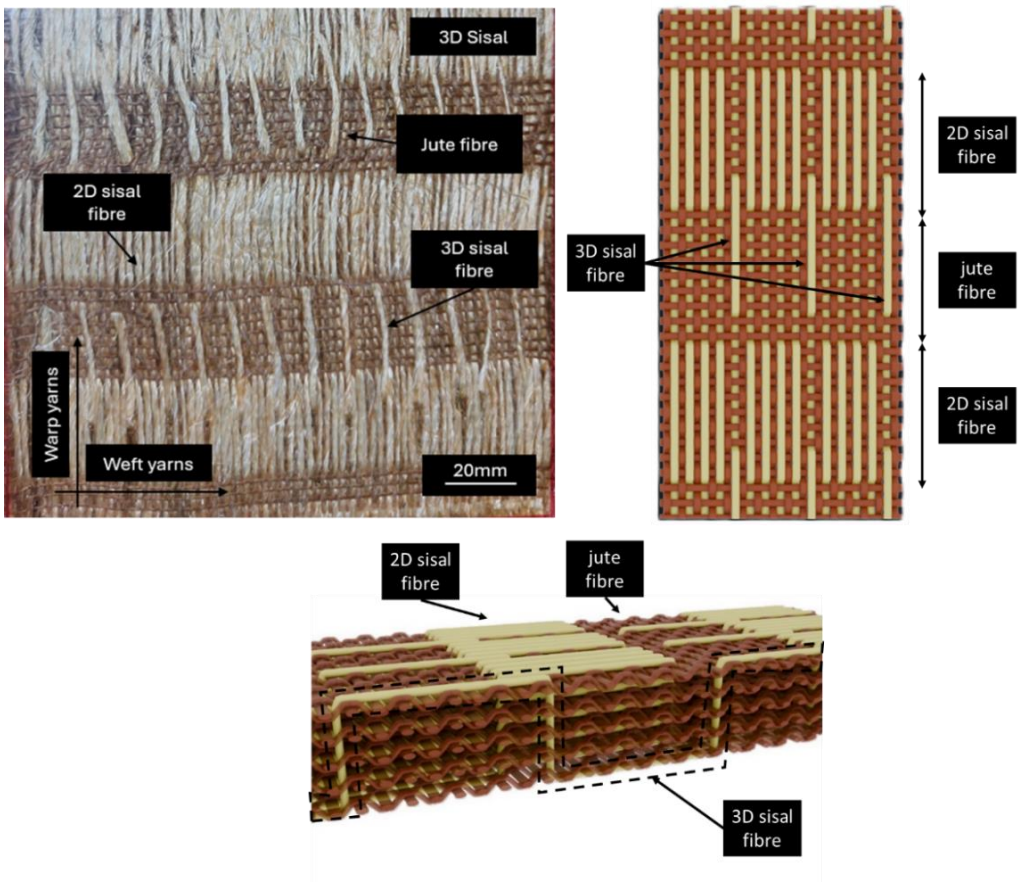
The compression moulding technique was applied to fabricate the composite plates with the aid of a steel mould and a heated hydraulic press, Solab SL 20 (São Paulo, Brazil). The composite curing was done at 70 degrees Celsius for 8 hours under pressure as per manufacturer guidelines. The composite thickness was approx. 6 mm and it was controlled through steel tabs. The test specimens were cut from the panels via a tungsten carbide blade. All specimens followed the international ASTM geometry guidelines for their respective tests. The specimens received a simple nomenclature as a function of type of fibre reinforcement, both nature and architecture, see Table 2. Figure 1 presents examples of finished composite plates in their 2D and 3D configurations. The 2D means only the intralaminar reinforcement is present (see Fig. 1b), while the 3D means that both the intralaminar and 3D OTT reinforcement architectures are present simultaneously (see Fig. 1a). The idealized schematic of the architecture can be seen in Fig. 1c-e. Dark brown is the main jute phase while the lighter brown are the secondary reinforcements (2D and 3D).

Table 2. Composite material nomenclature.

Composite code	Composite specimen
JFRP	Pure jute fibre-reinforced polymer composites
SISAL 2D	Jute fabric reinforced with woven sisal UD
SISAL 3D	SISAL 2D reinforced with transverse orthogonal sisal fibres
CURAUÁ 2D	Jute fabric reinforced with woven curauá UD
CURAUÁ 3D	CURAUÁ 2D reinforced with transverse orthogonal curauá fibres
GLASS 2D	Jute fabric reinforced with woven glass UD
GLASS 3D	2D reinforced with transverse orthogonal glass fibres
GFRP	Pure glass fibre-reinforced specimen



a)



b)

Figure 1. Representative a) SISAL 2D fabricated composite plate, b) SISAL 3D fabricated composite plate.

2.3 Test method

2.3.1 Mechanical testing

The composite materials were mechanically characterized via tensile tests by way of an Instron®5966 (Norwood, Massachusetts, USA) testing machine. A load cell of 10 kN was used and a speed of 1 mm/min was applied to the clamps**.** The flexural and short beam tests were carried out with the same machine (1kN load cell) at a test speed of 1 mm/min. The impact tests were carried out via a WPM PS 30 Leipzig impactor (error of 0.0075 kgf). Four specimens were tested for each group. All tests were conducted in accordance with their corresponding ASTM international standards.

2.3.2 SEM analysis

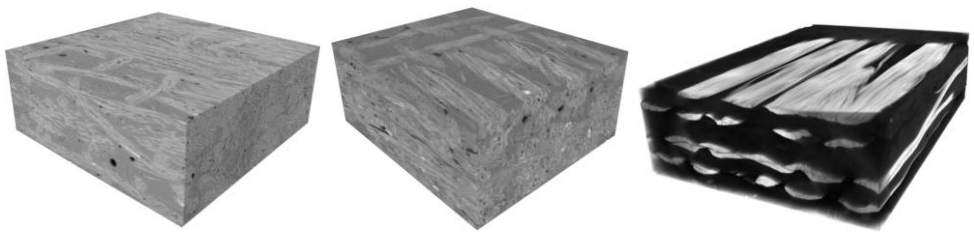
A SEM analysis was performed on the failure surfaces of the tensile specimens via a high-resolution Scanning Electron Microscope with X-Ray Microanalysis: JEOL - JSM-7100F found at the Nanotechnology Characterization Laboratory (CENANO) National Institute of Technology (INT), Rio de Janeiro, Brazil, using an acceleration of 15 KV. A coating of platinum (surface density of 21.53 g/cm^3) was done before examination.

2.3.3 MicroCT analysis

A XRANDIA 510 Versa microtomography microscope equipment available in Image Analysis and Digital Microscopy Group (MicDigi) in Chemical and Materials Engineering Department (PUC-Rio, Rio de Janeiro, Brazil) was used. The test evaluates the fibre distribution in the matrix as well as the presence of defects in the sample such as pores and voids. It is a non-destructive qualitative technique based on the principle of radiography that allows obtaining 2D and 3D images of bulk material. The images were processed using the Dragonfly© software. A reduction in computational demand was achieved by selecting smaller regions of interest surrounding the sample's image to remove the background. The tomography scan consisted of three samples (SISAL 2D, CURAUÁ 3D and GLASS 3D) and an empty background. The segmentate sample image used was a prism with dimensions as shown in Table 3 and representative isometric images of the scanned specimens can be seen in Fig. 2.

Table 3. Dimensions of the microCT samples.

Sample	Width (mm)	Height (mm)	Depth (mm)
SISAL 2D	10.36	5.02	11.95
CURAUÁ 3D	13.49	5.34	24.41
GLASS 3D	12.69	4.78	17.79



a) b) c)

Figure 2. Representative microCT images of the a) CURAUÁ 3D, b) SISAL 2D and c) GLASS 3D specimens.

3. RESULTS AND DISCUSSION

3.1 Mechanical properties

3.1.1 Tensile properties

Figure 3 presents representative stress-strain curves of all the tested specimens as a function of fibre architecture, while Fig. 4 presents the quantitative statistical data.

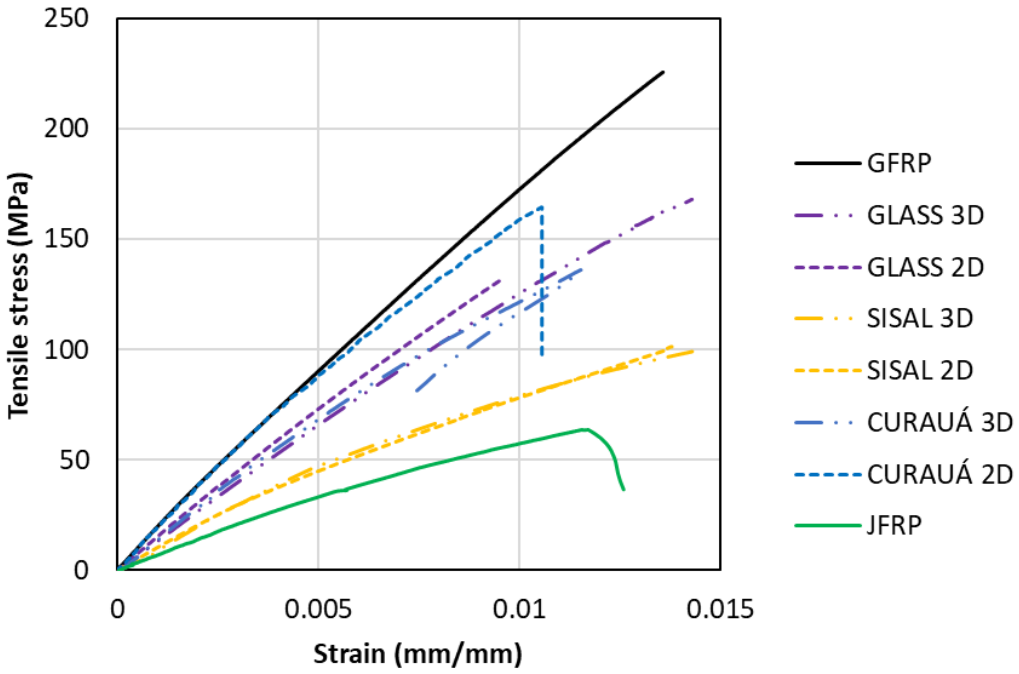
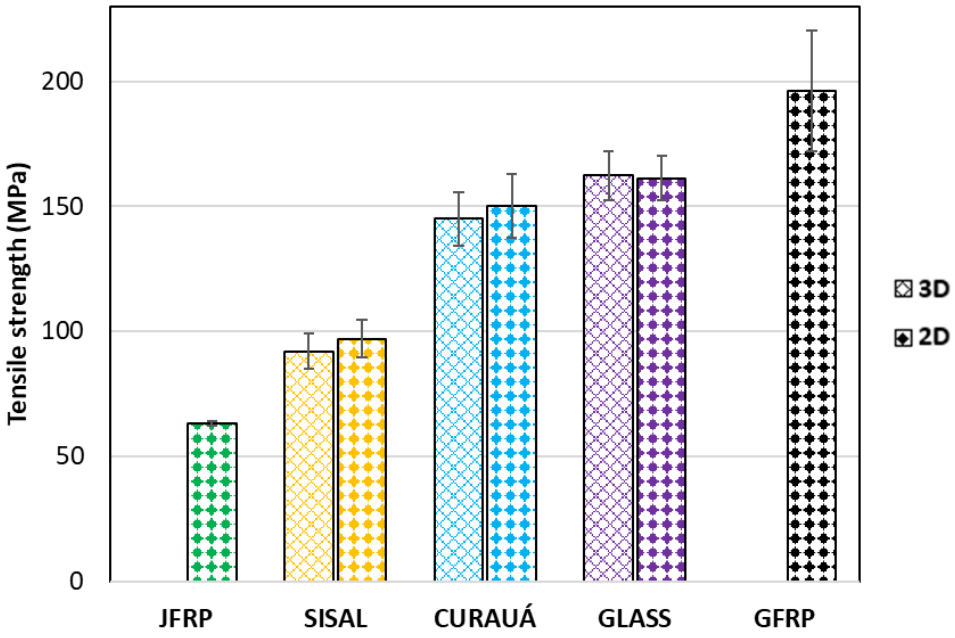


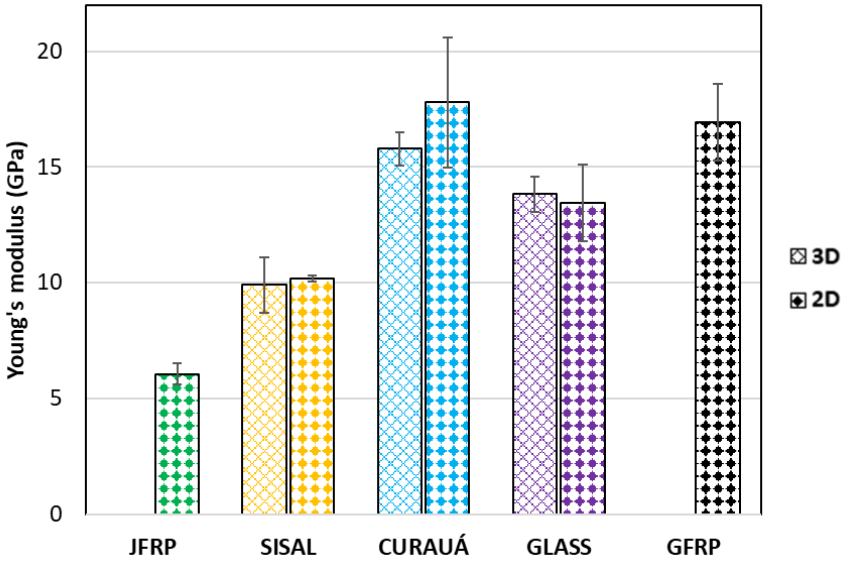
Figure 3. Representative stress-strain curves of all the tested specimens as a function of fibre architecture.

It can be seen from Fig. 3 that a significant variance in behaviour and rigidity occurs as a function of composite material. As expected, the neat synthetic composites presented the highest rigidity and stress at failure. The general behaviour evolution of the specimens was brittle, with a more mixed brittle/ductile behaviour observed for the natural hybrid composites. From Fig. 4, significant enhancements in tensile strength are visible for all cases when compared to the neat JFRP. For example, improvements of approx. 35%, 58% and 61% were observed when the SISAL, CURAUÁ and GLASS specimens are compared to the neat JFRP, see Fig. 4a. In a hybrid composite, the properties of the composite are mainly reliant on the stiffness and the ductility of the individual fibres. The stiffness of glass fibre is significantly higher than the one observed for the natural fibres used here, while the ductility of glass is low when compared to the sisal and curauá fibres

[4]. No significant variation was observed as a function of architecture (i.e., when the 3D composites are compared to their 2D counterpart). The data available for the 3D woven synthetic composites in the literature suggests a decrease of tensile strength as a function of z-binder (through-the-thickness reinforcement) fraction and have been attributed to waviness and crimping of in-plane fibres [17]. The lack of significant variation of tensile strength as a function of architecture indicates few significant fabrication defects for these composites. The neat synthetic specimens presented highly significant enhancements in tensile strength when compared to the neat JFRP, as expected (i.e., approx. 68%). It can also be observed from Fig. 4a, that variations in tensile strength occurred as a function of secondary fibre reinforcement type. For example, the CURAUÁ specimens presented an enhancement in tensile strength of approx. 35% when compared to the SISAL specimens. This is likely linked to the lower interface quality between the sisal fibre and the epoxy resin matrix (lower interfacial shear strength, IFSS) when compared to the curauá [13, 37]. However, when compared to the GLASS specimens, a lower variation was observed (i.e., an approx. 7% decrease in tensile strength). This small variation demonstrates the viability of curauá to substitute glass in certain applications as a function of architecture.



a)



b)

Figure 4. Tensile test data as a function of reinforcement architecture, a) tensile strength and b) Young's modulus.

The neat synthetic specimens presented increased tensile strength when compared to all the hybrid composites. It should be noted that, the CURAUÁ specimens managed to reach 77% of the GFRP's tensile strength, while being fully natural fibre reinforced and presenting likely significantly higher transverse material strength and toughness owing to its woven 3D architecture [15].

The variations of composite stiffness as a function of architecture can be seen in Fig. 4b. The trends are very similar to tensile strength, with the notable exception of the CURAUÁ specimens. All specimens presented significant enhancements in stiffness when compared to the neat JFRP specimens, due to the same reason as tensile strength (enhancements of approx. 40%, 66% and 55% when compared to the SISAL, CURAUÁ and GLASS specimens, respectively, while the synthetic specimens presented an enhancement of approx. 64%).

As a function of fibre architecture, the only significant variation, when the 3D specimens are compared to the 2D, was observed for the CURAUÁ cases, where the 2D specimens presented an enhancement of approx. 11% in stiffness. This is likely due to either a reduction in the in-plane fibre volume fraction or waviness/crimping of in-plane fibres (see Fig. 12d) [17]. However, significant variations of Young's modulus were observed

as a function of secondary reinforcement hybridization, (see Fig. 4b). For example, the CURAUÁ 3D specimens presented an improvement of approx. 43% and 24% in stiffness when compared to the SISAL 3D and GLASS 3D cases, respectively. Both the 2D and 3D CURAUÁ specimens presented a similar stiffness when compared to the GFRP case (i.e., approx. 7% decrease and 5% enhancement, respectively).

The tensile strain variations observed were for the most part not significant. The majority was close to the 1% value, a more brittle tendency, due to the fact that the hybridization was done using a jute bidirectional fabric. However, for the SISAL 3D and GLASS 2D and 3D specimens, a more significant increase in tensile strain was observed (i.e., tensile strains of 1.76% and 1.59%, respectively). This is due to the higher ductility of the secondary reinforcement fibres.

The trends described here for the tensile properties of the 3D composites are in line with the literature for synthetic 3D reinforced composites. Generally, it has been reported that the properties of 3D composites may fluctuate 0.8x to 1.2x when compared to their 2D counterparts [17] and has been observed here for the tensile strength and stiffness of the three-dimensional reinforced composites. This means that the existing models used to predict the behaviour of synthetic 3D composites may be adapted to 3D NFRCs.

3.1.2 Flexural properties

Figure 5 presents representative stress-strain curves of all the tested specimens as a function of fibre architecture, while Fig. 6 presents the quantitative statistical data. From Fig. 5, the behaviour up to failure in flexion of all the composites can be seen. The stiffness range was the same as observed for the tensile specimens. It is possible to observe a significant variation in behaviour. For instance, the GFRP presented a more ductile failure while developing a similar buckling compression failure. The behaviour evolution of the hybrid composites becomes more complex due to a mixed failure mode of compression and traction (see Fig. 5).

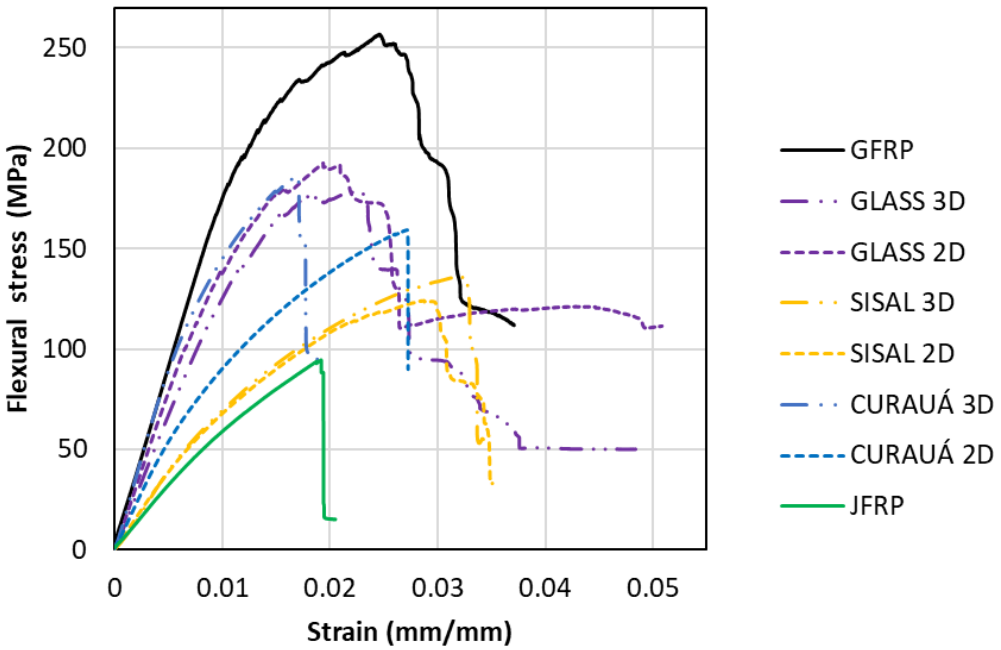
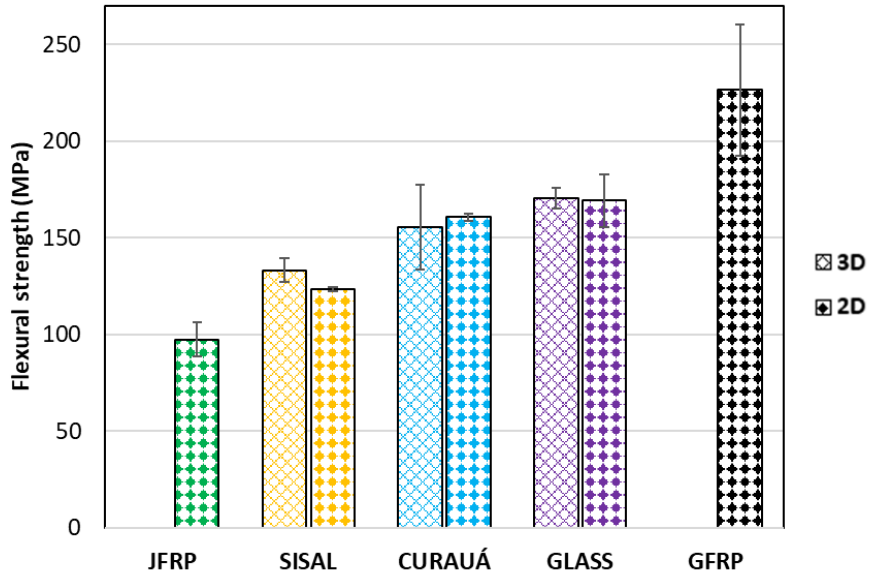


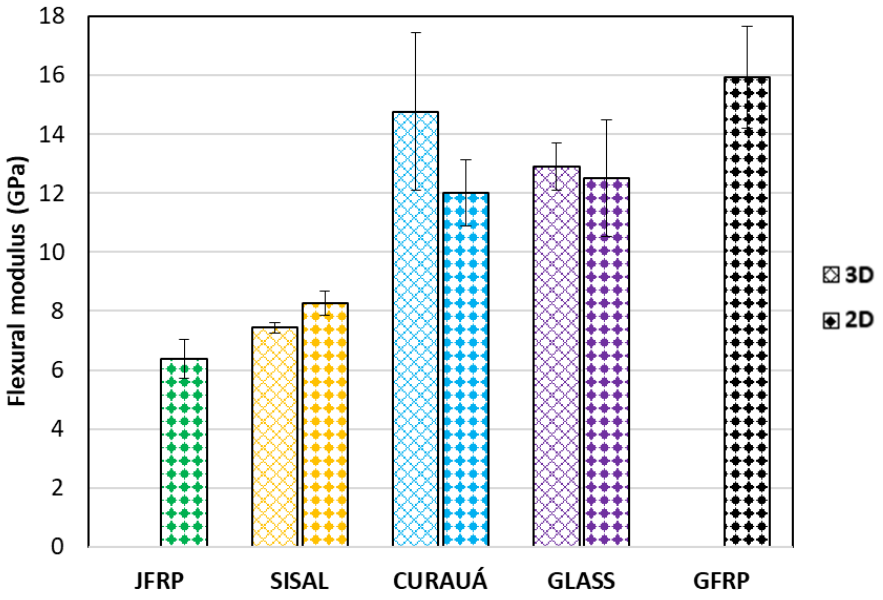
Figure 5. Representative flexural stress-strain curves of all the tested specimens as a function of fibre architecture.

From Fig. 6a the flexural strength data can be seen. A similar trend to the tensile strength is visible. All specimens presented significant improvements in flexural strength when compared to the neat JFRP (the SISAL, CURAUÁ and GLASS specimens presented an approx. 21%, 39% and 42% enhancement in flexural strength, respectively). Furthermore, the GFRP presented an approx. 57% improvement in flexural strength, compared to the JFRP.

As a function of secondary fibre reinforcement, the CURAUÁ specimens presented and enhancement of approx. 23% when compared to the SISAL specimens and no significant variation when compared to the GLASS ones. Regarding the effect of fibre architecture, the variations between 2D and 3D specimens for flexural strength were not significant (~8%). Similar to tensile strength and the general literature for synthetic woven 3D composites [17], this indicates that fabrication defects were not significant. Finally, it is noteworthy that the CURAUÁ specimens managed to reach 70% of the GFRP flexural strength, while presenting a unique architecture that affords it higher transverse strength and fracture toughness.



a)



b)

Figure 6. Flexural test data as a function of reinforcement architecture, a) tensile strength and b) flexural modulus.

The flexural modulus trends were once again similar to the tensile specimens (see Fig. 6b). The SISAL specimens presented enhancements when compared to the neat JFRP (approx. 23% enhancement for the 2D and 14% for the 3D specimens, respectively). The CURAUÁ specimens presented approx. 47% and 57% improvements in flexural modulus

for the 2D and 3D cases respectively, while the GLASS specimens presented an approx. 50% enhancement. These trends are linked to the higher mechanical properties and improved fibre/resin interface of the secondary fibres when compared to the jute main phase [13]. Finally, the GFRP showed an increment of 60% in flexural modulus, when compared to the JFRP. As a function of secondary reinforcement fibre, the CURAUÁ specimens presented significant improvements in flexural modulus when compared to SISAL, 31% for the 2D case and 50% for the 3D case, respectively. These enhancements are further linked to the good mechanical interface of the curauá/epoxy when compared to the sisal [37, 38]. However, when compared to the GLASS specimens, the 2D case presented no significant difference and the 3D presented a slight enhancement of approx. 13%. Finally, the CURAUÁ 3D specimens presented a similar flexural stiffness to the GFRP (an approx. decrease of 8%). Similar to the tensile properties, the general trends observed for the flexural material properties are in line with the estimated range of the synthetic 3D woven composites [17].

3.1.3 Impact properties

Figure 7 presents the quantitative statistical data of the impact tests. It can be seen that the impact energy was significantly affected by the type of fibre and reinforcement architecture. All cases presented an enhancement in impact energy when compared to the JFRP specimens. For example, for the 2D reinforced hybrids, improvements in impact energy were found to be approx. 82% for SISAL, 77% for CURAUÁ and 87% for the GLASS specimens, respectively.

For the 3D fibre reinforced specimens, these enhancements were approx. 96%, 78% and 91% for the SISAL, CURAUÁ and GLASS specimens, respectively. Regarding the synthetic composite, an enhancement of approx. 36% in impact energy was observed when the GFRP is compared to the JFRP. These significant enhancements compared to the JFRP are linked to the brittle nature of the fibre, given the dynamic fast load state of the impact test, the quick to fail nature of the jute leads to low absorption. For the GFRP and hybrid specimens, a tendency of significant deformation during impact while maintaining the coupon in one piece, served to absorb more energy in plastic deformation. This was observed to be more significant for the SISAL and GLASS specimens, likely due to the individual fibre's ductility [7, 13].

As a function of reinforcement architecture, all the 3D reinforced specimens presented different variations in impact energy, when compared to their 2D counterparts. For instance, the SISAL 3D presented the most significant energy absorbed at an approx. 79% improvement when compared to the 2D specimens. Similar trends were observed for the GLASS specimens (i.e., an improvement of approx. 29%), while for the CURAUÁ specimens, no significant variation in impact energy was reported as a function of fibre architecture. When compared to the synthetic specimens, all the 3D and 2D hybrid composites presented significant enhancements in impact energy. For the CURAUÁ specimens this improvement was at approx. 65% when compared to the GFRP. For the GLASS specimens, improvements of approx. 80% and 73% were observed for the 2D specimens and 86% and 81% for the 3D ones, respectively. Finally, for the SISAL specimens the enhancement in impact energy when compared to the synthetic specimen was approx. 71% for the 2D case and 94% for the 3D specimens, when compared to the GFRP. This has been observed previously in the literature where sisal has been shown to present a suitable alternative for impact applications [39]. In general, both the 2D and 3D architectures have been shown to be effective at enhancing impact energy absorption when compared to the more standard synthetic fibre composites. This is a relevant observation for applications where impact resistance is key such as the automotive industry.

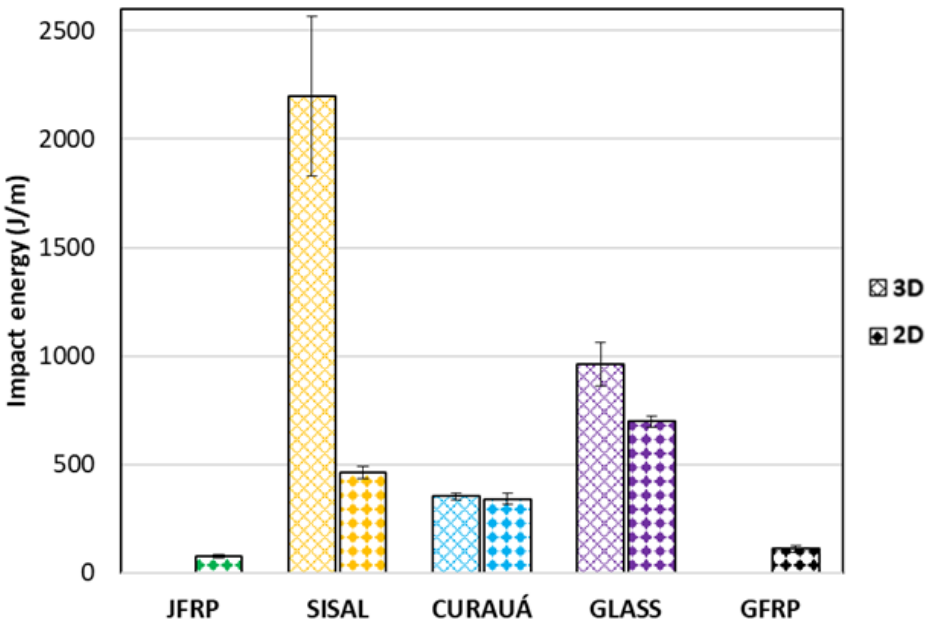


Figure 7. Impact test data as a function of reinforcement architecture.

3.1.4 Interlaminar Shear Strength (ILSS)

Figure 8 presents representative interlaminar shear stress-displacement curves of all the tested specimens as a function of fibre architecture, while Fig. 9 presents the quantitative statistical data.

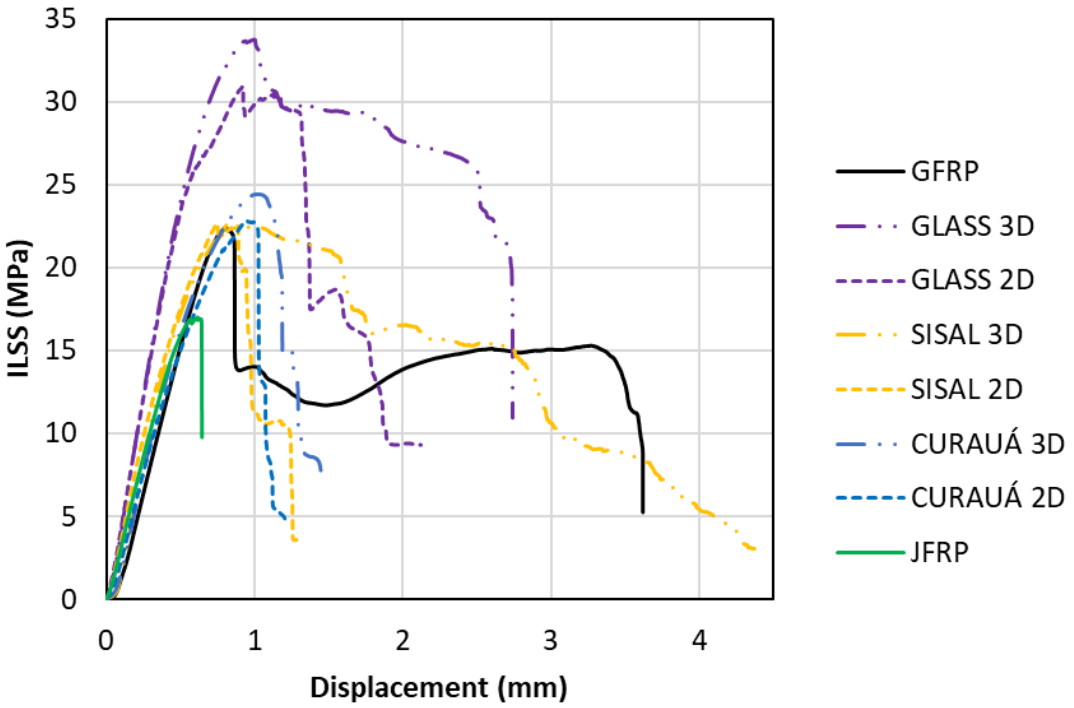


Figure 8. Representative interlaminar shear stress-displacement curves of all the tested specimens as a function of fibre architecture.

The general behaviour of the interlaminar shear failure of the short beam specimens show an apparent rigidity variation (Fig. 8). Interestingly, the GLASS hybrid specimens appear to have a slightly higher apparent interlaminar shearing stiffness. This observation correlates to the average ILSS values reported on Fig. 9. The failure behaviour also varied significantly with the type of fibre. For example, the JFRP presented the most brittle behaviour and earliest failure, while the hybrids presented a more ductile behaviour and failures at higher loads. From Fig. 9, the ILSS quantitative test data can be seen. It has been observed that, similar to the previous tests, all cases presented significant enhancements in the ILSS, when compared to the JFRP.

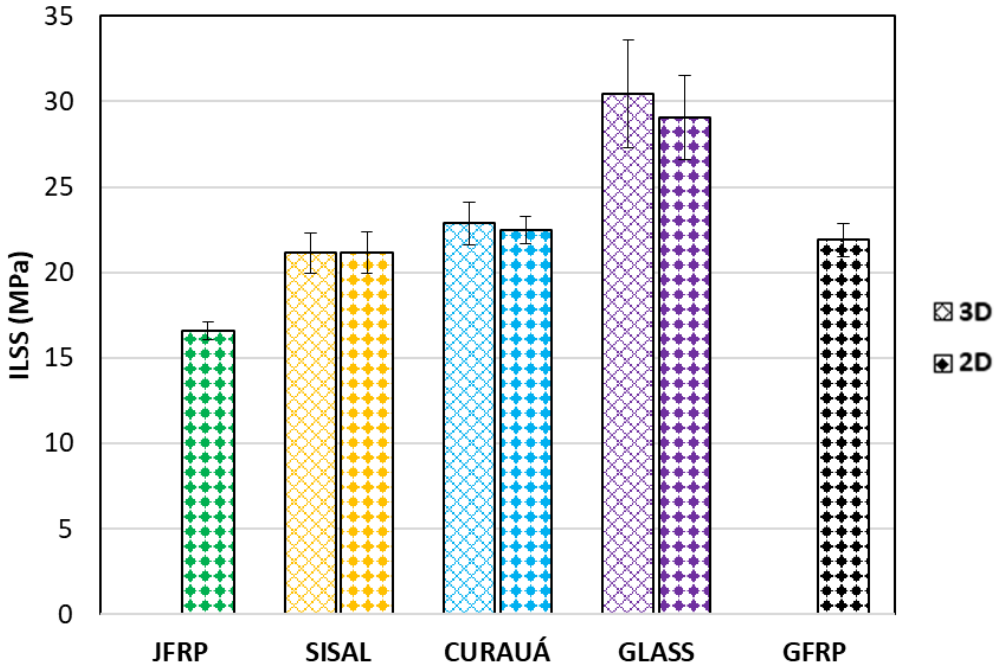


Figure 9. ILSS test data as a function of reinforcement architecture.

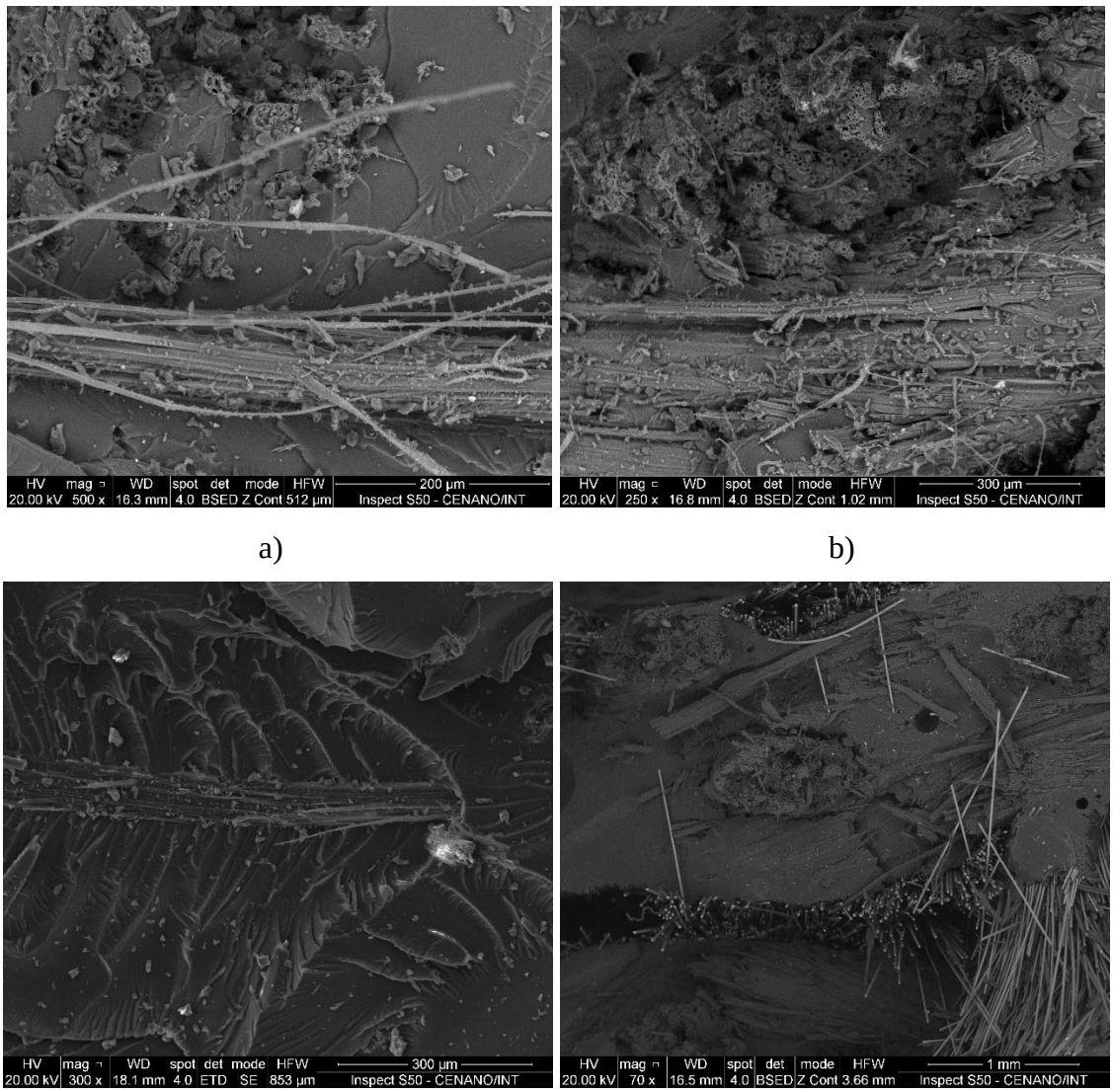
For example, for the 2D reinforced hybrids, improvements in ILSS were found to be approx. 21%, 26% and 43% for the SISAL, CURAUÁ and GLASS specimens, respectively. For the 3D fibre reinforced ones, these enhancements were approx. 22%, 28% and 46% for the SISAL, CURAUÁ and GLASS specimens, respectively. This is likely linked to the increase in interfacial surface area between the UD secondary fibre phases with the resin matrix, when compared to the neat jute. This increased mechanical interlocking with the surface fibrils and morphological structures of the secondary reinforcement significantly increased the required energy to shear the surfaces during testing [13].

As a function of reinforcement architecture, when the 3D specimens are compared to the 2D, the variations observed were not significant (~5%). This is likely due to the size of the specimen, since ILSS specimens are essentially three-point-bending specimens at a span to depth ratio of 4. Meaning that the specimens are quite small and therefore could only at most feature a single 3D fibre within its useful area. When compared to the synthetic specimens, the hybrid composites presented variations as a function of the type of fibre. For example, the SISAL and CURAUÁ specimens presented no significant variation in ILSS when compared to the GFRP, while the GLASS specimens presented

an enhancement of approx. 25% (see Fig. 9). This somewhat surprising result demonstrates that both the 3D and 2D architectures for the glass/jute hybrids, a good level of synergy between the fibre phases was reached and the ILSS was enhanced. This may be due to the vastly different surface morphologies of the fibre phases where the crack would have to transition between more smooth and rough fibres often, making it more difficult to propagate.

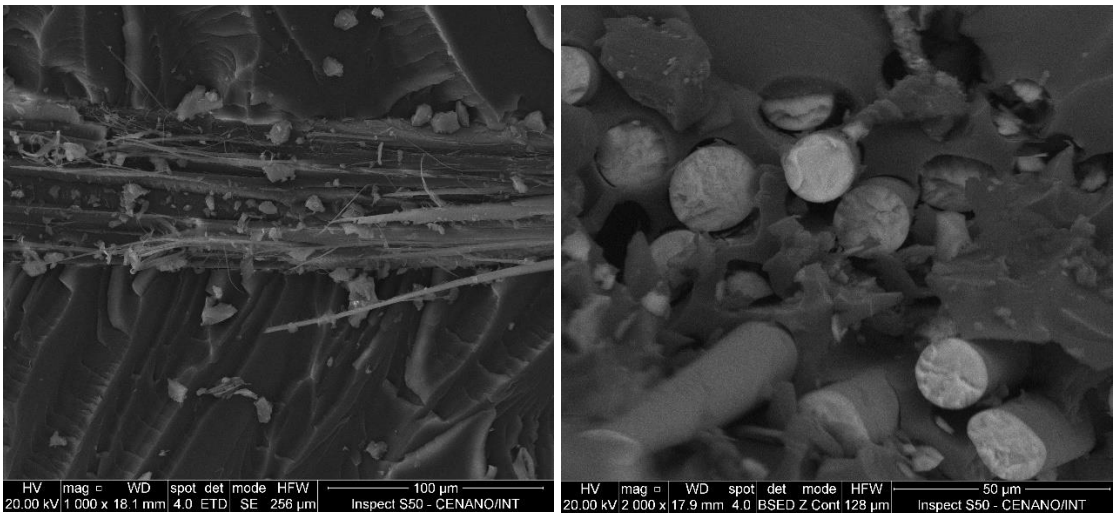
3.2 SEM fractography

From Fig. 10, representative SEM fractographic images can be seen. Not all specimens are shown due to failure mode similarities.



a) b)

c) d)



e) f)

Figure 10. Representative SEM images of a) CURAUÁ 2D, b) CURAUÁ 3D, c) SISAL 3D, d) GLASS 3D, e) detail of SISAL 3D and f) detail of GLASS 3D.

From Fig. 10a, the failure surface of the CURAUÁ 2D tensile specimens can be seen. The warp and weft fibres are visible along a mostly smooth (brittle) resin failure surface. The curauá/epoxy matrix interface is observed to be good, and no significant voids are visible. Similarly, from Fig. 10b, the CURAUÁ 3D failure can be observed. The warp and weft tows are also visible and good interface quality is seen. This was a general trend for the tested composites, and it is linked with the little variations found for the various mechanical tests carried out. From Fig. 10c, a detail of a partial debonding of a 3D fibre (transverse part) can be observed for the SISAL 3D specimen. It is noteworthy that the front of the crack propagation is at the edge of the transverse reinforcement (right side of the image) where the fibre enters the composite. This demonstrates the high stress state at the edge of the transverse reinforcement as a significant crack front is visible stemming from the edge and propagating throughout the partial debonding. The hollow remnant of where the transverse fibre used to be is visible along with some delaminated fibrils and the significant fibre cracking by scarfs and riverlines, indicates the strong adherence between the matrix and fibre [40]. Figure 10e, presents a close-up of the debonding and fibrils still attached to the resin are visible, evidencing a good interface between the 3D sisal reinforcement and the matrix. Finally, from Fig. 10d, the failure surface of the GLASS 3D specimens can be seen. Jute warp and weft tows can be seen as well as glass

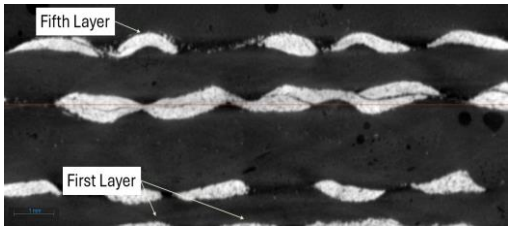
reinforcement. Overall, good fibre/matrix interfaces are visible with the expected glass fibre fibrillation failure [41]. From Fig. 10f, a close-up of the glass reinforcement presents the ductile failure of the glass fibres and a slight warping and debonding of the interface during failure.

3.3 MicroCT analysis

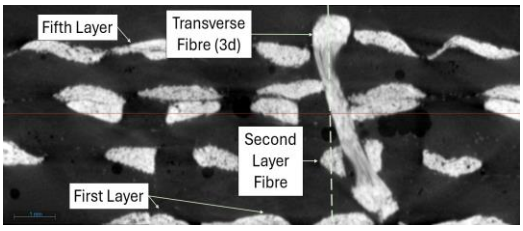
X-ray computed tomography is a powerful tool to non-destructively analyze the interior structure of multiphase materials such as fibre-reinforced composites. This is due to the high resolution and the ability to accurately visualize their internal 3D multi-scale structures [42]. The MicroCT analysis were done to identify the fibre fabric positions, reinforcement volumetric conditions and number and geometry of voids resulting from the manufacturing process. Figure 11 presents 2D slices of the GLASS 3D, SISAL 3D and CURAUÁ 3D samples. Figure 11a and b present different slices at different points in the length of the specimen (17.79 mm depth, see Table 2), in order to assess the general crimp of the reinforcement layers throughout the specimen. It can be seen from Fig. 11a that the composite presents very high anisotropy, as expected for these multi-phase composites [42]. For example, the intralaminar glass reinforcement can be seen in white, while the matrix and jute fibre phases are in darker colors. It is evident that due to the compression molding fabrication process, the glass fibre bundles were compressed unevenly, and the resin-rich interlaminar space between each glass layer diverges significantly. From Fig. 11b, the mid-point slice can be seen, and it is apparent that significant crimp is present for the interlaminar reinforcement layers due to their position relative to the previous slice. Furthermore, a transverse reinforcement fibre is visible crossing the height of the specimen at an angle significantly different from the idealized orthogonal (dotted line). Moreover, it is also visible that this transverse fibre has punctured through an intralaminar reinforcement fibre. It is noted that the micromechanical state and therefore the stress state prevailing within the composite is highly complex owing to the extreme anisotropy of the composite cross section. Despite this, no significant variation in mechanical properties was observed between the 3D and 2D composites, suggesting that the negative influence of the 3D fibre was compensated likely due to the part of the 3D weave that is in the main loading direction (top and bottom of the specimens).

From Fig. 11c and d, the microCT 2D cross-sections of the CURAUÁ 3D and SISAL 2D can be seen. It is possible to observe from Fig. 11c that an even higher anisotropic state prevails within the CURAUÁ 3D specimen when compared to the GLASS 3D. This is somewhat expected given the in-natura fibres used compared to the industry-made glass fibres. Curauá fibre bundles can be seen and a highly significant difference in cross section is visible from one fibre bundle to the next. This is due to the compression molding fabrication as well as the jute bidirectional fabric. Some fibre bundles compressed the jute weft tows more, others less. A similar situation can be seen for the SISAL 2D (see Fig. 11d), however, to a lesser extent given that an industrially made sisal roving was used as intralaminar reinforcement. Despite the more organized distribution of the SISAL 2D specimen, still a very high anisotropic state is observed.

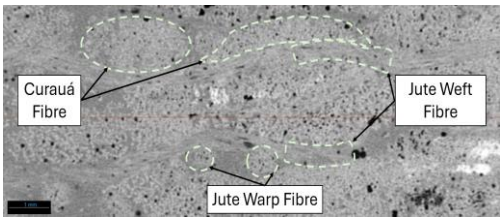
The segmentations of the samples were made in three distinct parts: matrix, reinforcement, and voids (see Fig. 11e and f). For the SISAL 2D, it was possible to highlight a fibre volumetric fraction of 57.50% (both jute and sisal), as well as a void fraction of 1.13%, demonstrating the efficiency of the hot compression process in impregnating the natural composite and the importance of high pressure in eliminating bubbles.



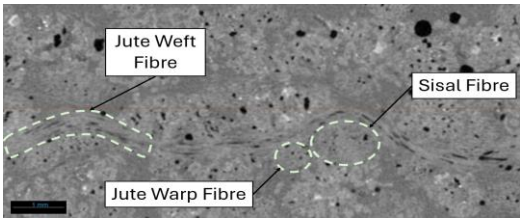
a)



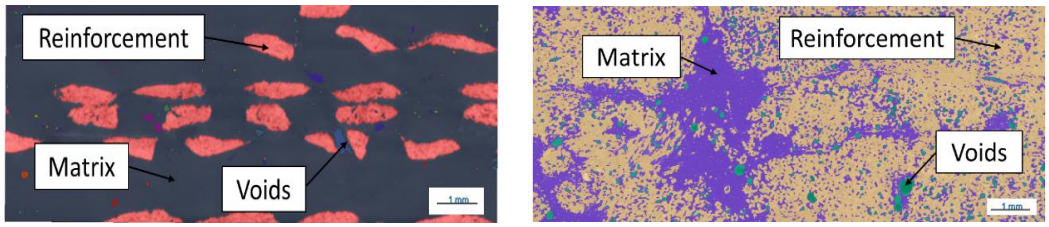
b)



c)



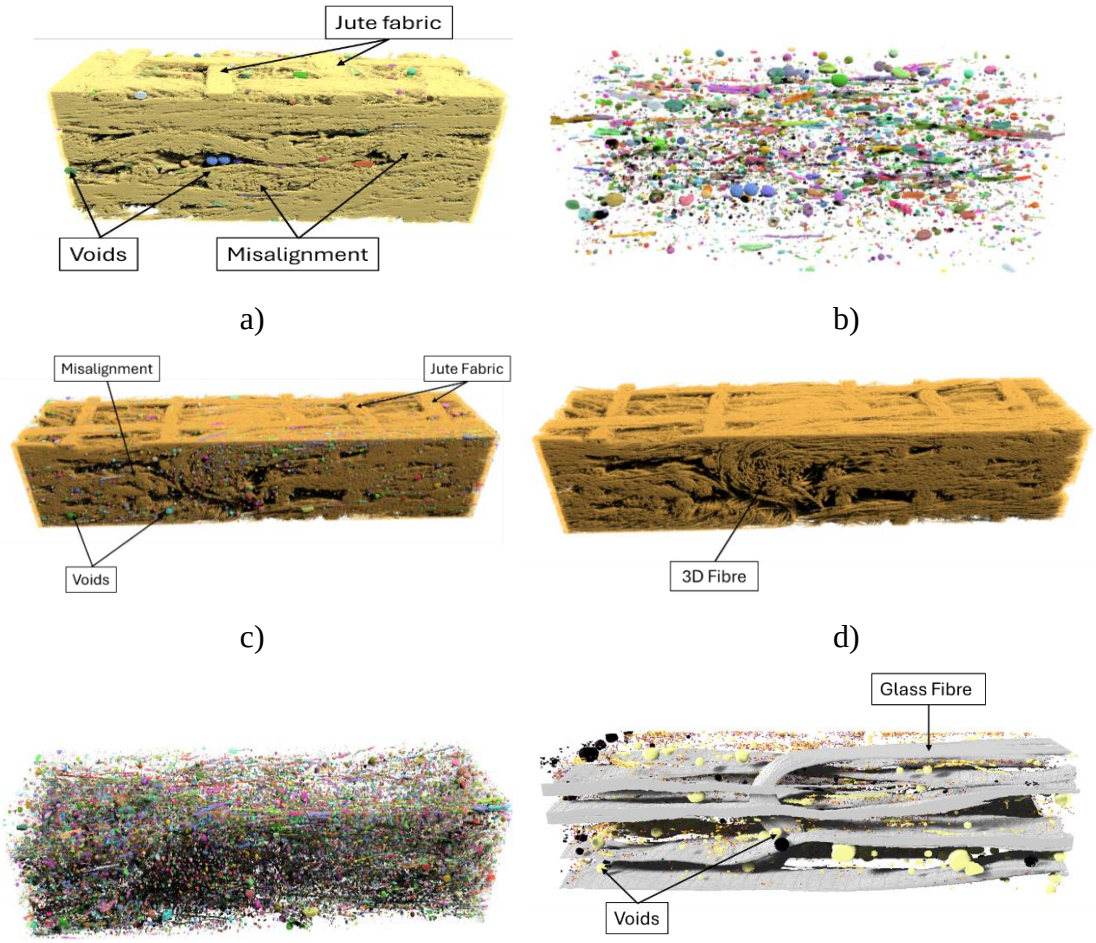
d)



e) f)

Figure 11. Representative cross-sections of the X-ray analysis: a) GLASS 3D (edge of specimen), b) GLASS 3D (middle of the specimen), c) CURAUÁ 3D, d) SISAL 2D, e) Segmented GLASS 3D and f) Segmented CURAUÁ 3D.

Through the segmentation of the fabric and voids (see Fig. 12) it is possible to observe the presence of misalignment areas, stemming from manufacturing issues that may have direct impacts on load transfer. Additionally, it can be noted that most voids (see Fig. 12a) are located externally to the yarns, indicating efficient impregnation within the yarn.



a) b)

c) d)

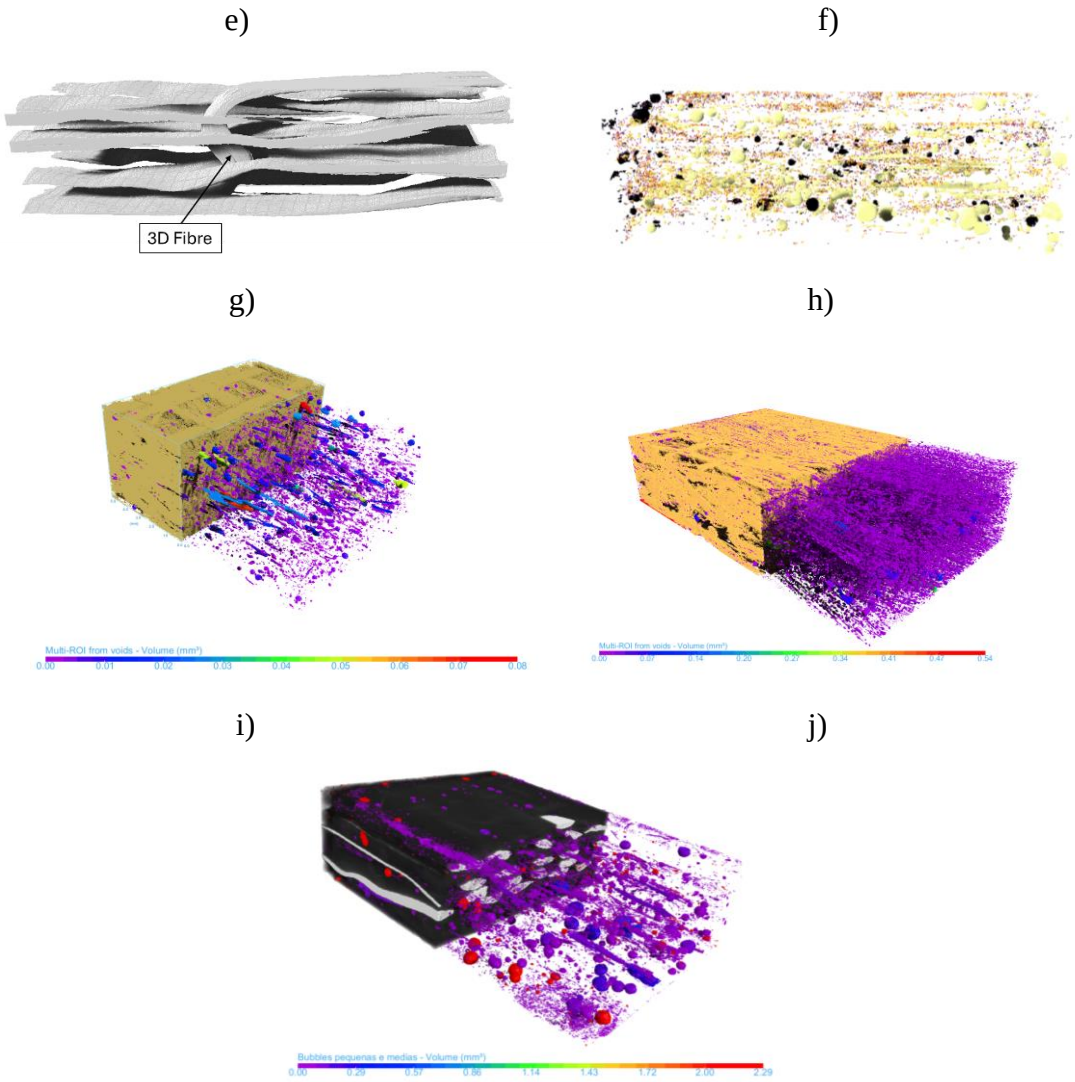


Figure 12. 3D segmentate model of a) 2D SISAL fabric and voids, b) 2D SISAL voids; c) CURAUÁ 3D fabric and voids d) CURAUÁ 3D fabric and e) CURAUÁ 3D voids; f) GLASS 3D fabric and voids g) GLASS 3D fabric, h) GLASS 3D voids and 3D model statistical analysis of the voids: i) SISAL 2D, j) CURAUÁ 3D and k) GLASS 3D.

The CURAUA 3D (see Fig. 12c, d and e) exhibits a fibre volumetric fraction of 62.14%, as well as a void fraction of 3.90%. Compared to the SISAL 2D, the concentration of voids is notably higher, this is likely due to the fibre bundle size differences. Since the curauá bundles were in-natura, their points of entry into the preform (transverse fibres), generated high pockets of resin rich zones and areas prone to void formation during curing. In this case, through segmentation, in addition to cases of misalignment and non-

uniform distribution, the voids (see Fig, 12c) are found both externally and internally to the yarns, indicating that the impregnation process was not sufficient for effective reduction of voids, thus suggesting an inefficient impregnation within the fabric. Furthermore, from Fig. 12d, significant transverse fibre crimp is visible, induced by the compression during fabrication. It can be seen that the fibre bundle collapsed and spread out, likely generating localized stresses. However, as evidenced by the mechanical properties, these discontinuities did not present significant decreases in the material characteristics.

Finally, the GLASS 3D (Fig. 12f, g and h) exhibited a glass fibre volumetric fraction of 17.48%, as well as a void fraction of 1.44%. Due to the high contrast of the resulting tomography, it was only possible to accurately calculate the synthetic fibre phase. During the segmentation of the fibres and voids (see Fig. 12f), the spacing between fibres is evident, unlike in previous cases. In this instance, the voids (Figure 12h) are dispersed within the matrix, indicating that, in this scenario, the presence of voids occurs due to inadequate pressure in the matrix, compromising the expulsion of bubbles. From Fig. 12g, the 3D fibre can be seen, and a high state of crimp and bending is visible at the surfaces. However, through the composite, the fibre is bent but no significant bundle collapse and opening is visible, distinct from the CURAUÁ 3D specimen.

Figure 12 presents the statistical distribution of the voids for the tested samples. For the SISAL 2D (see Fig. 12i), it is possible to identify that the primary type of void exhibits a regular shape (aspect ratio near 1) and low volume (less than 0.02 mm^3), indicating uneliminated bubbles in the composite. However, there are voids with larger volumes and less regular shapes, where one of their dimensions is notably greater than the others. These elements can be attributed to areas between fabrics where the process failed to achieve complete impregnation. The significant number of voids is reflected in the statistical analysis. For the CURAUÁ 3D specimen, the primary type of void exhibited a similar regular shape (aspect ratio near 1) and low volume (less than 0.01mm^3), with few instances of larger-sized elements (see Fig. 12j). This suggests that the main impregnation issue lies in the movement of resin within the fibre. Regarding the GLASS 3D sample, (see Fig. 12k), the first characteristic to be highlighted is that this type of void exhibits a more irregular shape (aspect ratio different than 1) and a low volume (less than 0.05mm^3). A few isolated bubbles were also identified in the matrix.

From Table 4, the total fibre volume and void fractions of the analysed samples can be seen. It has been reported that void fractions tend to increase when the fibre volume fraction exceeds 40% [43] and this was observed case when the SISAL 2D is compared to the CURAUÁ 3D. Higher void fractions are linked to lower composite mechanical properties, therefore, lower void fractions are crucial. The voids form when the resin is unable to displace trapped air within the stacked fibre fabrics during fabrication. In vacuum infusion processes these are linked to factors such as vacuum quality, resin viscosity reinforcement material permeability [6]. Nevertheless, this research shows the importance of the applied pressure during fabrication, as a hydraulic press is capable of generating much higher internal pressure in the composites during curing, displacing the air trapped within.

Table 4. Composite fibre volume and void fractions.

Sample	Fibre vol. (%)	Void fraction (%)
SISAL 2D	57.50	1.13
CURAUÁ 3D	62.14	3.90
GLASS 3D	17.48*	1.44

* Synthetic (intralaminar and transverse) fibre phases only.

From Table 4, it can be seen that the SISAL 2D and CURAUÁ 3D samples presented high fibre volumetric fractions for this manufacturing type (higher than 40%). For the GLASS 3D sample, only the synthetic phases (intralaminar and transverse) were viable to calculate due to the difficulty in separation of phases in the histogram. Despite this, as can be seen in Table 4, all total void fractions calculated via X-ray microCT were below 5%. Similar void fractions are reported in the literature, however, a more complex fabrication method was used [6]. These low void fractions are due to a combination of high pressures applied by the press and the fabrication methodology which via a silicone ring, was able to significantly increase the hydrostatic pressures during composite consolidation, while maintaining the orientation of the fibre fabrics. It is well known that different industrial sectors present different thresholds of internal discontinuities for composite materials and it has been reported that for sectors such as automotive and marine, void fractions at or below 5% are acceptable [44]. Therefore, this research presented a relatively simple fabrication technique for novel natural fibre hybrid composites which present good mechanical properties and low internal void fractions. It

is expected that will also lead to significantly increasing fracture toughness and delamination resistance owing to the transverse reinforcement (this aspect is investigated in ongoing research).

4. CONCLUSIONS

This research explored novel 3D fiber-reinforced hybrid composites, using jute bidirectional fabric with secondary reinforcement phases (sisal, curauá, and glass fibers). These were woven unidirectionally for 2D architecture and orthogonally for 3D architecture. Pure jute and glass fiber-reinforced composites were also tested for comparison. All hybrid composites showed improved properties compared to JFRP specimens, with a trend of increasing tensile and flexural strength and stiffness from natural to synthetic reinforcements. Curauá fibers matched GFRP stiffness, and sisal fibers showed superior impact absorption. Mechanical properties of 2D and 3D specimens were similar, with variations within 20%, consistent with existing literature. SEM microscopy revealed good fiber/matrix interfaces, while microCT showed high anisotropy and low void fractions (below 5%). These results highlight the potential of these composites for demanding engineering applications, contributing to the development of more sustainable and high-performing natural fiber-reinforced composites.

REFERENCES

1. Neto, J., et al., *A Review of Recent Advances in Hybrid Natural Fiber Reinforced Polymer Composites.* Journal of Renewable Materials, 2022. **10**(3): p. 561--589.
2. Pickering, K.L., M.G.A. Efendy, and T.M. Le, *A review of recent developments in natural fibre composites and their mechanical performance.* Composites Part A: Applied Science and Manufacturing, 2016. **83**: p. 98-112.
3. de Queiroz, H.F.M., M.D. Banea, and D.K.K. Cavalcanti, *Adhesively bonded joints of jute, glass and hybrid jute/glass fibre-reinforced polymer composites for automotive industry*. Applied Adhesion Science, 2021. **9**(1): p. 2.
4. de Queiroz, H.F.M., et al., *A novel 3D fibre-reinforcement architecture for high performance natural fibre reinforced composite adhesively bonded joints.* The Journal of Adhesion, 2023: p. 1-21.
5. Queiroz, H., et al., *Mechanical characterization of jute/carbon hybrid epoxy composites.* Proceedings of the Institution of Mechanical Engineers, Part L: Journal of Materials: Design and Applications, 2024: p. 14644207241233947.
6. Sezgin, H. and O.B. Berkalp, *The effect of hybridization on significant characteristics of jute/glass and jute/carbon-reinforced composites.* Journal of Industrial Textiles, 2017. **47**(3): p. 283-296.
7. Cavalcanti, D.K.K., et al., *Mechanical characterization of intralaminar natural fibre-reinforced hybrid composites.* Composites Part B: Engineering, 2019. **175**: p. 107149.
8. Awais, H., et al., *Effect of comingling techniques on mechanical properties of natural fibre reinforced cross-ply thermoplastic composites.* Composites Part B: Engineering, 2019. **177**: p. 107279.
9. Bahrami, M., et al., *Characterization of hybrid biocomposite Poly-Butyl-Succinate/Carbon fibers/Flax fibers.* Composites Part B: Engineering, 2021. **221**: p. 109033.
10. Chee, S.S., et al., *Thermomechanical and dynamic mechanical properties of bamboo/woven kenaf mat reinforced epoxy hybrid composites.* Composites Part B: Engineering, 2019. **163**: p. 165-174.
11. Fiore, V., et al., *Salt-fog spray aging of jute-basalt reinforced hybrid structures: Flexural and low velocity impact response.* Composites Part B: Engineering,

2017. **116**: p. 99-112.

12. Jawaid, M., et al., *Effect of jute fibre loading on tensile and dynamic mechanical properties of oil palm epoxy composites.* Composites Part B: Engineering, 2013. **45**(1): p. 619-624.
13. de Araujo Alves Lima, R., et al., *Effect of surface treatments on interfacial properties of natural intralaminar hybrid composites.* Polymer Composites, 2020. **41**(1): p. 314-325.
14. Ahmad, F., N. Yuvaraj, and P.K. Bajpai, *Effect of reinforcement architecture on the macroscopic mechanical properties of fiberous polymer composites: A review.* Polymer Composites, 2020. **41**(6): p. 2518-2534.
15. Stegschuster, G., et al., *Experimental determination of the mode I delamination fracture and fatigue properties of thin 3D woven composites.* Composites Part A: Applied Science and Manufacturing, 2016. **84**: p. 308-315.
16. Saleh, M.N. and C. Soutis, *Recent advancements in mechanical characterisation of 3D woven composites.* Mechanics of Advanced Materials and Modern Processes, 2017. **3**(1): p. 12.
17. Mouritz, A.P. and B.N. Cox, *A mechanistic interpretation of the comparative in-plane mechanical properties of 3D woven, stitched and pinned composites.* Composites Part A: Applied Science and Manufacturing, 2010. **41**(6): p. 709-728.
18. Liu, Q. and M. Hughes, *The fracture behaviour and toughness of woven flax fibre reinforced epoxy composites.* Composites Part A: Applied Science and Manufacturing, 2008. **39**(10): p. 1644-1652.
19. Bogdanovich, A.E., et al., *Experimental study of joining thick composites reinforced with non-crimp 3D orthogonal woven E-glass fabrics.* Composites Part A: Applied Science and Manufacturing, 2011. **42**(8): p. 896-905.
20. Ladani, R.B., et al., *Delamination toughening and healing performance of woven composites with hybrid z-fibre reinforcement.* Composites Part A: Applied Science and Manufacturing, 2018. **110**: p. 258-267.
21. Boussu, F., I. Cristian, and S. Nauman, *General definition of 3D warp interlock fabric architecture.* Composites Part B: Engineering, 2015. **81**: p. 171-188.
22. Tong, L., A.P. Mouritz, and M. Bannister, *3D fibre reinforced polymer composites*. 2002: Elsevier.

23. Clarke, J., et al., *A Cost Model for 3D Woven Preforms.* Journal of Composites Science, 2022. **6**(1): p. 18.
24. Nematollahi, M., et al., *Experimental and Numerical Study of the Critical Length of Short Kenaf Fiber Reinforced Polypropylene Composites.* Fibers and Polymers, 2020. **21**(4): p. 821-828.
25. Dai, S., et al., *Influence of fibre architecture on the tensile, compressive and flexural behaviour of 3D woven composites.* Composites Part A: Applied Science and Manufacturing, 2015. **69**: p. 195-207.
26. Guénon, V.A., T.W. Chou, and J.W. Gillespie, *Toughness properties of a three-dimensional carbon-epoxy composite.* Journal of Materials Science, 1989. **24**(11): p. 4168-4175.
27. Wielhorski, Y., et al., *Numerical modeling of 3D woven composite reinforcements: A review.* Composites Part A: Applied Science and Manufacturing, 2022. **154**: p. 106729.
28. Seltzer, R., et al., *X-ray microtomography analysis of the damage micromechanisms in 3D woven composites under low-velocity impact.* Composites Part A: Applied Science and Manufacturing, 2013. **45**: p. 49-60.
29. Jabbar, M., et al., *Effect of the stuffer yarns on the mechanical performance of novel 3D woven green composites.* Composite Structures, 2021. **269**: p. 114023.
30. Kashif, M., et al., *Optimization of 3D woven preform for improved mechanical performance.* Journal of Industrial Textiles, 2019. **48**(7): p. 1206-1227.
31. Hussain, M., et al., *Properties and characterization of novel 3D jute reinforced natural fibre aluminium laminates.* Journal of Composite Materials, 2021. **55**(14): p. 1879-1891.
32. Jabbar, M., et al., *Mechanical Response of Novel 3D Woven Flax Composites with Variation in Z Yarn Binding.* Journal of Natural Fibers, 2020. **17**(6): p. 890-905.
33. Khan, M.I., et al., *Development of composites, reinforced by novel 3D woven orthogonal fabrics with enhanced auxeticity.* Journal of Industrial Textiles, 2019. **49**(5): p. 676-690.
34. Nawab, Y., et al., *Development & Characterization of Green Composites Using Novel 3D Woven Preforms.* Applied Composite Materials, 2018. **25**(4): p. 747-759.

35. Chowdhury, S. and B.K. Behera, *Low-velocity impact response of 3D woven solid structures for multi-scale applications: role of yarn maneuverability and weave architecture.* Journal of the Brazilian Society of Mechanical Sciences and Engineering, 2024. **46**(3): p. 138.
36. Olhan, S., et al., *Investigating the impact of different machinability processes and fibre architecture on the bearing performance of pin-loaded textile structural composites for automotive applications: Experimental and finite element analysis.* Journal of Manufacturing Processes, 2023. **86**: p. 30-55.
37. Fiore, V., et al., *A new eco-friendly chemical treatment of natural fibres: Effect of sodium bicarbonate on properties of sisal fibre and its epoxy composites.* Composites Part B: Engineering, 2016. **85**: p. 150-160.
38. Neto, J.S.S., et al., *Effect of Multi-Walled Carbon Nanotubes on the Mechanical and Thermal Properties of Curauá Natural-Fiber-Reinforced Composites.* C, 2023. **9**(4): p. 102.
39. Rohen, L.A., et al., *Ballistic Efficiency of an Individual Epoxy Composite Reinforced with Sisal Fibers in Multilayered Armor.* Materials Research, 2015. **18**.
40. Yesgat, A.L. and R. Kitey, *Effect of filler geometry on fracture mechanisms in glass particle filled epoxy composites.* Engineering Fracture Mechanics, 2016. **160**: p. 22-41.
41. Ramesh, M., K. Palanikumar, and K.H. Reddy, *Mechanical property evaluation of sisal–jute–glass fiber reinforced polyester composites.* Composites Part B: Engineering, 2013. **48**: p. 1-9.
42. Gao, Y., et al., *A review of applications of CT imaging on fiber reinforced composites.* Journal of Composite Materials, 2022. **56**(1): p. 133-164.
43. Sreekala, M.S., et al., *The mechanical performance of hybrid phenol-formaldehyde-based composites reinforced with glass and oil palm fibres.* Composites Science and Technology, 2002. **62**(3): p. 339-353.
44. Shah, D.U., *Developing plant fibre composites for structural applications by optimising composite parameters: a critical review.* Journal of Materials Science, 2013. **48**(18): p. 6083-6107.

Paper 4

Impact response of novel 3D hybrid composites under perforation and low energy impact fatigue

Enhancement of impact behaviour of natural-fibre reinforced composites via 3D orthogonal architecture: perforation and impact fatigue analysis

H. F. M. de Queiroz[1], R. Ciardiello[2], M.D. Banea[1,3*]

[1]Federal Centre of Technological Education in Rio de Janeiro (CEFET/RJ), Brazil.

[2]Department of Mechanical and Aerospace Engineering, Politecnico di Torino, 10129 Turin, Italy

[3]CICECO - Aveiro Institute of Materials, Department of Materials and Ceramic Engineering, University of Aveiro, 3810-193 Aveiro, Portugal

Abstract

This research focuses on the dynamic response analysis of novel 3D natural fibre-reinforced hybrid composites. Natural fibre hybrid composites reinforced using two distinct techniques: intralaminar (2D) and orthogonal-through-the-thickness (3D-OTT) reinforcement were fabricated. Jute bidirectional fabric was used as the primary fibre phase, while secondary reinforcement phases (sisal and curauá) were unidirectionally woven through the jute fabric in the 2D intralaminar architecture. For the 3D architecture, a transverse fibre phase was additionally woven orthogonally through the thickness of the fibre preforms, providing through-the-thickness reinforcement. Pure jute fibre-reinforced composites were also fabricated and tested as comparison samples under low velocity impact (LVI). Both full-perforation and repeated LVI fatigue tests were conducted to assess the maximum energy absorption and load-bearing capacity of the composites, as well as their fatigue life under repeated low-energy impacts. These tests simulate real-life scenarios, such as hailstorms or falling debris, to evaluate the durability and impact resistance of the composites. It was found that for perforation the SISAL 2D specimens presented the highest absorbed energy and peak load due to the delamination of sisal fibres from the resin generating large debonding areas that absorb energy. Furthermore, for the 3D reinforcement, the impact fatigue life was significantly enhanced (i.e., 3.6x and 2x for the SISAL and CURAUÁ specimens, respectively). Micro-CT analysis showed distinct crack-arrest mechanisms for each fibre type (i.e. for SISAL, the 3D reinforcement substantially reduces crack initiation and propagation, while the CURAUÁ specimens exhibit a natural tendency for crack arrest due to the unique qualities of the

fibre/matrix interface.

Keywords: Composite structures, hybrid composites, natural fibre composites, 3D architectures.

1. INTRODUCTION

In the quest for advanced materials that exhibit superior mechanical performance while decreasing overall environmental impact, natural fibre-reinforced composites (NFRCs) have emerged as a prominent candidate. Natural fibres, such as jute, flax, hemp and sisal, are extracted from renewable sources and their use in composites contributes to sustainability goals by reducing reliance on non-renewable synthetic fibres. This reduction is directly linked to the overall trend across multiple industrial sectors to reduce as much as possible the carbon-footprint of composite structures [1]. Furthermore, natural fibres are biodegradable which further reduces their environmental impact at end-of-life. When compared to their synthetic counterparts, natural fibres present lower cost as well as lower structural weight [2]. Their specific strength and stiffness (i.e., relative to their weight) is high as well as their significant capacity to absorb vibration (damping) [3]. However, the use of NFRCs is hindered by significant drawbacks such as moisture absorption, variability of fibre properties and the possibility of a weak interface with the resin matrix [4]. There are several techniques that can be applied to resolve some of these issues, such as, interlaminar hybridization with synthetic fabrics to reduce water uptake and chemical treatments to enhance fibre/matrix interface [5]. The automotive industry has been in the process of increasingly integrating NFRCs into vehicle structures due to their many attractive characteristics [6]. During the service of vehicular structural components, low-velocity impact (LVI) events are expected. In particular, front and side collisions are of great concern to the safety obligations of the automotive sector [7]. The most common low-velocity impacts are falling objects or a particularly severe hailstorm. It is noteworthy that in the world of low velocity impacts, it is not necessary for the surface of a composite material to be visibly damaged for a significant crack development to occur inside the structure. Barely visible impact damage (BVID) may already have created sufficient internal cracks to significantly reduce the lifespan of a composite material [8]. Moreover, it is known in the literature that the performance of NFRCs is not optimized for impact resistance and perforation energy absorption. Even at LVIs that are

far below the perforation energy, through-the-thickness fibre failure is the most common damage mode for some natural fibre failures [9]. Therefore, the analysis of not only a single high energy complete perforation impact is necessary to ascertain the total energy a composite material may absorb, but also, lower energy repeated impacts are relevant to reach a more complete comprehension of the material damage evolution. Following an impact event, delamination-induced internal damage is very common in composite materials, leading to a reduction in material properties [10]. In order to surpass these drawbacks, 3D fibre architectures such as orthogonal through-the-thickness (OTT) reinforcements aim to enhance the transverse tensile strength, stiffness and delamination resistance of composite materials [11]. Traditional 2D composites, while offering excellent in-plane properties, often fall short in through-the-thickness performance and damage tolerance [12]. The effect of 3D fibre architectures in composite impact performance enhancement has been analysed by various authors [13-16]. Progress in the field of technical textiles and weaving technologies has allowed for the emergence of 3D woven textile composites as a substitute for 2D composites [6]. These distinctive features of through-the-thickness reinforcement has recently lead the automotive industry to utilize 3D woven composites [17-19]. More recently, the use of natural fibres in 3D reinforced composite materials is gaining attention due to their environmental benefits, cost-effectiveness, and satisfactory mechanical properties [20-27]. For instance, Queiroz et al. [28] showed that by using a transverse fibre reinforcement phase (OTT), an improvement was observed in the single lap bonded joint performance of the composites. This was due to the likely significantly improved fracture toughness of the adherend. Despite the potential applications of 3D woven composites, significant limitations exist. It is expected that the in-plane properties will decrease when compared to non-crimp 2D fabric composites (perhaps as much as 20%). This crimp is the undulation that results from the interlacing of the multiple fibre fractions and directions. Moreover, the damage mechanisms are complex and involve damage within and between yarns and resin rich regions as well as voids and geometrical imperfections due to the manufacturing compaction process. Recently, Olhan et al. [6] performed an experimental investigation to evaluate the drop-weight low-velocity impact (LVI) and quasi-static compression-after-impact (CAI) characteristics of unidirectional (UD) laminates, along with 2D and 3D textile composites made from basalt, glass, and sisal fibres using the VARTM

technique. All specimens were subjected to three different impact energy levels 20 J, 30 J, and 40 J. The resulting contact force–time, force–displacement, and energy–time curves were recorded and analysed. They found that the 3D woven samples absorbed more energy compared to the UD and 2D specimens across all impact energy levels.
However, additional mechanical characterization of these materials is necessary, as the field of three-dimensional fibre reinforcement in NFRCs is still in its early stages. To the knowledge of the authors, the analysis of perforation and repeated impact fatigue life of 3D fibre architectures in NFRCs has not been done in the literature to date. This paper explores the properties of 3D hybrid fibre-reinforced composites, focusing on their behaviour under two impact scenarios: full perforation and LVI repeated impacts. By examining factors such as fibre type, fibre/matrix interface quality and the three-dimensional arrangement of fibres, we aim to elucidate the mechanisms that contribute to enhanced impact resistance and impact fatigue life. Additionally, the study investigates the influence of hybridization on damage progression and energy dissipation during impact events.

2. MATERIALS AND METHODS

2.1. Materials

This research effort is part of an ongoing project of analysis of novel 3D reinforced NFRCs. The primary reinforcement phase consisted of pure jute fibre bidirectional fabrics, supplied by Sisalsul (São Paulo, Brazil), while curauá and sisal fibres were the secondary reinforcements for the 2D and 3D fibre preforms. The intralaminar reinforcement utilized a 2D configuration, where the secondary fibres were woven unidirectionally into a balanced 2x2 jute bidirectional fabric. Additionally, a tertiary fibre reinforcement was introduced in the through-the-thickness (transverse) direction, creating a 3D orthogonal through-thickness (OTT) fibre architecture for the NFRC preforms ((see Fig. 1). The curauá fibres used in this research were supplied by the Federal University of Pará, Brazil in-natura. The curauá fibres were washed to remove any dirt and debris then subsequently dried in an oven at 100 ºC until completely dry (controlled by weight). The sisal (APAEB 700/1, Bahia, Brazil) used were industrially made fibre rovings. For the 3D OTT preforms, the transverse reinforcement was woven through 5 layers of 2D intralaminar fabrics. A more detailed description of the fibre architecture reinforcement

fabrication (for both 2D and 3D) can be found in a previous research [28]. The mechanical properties of the fibres can be seen in Table 1. A bicomponent epoxy resin matrix, HEX 135 SLOW (Barracuda Advanced Composites, SP, Brazil), was used to fabricate the composite plates. The material properties of the resin matrix used can be seen in Table 2.

Table 1. Typical single fibre mechanical properties [32, 39].

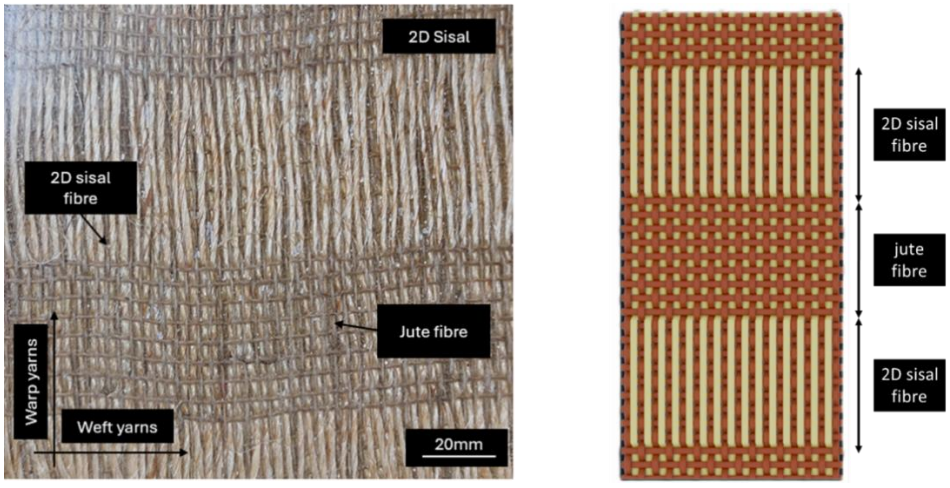
Fibre	Tensile strength (MPa)	Young's modulus (GPa)	Elongation at break (%)
Jute	254-773	22-26.5	1.5-2.5
Curauá	500-1900	44-128	3.7-4.3
Sisal	468-700	9.4-38	2-7

Table 2. Mechanical properties of the resin matrix used.

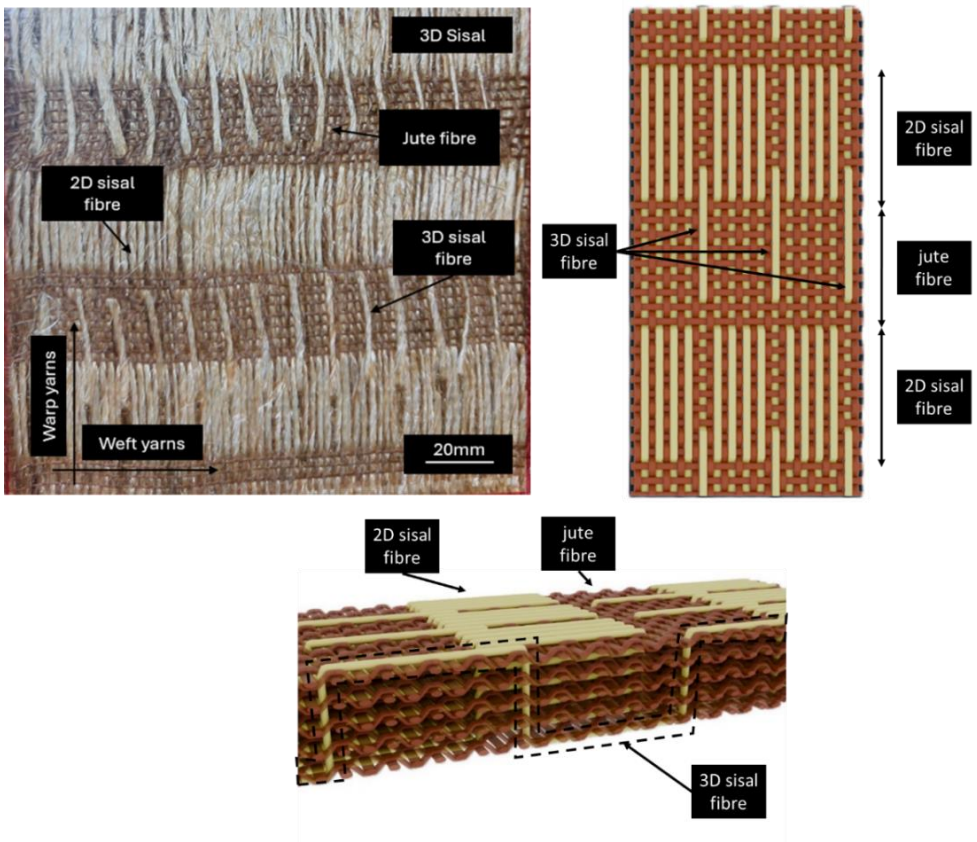
Polymer	Tensile strength (MPa)	Young's modulus (GPa)	Tensile strain (%)
HEX 135 SLOW	60.92 ± 1.42	3.25 ± 0.008	3.20 ± 0.20

Table 3. Composite material nomenclature and description.

Composite	Description
JFRP	Pure jute fibre-reinforced polymer composites
CURAUÁ 2D	Jute fabric reinforced with woven curauá UD
SISAL 2D	Jute fabric reinforced with woven sisal UD
CURAUÁ 3D	CURAUÁ 2D reinforced with transverse orthogonal curauá fibres
SISAL 3D	SISAL 2D reinforced with transverse orthogonal sisal fibres



a)



b)

Figure 1. Representative a) SISAL 2D fabricated composite plate and idealized schematic, b) SISAL 3D fabricated composite plate and idealized schematic [38].

2.2 Specimen fabrication

The composites were fabricated using the compression moulding technique via a steel mould and a heated hydraulic press, Solab SL 20 (São Paulo, Brazil). The composite curing followed the manufacturer's guidelines at 70 degrees Celsius for 8 hours under pressure. The composite panel thickness varied slightly as a function of fibre type and architecture (the JFRP was approx. 2 mm, while the SISAL 2D was 5.33 ± 0.11 mm, the SISAL 3D was 5.37 ± 0.06 mm, the CURAUÁ 2D was 5.09 ± 0.09 mm, and the CURAUÁ 3D was 4.96 ± 0.36 mm). The test specimens were cut from the panels via waterjet cutting machine. All specimens presented a 100x100 mm area. The specimens received a simple nomenclature as a function of type of fibre reinforcement (type and architecture), see Table 3. Figure 1 presents examples of finished composite plates in their 2D and 3D configuration (the 2D means only the intralaminar reinforcement is present,

while the 3D means that both the intralaminar (2D) and 3D OTT reinforcement architectures are present simultaneously).

2.4 Test methods

2.4.1 Impact tests

Impact tests were performed at Politecnico di Torino (Department of Mechanical and Aerospace Engineering, DIMEAS) on laminate specimens with dimensions of 100 mm × 100 mm, using a drop tower machine (Instron/CEAST Fractovis Plus) equipped with a hemispherical impactor instrumented with a piezoelectric load cell of 12.7 mm diameter at room temperature, see Fig. 2. The samples were clamped between two steel plates with a circular opening of 40 mm diameter. The full perforation impact tests were done at an energy level of 45 J to ensure complete penetration of the dart. Force-displacement and energy-displacement curves were calculated for each test based on the data acquisition system. Three different energy levels were tested: 3 J, 7 J, and 12 J, respectively for the repeated impact of the different materials. This was chosen due to the different material impact response and therefore the required energies to reach failure in a feasible amount of time. The lowest energy level was used for the JFRP specimens, while 7 J was used for the CURAUÁ 2D and 3D specimens. The highest energy level was used for the SISAL hybrid composites, both 2D and 3D. This was done in order to reach failure in a reasonable time (i.e., at lower energy levels the hybrid SISAL composites did not fail at over 200 impacts). A damage index (DI) was computed from the impact data. This index serves as a measure of damage propagation within the laminate as a function of test parameters [29]. Equation 1 presents the computation:

$$DI = \frac{E_a}{E_i}\frac{s_{\max}}{s_i} \qquad (1)$$

Where, E_a is the energy absorbed by the specimen during impact, E_i is the total impact energy s_{max} is the maximum displacement for each repeated impact and s_i is the average value of the displacement obtained in the perforation tests.

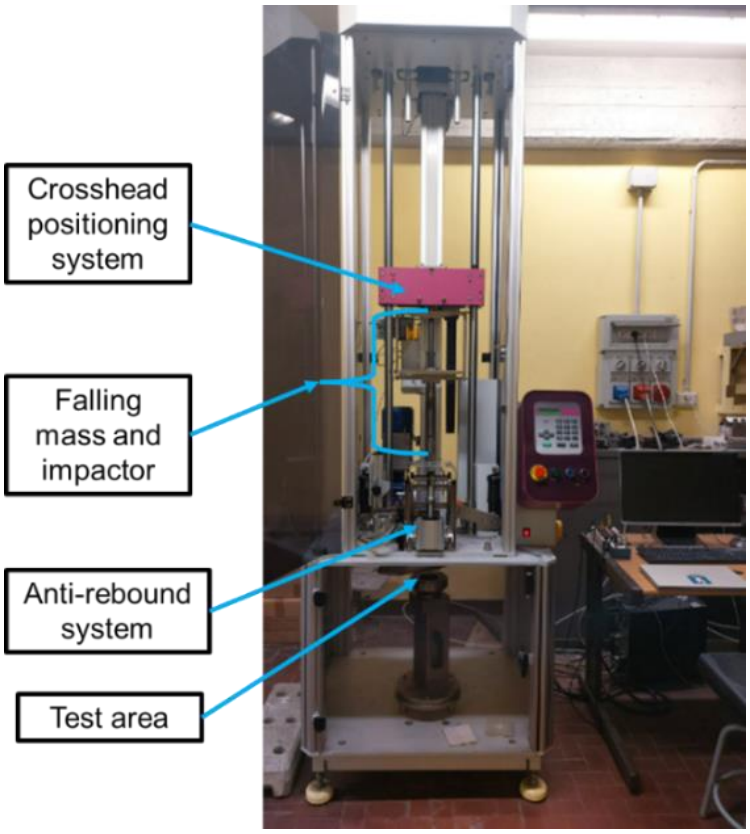


Figure 2. LVI test set up.

2.4.2 MicroCT analysis

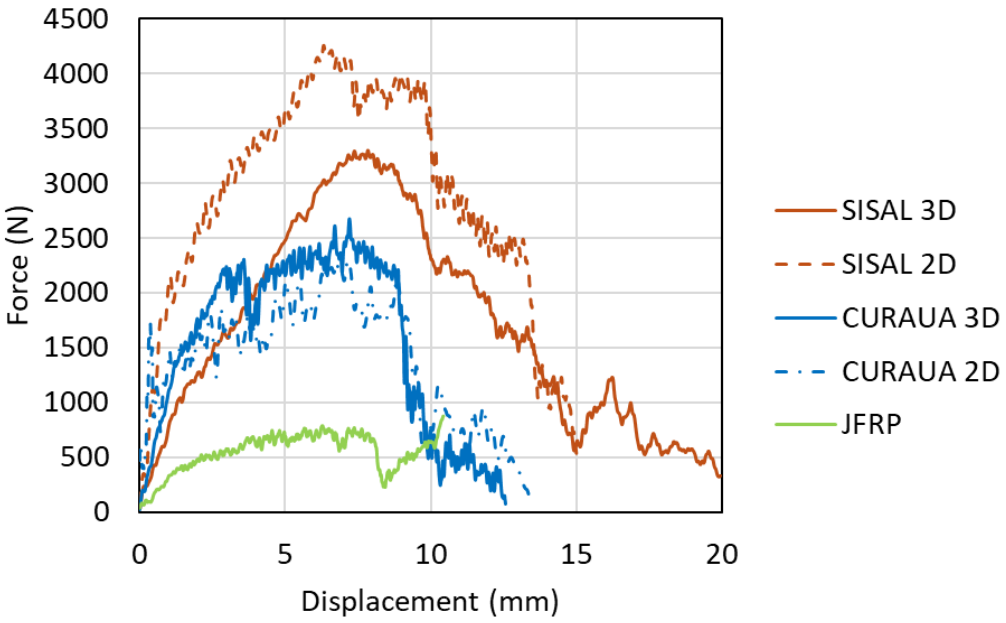
X-ray computed tomography (CT) was performed using a custom-made CT system located in Politecnico di Torino J-Tech@PoliTO laboratory (Torino, Italy). The facility is equipped with a 300 kV X-ray source and a 5 μm minimum focal spot size, along with a flat panel detector featuring 2048 × 2048 pixels. The working distance between the source and the sample, as well as between the source and the detector, can be adjusted as needed**.** The scanning parameters used were 80 kV and 110 μA, resulting in an electron beam power of 8.8 W and a final resolution of 13 μm per voxel. No physical filtering was applied to the X-rays. The reconstructed 3-D volume of the investigated specimens was obtained using the filtered back-projection algorithm through VG MAX 3.5 software (Volume Graphics GmbH, Heidelberg, Germany), utilizing a total of 1600 X-ray projections. During post-processing, the fibres were successfully separated from the matrix material, and the defects present in the different laminates were detected. Finally, the porosity of the laminates was computed

3. RESULTS AND DISCUSSION

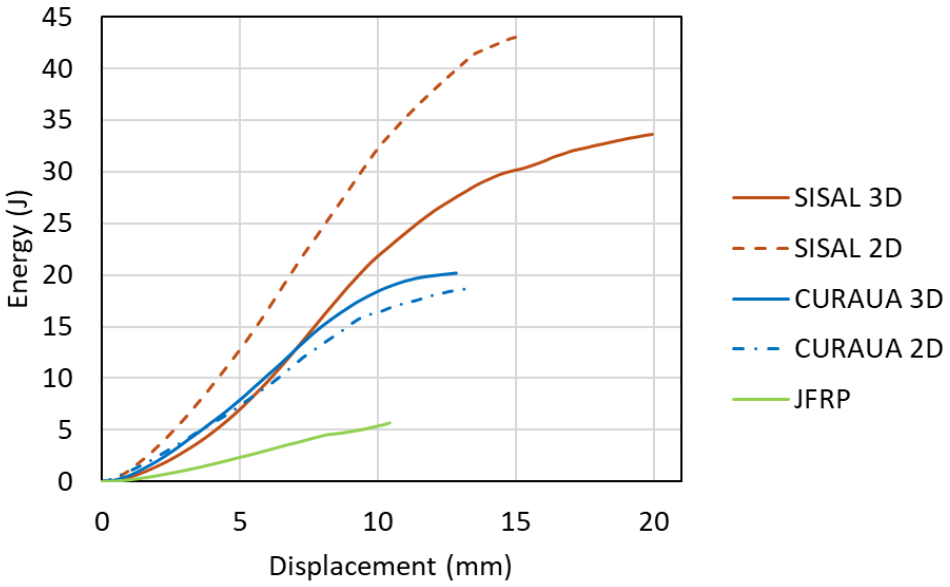
3.1 Perforation tests

Figure 3 and 4 presents a summary of the results of the impact test campaign. The force-displacement representative curves can be seen in Fig. 3a. A significantly different damage progression is visible as a function of composite material. It can be seen from the initial slope of the curves (i.e., the elastic range), how the stiffness varies as the damage propagates through the different materials. The change in slope at around 1 mm is due to initiation of damage such as matrix cracking. Later in the curves more significant slop changes as well as local oscillations are visible, indicating more severe damage such as delamination and fibre failures. Sudden drops in load are characteristic of fibre breakage of the surface layers. The trend for peak load observed is affected by the thickness [30], however, all hybrid composites are comparable. It is also noteworthy that the peak load is reached for the CURAUÁ specimens and the SISAL 2D at approx. 6 mm and is maintained somewhat until approx. 10 mm (see Fig. 3a). Similar behaviour has been previously reported for flax composites [31]. This interval was decreased for the SISAL 3D specimens to only approx. 1.2 mm. The JFRP barely presented a peak and absorbed very little energy due to its brittle failure mode (see Fig. 9a-b). The hybridization technique, as well as the architecture had a significant effect in the peak load, the time at peak load, and the behaviour to complete perforation. From Fig. 3b the energy-displacement representative curves for the perforation impact tests can be seen. The initial slope is linked to minor damage and deformation along the thickness direction caused by the transverse impact load. A cluster of initial slopes that are almost identical can be seen for the CURAUÁ 2D, 3D and SISAL 3D. However, higher deformation and damage can be seen for the SISAL 2D specimens. This trend continues until failure, and it is due to the damage progression within the laminates. From Fig. 4 the statistical data for the perforation tests can be seen. From Fig. 4a, it can be seen that all cases presented significant enhancements in the maximum absorbed energy (AE) when compared to the JFRP. For instance, the CURAUÁ specimens absorbed approx. 74% more energy, while the SISAL specimens approx. 86%. The SISAL specimens presented the highest overall absorbed energy of all tested specimens (i.e. approx. 36% and 45% more energy than the CURAUÁ for the 3D and 2D variants). This may be linked to the fact that the interfacial shear strength (IFSS) of CURAUÁ/epoxy is higher than SISAL/epoxy [32] and in an

impact scenario the chemical linkages between the fibre and matrix are broken and the fibres are separated from the matrix by parallel cracks. This occurs when the contact (IFSS) is weak, but the fibre is resistant. Given the creation of a debonding crack upon impact, a fresh surface is created and this encourages a cascade of fresh surfaces creation upon many fibres debonding but resisting failure, increasing the overall absorbed energy [8, 32]. Further evidence of this can be seen in Section 3.4 (see Fig. 10). From Fig 4b, all cases presented enhancements in peak load when compared to the JFRP (improvements of approx. 73% and 80% for the CURAUÁ 3D and SISAL 3D specimens, respectively). Finally, no significant variations of displacement for perforation tests can be seen in Fig. 4c

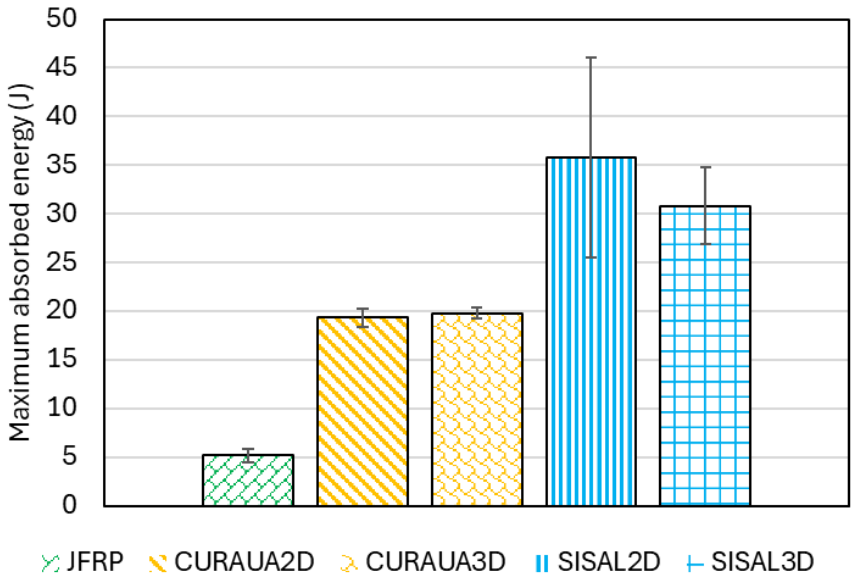


a)

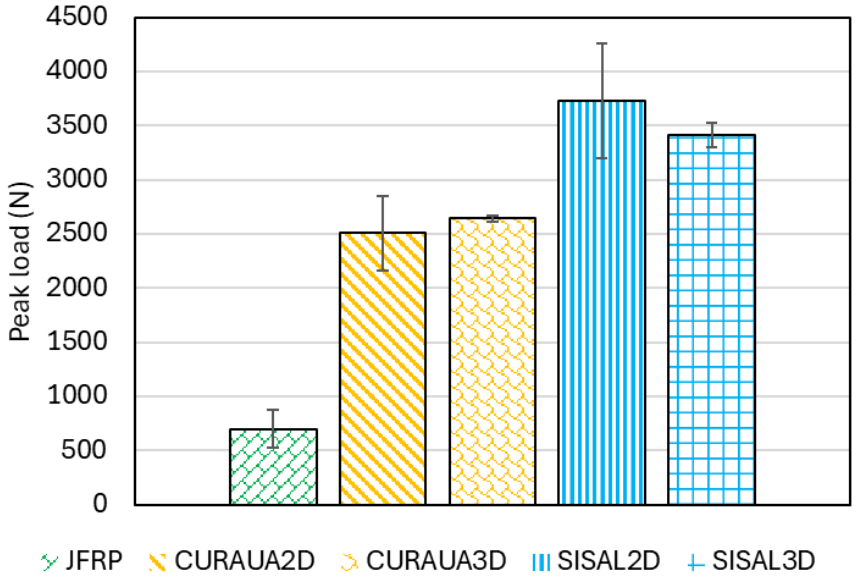


b)

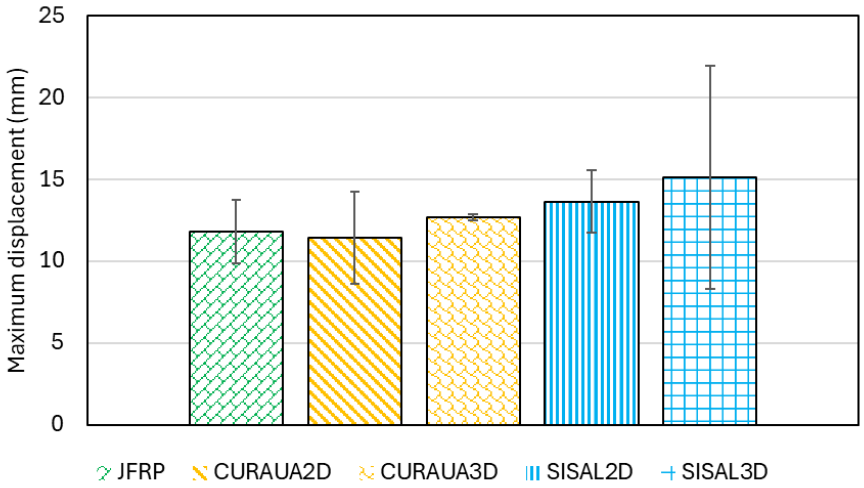
Figure 3. Impact test representative curves: a) Force-displacement and b) Energy-displacement.



a)



b)



c)

Figure 4. Statistical data for the perforation impact tests, a) maximum absorbed energy, b) peak load and c) maximum displacement.

3.2 Repeated impacts

Figure 5 presents representative energy-displacement curves for the composites studied here under repeated impacts.

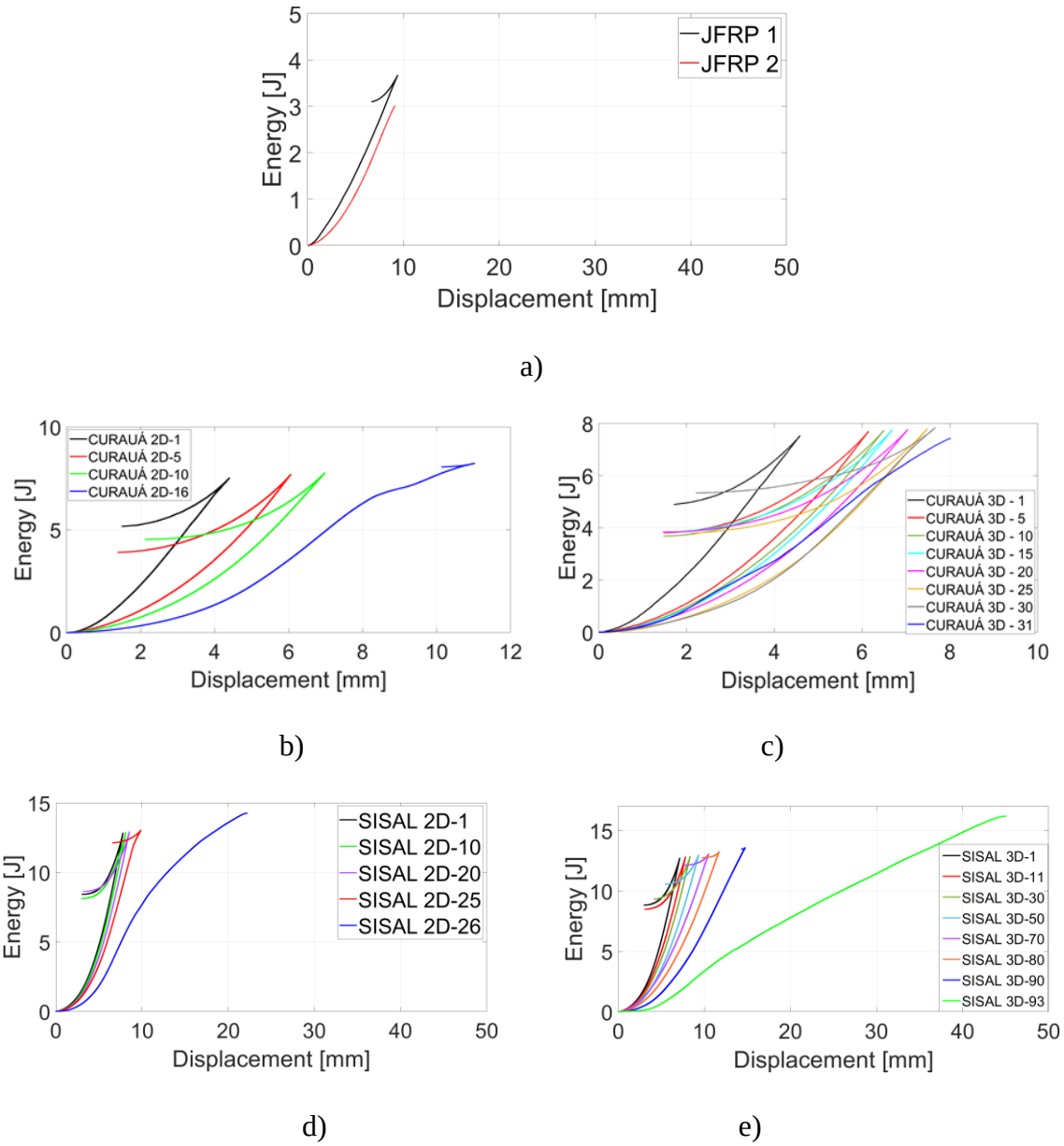
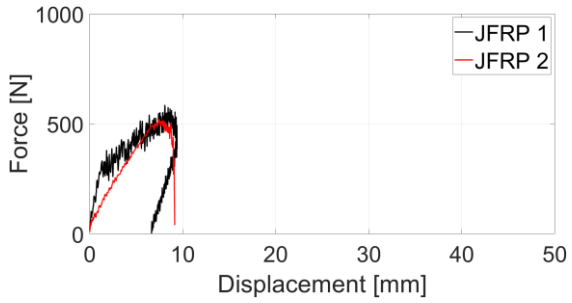


Figure 5. Energy-displacement curves for repeated impact tests, a) JFRP, b) CURAUÁ 2D, c) CURAUÁ 3D, d) SISAL 2D and e) SISAL 3D.

For the JFRP specimens, all curves are presented (see Fig. 5a), while for the hybrid specimens, due to the much higher number of impacts to failure, a different number of curves is presented (the number in the legend next to the name indicates the impact number). The elastic energy still stored within the specimen is depicted in the curves as a tail returning in the displacement (see Fig. 5). The 3D reinforcement significantly

improved the resistance to repeated impacts for both CURAUÁ and SISAL specimens. Specifically, the CURAUÁ 3D presented almost 2x the number of impacts to failure, while the SISAL 3D presented almost a 4x increase when compared to their 2D counterparts. It can be seen from Fig. 5c and d that the displacement increases much faster for the CURAUÁ 2D when compared to the 3D. For example, at approx. 7 mm, the peak of the 10th impact is visible for the CURAUÁ 2D, while for the 3D the same displacement correlated to the peak of the 20th impact. This suggests that the transverse fibres are acting to restrain the displacement of the specimen via crack arrestment mechanisms (delaying and bridging the cracks) [11]. Similarly for the SISAL specimens, the 10 mm displacement correlated to the peak of the 25th impact for the 2D specimens, while for the 3D, it correlates to the 70th (see Fig. 5d and e). Upon failure, the energy absorbed increases significantly for all hybrid specimens, especially for the SISAL specimens, due to the total release of the elastic energy [8]. It is observed that the 3D hybrid composites presented a higher number of impacts needed to fail when compared to the 2D. This higher damage tolerance of 3D architectures has been previously reported, however, there is limited literature available on repeated impact response of 3D composites [30]. This damage tolerance stems from the enhanced resistance to delamination and transverse matrix cracking afforded by the 3D reinforcement which suppresses deformation in the out-of-plane direction and restricts delamination propagation (i.e., most common failure modes in laminated structures) [6]. Figure 6 presents the representative load-displacement curves for all cases.



a)

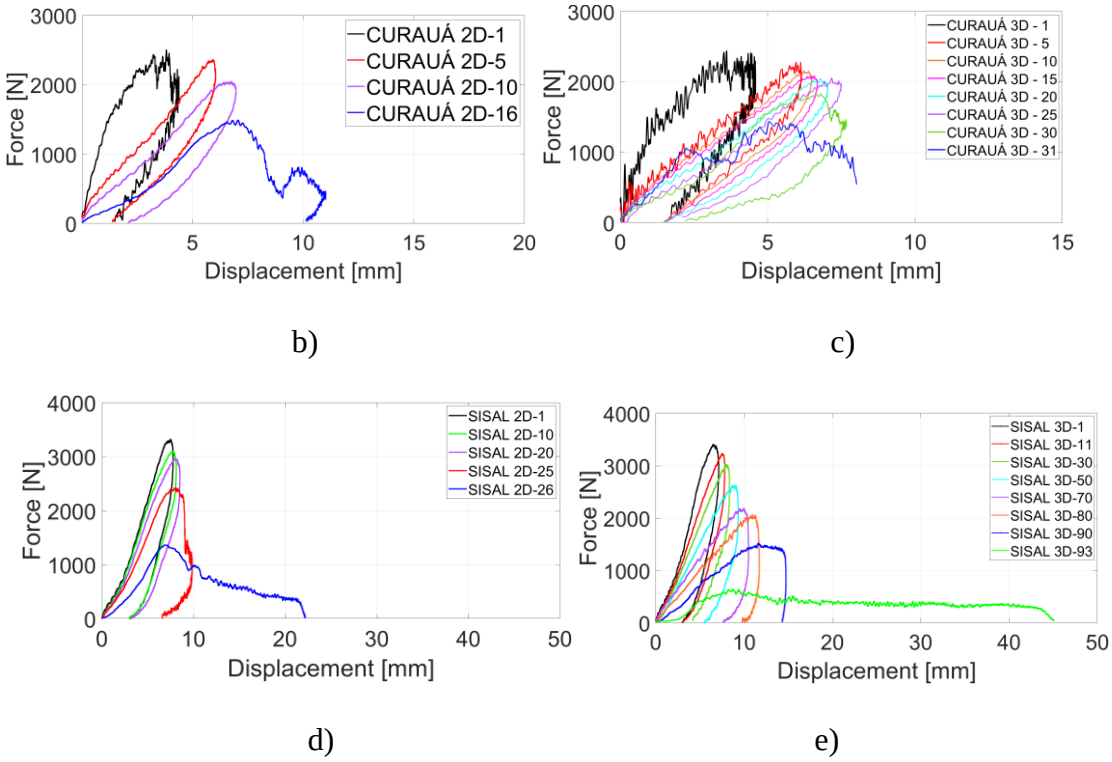


Figure 6. Force-displacement curves for repeated impact tests, a) JFRP, b) CURAUÁ 2D, c) CURAUÁ 3D, d) SISAL 2D and e) SISAL 3D.

All groups presented the expected trend of decreasing peak load and increasing displacement as a function of repeated impacts [29]. A significant variation in the slope of the curve from the first impact to the second is visible for all cases, with the exception of the SISAL specimens, likely due to the ability of the transverse fibres to maintain the integrity of the specimen at a relatively low energy level (12J). It is known that the behaviour of the curve is associated with the damage progressions within the specimen (matrix cracking, fibre failures) [8]. It is possible to observe that for neat specimens (i.e., JFRP), the first impact already presented significant damage propagation evidenced by the jitter in the curve following the initial slope (see Fig. 6a). For the JFRP, only one more impact failed the specimens at 3J. This is due to the inherently brittle nature of both reinforcement phases (i.e., matrix and jute fibre), as well as the fact that due to the nature of the jute fabric, large resin rich zones exist in the spaces formed by the warp-weft weave. A similar trend can be seen for the CURAUÁ specimens, where the first impact presented more apparent significant damage than the following (see Fig. 6b and c). The SISAL specimens, both 2D and 3D, break this trend since the initial curve and the following are much smoother and present much less accumulated internal damage per impact than the

other specimens. For the SISAL 2D, a more significant jitter in the curve is visible from the 25th impact (one before last), while for the 3D this becomes more apparent from the 70th impact (see Fig. 6d and e). This is evidence of how the secondary fibre phase's material properties affect the composite. The higher ductility and strength of both CURAUÁ and SISAL (see Table 1), completely change the material response to impact fatigue in both 2D and 3D variants. Figure 7 presents the progression of several material parameters as a function of repeated impacts.

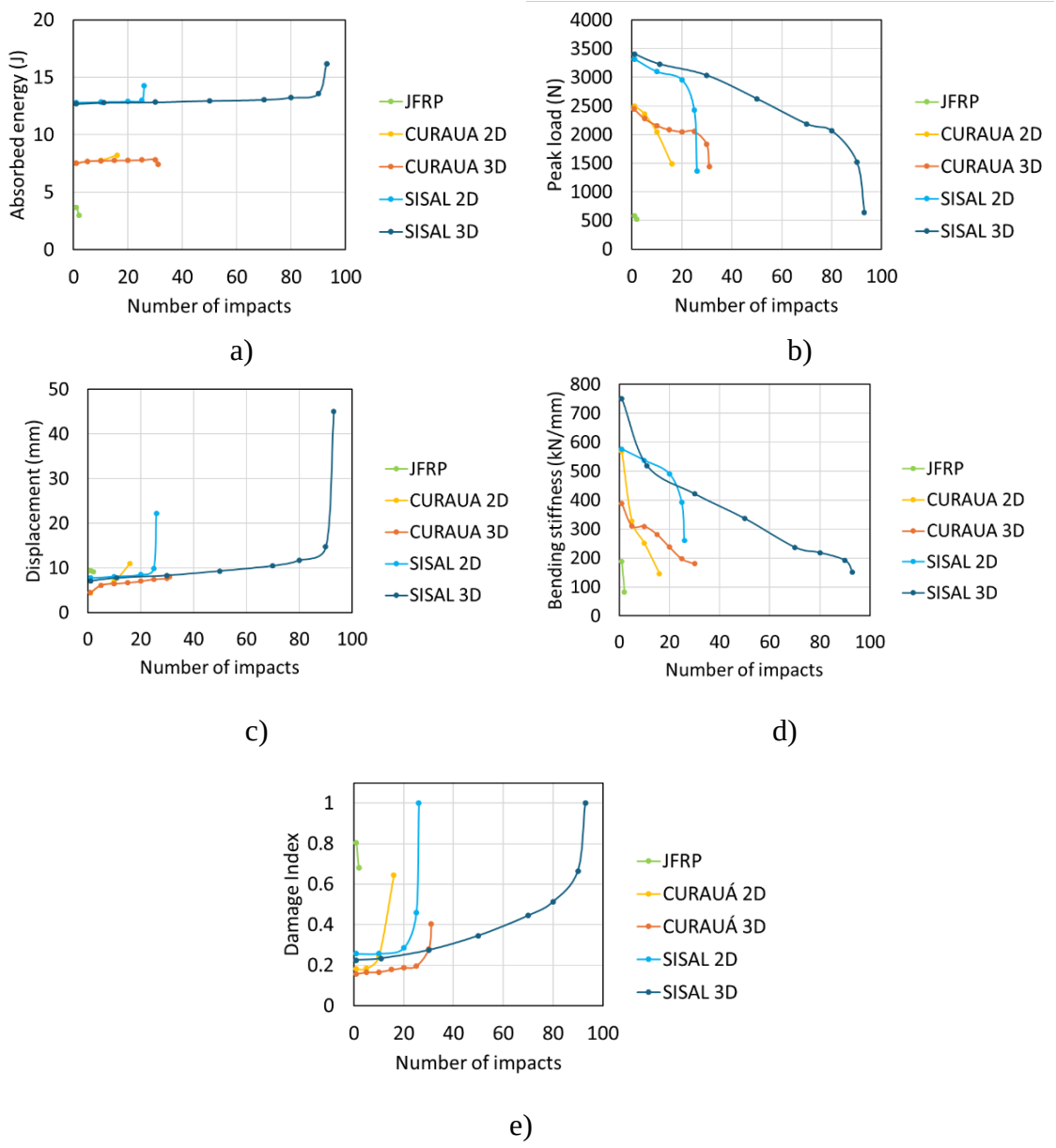


Figure 7. Material impact parameters as a function of repeated impacts: a) absorbed energy, b) peak load, c) displacement, d) bending stiffness and e) damage index.

From Fig. 7a, the evolution of the absorbed energy can be seen. For the neat jute specimens, a quick reduction in AE is visible as a function of impacts. This is mainly due to their brittle nature (i.e., low failure strains) [30]. For all the hybrid cases, a stable trend of AE is visible as the number of impacts increases. The progression for all these groups is quasi-linear. Furthermore, as a function of architecture, no significant variation in AE was found when the 2D is compared to the 3D for both CURAUÁ and SISAL. Therefore, the 3D OTT architecture significantly affects the impact fatigue life of the material without degrading the AE. The SISAL specimens however, presented a significant peak in energy absorption upon failure, due to significant deformation. From Fig. 7b, the progression of peak load as a function of impacts can be seen. It is known in the literature that three regions may be visible; The first region is characterized by a sharp drop in load due to reinforcement fibre micro-buckling and shear deformations; The second region is characterized by a plateau tendency, where the decrease in load continues but at a much slower pace, this is linked to the phenomenon of delamination saturation; In the third and final region, a sharp decrease in peak load is recorded along with significant matrix and fibre cracking and the onset of total specimen failure [30]. These regions are visible in Fig. 7b; however, they may be somewhat difficult to see considering that the energy levels were already significant (i.e., not a very high number of impacts). The regions tend to be more clearly visible at much lower energy impact-fatigue levels (i.e., a high number of impacts to failure). Nevertheless, for the SISAL 2D, 3D and CURAUÁ 3D, the regions are visible. Interestingly, none of these cases presented a sharp decrease from the first to the second impact. Rather, the first and second regions seemed to merge immediately, with a sharp decrease only clearly visible for the third region with the failure of the specimen. Figure 7c presents the progression of the maximum displacement as a function of impacts. It can be seen that very limited increases are observed from impact to impact for all cases. The only significant variations occur at failure and only for the SISAL specimens, likely owing to their higher ductility. Finally, regarding the bending stiffness as a function of repeated impacts, the progression can be seen in Fig. 7d. As expected, the material stiffness decreased as a function of continued impacts, however, different trends were observed as a function of material. For example, the JFRP specimens presented very sharp immediate and significant decreases failing right after. For the hybrid specimens

however, the effect of the 3D reinforcement was clearly defined. For both CURAUÁ and SISAL, the 3D reinforcement helped to decrease the initial drop in stiffness and presented a smoother decline. The CURAUÁ 2D presented a significant initial decline followed by slightly smoother decreases till failure. Meanwhile, for the 2D specimens, the SISAL presented a smoother decline at first following a steep decline at the final impact. Finally, from Fig. 7e, the damage index (DI) progression can be seen. This index is used to monitor the damage progression of composites subjected to repeated impacts as a function of the energy and displacement of both repeated and perforation impacts [29]. For both CURAUÁ and SISAL specimens a similar trend can be seen as a function of fibre architecture. The damage index presented a sharp increase for the 2D specimens, while for the 3D, a more linear progression was observed. This is linked to the much lower rate of damage propagation within the composite during repeated impacts for both 3D reinforced composites and further evidence of this is visible in the microCT images (see Section 3.4). Furthermore, the initial DI for all hybrids were in the range of 0.15 to 0.22, while the JFRP initiated at 0.8. This significant difference is linked to the fact that for the JFRP, both phases (i.e., matrix and fibre) are predominantly brittle and accumulate high damage at lower strains quickly. Both CURAUÁ and SISAL specimens, however, present higher inherent ductility and resistance when compared to jute (see Table 1) and significantly altered the tendency of the composite to accumulate damage at first impacts.

3.3 Impact failure modes

Following an impact event of a projectile to a composite material, different failure modes are possible. These include delamination, matrix cracking, fibre failure, fibre splitting and edge delamination. The type and severity of the failures will depend on parameters such as mass of the projectile/impactor, its geometry, the architecture of the reinforcement, material properties of the fibre and matrix and impact velocity [8]. Figure 8 presents representative side views of the failure modes of the hybrid composites subjected to perforation impact tests.

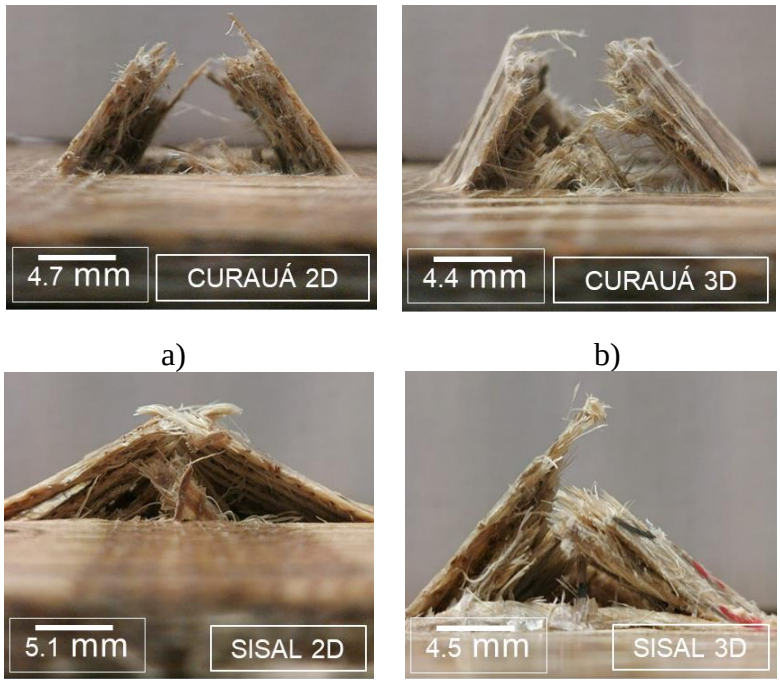


Figure 8. Representative failure modes of the hybrid composites for perforation impact tests: a) CURAUÁ 2D, b) CURAUÁ 3D, c) SISAL 2D and d) SISAL 3D.

From Fig. 8a, the CURAUÁ 2D perforation failure can be seen in better detail. A significant opening is visible, denoting total matrix and fibre failures in a mostly brittle behaviour. A very similar behaviour can be seen for the 3D counterpart in Fig. 8b. However, it was more difficult for the surfaces to completely separate, suggesting a bridging effect of the 3D fibres. For the SISAL specimens, however, a similar type of failure behaviour is visible for both 2D and 3D (see Fig. 8c and d). In both cases, total opening of the back face failure zone was not visible, the bridging effect was highly significant for both cases, likely due to the high resistance and ductility of the SISAL fibre. Figure 9 presents the representative failure mode progression of the repeated impacts of all cases, the number in the top left corner indicates which impact it is. The top image of each case depicts the impact contact face, while the bottom image shows the underside of the specimen. The failure zone on the top face presents the direct contact of the impactor, while the bottom face failure zone shows the damage propagation in order for the specimen to absorb the impact energy. As a reminder, the impactor was circular with a diameter of 12.7 mm. For the JFRP, from the first impact, a cross shaped crack is visible, followed by a severe brittle failure in the second impact (see Fig. 9a-b).

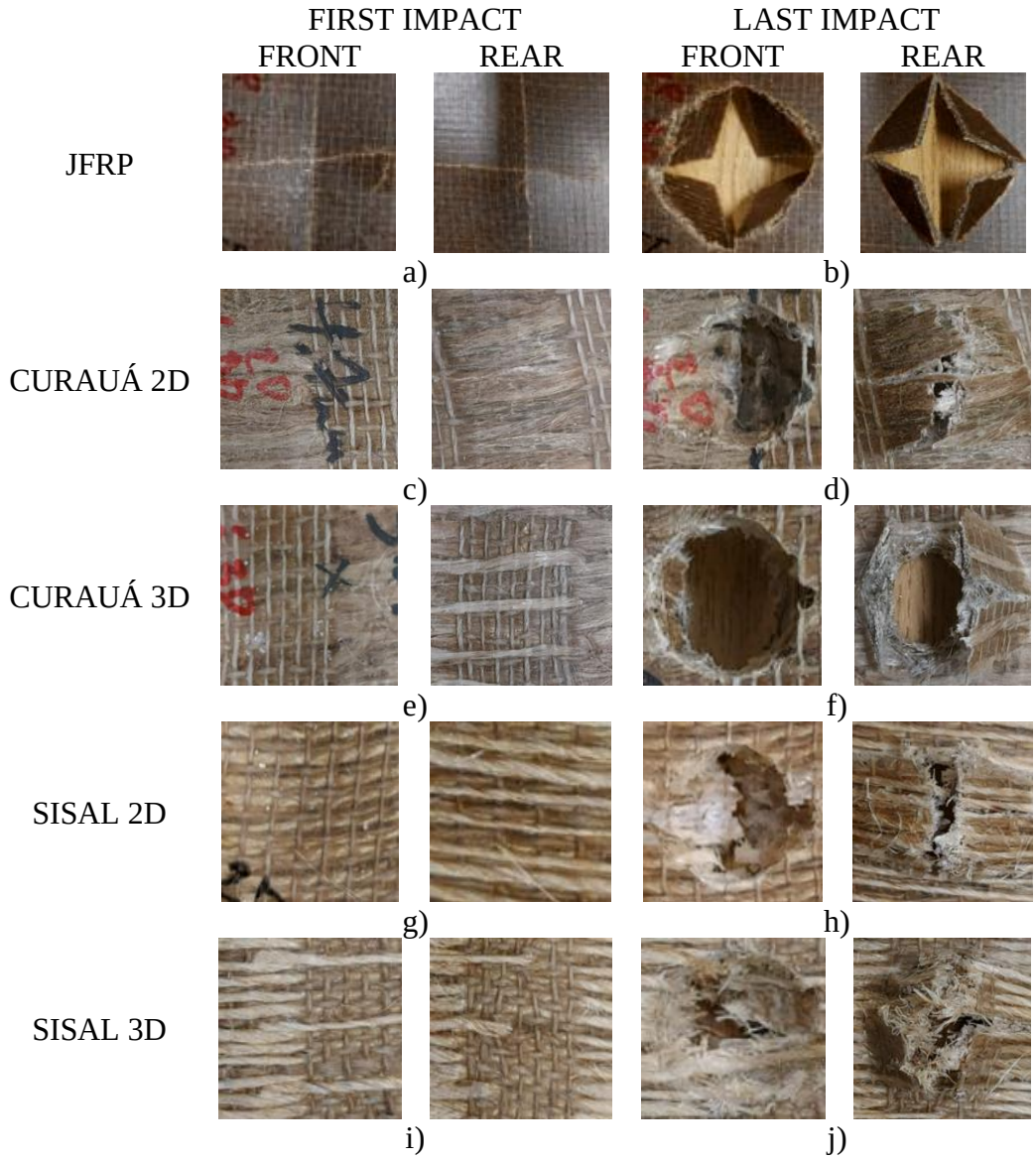


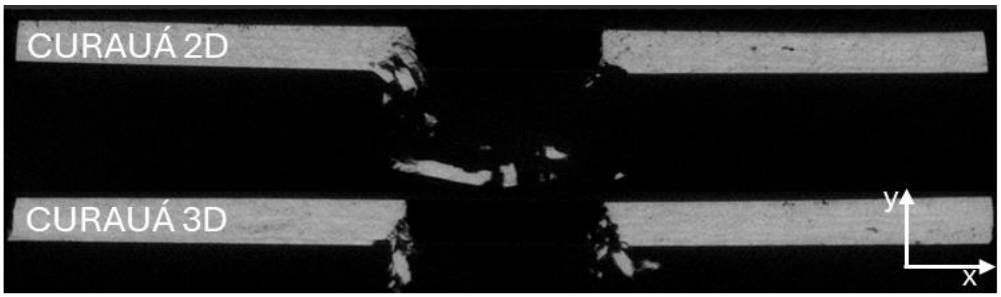
Figure 9. Representative failure modes for the repeated impact tests for all specimens.

This is due to the fact that both phases (fibre and matrix) and very brittle [33]. These types of impact failures for jute have been previously observed in the literature [34]. The failure progression changes drastically when the hybrid composites are compared to the neat ones. Not only does the failure progresses more slowly, the number of impacts to failure increases significantly. This is in part by the increase in the thickness of the composite [30], but also due to the higher ductility of the secondary and tertiary (3D) fibre phases, CURAUÁ and SISAL. For the CURAUÁ 2D specimens, the failure progression can be seen in Fig. 9c-d, while for the 3D it is visible in Fig. 9e-f. For the CURAUÁ 2D, the

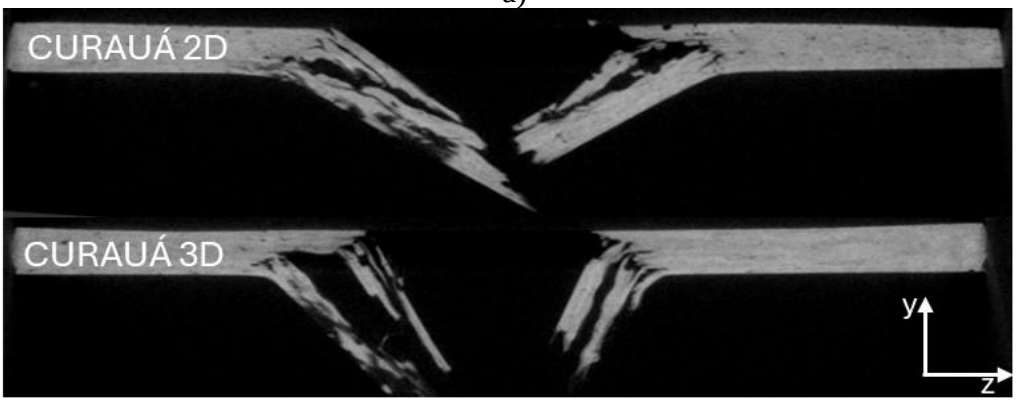
impactor contact left barely visible impact damage (BVID), while for the back face, crack propagation became easily recognizable near the surface crossing the CURAUÁ 2D fibre bundles at the 10th impact. By the 16th and final impact, a predominantly brittle failure can be seen on the top face, where an ellipsoidal cave in marks the total failure on the specimen, while on the back face a lifting of two surfaces with a total specimen crack in the middle is visible. Matrix cracking, and fibre failure are the dominant failure mechanisms. For the CURAUÁ 3D specimens, the failure became more significant closer to the 30th impact (see Fig. 8e and f) with a rounded cave in on the top face and a cross shaped crack on the back face. The following impact marked the composite failure and a similar failure to the CURAUÁ 3D is visible, however, at almost twice the number of impacts. The impact failure evolution for the SISAL 2D can be seen in Fig. 9g-h. It can be seen that the failure is similar to the previous hybrids in its predominant brittle tendency in matrix cracking and fibre failures, however, it can also be seen that a large crack began to form at the impact zone propagating to the ends of the specimen in the space between SISAL intralaminar reinforcement fibres (see Fig. 9h). This corroborates the hypothesis posited earlier that large surfaces are created during each impact as the resin progressively debonds from the SISAL fibres, absorbing significant amounts of energy. The failure modes of the SISAL 3D can be seen in Fig. 9i-j. Most notably, the damage was BVID, until close to the 60th impact, indicating the capacity of the SISAL transverse reinforcement to contain significant deformations. When the visible failures began, especially on the back face, fibre failure was more evident at first than matrix cracking. Even at the top face, the deformations were much more limited, especially when compared to the JFRP and SISAL 2D. Differently to the SISAL 2D, no massive cracks spanning the entire specimen were observed. This may be one of the reasons why the SISAL 2D absorbed more energy in perforation by being able to create large matrix debonding surfaces that were blocked from progressing by 3D fibre crack arrestment. Therefore, for the SISAL specimens, the 3D reinforcement offers a positive and a negative in terms of LVI, the 3D offers significantly higher impact fatigue life, however, a lower total AE at perforation is expected.

3.4 MicroCT analysis of impact specimens

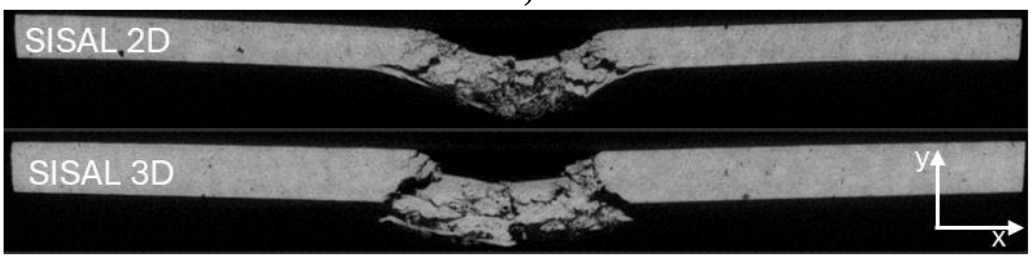
Figure 10 presents the micro tomography images of the impact specimens after full penetration (xy (normal) and zy (parallel to the fibres) plane views).



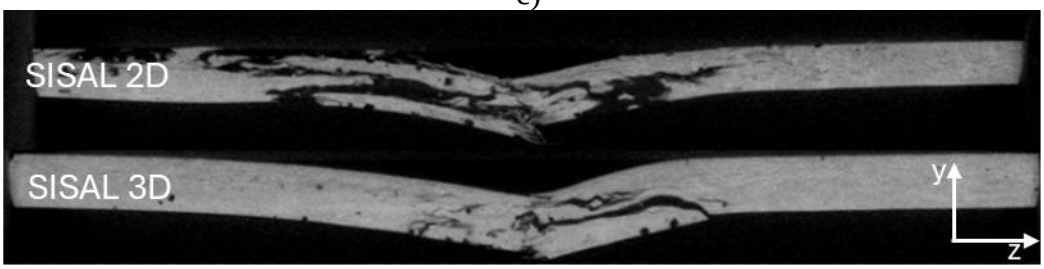
a)



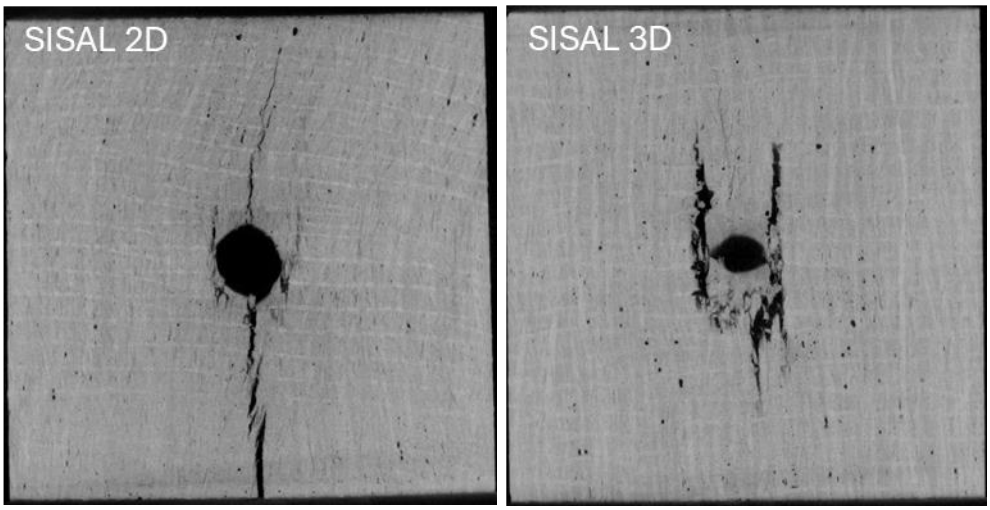
b)



c)



d)



e) f)

Figure 10. Representative microCT scans of all tested samples for perforation specimens on both cross-sectional planes, a) CURAUÁ 2D and 3D (xy plane), b) CURAUÁ 2D and 3D (zy plane), c) SISAL 2D and 3D (xy plane), d) SISAL 2D and 3D (zy plane), e) SISAL 2D (top surface) and f) SISAL 3D (top surface).

It can be seen that for all cases, no significant voids (dark dots) are interacting with any crack nucleation sites in a meaningful way, therefore it is assumed that they are not relevant for the large-scale damage propagation [35]. It is apparent that for all the CURAUÁ reinforced specimens, no significant crack propagation occurred from the main perforation site across the specimens on both planes (see Fig. 10a-b). This further supports the quantitative observation of the perforation impact dataset from section 3.1, where no significant variation was found in absorbed energy, peak load or deformation between the CURAUÁ 2D and 3D specimens. This is likely due to the strong fibre/matrix adhesion and mechanical interlocking of the CURAUÁ/epoxy, which makes it inherently difficult for interlaminar and interphase cracks to form and propagate [36]. Furthermore, the more brittle failure of the CURAUÁ specimens is also clear when compared to the SISAL specimens. In contrast, for the SISAL specimens a more significant variation in crack propagation as well as matrix cracking was observed as a function of architecture. From Fig. 10c and d, it can be seen that no significant cracks propagated on the xy plane, similar to the CURAUÁ, however, highly significant cracking was observed on the zy plane for the SISAL 2D case. The SISAL 3D case, one the other hand, presented a much more controlled crack development only near the main impact zone, without significant

cracks developing across the zy plane. From Fig. 10e and f the representative top view tomography of the impact side of the perforation SISAL specimens are visible. It is clear that a large crack propagated from the main impact zone in the zy plane all the way through the specimen for the SISAL 2D case. Furthermore, significant crack development is visible on either side of the mostly circular impact zone (stress concentrations, see Fig. 10e). Moreover, fibre bridging can be seen near the bottom of the image where SISAL tows diverted the crack as it developed through the matrix region between intralaminar reinforcements. On the other hand, for the SISAL 3D top failure view, a much more controlled crack development was observed, where the cracks propagated only on either side of the impact zone (see Fig. 10f). This is directly linked to the fibre architecture where the transverse reinforcement arrested the crack development. These microCT analyses corroborate the previous discussion whereby the mechanics of local debonding of fibre/matrix, very large new surface areas are formed and absorb significant energy in the process. This phenomenon is the main reason for the higher energy absorption of the SISAL 2D specimen under perforation impact testing, while for fatigue (repeated) LVI, the crack arrestment mechanism afforded by the transverse reinforcement nearly quadruples the impact life until failure. In other words, energy dissipation capacity is proportional to crack density [7, 37]. Furthermore, z-binder yarn debonding tendency during impact events is linked to differences in elastic modulus [17]. Therefore, design factors may be implemented such that if a significant single energy impact is expected at some point in the life of the part, the SISAL 2D architecture is preferable, however, if impact fatigue is likely, the 3D reinforcement is more effective.

4. CONCLUSIONS

In this research, novel 3D fibre reinforced hybrid composites were fabricated using two distinct techniques: intralaminar (2D) and orthogonal-through-the-thickness (3D-OTT). Perforation and repeated LVI fatigue tests were conducted to assess the maximum energy absorption and load-bearing capacity of the composites, as well as their fatigue life under repeated low-energy impacts. The main conclusions can be drawn:

- The 3D reinforcement was found to be very effective in keeping cracks from developing inside the specimens during impact. For the full perforation of the CURAUÁ specimens, absorbed energy and peak load showed no significant

variation between 2D and 3D configurations, due to minimal crack propagation and strong interlocking between fibres and the resin matrix. In SISAL specimens. The crack-blunting effect presented a decrease in the total energy absorbed under perforation testing when the SISAL 3D is compared to the 2D. This is linked to the fibre debonding phenomena for the SISAL specimens.

- For repeated impact tests, the 3D reinforcement architecture significantly improved performance, enhancing fatigue impact life by 2 times for CURAUÁ specimens and 3.6 times for SISAL specimens.
- Micro-CT imaging revealed distinct crack arrest mechanisms for the two fibre types. The CURAUÁ specimens presented an inherent crack-blunting effect for both 2D and 3D configuration, owing to the good fibre/matrix interface quality and mechanical interlocking. In contrast, the SISAL specimens presented significant crack development following impact (in the yz plane, parallel to the fibres) for both 2D and 3D configuration. However, the 3D case showed a higher capacity to limit crack propagation.

REFERENCES

1. Neto, J., et al., *A Review of Recent Advances in Hybrid Natural Fiber Reinforced Polymer Composites.* Journal of Renewable Materials, 2022. **10**(3): p. 561--589.
2. Neto, J.S.S., et al., *A Review on the Thermal Characterisation of Natural and Hybrid Fiber Composites.* Polymers, 2021. **13**(24): p. 4425.
3. Prasob, P.A. and M. Sasikumar, *Static and dynamic behavior of jute/epoxy composites with ZnO and TiO2 fillers at different temperature conditions.* Polymer Testing, 2018. **69**: p. 52-62.
4. de Seixas, G., et al., *Effect of water on the mechanical and thermal properties of natural fibre reinforced hybrid composites.* Journal of Composite Materials, 2023. **57**(11): p. 1941-1958.
5. de Queiroz, H.F.M. and M.D. Banea, *Methods to increase the mechanical performance of composite adhesive joints: An overview with focus on joints with natural fibre composite adherends.* Journal of Composite Materials, 2022. **56**(26): p. 3993-4010.
6. Olhan, S., B. Antil, and B.K. Behera, *Low-velocity impact and quasi-static post-impact compression analysis of woven structural composites for automotive: Influence of fibre types and architectural structures.* Composite Structures, 2025. **352**: p. 118676.
7. Pheysey, J., et al., *Low-velocity impact response of hybrid sheet moulding compound composite laminates.* Composites Part A: Applied Science and Manufacturing, 2025. **188**: p. 108527.
8. Chowdhury, S., L. Tripathi, and B.K. Behera, *Review: impact resistance and damage tolerance of 3D woven composites.* Journal of Materials Science, 2024. **59**(18): p. 7636-7699.
9. Javanshour, F., et al., *Modulating impact resistance of flax epoxy composites with thermoplastic interfacial toughening.* Composites Part A: Applied Science and Manufacturing, 2021. **150**: p. 106628.
10. Zhang, H., et al., *Experimental investigation of Z-pin insertion angles on the mechanical behavior and failure mechanism of compression after impact for CFRP laminates.* Composite Structures, 2023. **304**: p. 116476.
11. Mouritz, A.P. and B.N. Cox, *A mechanistic interpretation of the comparative in-*

plane mechanical properties of 3D woven, stitched and pinned composites. Composites Part A: Applied Science and Manufacturing, 2010. **41**(6): p. 709-728.

12. Pickering, K.L., M.G.A. Efendy, and T.M. Le, *A review of recent developments in natural fibre composites and their mechanical performance.* Composites Part A: Applied Science and Manufacturing, 2016. **83**: p. 98-112.
13. Zhu, X., et al., *Experimental investigation on high-velocity impact damage and compression after impact behavior of 2D and 3D textile composites.* Composite Structures, 2023. **303**: p. 116256.
14. He, Y., et al., *Drop-weight impact behaviour of stitched composites: Influence of stitching pattern and stitching space.* Composites Part A: Applied Science and Manufacturing, 2023. **172**: p. 107612.
15. Carvelli, V., et al., *Low velocity impact and CAI of woven carbon fibre reinforced highly polymerized thermoplastic epoxy modified with submicron diameter glass fibres.* Composite Structures, 2020. **236**: p. 111835.
16. Ma, B., et al., *A comparative study on the low velocity impact behavior of UD, woven, and hybrid UD/woven FRP composite laminates.* Composites Part B: Engineering, 2024. **271**: p. 111133.
17. Seltzer, R., et al., *X-ray microtomography analysis of the damage micromechanisms in 3D woven composites under low-velocity impact.* Composites Part A: Applied Science and Manufacturing, 2013. **45**: p. 49-60.
18. Gerlach, R., et al., *In-plane and through-thickness properties, failure modes, damage and delamination in 3D woven carbon fibre composites subjected to impact loading.* Composites Science and Technology, 2012. **72**(3): p. 397-411.
19. Olhan, S., et al., *Mechanical, thermal, and viscoelastic behavior of sisal fibre-based structural composites for automotive applications: Experimental and FEM analysis.* Composite Structures, 2023. **322**: p. 117427.
20. Jabbar, M., et al., *Effect of the stuffer yarns on the mechanical performance of novel 3D woven green composites.* Composite Structures, 2021. **269**: p. 114023.
21. Kashif, M., et al., *Optimization of 3D woven preform for improved mechanical performance.* Journal of Industrial Textiles, 2019. **48**(7): p. 1206-1227.
22. Hussain, M., et al., *Properties and characterization of novel 3D jute reinforced natural fibre aluminium laminates.* Journal of Composite Materials, 2021. **55**(14):

p. 1879-1891.

23. Jabbar, M., et al., *Mechanical Response of Novel 3D Woven Flax Composites with Variation in Z Yarn Binding.* Journal of Natural Fibers, 2020. **17**(6): p. 890-905.
24. Khan, M.I., et al., *Development of composites, reinforced by novel 3D woven orthogonal fabrics with enhanced auxeticity.* Journal of Industrial Textiles, 2019. **49**(5): p. 676-690.
25. Nawab, Y., et al., *Development & Characterization of Green Composites Using Novel 3D Woven Preforms.* Applied Composite Materials, 2018. **25**(4): p. 747-759.
26. Chowdhury, S. and B.K. Behera, *Low-velocity impact response of 3D woven solid structures for multi-scale applications: role of yarn maneuverability and weave architecture.* Journal of the Brazilian Society of Mechanical Sciences and Engineering, 2024. **46**(3): p. 138.
27. Olhan, S., et al., *Investigating the impact of different machinability processes and fibre architecture on the bearing performance of pin-loaded textile structural composites for automotive applications: Experimental and finite element analysis.* Journal of Manufacturing Processes, 2023. **86**: p. 30-55.
28. de Queiroz, H.F.M., et al., *A novel 3D fibre-reinforcement architecture for high performance natural fibre reinforced composite adhesively bonded joints.* Journal of Adhesion, 2024. **100**(2): p. 118-138.
29. Ciardiello, R., A. Benelli, and D.S. Paolino, *Static and Impact Properties of Flax-Reinforced Polymers Prepared with Conventional Epoxy and Sustainable Resins.* Polymers, 2024. **16**(2): p. 190.
30. Sadighi, M. and R. Alderliesten, *Impact fatigue, multiple and repeated low-velocity impacts on FRP composites: A review.* Composite Structures, 2022. **297**: p. 115962.
31. Giammaria, V., et al., *Material parameter optimization of flax/epoxy composite laminates under low-velocity impact.* Composite Structures, 2023. **321**: p. 117303.
32. de Araujo Alves Lima, R., et al., *Effect of surface treatments on interfacial properties of natural intralaminar hybrid composites.* Polymer Composites, 2020. **41**(1): p. 314-325.

33. de Queiroz, H.F.M., et al., *Effect of hybridization and composite architecture symmetry in the bonded joint performance of jute/carbon fibre-reinforced composites.* International Journal of Adhesion and Adhesives, 2024. **133**: p. 103745.
34. Fiore, V., et al., *Salt-fog spray aging of jute-basalt reinforced hybrid structures: Flexural and low velocity impact response.* Composites Part B: Engineering, 2017. **116**: p. 99-112.
35. Rouphael, S.E.K., et al., *Low energy impact behavior of unidirectional and cross-ply flax/epoxy laminates and comparison with similar glass/epoxy laminates.* Composites Part A: Applied Science and Manufacturing, 2023. **175**: p. 107746.
36. de Freitas, A.E.M., et al., *Curauá fiber from plants produced by tissue culture: thermal, mechanical, and morphological characterizations.* Cellulose, 2023. **30**(5): p. 2841-2858.
37. Ravindran, A.R., et al., *Improving the delamination resistance and impact damage tolerance of carbon fibre-epoxy composites using multi-scale fibre toughening.* Composites Part A: Applied Science and Manufacturing, 2021. **150**: p. 106624.
38. de Queiroz, H.F.M., et al., *Mechanical characterization of novel natural fibre-reinforced composites via a three-dimensional fibre architecture.* Composites Science and Technology, 2025. **261**.
39. Neto, J.S.S., et al., *Effect of chemical treatment on the thermal properties of hybrid natural fiber-reinforced composites.* Journal of Applied Polymer Science, 2019. **136**(10): p. 47154.

Paper 5

Tensile-tensile fatigue response of novel 3D hybrid composites

Fatigue analysis of novel 3D natural fibre-reinforced composites

H. F. M. de Queiroz[1], R. Ciardiello[2], M.D. Banea[1,3*]

[1]Federal Centre of Technological Education in Rio de Janeiro (CEFET/RJ), Brazil.

[2]Department of Mechanical and Aerospace Engineering, Politecnico di Torino, 10129 Turin, Italy

[3]CICECO - Aveiro Institute of Materials, Department of Materials and Ceramic Engineering, University of Aveiro, 3810-193 Aveiro, Portugal

Abstract

The increasing demand for sustainable materials in engineering applications has led to significant interest in natural fibre-reinforced composites (NFRCs). In this study, the fatigue behavior of a novel 3D woven orthogonal through-the-thickness natural fibre-reinforced composite was investigated. The unique structure of the composite, featuring a three-dimensional woven architecture, is examined for its impact on fatigue performance under cyclic loading conditions. Experimental testing is conducted to determine the fatigue life and failure modes, with a focus on the influence of fibre orientation, weave patterns, and matrix properties. The results show that the 3D woven structure significantly improves the fatigue resistance compared to conventional 2D fibre-reinforced composites, with enhanced through-the-thickness strength and durability. A detailed analysis of crack propagation, delamination, and damage evolution is presented, providing insights into the material's potential for automotive, aerospace, and other high-performance applications. This research contributes to the development of more sustainable, high-performance composites for advanced engineering applications, offering a promising alternative to traditional synthetic fibre-based materials.

K**eywords:** Natural fibres, 3D architecture, tensile-tensile fatigue

1. INTRODUCTION

The increasing demand for sustainable and environmentally friendly materials in engineering applications has led to significant advancements in the development of natural fibre-reinforced composites (NFRCs). These materials, which combine natural fibres such as flax, hemp, and jute with structural resins, offer an attractive alternative to conventional synthetic composites such as glass fibre (GFRP) [1-3]. Natural fibres have been gaining ground in the quest for carbon-footprint reduction of many structures such as automotive and marine applications [4]. However, they lack the mechanical performance and environmental resistance of synthetic fibres. Due to their hydrophilic tendency, they may create weak interfaces with the hydrophobic matrix (e.g., epoxy) and seriously compromise the composite material properties [5]. Therefore, researchers have attempted to enhance the mechanical properties of NFRCs to increase their competitiveness with their synthetic counterparts. This has been done by way of chemical and mechanical treatments as well as the hybridization technique [6-10]. The latter is by far the most common and well developed and it is defined as the use of two or more distinct fibre phases in the composite reinforcement architecture in order to extract the best qualities of both. For example, an interlaminar synthetic/natural hybrid composite with the synthetic part enveloping the natural core improves the longitudinal properties as well as creates a barrier for the entry of moisture in the composite [5]. Furthermore, this type of hybridization may also enhance the bonded joint performance of the composites [11, 12]. On the other hand, there are other material properties that are less obvious but no less important. The transverse properties of a composite material are very important for the application envelope of a given material, owing to the complex mechanical requirements a composite panel may face in the real world [13]. In this context, the potential of composites reinforced by 3D fibre-reinforcement architectures such as orthogonal through-the-thickness (OTT) is apparent [14]. These materials offer a solution to the long-standing issue of the mismatch between the longitudinal (main direction) properties of a conventional composite versus its out-of-plane (transverse) properties [15]. Moreover, they offer many advantages over their 2D counterparts, such as higher transverse strength, delamination resistance, single lap-joint bonded performance, higher modes I and II fracture toughness and impact resistance [13].

However, while much research has focused on the characterization of synthetic 3D OTT composites, very little attention has been given to NFRCs in this field. Fatigue, a process of progressive material degradation under repeated stress, is a critical factor in determining the longevity and reliability of composites in real-world applications. Understanding the fatigue behavior of 3D natural fibre-reinforced composites is essential for optimizing their design and performance, particularly in industries such as automotive, aerospace, and construction. The mechanical behaviour of 3D woven composites has been investigated in the literature for synthetic and natural composites [13, 16-19]. Variations of approx. 20% are expected when compared to their 2D counterparts regarding their classical properties. However, regarding fatigue, most of the literature for synthetic composites reports a reduction to the fatigue strength and fatigue life (number of cycles to failure) due to the z-binders (transverse fibres) [13, 19]. However, specifically for the case of 3D OTT NFRCs subjected to tension-tension fatigue, no works were found in the literature. This study aims to address this gap by conducting a comprehensive fatigue analysis of novel 3D OTT natural fibre-reinforced composites, with a focus on their resistance to fatigue failure under three loading levels (i.e., 70%, 60% and 50% of the UTS). A sinusoidal fatigue program was used at 5 Hz and R = 0.1. The materials were also analysed via X-Ray microCT and virgin tensile tests were compared to 1 million cycle-aged (50% UTS) composites to analyse the residual strength and stiffness effect of fatigue in these novel materials.

2. MATERIALS AND METHODS

2.1 Materials

This research effort is part of an ongoing project of analysis of novel 3D reinforced NFRCs. The primary reinforcement phase consisted of pure jute fibre bidirectional fabrics, supplied by Sisalsul (São Paulo, Brazil), while curauá and sisal fibres were the secondary reinforcements for the 2D and 3D fibre preforms. The intralaminar reinforcement utilized a 2D configuration, where the secondary fibres were woven unidirectionally into a balanced 2x2 jute bidirectional fabric. Additionally, a tertiary fibre reinforcement was introduced in the through-the-thickness (transverse) direction, creating a 3D orthogonal through-thickness (OTT) fibre architecture for the NFRC preforms (see Fig. 1). The curauá fibres used in this research were supplied by the Federal University

of Pará, Brazil in-natura. The curauá fibres were washed to remove any dirt and debris then subsequently dried in an oven at 100 ºC until completely dry (controlled by weight). The sisal (APAEB 700/1, Bahia, Brazil) used were industrially made fibre rovings. For the 3D OTT preforms, the transverse reinforcement was woven through 5 layers of 2D intralaminar fabrics. A more detailed description of the fibre architecture reinforcement fabrication (for both 2D and 3D) can be found in previous research [20]. A bicomponent epoxy resin matrix, HEX 135 SLOW (Barracuda Advanced Composites, SP, Brazil), was used to fabricate the composite plates. The material properties of the resin matrix used can be seen in Table 1, while Table 2 presents the nomenclature used for the composite materials.

Table 1. Mechanical properties of the resin matrix used [20].

Polymer	Tensile strength (MPa)	Young's modulus (GPa)	Tensile strain (%)
HEX 135 SLOW	60.92 ± 1.42	3.25 ± 0.008	3.20 ± 0.20

Table 2. Composite material nomenclature and description.

Composite	Description
CURAUÁ 2D	Jute fabric reinforced with woven curauá UD
SISAL 2D	Jute fabric reinforced with woven sisal UD
CURAUÁ 3D	CURAUÁ 2D reinforced with transverse orthogonal curauá fibres
SISAL 3D	SISAL 2D reinforced with transverse orthogonal sisal fibres

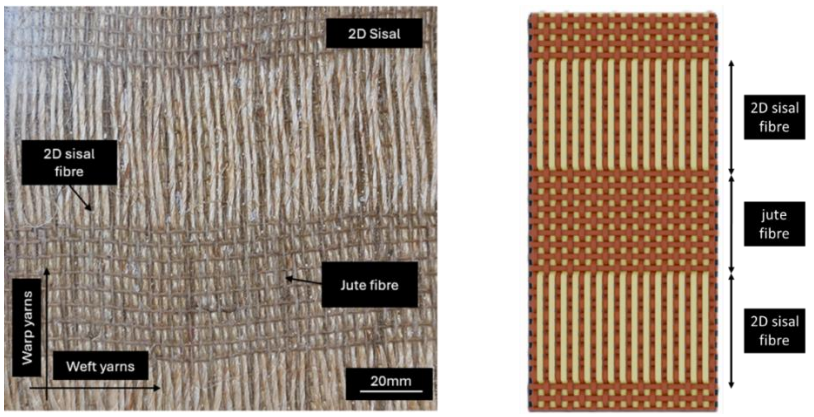
2.2 Specimen fabrication

The composites were fabricated using the compression moulding technique via a steel mould and a heated hydraulic press, Solab SL 20 (São Paulo, Brazil). The composite curing followed the manufacturer's guidelines at 70 degrees Celsius for 8 hours under pressure. The composite panel thickness varied slightly as a function of fibre type and architecture (the JFRP was approx. 2 mm, while the SISAL 2D was 5.33 ± 0.11 mm, the SISAL 3D was 5.37 ± 0.06 mm, the CURAUÁ 2D was 5.09 ± 0.09 mm, and the CURAUÁ 3D was 4.96 ± 0.36 mm). The test specimens were cut from the panels via waterjet cutting machine. Specimen geometry was approx. 220 x 13 x t mm, where t is the specimen thickness. The specimens received a simple nomenclature as a function of type of fibre reinforcement (type and architecture), see Table 3. Figure 1 presents examples of finished composite plates in their 2D and 3D configuration (the 2D means

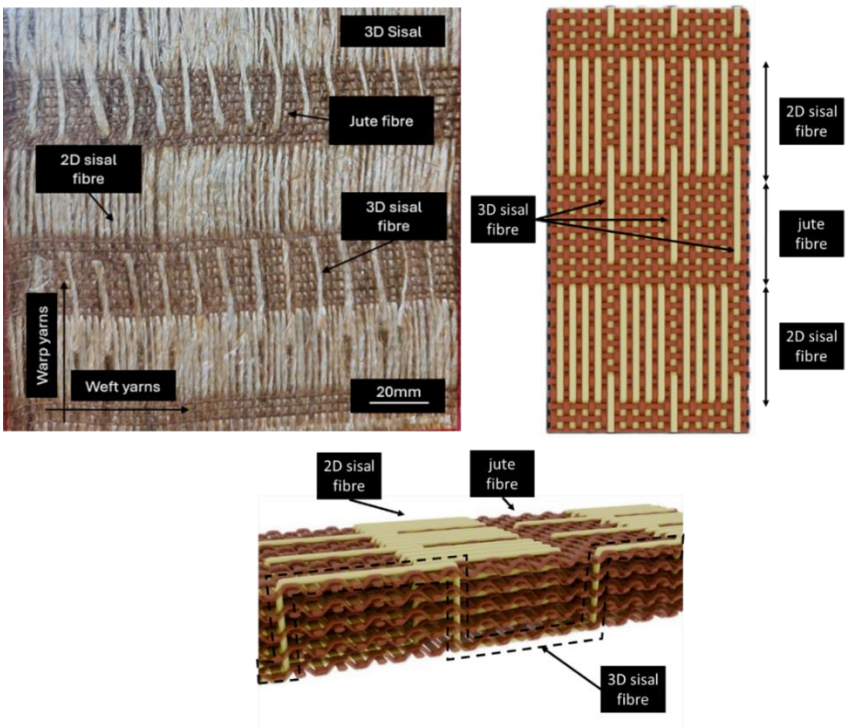
only the intralaminar reinforcement is present, while the 3D means that both the intralaminar (2D) and 3D OTT reinforcement architectures are present simultaneously). Table 3 presents the virgin material tensile properties.

Table 3. Mechanical properties of the virgin composite materials [20].

Composite type	Tensile strength (MPa)	Young's modulus (GPa)	Tensile strain (%)
SISAL 2D	96.98 ± 7.57	10.16 ± 0.12	1.04 ± 0.002
SISAL 3D	91.88 ± 7.04	9.90 ± 1.19	1.76 ± 0.006
CURAUÁ 2D	150.26 ± 12.72	17.79 ± 2.81	1.04 ± 0.002
CURAUÁ 3D	145.01 ± 10.81	15.78 ± 0.72	1.08 ± 0.001



a)



b)

Figure 1. Representative a) SISAL 2D fabricated composite plate and idealized schematic, b) SISAL 3D fabricated composite plate and idealized schematic.

2.3 Test methods

2.3.1 Fatigue tests

For the fatigue testing of the composite materials, a WinTest TA ElectroForce testing machine present at the DYNLAB facility at Politecnico di Torino with a 15 kN load cell was used, see Fig. 2. The size and geometry of the specimens were based on the ASTM D3479 [39] international standard. The testing was conducted with a targeted R ratio of 0.1, sine wave and a test frequency of 5 Hz in all cases. The load levels analyzed were chosen to be 0.7, 0.6 and 0.5 of the UTS of the individual materials. A limit of 1 million cycles was stipulated and any specimen that did not break at that level was considered a run out. A damage index was calculated as a function of the apparent modulus (i.e., no extensometer was used to obtain true strain). However, given that the test system was maintained and the compliance unchanged, a qualitative comparison analysis between the cases is possible. Equation 1 was used to calculate the damage index, D [21], where E is the apparent stiffness (N/mm) during tensile fatigue loading.

$$D = 1 - \frac{E(N)}{E_0} \tag{1}$$



a) b)

Figure 2. Fatigue machine used (a), and example of test set-up (b).

2.3.2 MicroCT analysis

X-ray computed tomography (CT) was performed using a custom-made CT system located in Politecnico di Torino J-Tech@PoliTO laboratory (Torino, Italy). The facility is equipped with a 300 kV X-ray source and a 5 μm minimum focal spot size, along with a flat panel detector featuring 2048 × 2048 pixels. The working distance between the source and the sample, as well as between the source and the detector, can be adjusted as needed**.** The scanning parameters used were 80 kV and 110 μA, resulting in an electron beam power of 8.8 W and a final resolution of 13 μm per voxel. No physical filtering was applied to the X-rays. The reconstructed 3-D volume of the investigated specimens was obtained using the filtered back-projection algorithm through VG MAX 3.5 software (Volume Graphics GmbH, Heidelberg, Germany), utilizing a total of 1600 X-ray

projections. During post-processing, the fibres were successfully separated from the matrix material, and the defects present in the different laminates were detected. Finally, the porosity of the laminates was computed.

3. RESULTS AND DISCUSSION

3.1 Tensile-tensile fatigue behaviour of 3D NFRCs

S-N curves for tensile-tensile fatigue tests at 5 Hz are presented in Fig. 3. The results are all within the low cycle fatigue range. For all cases, a decline in fatigue strength with increasing number of fatigue cycles was observed. For all loading levels (i.e.,0.7, 0.6 and 0.5 UTS) data dispersion in fatigue life was found. The order of magnitude of this dispersion is in line with other NFRC fatigue data from the literature [22, 23]. From Fig. 3 it can be seen that from the linear fit lines, the fatigue resistance increases (i.e., left to right, bottom to top), indicating that the reinforcement architecture had a significant effect on fatigue life. It can be seen that the 3D specimens presented higher fatigue lives and a general trend of higher resistance than their 2D counterparts. The arrow represents “run out” specimens, where some of the specimens did not fail after 1 million cycles at 0.5 UTS. This occurred for all cases studied. The surviving specimens were later tested in quasi-static monotonic tensile tests and compared to their virgin material counterparts and the results are presented and discussed in section 3.2. It has been observed in the literature that SISAL fibres have survived 1 million fatigue cycles at UTS 0.5 and failed in fatigue for ratios of 0.6 and 0.8 for fatigue lives between 10^3 and 10^6, respectively [24].

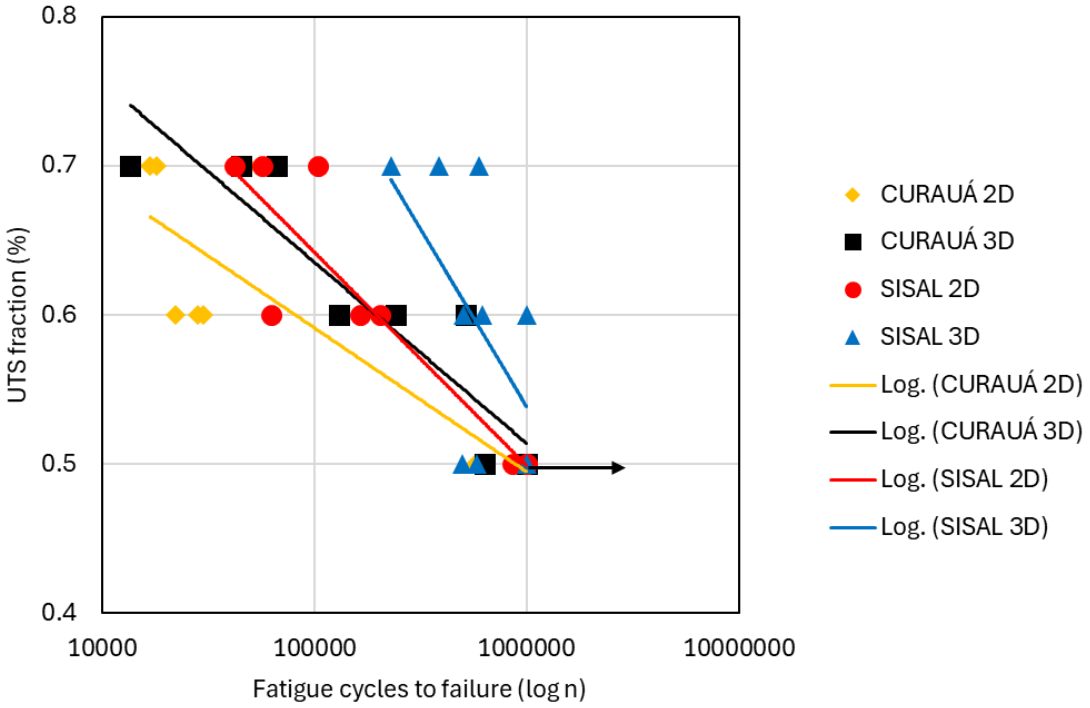


Figure 3. S-N curves of all tested specimens.

Table 4 presents the average fatigue life data for all specimens. It can be seen that the 3D specimens presented enhancements when compared to the 2D mainly for the 0.7 and 0.6 UTS load levels. The SISAL 3D presented an enhancement in fatigue life of approx. 80% when compared to the SISAL 2D for both 0.7 and 0.6 UTS load levels. On the other hand, the CURAUÁ 3D presented improvements of approx. 34% and 91% when compared to the 2D specimens for the 0.7 and 0,6 UTS load levels, respectively. Despite the dispersion, this suggests a clear trend of higher fatigue life for higher load levels. However, for the 0.5 UTS level, the SISAL 2D presented a higher life of approx. 34% while the CURAUÁ specimens did not present a significant variation, essentially plateauing. Therefore, it can be concluded that the improvements brought by the 3D architecture tend to stabilize at lower UTS fractions for tensile-tensile fatigue. A similar trend has been observed in the literature for SISAL composites as a result of alkalization treatment [25]. It was observed in general, for all specimens, that an increase in loading level significantly decreased the fatigue lives of the materials, likely due to the effect of internal manufacturing defects such as resin-rich zones, microcracks, bubbles and fibre misalignments that served as crack nucleation sites and decreased the fatigue life of the

material [26].

Table 4. Average fatigue life for all tested materials.

Composite	0.7 UTS	0.6 UTS	0.5 UTS
SISAL 2D	67,666	144,116	951,733
SISAL 3D	335,732	708,078	693,000
CURAUÁ 2D	27,816	26,850	858,191
CURAUÁ 3D	41,908	297,950	877,075

These trends are interesting because they are essentially in disagreement with the existing synthetic 3D composite fatigue literature [13]. Since, from the time of writing, no study of NFRC 3D OTT material has been found in the literature, comparisons are not possible with similar materials. Similarly, no research effort for the fatigue performance of CURAUÁ fibre-reinforced composites were found. However, this trend may be at least partially due to the completely different morphology of natural fibres compared to synthetic ones. The smoother surfaces of glass and carbon tows along with the much thinner fibres themselves may generate larger resin-rich zones around the z-binders than the case of NFRCs. On the other hand, for NFRCs, these zones surrounding the z-binder tend to be much smaller and the z-binder much more closely compacted with the surrounding main-direction fibres (compare Fig. 4 and Fig. 9a). Moreover, the 3D architecture geometry plays a crucial role in the material properties of 3D composites compared to their 2D counterparts. This research utilized an architecture where the in-plane aligned part of the z-binder (surface part) is approx. 7x the length of the orthogonal section (through-the-thickness) [20]. In the synthetic literature, more compact geometries are used where 2 rows are commonly skipped in the fabrication of the 3D preform [19]. This is also a key factor in the different trend observed in this research when compared to the general synthetic literature trends.

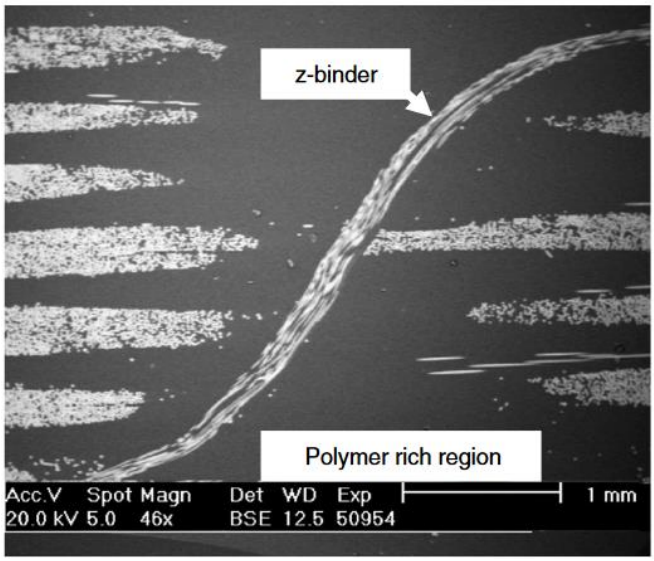
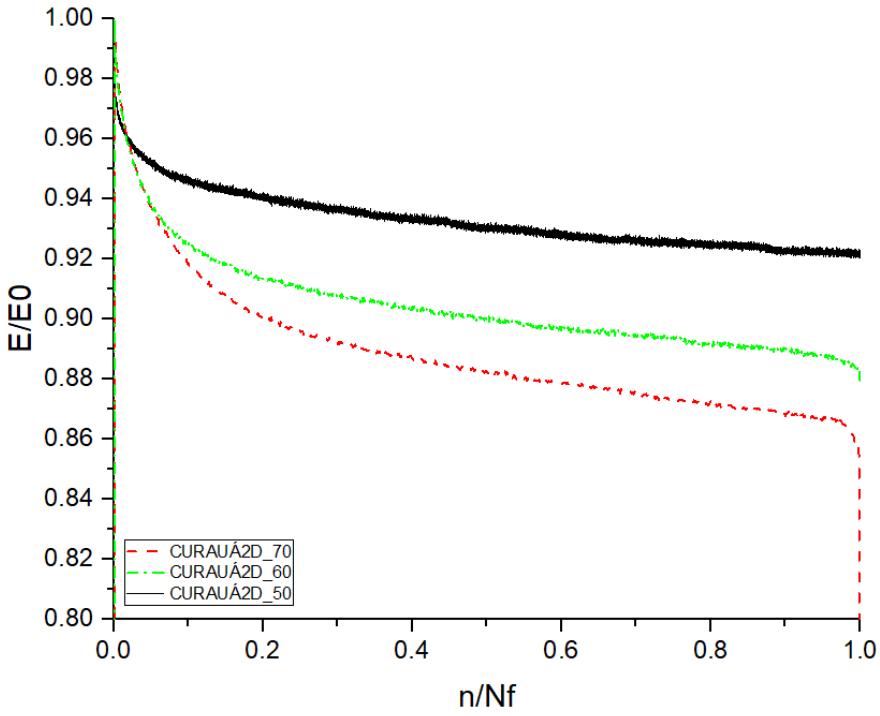


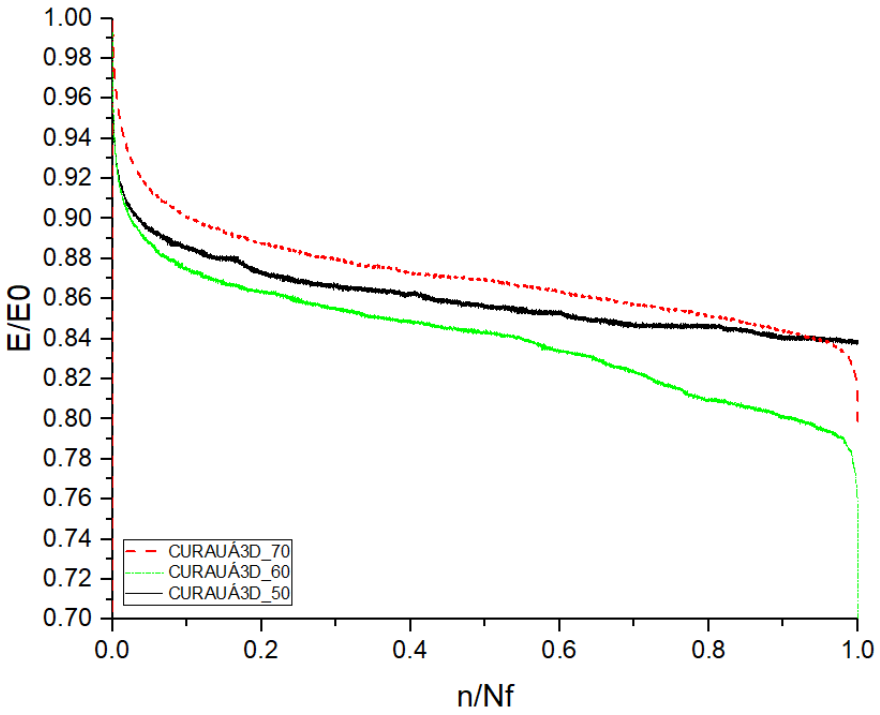
Figure 4. Cross-sectional view of a 3D carbon-fibre composite demonstrating the large resin-rich zones surrounding the z-binder [19].

Fatigue longevity alone is not sufficient to characterize the performance of these novel composites, since the material degradation behaviour may be different from one architecture to the next. It is expected that most fibre-reinforced composites analysed under stress-controlled fatigue loading would present a progressive stiffness degradation and this degradation would follow a 3-stage rotated sigmoidal trend [27]. The first and last stages are characterized by rapid degradation while the middle stage, stage 2, is usually longer and may present slower degradation or stable stiffness. Figure 5 presents the representative apparent modulus degradation curves for all specimens at the three studied load levels. This calculation is called apparent since no extensometer was used during fatigue testing, so the system compliance is not removed. However, since the same system was always used, a comparison between cases is fair. From Fig. 5a the stiffness degradation of CURAUÁ 2D can be seen. It is possible to see that the degradation trend was a function of the load levels, increasing from 0.5 to 0.7 UTS. From Fig. 5b the CURAUÁ 3D degradation is visible, and a slightly different trend is observed. Much closer degradation occurred where little variation was found except for stage 3 of the 0.6 UTS case. For the SISAL 2D case, the stiffness degradation trend was unchanged for stage 1, while higher deviation occurred for stages 2 and 3, where higher damage was observed as a function of increasing load levels (see Fig. 5c). Finally for SISAL 3D, the trends are slightly changed, where the 0.7 UTS accumulated less damage and the 0.6 and

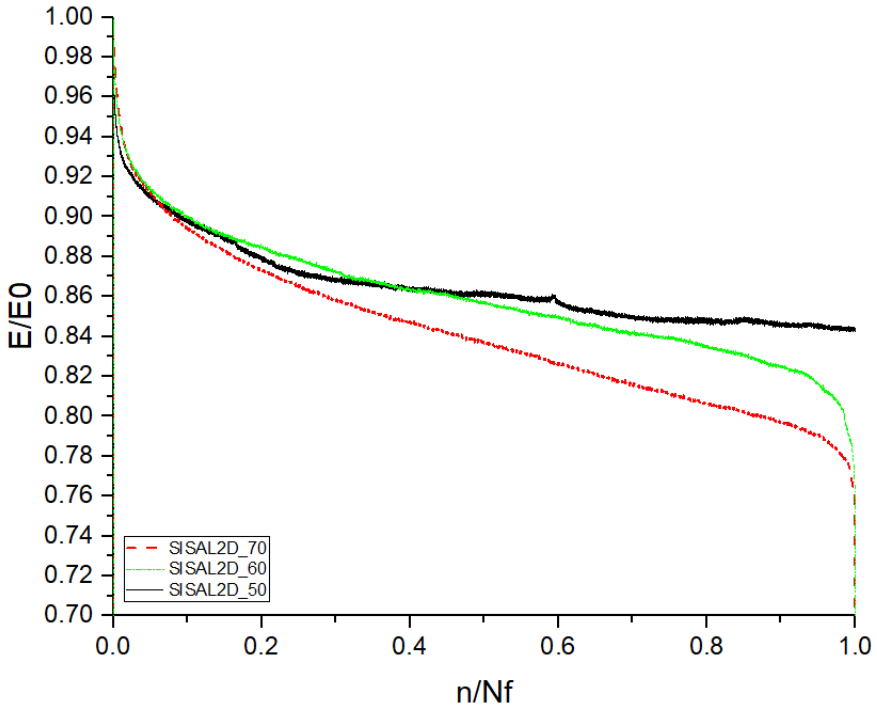
0.5 UTS cases presented similar behaviour and an interesting stiffening and softening trend within a larger scale generalized degradation trend.



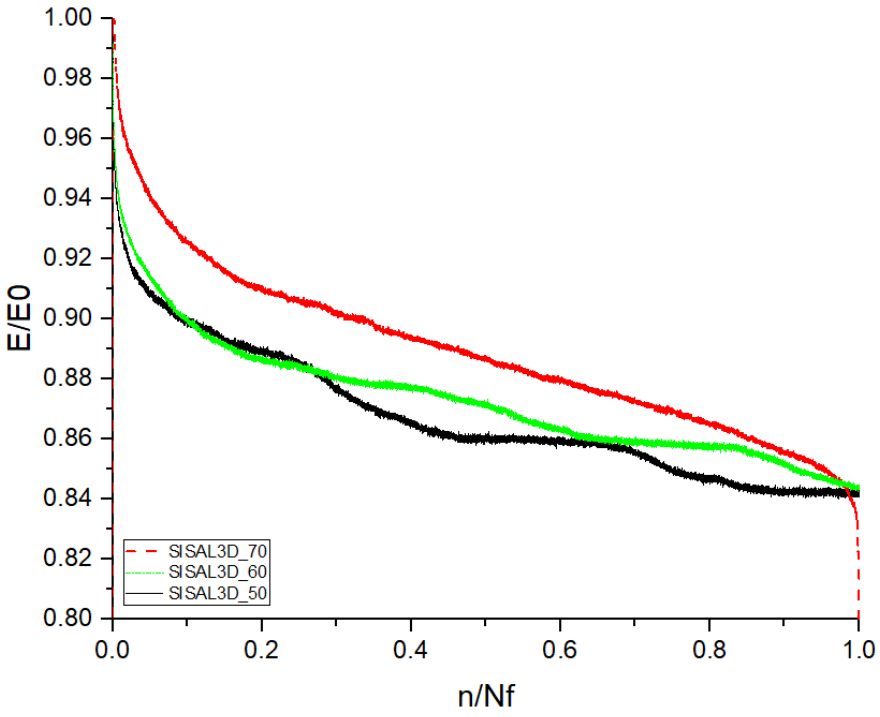
a)



b)



c)

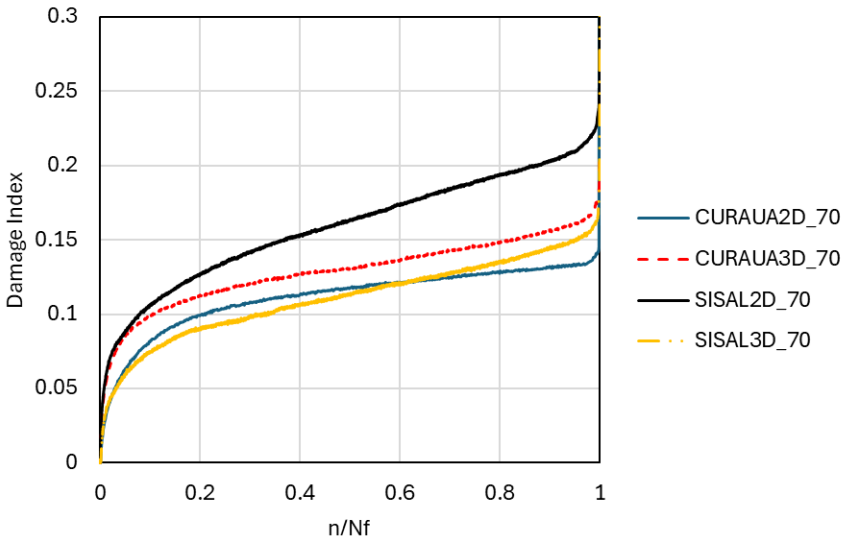


d)

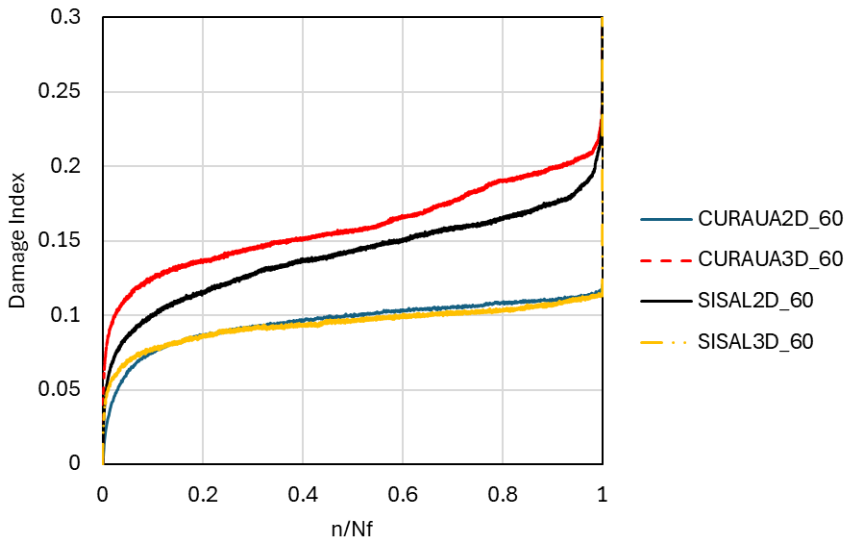
Figure 5. Representative apparent modulus degradation curves of CURAUÁ 2D (a), CURAUÁ 3D, (b) SISAL 2D (c) and SISAL 3D (d).

For a clearer view of the degradation trends, a damage evolution variable defined as a function of stiffness loss was calculated and charted in Fig. 6. Damage D is defined in

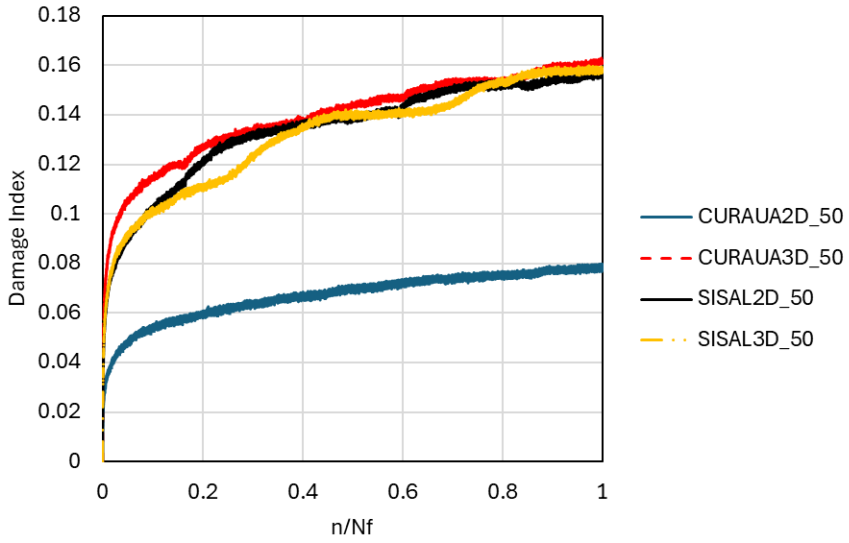
terms of normalized modulus as stiffness degradation and damage growth are interchangeable metrics, damage evolution reflects the stiffness trends [28]. Figure 6 presents the damage index, D, as representative curves for all specimens as a function of fatigue load level. From Fig. 6a, the damage index evolution of the 0.7 UTS load level can be seen. The SISAL 3D accumulated less damage than the 2D specimens, while for the CURAUÁ the opposite trend was observed. However, the variations were very small. For the 0.6 UTS specimens, the opposite trends were found where the SISAL 2D presented higher damage than the 3D and the CURAUÁ 2D less than the 3D. It is also interesting to see that for the SISAL 3D and CURAUÁ 2D, a very stable and large stage 2 was observed (see Fig. 6b). From Fig. 6c the damage index of the 0.5 UTS specimens can be seen. It is observed that very little variation was found for the CURAUÁ 3D, SISAL 3D and 2D, while the CURAUÁ 2D case presented the same behaviour at a lower damage index.



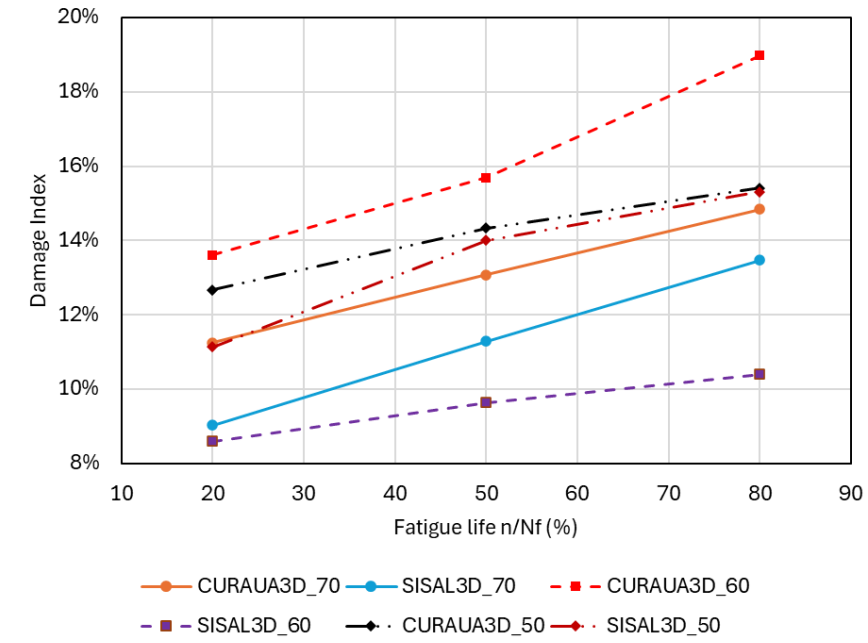
a)


0.3
0.25
0.2
0.15
0.1
0.05
0
Damage Index
0
0.2
0.4
0.6
0.8
1
n/Nf
CURAUA2D_60
CURAUA3D_60
SISAL2D_60
SISAL3D_60

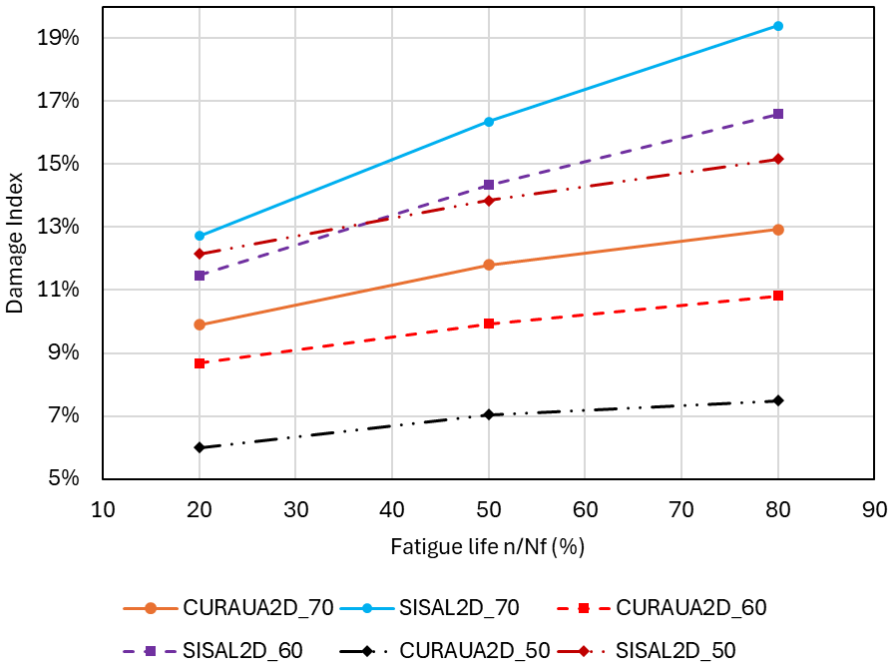
b)


0.18
0.16
0.14
0.12
0.1
0.08
0.06
0.04
0.02
0
Damage Index
0
0.2
0.4
0.6
0.8
1
n/Nf
CURAUA2D_50
CURAUA3D_50
SISAL2D_50
SISAL3D_50

c)



d)

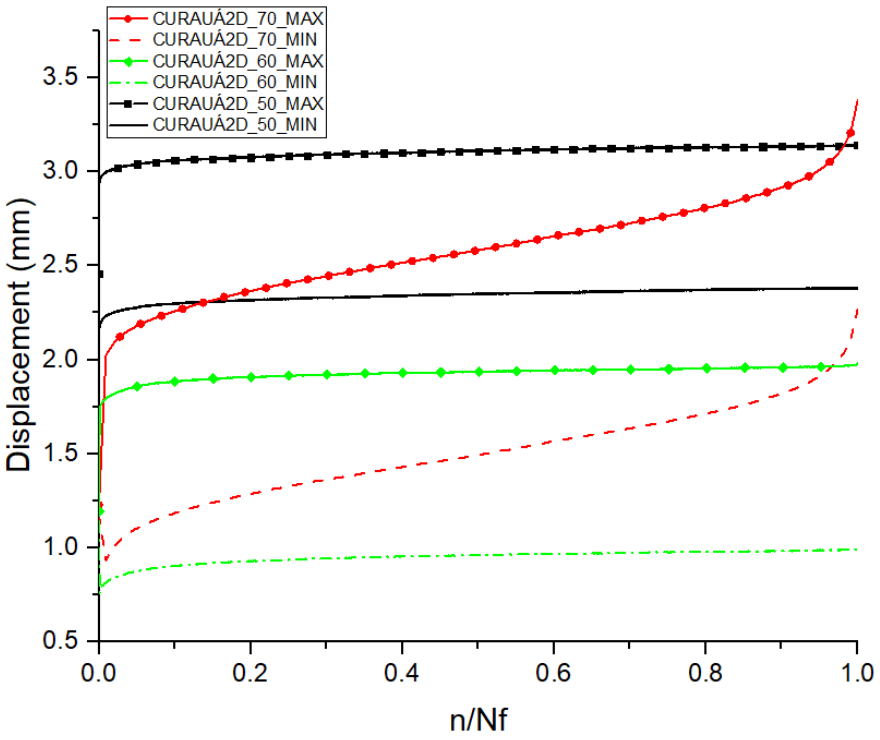


e)

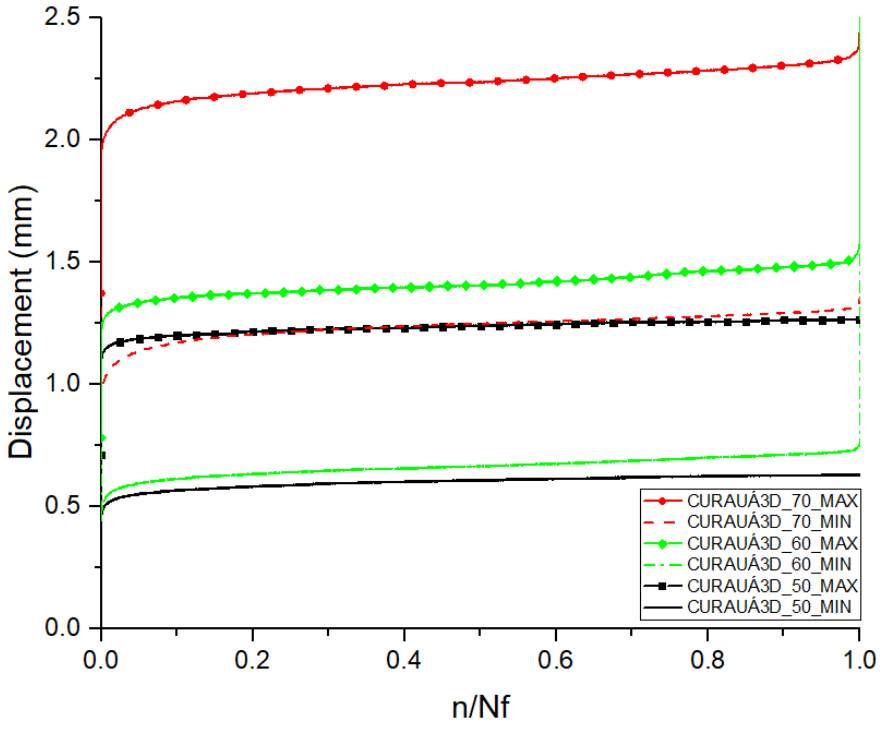
Figure 6. Fatigue damage index representative curves for all specimens under (a) 70%, (b) 60%, (c) 50% UTS, (d) Damage Index versus fatigue life expressed in percentages for the 3D cases and (e) 2D specimens.

These trends can be misleading however, since the actual differences between them sometimes span only a few percentage points (see the y axis). Therefore, for higher clarity, the damage index is also presented in percentage form and in three distinct sections of the fatigue life cycle (n/Nf), that is at 20, 50 and 80% of the fatigue life (see Fig. 6d and e). From Fig. 6d, the damage index expressed in percentages for the 3D specimens can be seen. For the CURAUÁ specimens, it can be seen that the trend over the fatigue life is a linear increase in damage for the 0.7 UTS while the trend is damage decrease for the 0.6 is slightly non-linear increase and the opposite for the 0.5 UTS case. However, the actual quantitative variations are in the 2-5% range. For the SISAL 3D specimens, a sharper linear trend of damage increase over fatigue life was observed for the 0.7 UTS case, while for both 0.6 and 0.5 UTS, a trend of decrease was found. The quantitative percentage variations are also in the range of approx. 5%. Figure 6b presents the damage index percentage variation for the 2D specimens. For the CURAUÁ specimens a similar quasi-linear trend of damage decrease over fatigue life was observed for all cases, however, lower damage was linked to lower UTS fractions. The variations were once more approx. 5%. Finally, for the SISAL 2D specimens, a similar trend was found, however a slightly higher damage increase tendency was found and a closer interaction between the 0.6 and 0.5 UTS cases was observed for stage 1 (approx. 20% life). The variations for the SISAL 2D were in the range of 2-5%. Therefore, the trends differ slightly for all cases, however in terms of percentage variations of damage index, no highly significant effect was found as a function of architecture or UTS load level (i.e., approx. 5% for each material type).

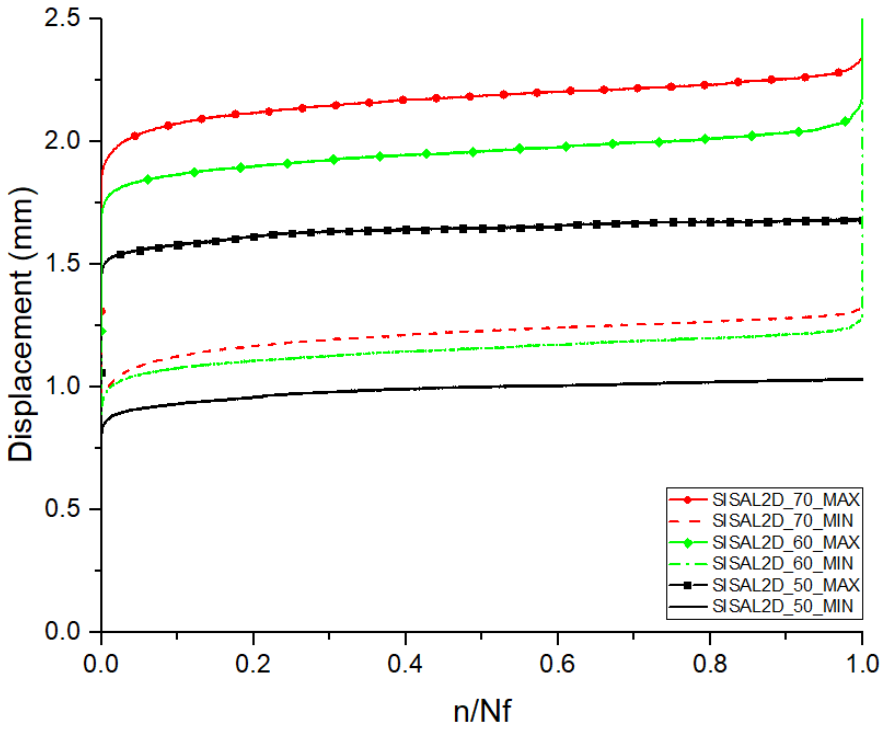
Figure 7 presents the representative displacement hysteresis (maximum and minimum displacement) of all the tested specimens as well as the hysteresis delta for three key points of the fatigue life. Overall, it can be seen that a very clear stage differentiation can be seen for the hysteresis loops, similar to the stiffness trends. All cases presented a rapid increase at stage 1 and quickly stabilized for a long stage 2 before a failure or run out after stage 3, apart from CURAUÁ 2D at 0.7 UTS.


CURAUÁ2D_70_MAX
CURAUÁ2D_70_MIN
CURAUÁ2D_60_MAX
CURAUÁ2D_60_MIN
CURAUÁ2D_50_MAX
CURAUÁ2D_50_MIN
Displacement (mm)
n/Nf
0.5
1.0
1.5
2.0
2.5
3.0
3.5
0.0
0.2
0.4
0.6
0.8
1.0

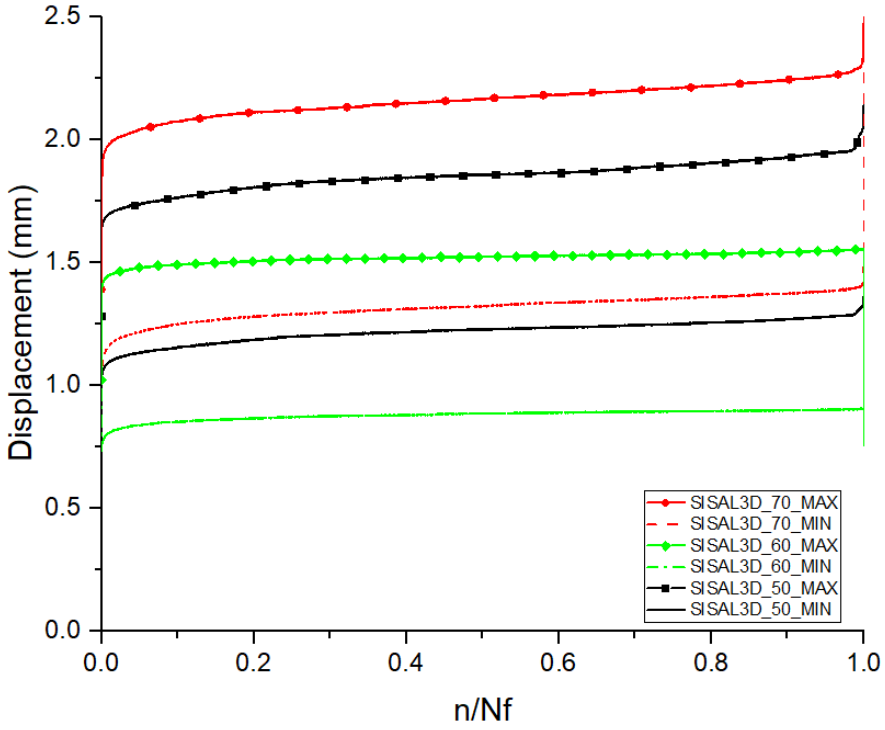
a)


CURAUÁ3D_70_MAX
CURAUÁ3D_70_MIN
CURAUÁ3D_60_MAX
CURAUÁ3D_60_MIN
CURAUÁ3D_50_MAX
CURAUÁ3D_50_MIN
Displacement (mm)
n/Nf
0.0
0.5
1.0
1.5
2.0
2.5
0.0
0.2
0.4
0.6
0.8
1.0

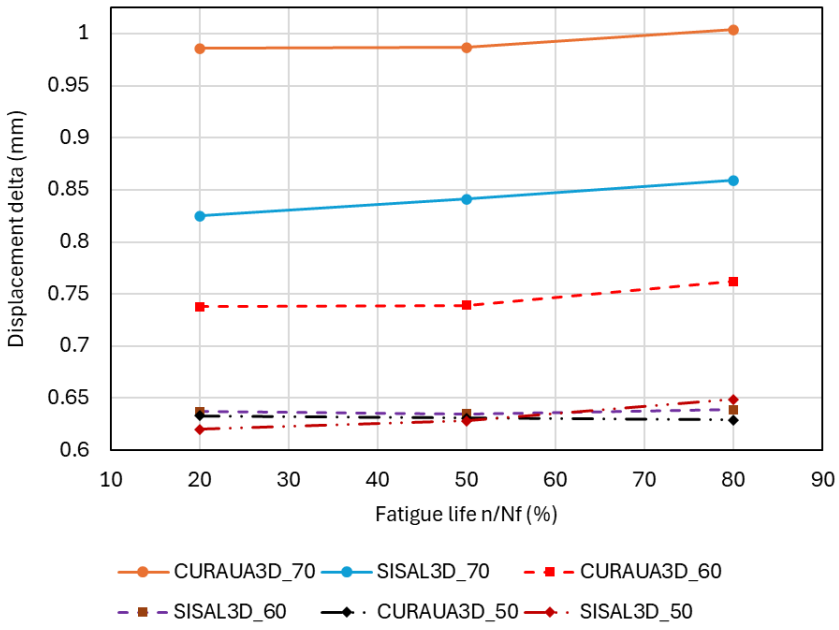
b)


Displacement (mm)
n/Nf
SISAL2D_70_MAX
SISAL2D_70_MIN
SISAL2D_60_MAX
SISAL2D_60_MIN
SISAL2D_50_MAX
SISAL2D_50_MIN

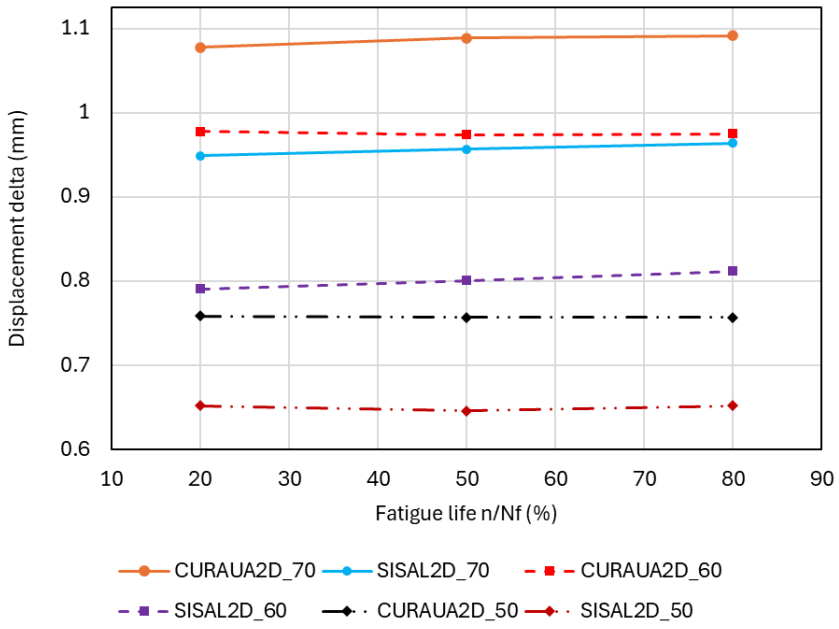
c)


Displacement (mm)
n/Nf
SISAL3D_70_MAX
SISAL3D_70_MIN
SISAL3D_60_MAX
SISAL3D_60_MIN
SISAL3D_50_MAX
SISAL3D_50_MIN

d)



e)



f)

Figure 7. Representative displacement hysteresis for the CURAUÁ 2D (a), CURAUÁ 3D (b), SISAL 2D (c), SISAL 3D and displacement delta versus fatigue life for the (e) 3D cases and (f) 2D specimens.

For a clearer understanding of the displacement behaviour of these novel materials under tensile-tensile fatigue loading, Fig. 7e and f present the displacement delta (maximum

minus minimum) of the hysteresis loop at 3 distinct key points of the fatigue life (i.e., 20, 50 and 80%). From Fig. 7e, a trend of non-linear decreased displacement can be seen as a function of load level, (i.e., higher displacement for higher load levels). This was observed for both CURAUÁ and SISAL, however, the SISAL specimens presented no significant variation between the 0.6 and 0.5 UTS levels. For the 2D specimens, a similar trend was observed for the CURAUÁ specimens, however, higher displacement deltas were observed, indicating that the 3D architecture decreased the deformation tendency of the specimen (see Fig. 7f). A similar trend was observed for the SISAL 2D specimens, where the 3D specimens presented lower displacement deltas. Furthermore, a larger gap was found between the 0.6 and 0.5 UTS fractions. Overall, no significant variation of displacement delta was found for all 3 fatigue life points analysed, indicating that deformation stability over fatigue life is independent of reinforcement architecture.

3.2 Effect of cyclic ageing in the residual tensile properties of the novel composites

As previously described in Section 3.1, all specimen cases presented at least one run out specimen that survived 1 million cycles at 0.5 UTS load level. To assess the true effect in the material properties of the materials, these run out specimens were tested in uniaxial quasi-static tension and compared to the virgin materials. Figure 8 presents the representative stress-strain curves of these materials. The general behaviour to failure did not significantly change, however both the stress at failure and the stiffness varied as a function of architecture. For the CURAUÁ specimens, the tensile strength decreased by approx. 41% and 27% when the aged specimens are compared to the virgin ones for the 3D and 2D cases, respectively. For the SISAL specimens, a decrease of approx. 24% and 15% was found when the 3D and 2D cases are compared to the virgin ones, respectively. These significant variations are expected and are a function of the ageing process where microcracks, local delaminations, fibre splitting and matrix cracking develop within the composite as a function of fatigue cycling [21]. The higher decrease of the CURAUÁ specimens compared to the SISAL, may be due to defects caused by the crushing of the z-binders that can split and cause high local anisotropy and sites of crack nucleation and propagation [14].

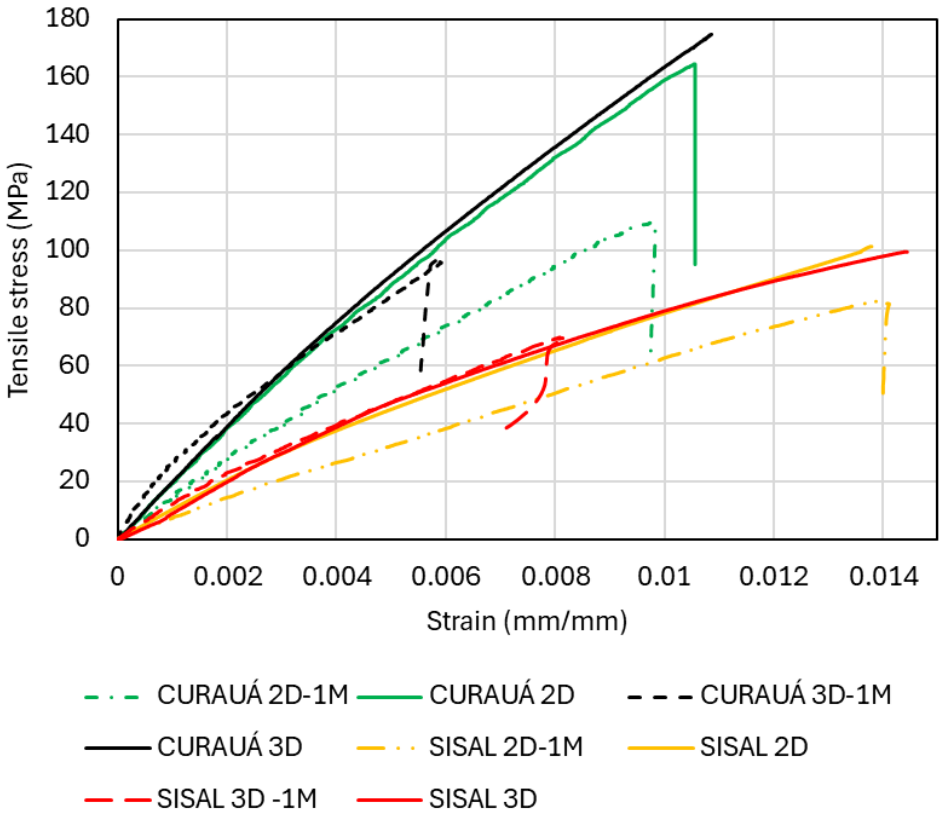


Figure 8. Representative stress-strain curves of unaged and fatigue cyclic aged composites.

On the other hand, when the stiffness of the aged specimens is compared to the virgin ones, a very different trend emerges. The decrease in stiffness for the CURAUÁ 2D specimens was approx. 26% when compared to the virgin material. Regarding the CURAUÁ 3D specimens, an approx. stiffness decrease of 10% was observed for the fatigue aged specimen when compared to the neat. For the SISAL specimens, the stiffness decrease was approx. 38% and 5%, when compared to the 2D and 3D virgin specimens, respectively. Therefore, a trend of stiffness retention after cyclic ageing was found for the 3D reinforced specimens. It is noteworthy that the previous discussion of the damage index, which was calculated based on the apparent modulus, both under and overpredicts the real stiffness degradation and should be used only as a tool for qualitative analysis between the groups that were tested in the same conditions. This is due to the effect of the testing machine's compliance which was not removed via an extensometer.

3.3 MicroCT analysis

MicroCT analysis was done to assess the state of voids and microcracks before and after cyclic ageing. Figure 9 presents representative scans of CURAUÁ 3D before and after cyclic ageing at 0.5 UTS (run out specimens). It can be seen from Fig. 9a and b that around and within the z-binder, higher volume voids are visible (red areas), and they follow the fibre all the way from entrance to the orthogonal directional change near the surface. Moreover, from Fig. 9a, it can be seen that the angle of the z-binder differs from the idealized 90 degrees. From the void formation in Fig. 9b, it can be inferred that the z-binder suffered a crushing and splitting during composite compression fabrication. Figure 9c and d a scan of aged CURAUÁ 3D specimen can be seen. This section is different from the previous in order to remove the pre-existing z-binder voids and analyse only voids created due to fatigue ageing. It can be seen that significant voids developed as a function of ageing (red areas) close to one of the specimen edges and between fibre tows. It is important to notice the scale, where the aged specimen voids are two orders of magnitude more severe than the unaged. Only the CURAUÁ specimen was described due to the similarity of the trends observed for the other cases.

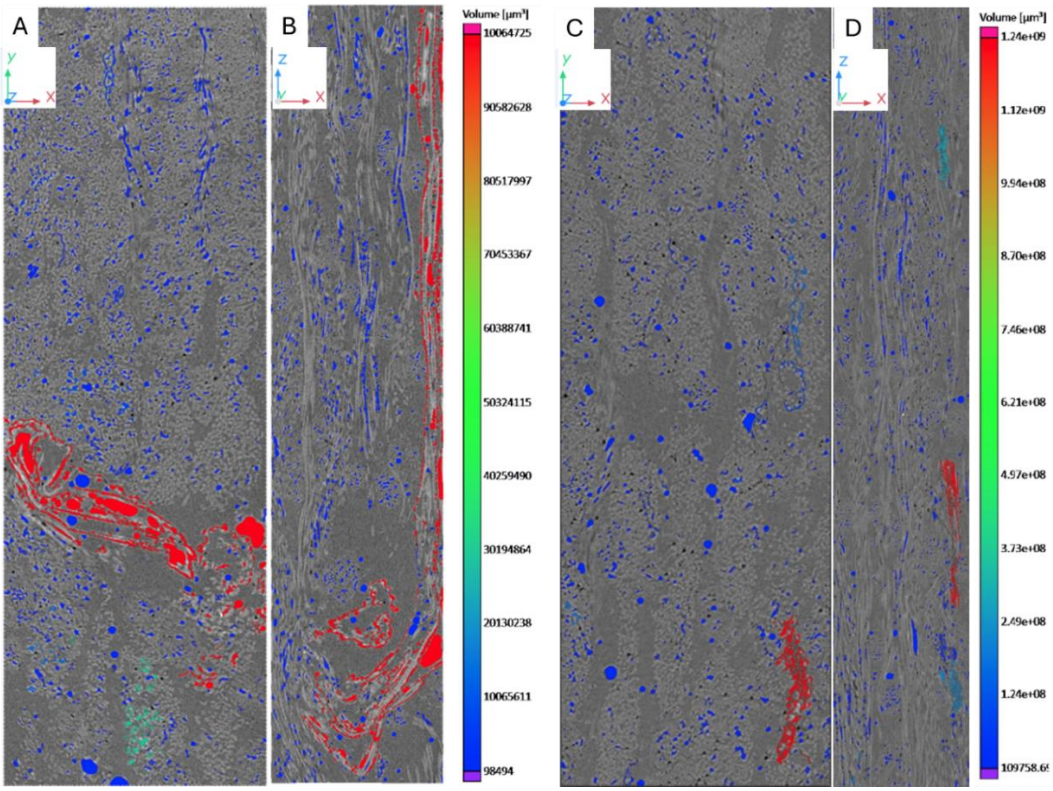


Figure 9. Representative scans of neat CURAUÁ 3D specimens neat (A,B) and after fatigue cycling (C,D).

4. Conclusions

This research focused on the analysis of novel 3D OTT NFRCs under tensile-tensile fatigue cyclic loading. Three loading levels were considered (i.e., 0.7, 0.6, 0,5 UTS). The following conclusions can be drawn:

- The fatigue life of these novel composites was significantly affected by the 3D architecture at higher load levels (i.e., 70 and 60%), while a tendency of stabilization was found for the 50% UTS fatigue life. Enhancements in fatigue life ranged from 80% to 91% for the SISAL and CURAUÁ specimens, respectively.
- All specimens presented varying degrees of stiffness degradation as a function of fatigue cycling. The damage index varied as a function of both loading level and architecture. However, the overall trends were not highly significant with variations of approx. 5%.
- The displacement hysteresis loops of all cases were well defined, and the 3-stage evolution could be identified. The displacement delta of all cases was not highly significant with variations of approx. 5%.
- By comparing uniaxial tensile testing of virgin and 0.5 UTS fatigue aged specimens (1 million cycles); it was found that the tensile strength always decreases significantly (i.e., up to 41%), while the 3D architecture provides a significant stiffness retention post-ageing (approx. 5-10%).
- MicroCT analysis revealed that void fraction significantly increases in volume as a function of cyclic ageing (i.e., approx. two orders of magnitude for 1 million cycles at 0.5 UTS).

REFERENCES

1. Neto, J., et al., *A Review of Recent Advances in Hybrid Natural Fiber Reinforced Polymer Composites.* Journal of Renewable Materials, 2022. **10**(3): p. 561--589.
2. Bhowmik, S., S. Kumar, and V.K. Mahakur, *Various factors affecting the fatigue performance of natural fiber-reinforced polymer composites: a systematic review.* Iranian Polymer Journal, 2024. **33**(2): p. 249-271.
3. Hallak Panzera, T., et al., *Static, fatigue and impact behaviour of an autoclaved flax fibre reinforced composite for aerospace engineering.* Composites Part B: Engineering, 2020. **197**: p. 108049.
4. Pickering, K.L., M.G.A. Efendy, and T.M. Le, *A review of recent developments in natural fibre composites and their mechanical performance.* Composites Part A: Applied Science and Manufacturing, 2016. **83**: p. 98-112.
5. de Seixas, G., et al., *Effect of water on the mechanical and thermal properties of natural fibre reinforced hybrid composites.* Journal of Composite Materials, 2023. **57**(11): p. 1941-1958.
6. de Araujo Alves Lima, R., et al., *Effect of surface treatments on interfacial properties of natural intralaminar hybrid composites.* Polymer Composites, 2020. **41**(1): p. 314-325.
7. Neto, J.S.S., et al., *Effect of chemical treatment on the thermal properties of hybrid natural fiber-reinforced composites.* Journal of Applied Polymer Science, 2019. **136**(10): p. 47154.
8. de Queiroz, H.F.M. and M.D. Banea, *Methods to increase the mechanical performance of composite adhesive joints: An overview with focus on joints with natural fibre composite adherends.* Journal of Composite Materials, 2022. **56**(26): p. 3993-4010.
9. Mostafa, N.H., *Tensile and fatigue properties of Jute-Glass hybrid fibre reinforced epoxy composites.* Materials Research Express, 2019. **6**(8): p. 085102.
10. Nugraha, A.D., et al., *Recent Progress on Natural Fibers Mixed with CFRP and GFRP: Properties, Characteristics, and Failure Behaviour.* Polymers, 2022. **14**(23): p. 5138.
11. de Queiroz, H.F.M., et al., *Effect of hybridization and composite architecture symmetry in the bonded joint performance of jute/carbon fibre-reinforced*

composites. International Journal of Adhesion and Adhesives, 2024. **133**: p. 103745.

12. de Queiroz, H.F.M., M.D. Banea, and D.K.K. Cavalcanti, *Adhesively bonded joints of jute, glass and hybrid jute/glass fibre-reinforced polymer composites for automotive industry*. Applied Adhesion Science, 2021. **9**(1): p. 2.
13. Mouritz, A.P. and B.N. Cox, *A mechanistic interpretation of the comparative in-plane mechanical properties of 3D woven, stitched and pinned composites.* Composites Part A: Applied Science and Manufacturing, 2010. **41**(6): p. 709-728.
14. de Queiroz, H.F.M., et al., *Mechanical characterization of novel natural fibre-reinforced composites via a three-dimensional fibre architecture.* Composites Science and Technology, 2025. **261**: p. 110996.
15. Barouni, A., et al., *Investigation into the fatigue properties of flax fibre epoxy composites and hybrid composites based on flax and glass fibres.* Composite Structures, 2022. **281**: p. 115046.
16. Olhan, S., et al., *Mechanical, thermal, and viscoelastic behavior of sisal fibre-based structural composites for automotive applications: Experimental and FEM analysis.* Composite Structures, 2023. **322**: p. 117427.
17. Paul, P., M. Ahirwar, and B.K. Behera, *Acoustic behavior of three-dimensional woven fabrics and their composites: role of fiber type and weave architecture.* The Journal of The Textile Institute, 2024. **115**(11): p. 2258-2271.
18. Jabbar, M., et al., *Effect of the stuffer yarns on the mechanical performance of novel 3D woven green composites.* Composite Structures, 2021. **269**: p. 114023.
19. Rudov-Clark, S. and A.P. Mouritz, *Tensile fatigue properties of a 3D orthogonal woven composite.* Composites Part A: Applied Science and Manufacturing, 2008. **39**(6): p. 1018-1024.
20. de Queiroz, H.F.M., et al., *A novel 3D fibre-reinforcement architecture for high performance natural fibre reinforced composite adhesively bonded joints.* The Journal of Adhesion, 2024. **100**(2): p. 118-138.
21. Ma, Z., P. Zhang, and J. Zhu, *Review on the fatigue properties of 3D woven fiber/epoxy composites: testing and modelling strategies.* Journal of Industrial Textiles, 2022. **51**(5_suppl): p. 7755S-7795S.
22. Jeannin, T., et al., *About the fatigue endurance of unidirectional flax-epoxy*

composite laminates. Composites Part B: Engineering, 2019. **165**: p. 690-701.

23. Jeannin, T., et al., *Influence of hydrothermal ageing on the fatigue behaviour of a unidirectional flax-epoxy laminate.* Composites Part B: Engineering, 2019. **174**: p. 107056.
24. Silva, F.d.A., N. Chawla, and R.D. de Toledo Filho, *An experimental investigation of the fatigue behavior of sisal fibers.* Materials Science and Engineering: A, 2009. **516**(1): p. 90-95.
25. Towo, A.N. and M.P. Ansell, *Fatigue evaluation and dynamic mechanical thermal analysis of sisal fibre–thermosetting resin composites.* Composites Science and Technology, 2008. **68**(3): p. 925-932.
26. Suriani, M.J., et al., *Delamination and Manufacturing Defects in Natural Fiber-Reinforced Hybrid Composite: A Review.* Polymers, 2021. **13**(8): p. 1323.
27. Mahboob, Z. and H. Bougherara, *Fatigue of flax-epoxy and other plant fibre composites: Critical review and analysis.* Composites Part A: Applied Science and Manufacturing, 2018. **109**: p. 440-462.
28. Al-Hajaj, Z., R. Zdero, and H. Bougherara, *Tensile fatigue response of a novel carbon/flax/epoxy hybrid composite under strain-controlled and stress-controlled amplitude.* Proceedings of the Institution of Mechanical Engineers, Part L: Journal of Materials: Design and Applications, 2021. **235**(11): p. 2588-2599.